DSPACE

https://dspace.org/

Spatial interpolation of extreme rainfall events over the past 50 years (1970 - 2019): a case study from central Southern Africa

Tumane, Maitshoko

2022
https://hdl.handle.net/10539/35494

Downloaded from a DSpace repository. https://dspace.org/



Maitshoko Tumane

Student Number: 1534778

School of Geography Archaeology and Environmental Studies

MSc GIS and RS Research Report

Spatial interpolation of extreme rainfall events over the past 50 years (1970 – 2019): a case study from central Southern Africa

Supervisor: Prof Jennifer Fitchett
Co-Supervisors: Dr Adriaan Van Der Walt, Prof Amanda Esterhuysen

April 2022

Declaration

I, Maitshoko Gloria Tumane (Student No 1534778) declare that this research report submitted for MSc in GIS and Remote Sensing at the University of Witwatersrand has not been previously submitted for a degree at this or any other University, in part or in full, all the sources of information have been fully acknowledged in the references.

Signed:  Date: 05 April 2022

Maitshoko Gloria Tumane

Abstract

Droughts have been identified as recurring natural hazards in various parts of the world. The study region is in a semi-arid area and this area exhibits high climate variability, and the frequency of this variability has been increasing in recent years. The present study was conducted to analyse the spatiotemporal distribution of extreme rainfall events in the central region of southern Africa. Rainfall data used in this research was obtained from the Botswana Meteorological Office and the South African Weather Service. The analysis spans a period from 1970 to 2019. Climate data obtained from the two meteorological offices was analysed using three methods, Standardized Precipitation Index (SPI), Inverse Discrete Weighing (IDW) and Ordinary Kriging (OK). The interpolation methods used in this study were applied to spatially distributed precipitation data. Based on the results of the study, various drought occurrences have been identified at the weather stations. In the study region, normal drought conditions prevail, followed by moderately dry drought conditions. The El Niño years that coincide with droughts in the study region are 1963/1964, 1994/1995, 2002/2003, 2004/2005, 2006/2007, 2015/2016. As per SPI calculations, the years 1991 and 1992 had more than 10 weather stations experiencing dry drought conditions. The years 1999 and 2005 had the most weather stations recording the occurrence of wet drought conditions. The average precipitation of the area shows that the region is experiencing a decrease in precipitation at the rate of change of -2.42. This study has provided new insights into the occurrence of droughts and floods in central southern Africa and has further indicated there has been an increase in the frequency and intensity of droughts in this region over recent decades.

Keywords: Inverse Distance Weighing, Ordinary Kriging, Droughts, Standardised Precipitation Index, Frequency, Southern Africa.

Acknowledgements

My thanks and gratitude goes to the Lord Almighty for keeping me strong through the years and enabling me to finish this research report despite all the ups and downs that occurred. I'm more than grateful to my supervisors Prof Fitchett, Dr Van Der Walt, and Prof Esterhuysen for being my supervisors and source of guidance. I'll also like to acknowledge Dr Merlo for organizing climate data from the SAWS and BMO as well as assisting with the early stages of my research report. To all my friends who have been supportive throughout my research report. To my mother, who has been by my side through thick and thin, you will always be appreciated, and to my uncles and aunts, I will forever be grateful for your support. I would like to thank Marike Klutys from the Wits Science Writing Centre for all the academic support. Finally, I would also like to thank Nedbank Eyethu, the Metsemegologolo project, and the Environmental Resources Management for funding my research report.

Table of Contents

Declaration i
Abstract ii
Acknowledgments iii
List of Figures vi
List of Tables vii
List of Acronyms and Scientific Terms viii
Chapter 1: INTRODUCTION 1
1.1. Background to the study 1
1.2. Significance of the Study 2
1.3. Problem Statement 4
1.4. Research Questions 5
1.5. Aim and Objectives 5
1.6. Overview of the Project 5
Chapter 2: LITERATURE REVIEW 7
2.1. Introduction 7
2.2. Drivers of climate in southern Africa 7
2.3. Methods for exploring key drivers of climate change 14
2.4. Occurrence of droughts and floods in southern Africa 16
2.5. Spatial interpolation of climate data 19
2.6. Conclusion 21
Chapter 3: METHODOLOGY 22
3.1. Introduction 22
3.2. Study Region 22
3.2.1. Climate and Geography 23
3.2.2. Data Acquisition (Data Quality and Limitations) 24
3.3. Data Analysis Procedures 26
3.3.1. SPI Analysis 26
3.3.2. Interpolation Methods 27
3.3.3. ENSO 29
Chapter 4: RESULTS 30
4.1. Introduction 30
4.2. Temporal frequency of droughts 30
4.3. Spatial Distribution of Droughts Events 36
4.3.1. IDW 36
4.3.2. OK 41
4.4. Annual rainfall statistical results 42

4.5. Conclusion 49
Chapter 5: DISCUSSION 50
5.1. Temporal frequency of droughts 50
5.2. Spatial frequency of droughts 52
5.3. Contemporary issues related to droughts 53
5.4. Limitations of the study 56
Chapter 6: CONCLUSION 58
6.1. Achievement of Aims and Objectives 59
6.2. Areas for future study 60
Chapter 7: REFERENCES 62
Chapter 8: APPENDICES i
8.1. Annual Rainfall Plots i
8.2. SPI Results (The 12-month Standard Precipitation Index (SPI)) xxix
8.3. Inverse Distance Weighting i
8.4. Ordinary Kriging xxvi

List of Figures

Figure 1: Distribution of weather stations around the study region. Sources: DIVA-GIS, South African Weather Service (SAWS) and Botswana Meteorological Office (BMO). 23

Figure 2: The 12-month SPI for Schietfontein 32

Figure 3: The 12-month SPI for Leeupoort. 32

Figure 4: SPI Values below -1, 1973-2019 35

Figure 5: SPI Values Wet Drought conditions, 1913-2019 35

Figure 6: Delineations in the study region 36

Figure 7: Average SPI using IDW, 1970-2019 37

Figure 8: Average SPI using OK, 1970-2019 41

Figure 9: Rainfall data Matsiloje 42

Figure 10: Rainfall data Shakawe 43

Figure 11: Average Precipitation 1913-2019 44

List of Tables

Table 1: Weather Stations with precipitation data.. 25

Table 2: SPI Values 27

Table 3: Accuracy Assessment IDW and OK 41

Table 4: Statistical results for the total annual precipitation 45

Table 5: Weather Stations showing the occurrence of Wet and Dry drought conditions during the occurrence of El Niño 47

Table 6: Weather Stations showing the occurrence of Wet and Dry drought conditions during the occurrence of La Niña 48

List of Acronyms and Scientific Terms

AMO - Atlantic Multi-decadal Oscillation

ASE - Average Standard Error

BMO - Botswana Meteorological Office

CE - Coefficient of Efficiency

CGCM - Coupled General Circulation Model

CRS - Completely Regularity Spline

CZI - China Z Index

d - Index of agreement

EBK - Empirical Bayesian Kriging

ENSO - El Niño Southern Oscillation

GIS - Geographic Information Systems

HPa - Hectopascals

IDW - Inverse Discrete Weighing

ITCZ - Inter-Tropical Convergence Zone

KED - Kriging with External Drift

m/s – Meters per second

MAE - Mean Absolute Error

MJO - Madden-Julian Oscillation

NDVI - Normalized Difference Vegetation Index

NDWI - Normalized Difference Water Index

NE – Northeast

NN - Natural neighbour

NNRK - Neural Network Residual Kriging

NOAA - National Oceanic and Atmospheric Administration

NRN - Nearest Neighbour

NW - Northwest

OCK - Ordinary Cokriging

OK - Ordinary Kriging

PDO - Pacific Decadal Oscillation

PDSI - Palmer Drought Severity Index

QBO - Quasi-Biennial Oscillation

R^2 - Coefficient of determination

RK - Regression Kriging

RKNNRK - Regression Kriging and Artificial Neural Network Residual Kriging

RMSE - Root Mean Square Error

S - South

SAM - Southern Angular Mode

SAWS - South African Weather Service

SE - Southeast

SIOD - Southern Indian Ocean Dipole

SLP - Sea Level Pressure

SPI - Standardized Precipitation Index

SPT - Spline Tension

SST - Sea Surface Temperature

SW - Southwest

SW – Southwest

TLI - Triangulation with linear interpolation

UK - Universal Kriging

ZSI – Z Score Index

Chapter 1: INTRODUCTION

1.1. Background to the study

Characteristics of extreme climate events are anticipated to change as global average temperatures increase, heightening the frequency and severity of extreme climate events (Ummenhofer and Meehl, 2017; Giorgi *et al.,* 2019; Guo *et al.,* 2019; Mbokodo *et al.,* 2020). One of the greatest concerns which arise due to climate change is the response of the Earth's hydrological system (Giorgi *et al.,* 2019). There have been continual changes in the spatiotemporal patterns of precipitation, and for most regions in the world, there has been an increase in the occurrence of droughts and floods (Guo *et al.,* 2019). Droughts are defined as prolonged periods of precipitation that is significantly below the mean (Hanel *et al.,* 2018; Haile *et al.,* 2020).

Droughts are classified into four categories: Meteorological, Hydrological, Agricultural and Socio-economic droughts (Wang *et al*., 2016; Sun *et al*., 2019). Meteorological droughts are defined by the degree of dryness, as compared to the normal or an average amount, as well as the duration of the dry conditions (Depsky and Pons, 2020). Hydrological droughts are associated with the effects of precipitation deficits on surface or subsurface water supply (Alvarez-Garreton *et al.,* 2021). Agricultural droughts are associated with the different characteristics of hydrological or meteorological droughts to agricultural impacts, focusing on precipitation shortages, lack of soil moisture, reduced groundwater levels, and the differences between actual and potential evapotranspiration (Zhu *et al.,* 2021). Socio-economic droughts can be identified or classified based on supply and demand processes over time and space (Nasirudeen *et al.,* 2021).

The translation of meteorological drought to hydrological drought has a major impact on water resource management (Borgomeo *et al.,* 2015; Van Loon, 2015; Wu *et al.,* 2018). Once a hydrological drought occurs it is more likely for agricultural and socio-economic droughts to take place (Mtilatila *et al.,* 2020). In the central region of southern Africa, a limited number of studies have been undertaken to explore extreme precipitation events (Pinto *et al*., 2016; Davis and Vincent, 2017). This research will analyse extreme precipitation events (droughts and floods), that have occurred in central southern Africa over the past 40-50 years. The study will be carried out using Geographic Information Systems (GIS). GIS software includes tools that can address both spatial statistics and spatial analysis (Machiwal *et al.,* 2018). These have become increasingly important in mapping the spatiotemporal distribution of climate variables (Rogan and Chen, 2004).

1.2. Significance of the study

99.9% of the scientific evidence indicates that the world's climate has been changing at an accelerated rate (Lenton *et al.,* 2019; Muthoni *et al.,* 2019; Lynas *et al.,* 2021). 88125 climate-related studies published between 2012 and November 2020 concluded that warming temperatures and increased frequency of extreme events are all related to anthropogenic activities (Dunleavy, 2021). Climate change, climate variability and extreme weather conditions are influenced by the atmospheric emission of greenhouse gases (Beckage *et al.*, 2018). Southern African countries are at risk of experiencing extreme weather events such as droughts and floods (He *et al.,* 2020), due to the vulnerability to climate change that is more rapid than the global average and low adaptive capacity (Tadross *et al.,* 2017; Beraki *et al.,* 2020). Climate models have predicted an increase in the intensity of extreme rainfall over southern Africa

(Ayanlade *et al.,* 2018), accompanied by an increase in dry conditions in the western region of southern Africa, during the austral summer months of December through to February (Maúre *et al.,* 2018). The occurrences of these precipitation extremes are linked to climate drivers (Nkemelang *et al.,* 2018; Li *et al.,* 2021), climate drivers which have a direct impact on the weather and climate of Southern Africa include the El Niño Southern Oscillation (ENSO), Southern Angular Mode (SAM), Southern Indian Ocean Dipole (SIOD), Madden-Julian Oscillation (MJO), Quasi-Biennial Oscillation (QBO; Lim *et al.,* 2019).

A range of studies have explored the effects of climate drivers in the eastern half of southern Africa (Reason *et al.,* 2005; Ngongondo *et al.,* 2011; Dougherty *et al.,* 2020; Makondo and Thomas, 2020; Tanyanyiwa and Mufunda, 2020), however, the central part of southern Africa has not been studied in detail. Understanding extreme rainfall events can lead to a better understanding of the relationship between these events and their key drivers (Sillmann *et al.,* 2017). This research is conducted under the umbrella of the Metsemegologolo project, which explores early historic Tswana urbanism in southern Africa. The project is structured in nine closely related work packages, one of which explores climate variables in the area. This research is part of the climate work pack of the Metsemegologolo project which aims at creating an open-source multimodal online platform for archival materials on early Tswana urban spaces straddling the South Africa-Botswana border in the 18th-20th century. The climate section looks at providing a climate and environmental backdrop against which a diverse range of archives can be interpreted. The methods for the climate work explore climate data identification and interpretation and climate time-slice mapping over a

continuous layer. This project looks at identifying climate weather extremes that occurred in this region between the years 1970-2019.

Understanding past climates in periods before regular record keeping can be improved through the analysis of trends and mean conditions in the contemporary climate (Brown *et al*., 2020). Annual rainfall variations across southern Africa have significant impacts on human livelihoods through their impacts on water supply and agriculture (Hannaford *et al.,* 2014; Kusangaya *et al.,* 2014; Neukom *et al.,* 2014; Nash *et al.,*2016; Bhaga *et al.,* 2020). Rainfall distribution in the subcontinent is seasonal and influenced by a variety of atmospheric and oceanic circulation systems (Neukom *et al.,* 2014). The area under investigation has instrumental data available for the past 40-50 years with the earliest records dating back to 1913 in Leeupoort which is one of the weather stations located in South Africa.

1.3. Problem Statement

Climate extremes affect day-to-day weather, and the overall climate of an area (Lovino *et al.,* 2018). Due to a changing climate in central parts of southern Africa, there has been an increase in the frequency of extreme events such as droughts and floods (Nangombe *et al.,* 2018). Technological advancements have allowed for the modelling of palaeoclimate, through the combination of instrumental data and technological tools (Haywood *et al.,* 2019). This study will assist in understanding the extreme rainfall events which have occurred in the central region of southern Africa from the 1970s onwards. This knowledge will be used as a basis to understand events that may have been recorded in the historical records.

1.4. Research Questions

The study answers the following research questions:

- What extreme climate (flood and drought) events occurred in the central region of southern Africa from the 1970s to the present?
- Which climatic drivers are responsible for the distribution of extreme precipitation events, over the central parts of southern Africa over the past 50 years?

1.5. Aim and Objectives

The primary aim of the research is to assess contemporary spatiotemporal variation of extreme precipitation events in the central part of southern Africa from 1970 to 2019. The objectives include:

- Calculating the standardized precipitation index (SPI) over the past 50 years for each meteorological station in the study region.
- Visualising spatiotemporal trends via the use of two different spatial interpolation methods and assessing their accuracy.

1.6. Overview of the Project

The main aim of the study is to evaluate the contemporary spatiotemporal variation of the extreme precipitation events in the central part of southern Africa from 1970 to 2019. Chapter 2 examines the key drivers of climate in southern Africa, how these climate drivers have been explored, the occurrence of droughts and floods in southern Africa as well as spatial interpolation of climate data using GIS methods. Chapter 3 explores the geography and climate of the study region, the importance of transnational studies, data analysis procedures including SPI analysis and

interpolation methods. Chapter 4 analyses the spatiotemporal frequencies of droughts and floods in the study region using the two interpolation methods, OK and IDW. Chapter 5 explores the importance as well as the relevance of this study's results and how this relates to the studies which have been conducted in the past. Chapter 6 examines the extent to which the aims and the objectives of this study have been achieved and the limitations of the study.

Chapter 2: LITERATURE REVIEW

2.1. Introduction

The climate of various parts of the world is driven to various degrees by different phenomena (Van Aalst, 2006). The literature review section will outline and examine the key climate drivers in southern Africa. This section will further unpack the occurrence of extreme floods and droughts, and interpolation methods that can be used to map these events will be outlined.

2.2. Drivers of climate in southern Africa

The North West Province of South Africa and southern Botswana are both located within the subtropical high-pressure belt, exposing this region to significant climate variability and semi-arid conditions (Washington and Preston, 2006; Driver and Reason, 2017; Hoell *et al.,* 2018). In this region, rainfall varies both spatially and temporally and it is influenced by several weather patterns (Maruatona and Moses, 2021). The Inter-Tropical Convergence Zone (ITCZ) is one of the systems which affects the weather in this region (Maruatona and Moses, 2021). The effects of the ITCZ are often experienced in January and February when it is located over southern Zambia (Maruatona and Moses, 2021). Over southern Africa, temperate troughs are the rain-bearing systems, and they are short-lived bands of northward-southward tilted convective clouds (Todd *et al.,* 2004; Ratna *et al.*, 2012). Through the interactivity between Rossby waves and moisture convergence over southern Africa, these temperate troughs connect the tropics to the mid-latitudes (Todd *et al.,* 2004; Ratna *et al.*, 2012). Tropical cyclones occasionally make landfall and move through this region (Sithole *et al.,* 2009; Moses and Ramotonto, 2018; Xulu *et al.,* 2020).

During austral spring, summer, and early autumn the Botswana High is a critical component of the regional atmospheric circulation over southern Africa (Reason, 2019). The Botswana High is a semi-permanent anticyclone that is found in the mid-level troposphere over subtropical landmasses, best expressed at 500hPa (Reason, 2016). This anticyclone is believed to be thermally induced as a response to the heat released by tropical regions of high precipitation (Reason, 2016). This high-pressure cell forms in the early spring, and it strengthens and moves southwards towards Botswana and Namibia during austral summer (Driver and Reason, 2017; Reason 2019). It centres at 18°S in October, it moves closer to 23°S in February, and it slightly retreats and weakens in March (Reason, 2019).

In southern Africa, for precipitation to occur it requires a weakening or shifting of the Botswana High (Reason, 2019). There is a strong connection between Botswana High and rainfall over southern Africa (Driver and Reason, 2016; Reason, 2019). Austral summers which are associated with stronger and/or north shifted Botswana High are typically drier, there is less cloud cover and surface temperatures are warmer (Manatsa and Reason, 2017; Driver *et al.,* 2019). A weaker and or shifted Botswana high implies reduced mid-troposphere subsidence over the region, hence more rainfall occurs (Reason, 2019).

Stronger mid-to-upper-level subsidence over southern Africa is a result of the high-pressure system over southern Africa (Blamey *et al.,* 2018; Rapolaki *et al.,* 2021). In addition to the subsidence, less moisture transport into the region was also a contributing factor to 2015's unusually dry October, November, and December. (Blamey *et al.,* 2018; Kruger and Nxumalo, 2017). There is less evidence to suggest

that during the 1982 and 1997 drought events, there was a similar response to the stronger Botswana High. However, during the 1997 and 1982 drought seasons, there was an anomalous descending movement in the mid-to-upper levels in October, November, and December 1982, which became stronger in January, February, and March 1983. The downward motion in January, February, and March in 1983 is likely associated with the presence of stronger Botswana High during this period (Blamey *et al.,* 2018).

ENSO refers to the interaction of the ocean and the atmosphere in the tropical Pacific Ocean, and it affects weather patterns globally through teleconnections (Takahashi and Martínez, 2019; Rashid, 2020; Zhao and Di Lorenzo, 2020). In the late Boreal winter and spring, ENSO events are thought to be influenced by surface zonal winds anomalies over the western equatorial Pacific and by the displacement of the thermocline in the eastern equatorial Pacific (Terray and Dominiak, 2005; Domeisen *et al.,* 2019; Sun and Okumura, 2020). The surface wind anomalies which later lead to ENSO events are associated with the inter-basin Sea Surface Temperature (SST) contrast between the tropical Pacific and the Indian/Atlantic Ocean (Li *et al.,* 2018; Wang, 2019). According to scientists, the phenomenon of ENSO has been associated with heavy rainfall in southern Africa since the late 1970s (Gaughan *et al.,* 2016; Manatsa *et al.*, 2017; Hoell and Cheng, 2018).

The spatiotemporal structure of rainfall anomalies between the three El Niño events differs significantly despite the strong correlation between ENSO and southern African rainfall (Marumbwa *et al.,* 2019; Kolusu *et al.,* 2019). Summer droughts in 2015/2016 were far more extreme as compared to 1982/1983 and 1997/1998 (Marumbwa *et al.,*

2019; Kolusu *et al.,* 2019). The 1997/1998 drought events resulted in predominantly dry conditions in October, November, and December but not much in Botswana, Namibia, Mozambique, or north-eastern South Africa (Blamey *et al.,* 2018). Some of the drier and warmer summers in southern Africa have been associated with El Niño (Manatsa and Reason, 2017; Driver *et al.,* 2019).

Increases in western wind anomalies result in more El Niño events and fewer La Niña events occurring over the western equatorial Pacific, while tropical cooling of the Pacific results in fewer El Niño events and more La Niña (Khodri *et al.*, 2017, Wu *et al.,* 2019). Decadal variability has been seen to enhance the effects of both El Niño and La Niña events, which affects the probability of extreme events (Okumura *et al.,* 2017). Meteorological droughts are triggered by large-scale atmospheric circulations such as the Hadley and Walker systems, Rossby waves and atmospheric teleconnections (Schubert *et al.,* 2016; Battisti *et al.,* 2019).

ENSO has both regional and inter-annual variation in the climate of southern Africa; hence it can be a good predictor for seasonal forecasts over certain parts of southern Africa (Monerie *et al.,* 2019). The major climate influences over southern Africa include tropical cyclones, jet streams, and teleconnections with regional large scale quasi-periodic climate systems (e.g., QBO) and Intraseasonal waves (Woodworth *et al.,* 2019). La Niña and El Niño events have been identified as having strong impacts on the precipitation patterns in southern Africa (Blamey *et al*., 2018). Late summer variability is linked to changes in the hemisphere's circulation, which can be observed in the SAM (Pohl and Fauchereau, 2012; Clem *et al.,* 2017; Dätwyler *et al.,* 2018).

SAM is a phenomenon that affects the atmosphere from the mid-latitudes to the Antarctic (Dätwyler *et al.*, 2018). SAM indices are approximated based on atmospheric mass conservation between Polar Regions and mid-latitudes (Yuan and Yonekura, 2011). SAM is associated with shifting latitudinal positions of the westerlies, which influences the position of mid-latitude storm tracks (Li and Wang, 2016). This alters surface wind shear, and evaporation through changes in latent heat flux (Li and Wang, 2016).

SAM and ENSO correlate negatively at seasonal scales, however, summer rainfall and SAM have a positive correlation (Montazerolghaem *et al.,* 2016). In summer, a positive SAM is caused by the southward displacement of the subtropical jet, which relates to wet conditions over southern Africa (Malherbe *et al.,* 2016). High-pressure anomalies have been shown to exist over the African subcontinent from December and January to March (Cook *et al.,* 2004; Malherbe *et al.*, 2016). Over summer rainfall regions, these highs are often associated with periods of drought (Cook *et al.,* 2004; Malherbe *et al.*, 2016). The positive state of SAM has been associated with increased precipitation in southern Africa (King *et al.*, 2020).

MJO phenomenon occurs in the tropics of the hemisphere that experiences summer (Yuan *et al.,* 2018). MJO is a coupled ocean-atmosphere system that organizes tropical convection at planetary scales into alternating zones of enhanced and suppressed convection (Notaro, 2018). It is a phenomenon that leads to the alternation in tropical precipitation between amplified and suppressed periods within a season (Zhang, 2013; Moron *et al.,* 2015; Koplitz *et al.,* 2018). MJO produce a region of increased precipitation as it travels eastwards along the equator for a period of 40 to

45 days (Serra *et al.,* 2014; Nicholson, 2017). MJOs are associated with increased precipitation and wind anomalies, beginning in the equatorial Indian Ocean, and gradually moving eastward into the West Pacific at the speed of 5m/s (Haertel, 2018; Wei *et al.,* 2020).

Wind converges in regions of the enhanced MJO and diverges in the upper troposphere (Adames *et al.,* 2014; Maloney *et al.,* 2019; Yang and Wang, 2019). Precipitation occurs in the lower troposphere, and areas of suppressed precipitation are followed by enhanced precipitation in about 20 to 25 days (Berhane *et al.,* 2015; Maloney *et al.,* 2019). Tropical MJOs play a key role in regulating tropical cyclones in the eastern Pacific Ocean and the Atlantic Ocean and beginning the ENSO cycle (Klotzbach and Oliver, 2015; Lin *et al.,* 2020). MJO modulates extreme events in southern Africa and these extreme events include floods, tropical cyclones, droughts, and heatwaves (Banhoizer *et al.,* 2014; Vitart and Robertson, 2018).

Over southern Africa, composite maps of the incoming longwave radiation (OLR) anomalies reveal very strong intra-seasonal fluctuations. (Pohl *et al.,* 2007; Kikuchi, 2020). The period it takes for the MJO to rejuvenate in the Indian Ocean region is 40 to 45 days (Pohl *et al.,* 2007; Stan *et al.,* 2017). MJO strongly interacts with the Indian and Australian monsoon systems. In the hemisphere experiencing summer, MJO is located at 10° to 15° (Hadi *et al.,* 2020). MJOs are often accompanied by convective anomalies in the eastern hemisphere during the austral summer (Pohl *et al.,* 2007; Kim *et al.,* 2017). Local nodes of African convective variability suggest that southern African rainfall is significantly modulated by MJO at different intra-seasonal timescales (Pourasghar *et al.,* 2015).

SIOD is a phenomenon that usually occurs due to latent heat flux anomalies, which are linked with differences in the Mascarene High and it is maintained through positive feedback of the air-ocean interaction over the south Indian Ocean (Gong *et al.,* 2019). Austral summer is characterized by a negative SIOD, which has a dipole pattern in the SST anomaly in the southern Indian Ocean with a cold south-western pole and a warm north-eastern pole (Ash and Matyas, 2012; Zhang *et al.,* 2019). The anomalous Subtropical High results in enhanced latent heat loss and a thick mixed layer over the north-eastern pole and the opposite in the south-western pole (Morioka *et al.,* 2011; Zhang *et al.,* 2020).

The positive SIOD leads to enhanced convective activity in southern Africa, which results in increased rainfall over the region and an increased moisture divergence from the eastern subtropical Indian Ocean (Ogwang *et al.,* 2020). Studies suggest that SIOD might have an influence on ENSO and Indian as well as Austral summer monsoon (Zinke *et al.,* 2004; Manatsa *et al.,* 2011; Ash and Matyas, 2012; Gong *et al.,* 2019; Monerie *et al.,* 2019). The anticyclonic and convective anomalies shift eastward to Australia when ENSO and SIOD are out of phase, and this induces negative rainfall anomalies in northern Australia (Gong *et al.,* 2019).

QBO is a periodic phenomenon that occurs in the form of oscillations in the zonal wind anomalies within the tropical stratosphere (Toms *et al.,* 2020). The single cycle of QBO takes about 28 months, where equatorial stratospheric (between 30 and 50hPa) winds whose maximum amplitude is along the equator (Anstey and Shepherd, 2014; Toms *et al.,* 2020). QBO can be predicted accurately due to ocean tides, however, there is variability in the duration of both the east and the west phases (Raphaldini *et*

al., 2021). Phase QBO of tropical stratospheric zonal winds appears to be an important variable controlling the atmospheric response to solar activity (Rao *et al.,* 2019).

The Southern Oscillation and South African rainfall associations are modulated only when tropical rainfall producing systems are dominant over the summer rainfall region (Zhang *et al.,* 2015; Daron *et al.,* 2019). South Africa's early summer season (October to December) is characterized by temperate synoptic systems (Mulenga *et al.,* 2003; Kane *et al.,* 2009; Lüdecke *et al.,* 2021). There is no difference in the southern oscillation and South African rainfall association between westerly and easterly QBO (Mulenga *et al.,* 2003; Kane *et al.,* 2009; Lüdecke *et al.,* 2021).

2.3. Methods for exploring key drivers of climate change

Integrating weather stations and remote sensing data has been used to monitor the occurrence of droughts and decadal variability in southern Africa (Mariano *et al.,* 2018; Park *et al.,* 2020). The use of both datasets facilitates effective tracking of drought intensity and frequency, by studying the relationship between SPI indices, worldwide SST and sea level pressure (SLP) in the southern hemisphere, where the mean SLP can be used to infer monthly atmospheric circulations in the southern hemisphere (Malherbe *et al.,* 2016; Di Capua *et al.,* 2020). One of the methods that have been undertaken in Colorado is the reconstruction of Atlantic Multi-decadal Oscillation (AMO) and Pacific Decadal Oscillation (PDO) using captured steam flow data (Nowak *et al.,* 2012).

Several countries have used the SPI to monitor droughts and floods, demonstrating that it can monitor dry conditions at some timescales and wet conditions at others

(Mathbout *et al.*, 2018). SPI calculations enable researchers to link the occurrence of wet conditions with La Niña events and dry conditions with El Niño events (Sobral *et al.,* 2019). PDO is the dominant mode of decadal to multidecadal variability, characterized by smaller variations in the SST anomaly patterns associated with ENSO (Lyu *et al.*, 2017). It was determined in these experiments that a negative PDO phase is accompanied by weakened atmospheric circulation systems, including the East Asian trough, the Asian continental High, and the Aleutian low (Qin *et al.*, 2020).

Reconstruction of decadal variability using instrumental data has been used by several authors, however, the data only exists for a shorter period (Zhang *et al.*, 2018). SAM indices are approximated based on atmospheric mass conservation between Polar Regions and mid-latitudes (Yuan and Yonekura, 2011). The inter-annual occurrence of the SIOD has been explored using observational and re-analysed datasets (Suzuki *et al*., 2004; Hoell and Cheng, 2018). Raw SST anomalies have been used to visually inspect the presence of SIOD in Coupled General Circulation Model (CGCM) simulations (Suzuki *et al.*, 2004).

Various indices have been used to map droughts (Mondol *et al.*, 2017). The SPI is one of the many indices that have been used to map the occurrence of both dry and wet conditions (Al-Quraishi *et al.,* 2020). Most of these indices have a fixed time scale, for instance, the Palmer Drought Severity Index (PDSI), this index has a time scale of 9 months, Z Score Index (ZSI) and China Z Index (CZI) are both sensitive to lower timescales (Zhao *et al.,* 2017; Payab and Türker, 2019). Timescales are not the only issue associated with these indices; however, calibration and spatial calibration are some of the issues associated with PDSI (Zhao *et al.,* 2017; Ogunrinde *et al.,* 2020).

The advantage of using SPI to map the distribution of dry and wet conditions is that it can be calculated at different timescales, and it is comparable at varying spatiotemporal scales (Zhao *et al*., 2017).

2.4. Occurrence of droughts and floods in southern Africa

Due to the decrease in precipitation in certain parts of the world, drought distribution has been mapped to understand the severity, duration, frequency, and the areal distribution of the droughts (Mathbout *et al.,* 2020). In southern Africa, the occurrence of El Niño was associated with droughts in the years 1991/1992, 2002/2003, 2015/2016 (Malherbe *et al.*, 2020). The occurrence of both droughts and floods can have an impact on agriculture, water resources and human health (Nobre *et al.,* 2019).

Since 1900, the amount of ENSO activity has intensified, which has resulted in increased floods and droughts (Kusangaya *et al.,* 2021). The frequency and magnitude of extreme precipitation associated with floods may increase in some regions, while precipitation may decrease in other areas (Madsen *et al.,* 2014; Bhatti *et al.,* 2020; Tabari, 2020). Countries including Mozambique, South Africa, Malawi, and Zimbabwe are already experiencing increased occurrences of both droughts and floods (Kusangaya *et al*., 2021). In Zambia rainfall is influenced by the movement of the ITCZ and ENSO phenomenon with rainfall ranging between 600mm in the south to 1300mm in the north (Kusangaya *et al*., 2021). The effects of weather extremes in Zambia lead to widespread damage and severe alterations in the normal functioning of household agricultural production (Chonabayashi *et al.,* 2020; Kusangaya *et al*., 2021). Zambia has also experienced the occurrence of droughts that have affected over 1.2 million people between the years 2004 to 2005 (Lekprichakul, 2008;

Kusangaya *et al*., 2021). There is a high incidence of occurrence of droughts and floods in the Luvuvhu River catchment of Limpopo, South Africa and these occurrences have a negative impact on crop production, agricultural income, crop sales, harvest, and livestock (Tshililo, 2017). The 2015/2016 El Niño occurred directly after the 2014/2015 El Niño events which led to the poorest rainfall season in 35 years (Masih *et al.,* 2014; Khan *et al.,* 2021).

The available data on droughts estimates that there have been 642 droughts during the 1900 to 2013 period, affecting 2 billion people and leading to the deaths of about 12 million people globally (Masih *et al.,* 2014). A global drought review conducted by Dai *et al.,* (2011) has indicated that there has been an increased frequency of the occurrence of droughts over the past years. Severe and multiyear droughts have been identified in North America, Africa, and China (Masih *et al.,* 2014; Yu *et al*., 2014; Du *et al.,* 2018; Goulden *et al.,* 2019).

SPI was used to categorize the occurrence of droughts in Zambia, and it successfully categorised the occurrence of extremely dry drought conditions (≤ -2) over the years 1992 and 2015, severely dry drought conditions (-1.9 to -1.5) in the year 1995, moderately dry drought conditions (-1.4 to -1.0) in the years 1972, 1980, 1987, 1999, 2005 and the remaining 26 years recorded normal drought conditions (-0.9 to 0.9) (Libanda *et al.,* 2019). Mahalapye, Botswana, experienced the occurrence of a storm in December 2018 (Moses, 2019). Even though the country has experienced droughts over the years, floods have also occurred, and they have destroyed infrastructure, agriculture, and the livelihood of people (Moses, 2019). Weather systems that have

been associated with the occurrence of this storm are the surface low and the westerly trough (Moses, 2019).

In January 2013 an extreme flood event occurred in south-eastern Africa which led to devastating impacts (Manhique *et al.,* 2015). During this period, the South Indian Convergence Zone (SICZ) stretched from Zambia to the east of South Africa (Manhique *et al.,* 2015). During the 10 days, over 200mm of rainfall was recorded over southern and central Mozambique, parts of south Zimbabwe and north-eastern South Africa (Manhique *et al.,* 2015). The January 2013 floods occurred about 15 years after the occurrence of the 1999/2000 droughts which occurred due to an active tropical cyclone season in this region (Manhiques *et al.,* 2015).

According to research, the Angolan low may be a precursor to the Tropical Temperate Trough (TTT), which contributes to a significant proportion of the rainfall in southern Africa (Todd and Washington, 1999; Hart *et al.,* 2010; Howard and Washington, 2018). The Angola low allows for the southward transport of atmospheric water vapour from the tropics and this water vapour is important for the development of the TTT (Howard and Washington, 2018). The 1982/1983 and 2015/2016 El Niño events both took place in years where the Angolan low was weak and resulted in severe droughts (Howard and Washington, 2018). Whereas the 1997/1998 El Niño events coincided with strong Angola Low hence fewer droughts were recorded (Howard and Washington, 2018).

The February to March 2009 floods that affected Angola and Namibia have led to the loss of lives and thousands of people were displaced due to infrastructure damages

which led to the affected areas being inaccessible (Madzudzo *et al.,* 2018). In 2013, heavy rains led to extensive floods and extreme infrastructure damage in central Botswana (Wiston and Mphale, 2019). Various countries which have recorded the occurrence of floods have also experienced extensive damage to infrastructure making it difficult to mitigate the aftermaths of the floods (Madzudzo *et al.,* 2018; Mind'je *et al.,* 2019; Adeel *et al*., 2020; Munawar, 2020; Njogu, 2021).

2.5. Spatial interpolation of climate data

Interpolation is often applied and is defined as a precursor to creating contour or isoline plots (lines of equal value) to produce a realistic surface between the points where measurements were obtained (Zhang *et al.*, 2016). Two groups of interpolation methods include deterministic and geostatistical methods (Zhang *et al.,* 2016). Deterministic interpolation methods create a surface from observed points based on either the extent of similarity (e.g., IDW) or the degree of smoothing (Completely Regularity Spline (CRS; Childs, 2004). Geostatistical methods (e.g., kriging and cokriging) use statistical properties of the known points (Apaydin *et al.,* 2004).

To determine values of unsampled locations, spatial correlation between the neighbouring observations is considered. Geostatistical methods yield better spatial representations of climatological data in comparison to traditional methods (Thiessen polygons (Ly *et al.,* 2013). Areas of low network density of rain gauges often require the inclusion of explanatory variables such as elevation to increase the reliability of rainfall estimates (Cheng *et al.,* 2008; de Amorim Borges *et al.,* 2016). Interpolation methods are more accurate when variables that represent precipitation drivers are included (de Amorim Borges *et al.*, 2016). Precipitation has been correlated with

geographic factors, such as height above sea level, longitude, and latitude (de Amorim Borges *et al.,* 2016; Muthusamy *et al.,* 2017).

Different estimation methods have been proposed for different climate data however, the performance of these methods depends on a variety of factors, such as the selected interpolation method, station network configuration, temporal data resolution and spatial variability (McKee and Binns, 2016; Berndt and Haberlandt, 2018). As a result of geostatistical methods such as kriging, adjacent observations can be correlated spatially and the unknown location can be estimated (Trangmar *et al.,* 1986; Wu, and Li, 2013; Jalali *et al.,* 2016; Berndt and Haberlandt, 2018; Das, 2021). A study conducted in Calabria used various interpolation methods, OK, IDW, Kriging with External Drift (KED), Ordinary Cokriging (OCK) and Empirical Bayesian Kriging (EBK) to produce month rainfall results for the study region (Antal *et al.,* 2021).

Seo *et al.,* (2015) has used Regression Kriging and Artificial Neural Network Residual Kriging (RKNNRK) hybrid approach to estimate the spatial precipitation in Jeju Island, South Korea. This method was compared to other methods such as OK, Universal Kriging (UK), Regression Kriging (RK), Neural Network Residual Kriging (NNRK; Seo *et al.,* 2015). A study administered by Ly *et al.,* (2015) to interpolate daily rainfall data at the Ourthe and Ambleve catchments in Belgium, has used five different interpolation methods to interpolate the rainfall data which include, OK, UK, KED, OCK, IDW. IDW and OK were considered the best methods as they provide the smallest RMSE for nearly all the cases (Ly *et al.,* 2015). It was found that integrating elevation data into KED and OK did not improve the interpolation accuracy for daily rainfall (Ly *et al.,* 2015). Interpolation of monthly rainfall over the state of Rio de Janeiro in southeast

Brazil was conducted using five deterministic methods (Lyra *et al.,* 2018). These methods include IDW, Nearest Neighbour (NRN), Triangulation with Linear Interpolation (TLI), Natural Neighbour (NN) and Spline Tension (SPT; Lyra *et al.,* 2018). These methods were tested using 110 weather stations. In comparison with the other methods, SPT yielded the highest level of precision and accuracy (Lyra *et al.,* 2018).

2.6. Conclusion

As outlined in the literature section, a range of studies have examined droughts and floods occurrences in southern Africa and other parts of the world. Methods such as SPI, ZSI, CZI, and PDSI have been used to calculate the occurrence of droughts and floods. Geostatistical and deterministic methods have been used to interpolate areas that have limited or no climate data. However, in central southern Africa, fewer studies have been conducted using SPI and geostatistical methods (OK) and deterministic methods (IDW). This study is therefore important in identifying the extreme weather events that have occurred in the region, using varying methods.

Chapter 3: METHODOLOGY

3.1. Introduction

This study adopts methods from several studies (Güner Bacanlı, 2017; Hodam *et al.,* 2017; Hirota *et al.,* 2018; Reddy and Venkatramana, 2018; Coria-Monter *et al.,* 2019). This includes SPI analysis which was carried out using monthly rainfall data and was calculated for a 12-month period. The 12-month SPI was used as the aim was to calculate hydrological droughts in the study region. At this 12-month timescale, SPI reflects long-term precipitation patterns (WMO, 2012). In areas with unknown precipitation values, spatial interpolation methods, IDW and OK were used to identify extreme precipitation events.

This study is carried out in two countries: South Africa and Botswana. Transnational projects have been more commonly conducted in Europe, and they have yielded positive results. These positive results include the ability of different territories to learn from one another and bridging the gaps between countries, such as the availability of data and access to skilled personnel required to perform certain tasks.

3.2. Study Region

The study region is in the central region of southern Africa, and it includes Botswana, the North West and portions of the Limpopo Province, these region boundaries were developed by the Metsemegologolo project (Figure 1). The Metsemegologolo project chose the area straddling the South African and Botswanan border as the study region, to create an online archive for information about early Tswana urbanisation.

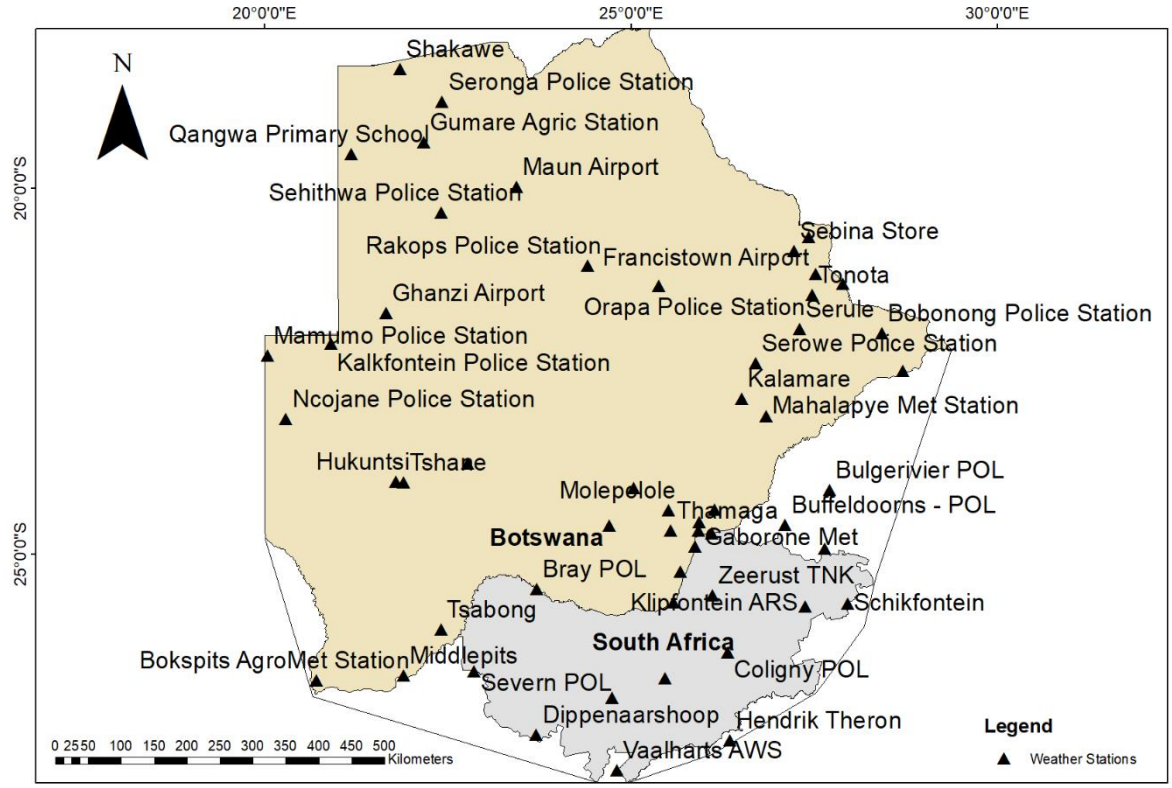

Figure 1: Distribution of weather stations around the study region (DIVA-GIS, South African Weather Service (SAWS) and Botswana Meteorological Office (BMO)).

3.2.1. Climate and Geography

Botswana's climate is classified as semi-arid with low rainfall ranging between 200 to 600 mm annually and with hot summer months (October to April; Byakatonda *et al.,* 2019). Evaporation rates range between 1800 to 2100mm per year which is higher compared to the annual rainfall (Batisani, 2012; Byakatonda *et al.,* 2016, 2019). Tropical easterly systems, thunderstorms and continental troughs bring precipitation to the region from October to April. (Nkemelang *et al.,* 2018). During the El Niño episodes, the rainfall of the area is mostly suppressed (Byakatonda *et al.,* 2016). The region's precipitation varies spatially, and rainfall increases moving from the west to the east (McKenna, 2020). Rainfall is dominant in the northeast at Kasane and decreases in the West at Ghanzi and is lowest recorded in the southwest of Tsabong (Byakatonda *et al.,* 2020). In the North West province, there is almost year-round

sunshine, with an average rainfall of 400mm annually (Adisa *et al*., 2021). The North West Province records temperatures ranging between 2°C in winter and 31°C in summer (Amin *et al.,* 2008; Phora, 2018; Adisa *et al*., 2021). Botswana records temperatures ranging between 3°C in winter and 35°C in summer (Maruatona and Moses, 2021). The cold fronts associated with mid-latitude cyclones have a large impact on the winter temperatures in Botswana (Nkemelang *et al.,* 2018).

The geography of central southern Africa is characterised by landscapes that are flat to gently steeped (Logan and Silberbauer, 2019). These flat areas are mostly covered by grass and low shrubs. Aridity decreases as one moves from the west to the east (Parsons, 2020). The Kalahari Desert which is the 8th largest desert in the world forms part of the study region and covers an area of 569,797km^2 (McKenna, 2020). The central region of southern Africa covers an area of 829,185km^2 (McKenna, 2020).

3.2.2. Data Acquisition (Data Quality and Limitations)

Data used in this research is made up of average monthly observations obtained from the BMO and the SAWS. The observations obtained include average monthly precipitation values. This study considers a time series with 14 weather stations in South Africa and 42 in Botswana. Data from the BMO did not include geographic coordinates with the exact location of the weather stations. However, knowing that the weather stations are situated in Police stations and schools, the coordinates of these stations were thus determined using Google Earth Pro. Coordinates obtained were then converted into a point shapefile.

Table 1: Weather Stations with precipitation data (BMO and SAWS).

Station	Elevation	Time Series	X-Coordinates	Y-Coordinates
Botswana				
Bainesdrift Police Station	700m	1971 - 2000	22°29'33.71''	-28°42'14.34"
Bobonong Police Station	699m	1979 - 2015	21°58'33.64"	-28°25'7.02"
Bokspits-AgroMet Station	912m	1979 - 2015	26°42'43.26"	-20°42'7.17"
Francistown Airport	1000m	1979 - 2015	21°09'57.96"	-27°30'51.70"
Gaborone Met	983m	1980 - 2016	24°40'00.50''	-25°55'00.05''
Ghanzi Airport	1156m	1971 - 2015	21°40'14.73"	-21°36'09.00"
Gumare Agric Station	967m	1979 - 2014	19°21'.59.76''	-22°10'0.12''
Hukuntsi	1129m	1983 - 2015	23°59'56.66"	-21°46'47.96"
Jwaneng	1199m	1988 - 2015	24°31'26.45"	-24°43'12.82"
Kalamare	1264m	1980 - 2016	22°52'06.35''	-26°30'01.68''
Kalkfontein Police Station	1182m	1971 - 2016	22°7'	-20°54'
Kang-AgroMet Station	1136m	1981 - 2015	23°45'15.89"	-22°3538.64"
Letlhakeng Police Station	1094m	1979 - 2015	24°5'6.48"	-25°1'53.08"
Lobatse Police Station	1192m	1971 - 2015	25°13'47.46"	-25°40'13.76"
Mahalapye	1012m	1971 - 2015	23°06'28.08"	-26°49'55.68"
Mamumo Police Station	1252m	1971 - 2013	22°17'0.12''	-20°02'0.01''
Masunga Police Station	1187m	1980 - 2014	20°40'10.90''	-27°24'22.90''
Matsiloje	934m	1981 - 2012	21°18'2.14''	-27°45'14.29''
Maun Airport	946m	1979 - 2013	19°59'42.94"	-23°25'05.08"
Middlepits	947m	1988 - 2014	26°39'07.59''	-21°53'34.99''
Mochudi Police Station	945m	1980 - 2015	24°23'	-26°8'
Molepolole	1147m	1979 - 2015	24°23'38.97"	-25°29'38.27''
Ncojane Police Station	1250m	1971 - 2013	23°09'S	-20°17'
Orapa Police Station	973m	1968 - 2014	21°19'40.97"	-25°22'12.86"
Palapye Police Station	908m	1972 - 2015	22°34'	-27°09'
Pitshane Molopo Police Station	1140m	1971 - 2015	24°45'	-25°6'
Qangwa Primary School	1063m	1982 - 2014	19°31'51.67''	-21°10'44.75''
Rakops Police Station	914m	1971 - 2000	21°3'	-24°23'
Ramatlabama Police Station	1275m	1961 - 2015	25°39'	-25°34'0.12"
Ramotswa Station	1020m	1971 - 2014	24°53'	-25°52'
Sebina Store	1065m	1971 - 2014	20°51'	-27°13'
Sehitwa Police Station	928m	1970 - 2014	20°20'0.43''	-22°24'4.53''
Serongwa Police Station	988m	1978-2013	18°49'18.00''	-22°24'57.37''
Serowe Police Station	1140m	1971 - 2016	22°23'17.96"	-26°41'45.19"
Serule	954m	1985 - 2016	21°55'23.34"	-27°17'11.40"
Shakawe	1030m	1971 - 2014	18°22'02.41"	-21°50'20.30"
Sir Seretse Khama Airport, Gaborone	1012m	1984 - 2013	24°33'29.03"	-25°55'27.42"
Thamaga	1079m	1986 - 2016	24°39'59.19''	-25°31'57.29''
Tlokweng Border	1060m	1980 - 2014	24°42'19.67"	-26°5'32.28"
Tonota	958m	1971 - 2014	21°27'	-27°28'
Tsabong	963m	1979 - 2015	26°01'14.81"	-22°24'40.55"
Tshane	1110m	1979 - 2015	24°01'01.06"	-21°53'33.47"
South Africa				
Bray- POL	1051m	1947 - 2019	25°28'07.02"	-23°42'10.93"
Buffeldoorns - POL	967m	1934 - 2019	24°35'48.74"	-27°05'.53.55"
Bulgerivier - POL	1046m	1969 - 2019	24°07'00.00"	-27°42'00.00"
Coligny - POL	1492m	1967 - 2016	26°19'52.96"	-26°18'36.66"
Delareyville Rietpan 2	1361m	1927 - 2014	26°41'05.97"	-25°27'41.43"
Dippenaarshoop	1099m	1979 - 2019	27°27'14.22"	-23°42'04.94"
Hendrik Theron	1265m	1932 - 2019	27°31'49.21"	-26°20'34.14"

Klipfontein ARS	1188m	1929 - 2017	25°42’16.31”	-27°21’57.64”
Leeupoort - MUN	1017m	1913 - 2019	24°55’13.35”	-27°38’25.98”
Schietfontein	1266m	1920 - 2019	25°39’35.05”	-27°55’26.62”
Severn - POL	1018m	1961 - 2019	26°35’36.44”	-22°51’15.20”
Vaalharts AWS	1142m	1935 - 2019	27°56’47.97”	-24°48’12.00”
Vryburg Tipperary	1199m	1986 - 2019	26°57’29.45”	-24°43’47.50”
Zeerust -TNK	1183m	1940 - 2019	25°33’08.44”	-26°06’01.76”

3.3. Data Analysis Procedures

Precipitation data obtained from different weather stations will be organized in terms of average annual precipitation values. These geocoded data points will then be used to calculate SPI values which will be used to create spatial interpolation maps.

3.3.1. SPI Analysis

SPI can be defined as the difference between the monthly precipitation (xi) and the mean value (O), divided by the standard deviation(s) (Güner Bacanlı, 2017). For this study, SPI was calculated for 12 months since the aim was to calculate hydrological droughts which have occurred in the study region. Monthly data was available for both Botswana and South Africa and this was used as input data. The cut off for drought is -1. In this study, SPI was used due to its simplicity as it only uses precipitation as an input and it can assess both wet and dry conditions (Mazibuko *et al.,* 2021).

Table 2: SPI Values (WMO, 2012).

SPI Values	Drought Condition
≥ 2	Extremely Wet
1.5 to 1.99	Very Wet
1.0 to 1.49	Moderately Wet
-.99 to .99	Normal
-1.0 to -1.49	Moderately Dry
-1.5 to -1.99	Severely Dry
≤-2	Extremely Dry

3.3.2. Interpolation Methods

Spatial interpolation has been employed in this study to map spatiotemporal precipitation trends in the study region. Two interpolation methods were used including IDW and OK. IDW considers that objects which are close to one another are more similar than those that are far apart (Reddy and Venkatramana, 2018). The general equation for IDW is:

$$\hat{Z}(s_0) = \sum_{i=0}^{n} \lambda_i \; Z(s_i)$$

1

$Z(s_0)$ - Predicted value

s_0 - Location

n - Number of measured samples surrounding the predicted location.

x_i - Weight assigned to each measured point used, with distance weights decrease.

Z(s_0) observed value at location s_i

At the location, s_i weights can be determined by

$$\lambda_i = d_{i0}^{-p} \quad (2)$$

As the distance increases weights are predicted by a factor of p. d_{i0} distance between prediction location s_0 and each measure location s_i.

Kriging minimizes the degree of spatial dependence among known points in terms of semi-variance. Semi-variance increases as h (lag) increases. Ordinary kriging assumes that drift is absent in the variable of interest (Hodam *et al.,* 2017).

General equation

$$z(x_0) = \sum_{i=1}^{n} \lambda_i . z(x_i) \quad (3)$$

$z(x_0)$ - Estimate the variable at an unknown location (x_0)

$z(x_i)$ Value of the variable z at a known location.

x_i, λ_i the weight assigned to $z(x_i)$ and n the number of known points used in estimation.

IDW and OK were performed using the Geostatistical Analyst tool IDW and OK ArcMap software. IDW was used to measure values surrounding the prediction location, like kriging. IDW directly implies that the values of the attribute at an unknown location are the weighted average of known values within the area surrounding the un-

sampled location (Mokarram and Hojati, 2017). IDW and OK have been used based on SPI, instead of the raw rainfall data.

3.3.3. ENSO

In Chapter 2, a range of studies identified various occurrences of ENSO. These studies have aided in a better understanding of the driving forces of various drought events, which have occurred in the study region. ENSO occurrences that have been identified in various literature have been compared with drought occurrences identified in this study (Masih *et al.,* 2014; Blamey *et al.,* 2018; Howard and Washington, 2018; Khan *et al.,* 2021). This comparison has aided in understanding whether the drought and flood events in the central portion of southern Africa can be attributed to La Niña or El Niño events.

Chapter 4: RESULTS

4.1. Introduction

This results section will outline and describe the spatiotemporal frequency of droughts and floods. The spatiotemporal frequency of both droughts and floods will be analysed based on the results obtained from the two interpolation methods viz. IDW and OK.

4.2. Temporal frequency of droughts

Schietfontein is a weather station with the longest rainfall data record. Moderately dry drought conditions were experienced in Schietfontein in the years 1924, 1926 and 1927 (Figure 2). In 1925 the weather station calculated normal drought conditions (Figure 2). Leeupoort experienced the occurrence of droughts for four consecutive years 1933 to 1936 and 1962 to 1966 excluding 1964 (Figure 3). In 1964 the weather station recorded the occurrence of normal drought conditions with an average SPI value of -0.98. In the years 1933, 1934 and 1936 Leeupoort station recorded moderately dry drought conditions, whereas in 1935 the station experienced severely dry drought conditions. The station experienced the occurrence of extremely wet drought conditions in the years 1944 and 2000 with SPI values of 2.26 and 2.01, respectively. The 2000 wet drought conditions are attributed to the occurrence of a strong La Niña event. The station recorded the occurrence of severely wet drought conditions in the year 1967, which was after the occurrence of the 1962 to 1966 dry drought conditions.

In the years 1962 and 1965 Leeupoort weather station recorded moderately dry drought conditions and severely dry drought conditions in 1963 and 1966. In Leeupoort the years 1918, 1967, 1971, 1974, 1976, 1978, 2000, 2006, 2008, 2010, 2011, 2014,

and 2017 recorded severely to extremely wet drought conditions. In the years 1918 and 2008, the station calculated extremely wet drought conditions, with SPI values of 2.25 and 2.48 respectively. Moderate dry drought conditions were calculated in 1965 at five stations, viz. Zeerust, Delareyville, Hendrik Theron, Schietfontein and Leeupoort, these stations are situated in the eastern and SE parts of the study region. In the year 1966, six stations calculated the occurrence of moderately to severely dry drought conditions. Stations that calculated moderately dry drought conditions include Zeerust, Vaalharts, Buffeldoorns and Hendrik Theron and those which calculated severely dry drought conditions include Klipfontein and Leeupoort. In 1967, Hendrik Theron, Buffeldoorns, Klipfontein, Leeupoort, Schietfontein and Zeerust recorded the occurrence of wet drought conditions with SPI values of 1.5, 1.44, 2.39, 1.71, 1.72, and 1.96, respectively.

Four stations recorded the occurrence of moderate to severe dry drought conditions in the years 1984 and 1985. Gaborone and Lobatse calculated moderately dry drought conditions in both years, whereas Zeerust and Molepolole calculated moderately dry drought conditions in 1984 followed by severely dry drought conditions in 1985. Molepolole recorded moderately dry drought conditions in 1986, whereas Zeerust recorded severely dry drought conditions, and in 1987 Zeerust recorded moderately dry drought conditions. None of the stations recorded the occurrence of wet drought conditions in 1984. In 1985 Schietfontein calculated the occurrence of wet drought conditions and in 1986 Shakawe calculated wet drought conditions, with SPI values of 1.32 and 1.18, respectively.

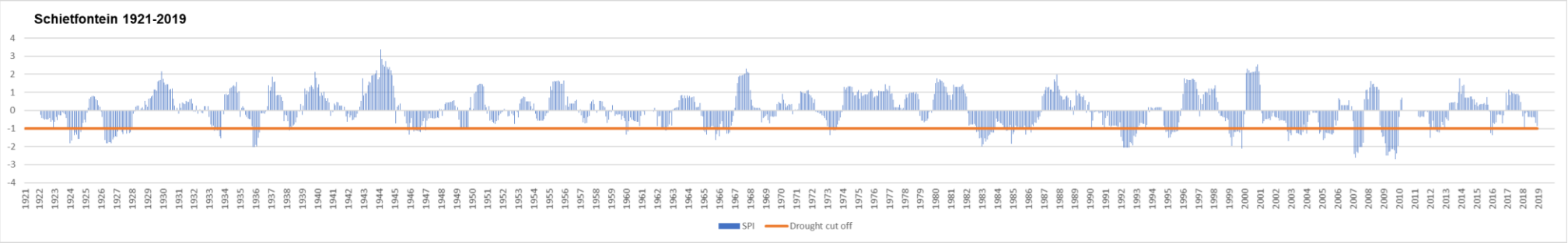

Figure 2: The 12-month SPI for Schietfontein.

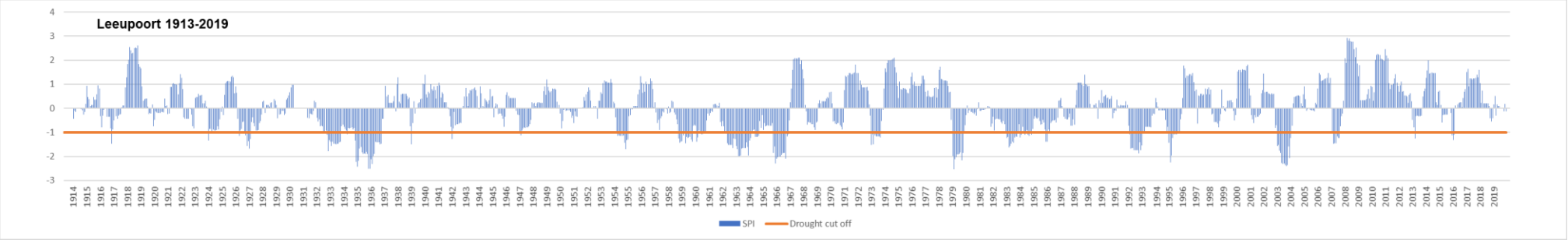

Figure 3: The 12-month SPI for Leeupoort.

Weather stations including Ramotswa, Tsabong, Gaborone, Palapye, Lobatse, Serowe, Molepolole, Pitshane Molopo, Ramatlabama, Thamaga and Francistown recorded the occurrence of dry drought conditions in the years 1991 and 1992. Tsabong and Pitshane Molopo are both found in the SW section of the study region. Palapye, Serowe and Francistown are in the NE portion of the study region. Palapye, Serowe, Molepolole, and Francistown calculated moderately dry drought conditions for the two consecutive years 1991 and 1992.

Lobatse and Thamaga recorded extremely dry drought conditions in 1991 and moderately dry drought conditions in 1992. Lobatse is in the SE region of the study region, whereas Thamaga is in the west of Gaborone. In the years 1991 and 1992, none of the weather stations in the NW region of the study region calculated any drought events. Hendrik Theron, located further SE of the study area, recorded severely wet drought conditions.

Mochudi, Palapye, Vaalharts, Leeupoort, and Bulgerivier recorded the occurrence of dry drought conditions in the years 1992 and 1993. These stations are in various regions of the study region. Mochudi, Vaalharts, Bulgerivier, and Leeupoort are located in the SE region, Palapye in the NE portion of the study region. Mochudi experienced moderately dry drought conditions, Bulgerivier recorded the occurrence of severely dry drought conditions in 1992 followed by moderately dry drought conditions in 1993. Vaalharts experienced moderately dry drought conditions in 1992 followed by extremely dry drought conditions in 1993. Palapye experienced the occurrence of moderately dry drought conditions in 1992 followed by the occurrence of severely dry drought conditions in 1993.

Six weather stations in the study region recorded moderately dry drought conditions in 2016. These stations include Bray Pol, Vryburg, Hendrik Theron, Dippenaarshoop, Zeerust and Bulgerivier. In 2017 the area calculated normal drought conditions, and five stations calculated moderately dry drought conditions. These stations include Hendrik Theron, Vryburg, Klipfontein Schietfontein, Leeupoort and Buffeldoorns.

As per (Figure 4) the years 1965, 1966, 1984, 1985, 1986, 1987, 1991 and 1992, had the most widespread dry droughts in the study region, these droughts ranged from moderately to extremely dry drought conditions. The study region from the 1980s has been recording the frequent occurrence of droughts and these droughts are mostly moderate to severely dry drought conditions. The years 1974, 1975, 1976, 1987, 1988, 1996, 1999, 2000, 2005, 2008, 2010 calculated the widespread occurrence of wet drought conditions and these years correlate with the occurrence of La Niña events excluding the occurrence of the 2010 wet drought which correlated with an El Niño event.

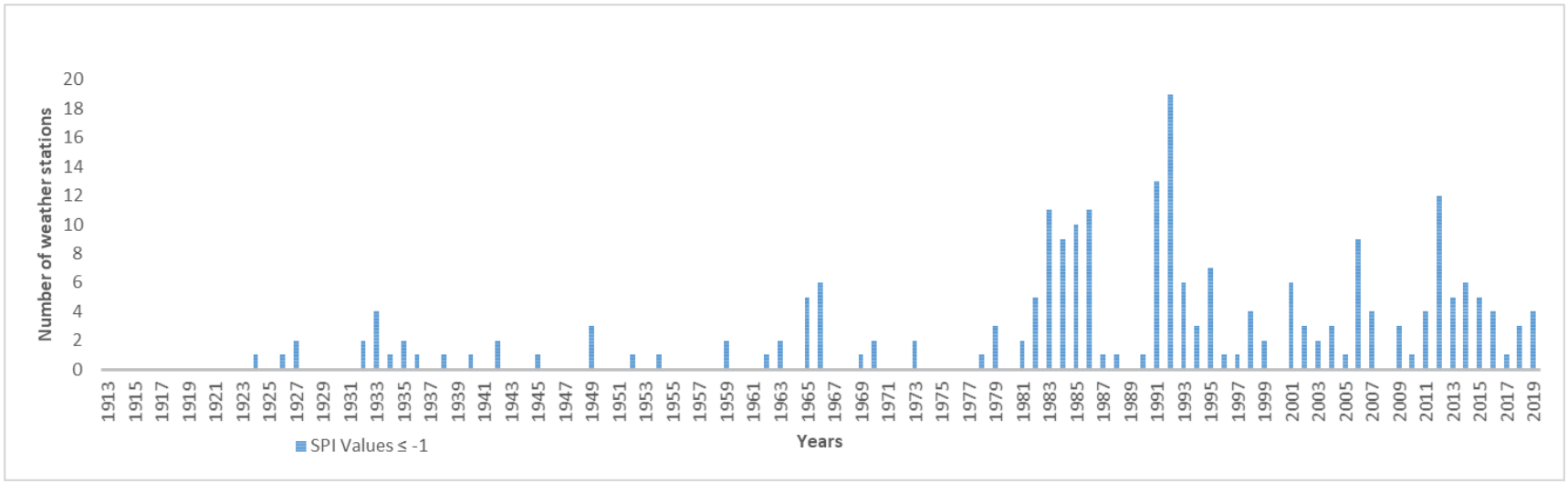

Figure 4: SPI Values below -1, 1913-2019

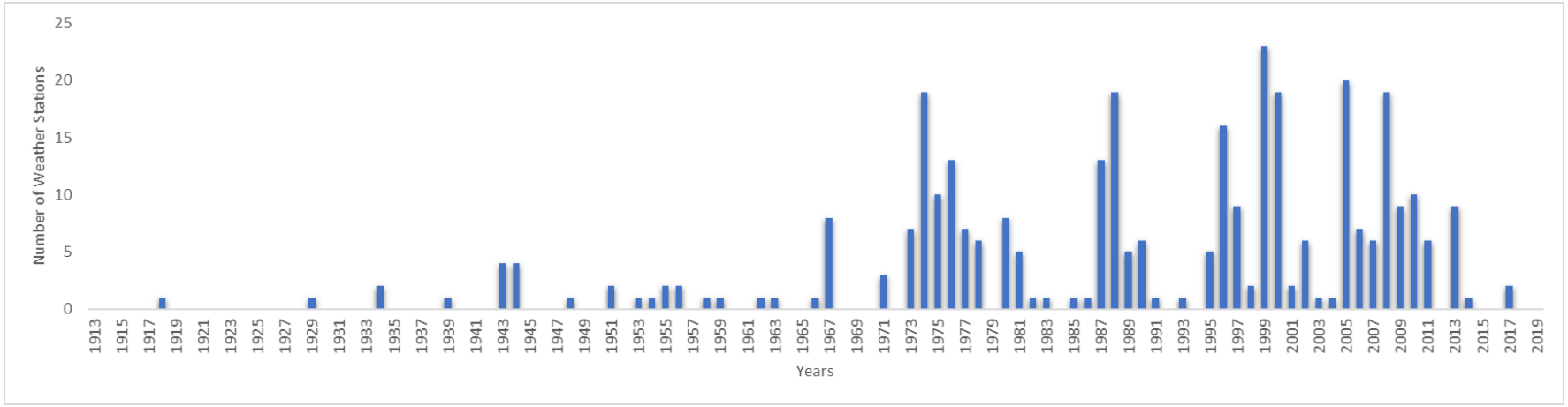

Figure 5: SPI Values Wet Drought conditions, 1913-2019

4.3. Spatial Distribution of Droughts Events

The spatial distribution of droughts was visualized using SPI values and applying the spatial interpolation methods IDW and OK. The study region is further divided into 4 different sections; Southwest (SW), Northwest (NW), Southeast (SE) and Northeast (NE) to present the results more simply and to make the analysis of the results easier to comprehend (Figure 6).

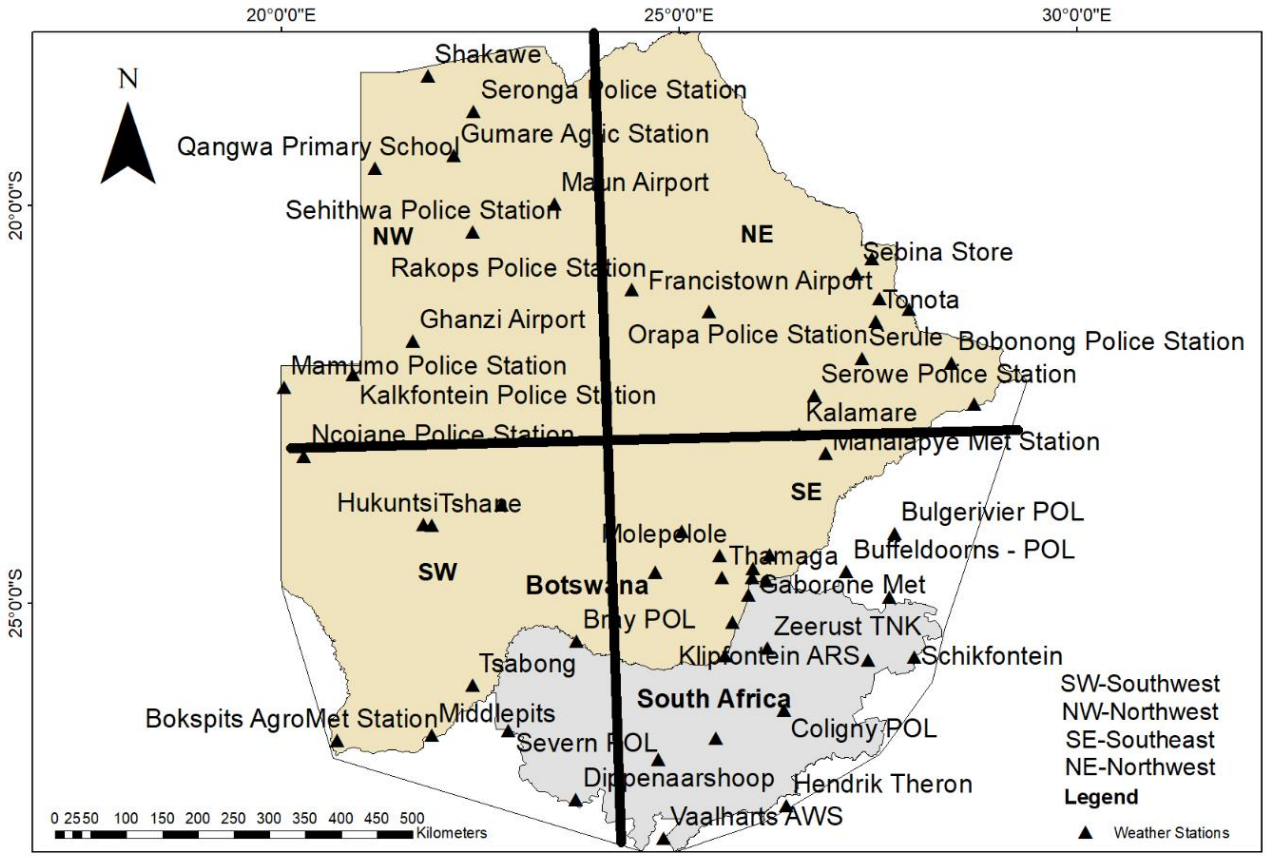

Figure 6: Delineations in the study region

4.3.1. IDW

This method was used to show the distribution of the occurrence of droughts and floods in the study region. The results of this method indicate that there is a distribution of various drought types in the study region. In the NW portion of the study region, one

of the weather stations Serongwa recorded the occurrence of severely dry drought conditions with the surrounding areas calculating moderately to normal drought conditions (Figure 7). The rest of the study region calculated the occurrence of normal drought conditions.

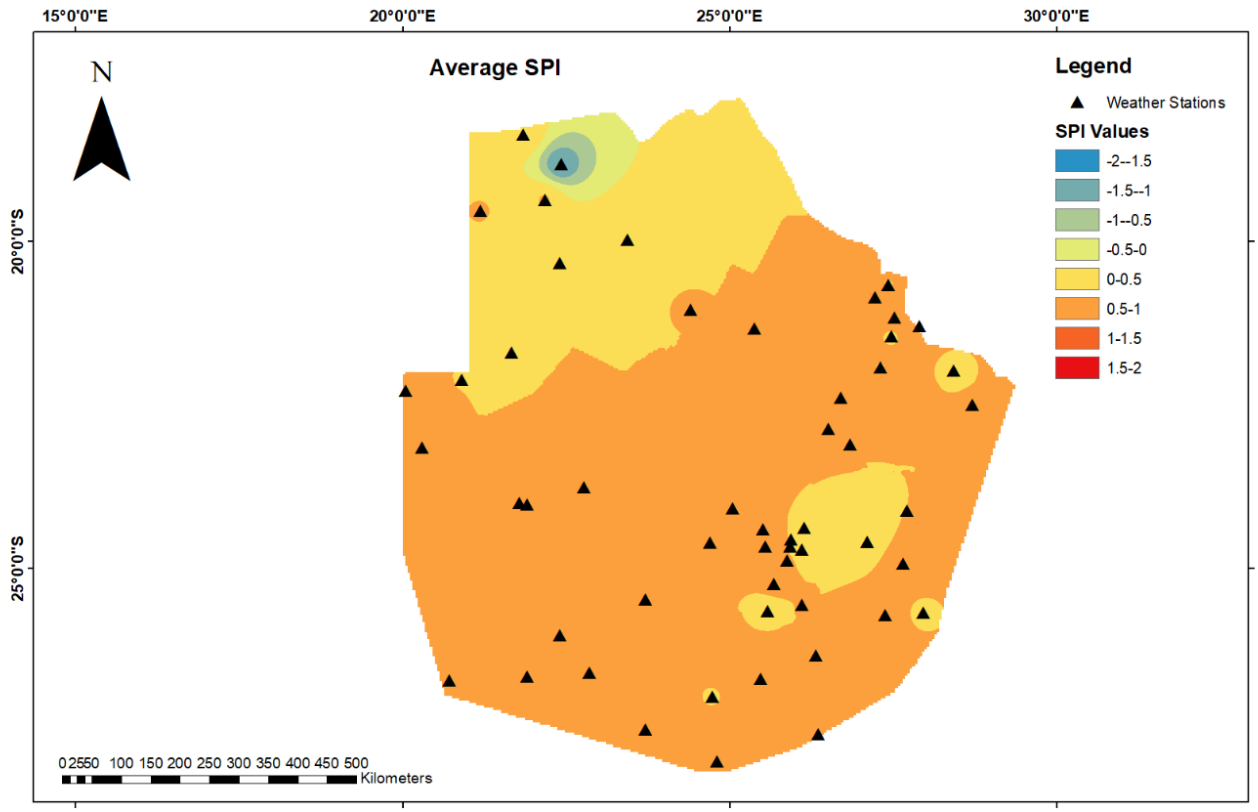

Figure 7: Average SPI using IDW, 1970-2019

The study region experienced normal drought conditions in 1973, and the NW section of the study region calculated moderately to severely wet drought conditions. In 1974 the study region recorded the occurrence of normal drought conditions. Areas around the SE and the NW section of the study region recorded the occurrence of moderately to severely dry drought conditions. In the year 1976, the central, SW, NW and NE sections of the study region experienced normal drought conditions.

In the year 1981, the northern section of the study region recorded the occurrence of moderately dry drought and the entirety of the region calculated normal drought

conditions. In the year 1982, areas in the northern section towards the SE section of the study region calculated moderately dry drought conditions. The central section towards the SW and NW section of the study region showed normal drought conditions, with one station in the west showing the occurrence of severely dry drought conditions.

The central section, towards the north and NE section of the study region, indicates the occurrence of normal drought conditions in 1983. In 1984 the NE towards the SW section of the study region calculated moderately dry drought conditions with the western and parts of the central region experiencing normal drought conditions. In the year 1985, moderate dry drought conditions were computed for the entirety of the study region, while normal drought conditions were computed in the SW and NW sections.

In the year 1986, the central region of the study area towards the NE and the SE edge of the study region experienced the occurrence of moderately dry drought conditions followed by normal drought conditions. The southern and the northern section of the study region calculated the occurrence of normal drought conditions followed by a band of moderately wet drought conditions running from the west towards the NE. In the year 1989, the southern and NW sections of the study region recorded the occurrence of moderately dry drought conditions. The years 1981, 1982, 1983, 1984, 1985, and 1986 recorded the occurrence of widespread drought conditions.

The study region indicated normal drought conditions in 1990 with moderately wet drought conditions in the central section of the study region. Moderately to severely

dry drought conditions were calculated with normal drought conditions in the eastern margin of the study region. In 1993 the study region recorded moderately to severe dry drought conditions in the eastern and parts of the western section. The northern and the southern sections of the study region calculated the occurrence of moderately dry drought conditions. The eastern section and parts of the central portion of the study region calculated the occurrence of normal drought conditions. In the year 1995, the southern section of the study region calculated the occurrence of moderately to severely dry drought conditions, and parts of the northern section recorded the occurrence of moderately wet drought conditions.

In the year 1996, the central section towards the NW and the SE sections of the study region calculated the occurrence of moderately wet drought conditions. Two weather stations, (Bokspits and Shakawe) and their surrounding areas located on the SW edge of the study region calculated the occurrence of moderately to severely dry drought conditions. In 1997 the southern section of the study region calculated the occurrence of moderately to severely wet drought conditions. In 1998 parts of the western and central section of the study region experienced the occurrence of moderately to severely dry drought conditions. In the year 1999 the SW, the central, the northern, and the NE sections of the study region calculated the occurrence of moderately to severely wet drought conditions. It was determined that minimal to widespread dry drought conditions occurred in 1990, 1993, 1995, 1997, 1998, and the years 1996 and 1999 calculated the occurrence of moderately to severely wet drought conditions.

In the year 2000 the central, NE, SW, SE, and the eastern portion of the study region recorded moderately to severely wet drought conditions. In the year 2001, the north

towards the eastern section of the study section calculated the occurrence of moderately to severely dry drought conditions. In the year 2002, the NW section of the study region calculated the occurrence of moderately dry drought conditions. The southern section calculated moderately to severely wet drought conditions.

In the year 2003, the SE section recorded moderately dry drought conditions and in the year 2004, the NE section of the area recorded moderately dry drought conditions. In the year 2007 the NE section recorded moderately wet drought conditions; the SE section calculated moderately dry drought conditions. In the year 2008 the central, SE, and SW calculated moderately wet drought conditions. In 2011 the NE section calculated moderately dry drought conditions; the southern section calculated moderately to severely wet drought conditions. In 2012, the study region recorded moderately to severely dry drought conditions. In the year 2013 the NW, NE and northern sections of the study region calculated the occurrence of moderately wet drought conditions. The southern section calculated moderately dry drought conditions. In the year 2014, the SW and the SE calculated moderately dry drought conditions and the eastern and the SE calculated the occurrence of moderately wet drought conditions. In the years 2018 and 2019, the SW portion of the study region calculated moderately dry drought conditions and the rest of the study region calculated normal drought conditions.

4.3.2. OK

Ordinary Kriging is one of the geostatistical methods that was used to interpolate SPI data in the study region. The results of this method are similar to the results obtained from the IDW method, they indicate that the study region calculated the occurrence of normal drought conditions, whereas the northern portion of the study region indicates the occurrence of severely to moderately dry drought conditions (Figure 8). The station which calculated this occurrence is the same station that calculated this drought condition using the IDW method.

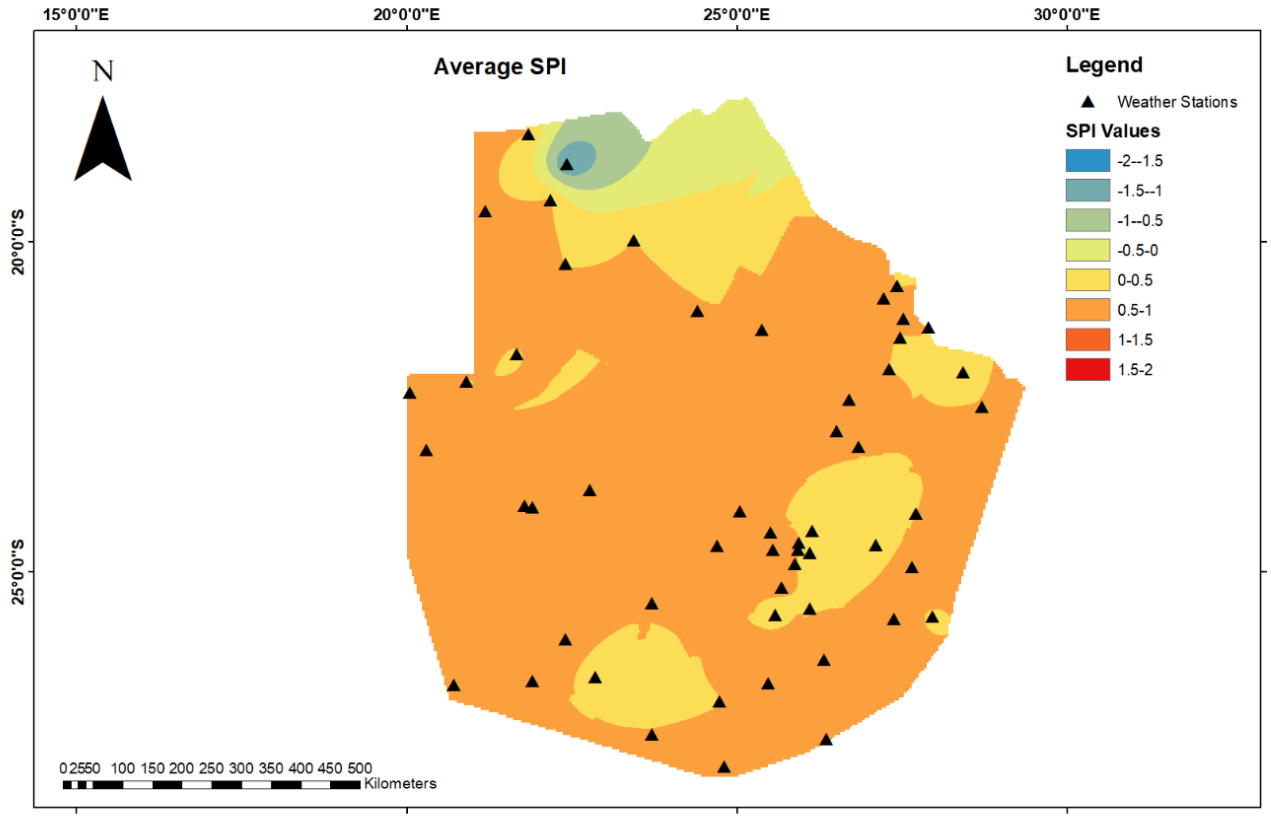

Figure 8: Average SPI using OK, 1970-2019

Based on the two interpolation methods the accuracy assessment shows that OK outperformed IDW at interpolating precipitation data, with a RMSE of 0.33 (Table 3).

Table 3: Accuracy Assessment IDW and OK

Interpolation Method	RMSE	MSE
IDW	0.37	$-1.557E^{-02}$

OK	0.33	0.008

4.4. Annual rainfall statistical results

The 54 weather stations are spatially distributed across the study region. In some years, certain weather stations recorded more precipitation than others. The station which recorded the least precipitation is Matsiloje, which recorded 9.1mm of rainfall in the year 1993 with a corresponding SPI value of -3.6 which indicates the occurrence of extremely dry drought conditions (Figure 9). Shakawe recorded the highest precipitation of about 1101.4mm in the year 1973 with a corresponding SPI value of 1.7 which indicates the occurrence of severely wet drought conditions (Figure 10). Shakawe is in the NW region of the study region and Matsiloje is located in the NE region of the study region. The two weather stations were selected based on the fact that one of them shows the lowest amount of precipitation recorded in the region and the other station shows the highest amount of precipitation.

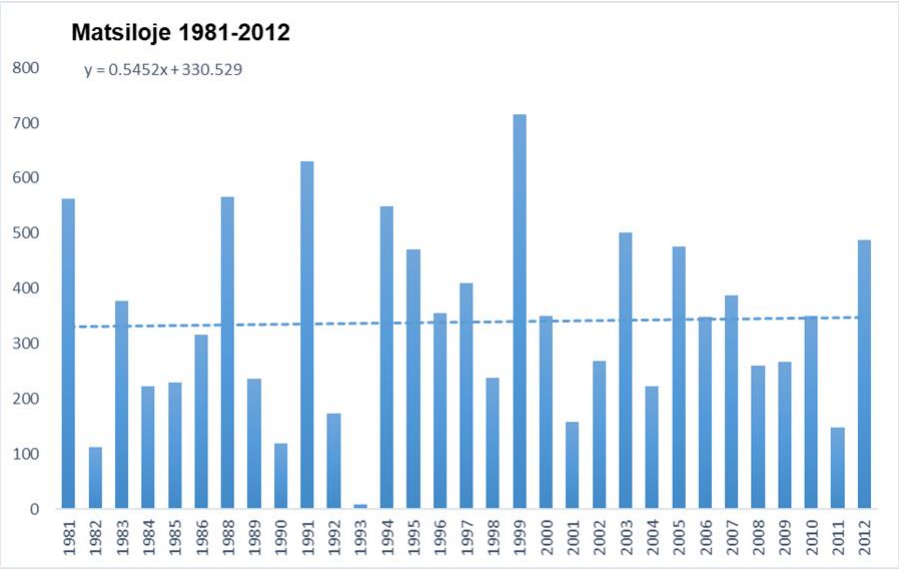

Figure 9: Rainfall data Matsiloje

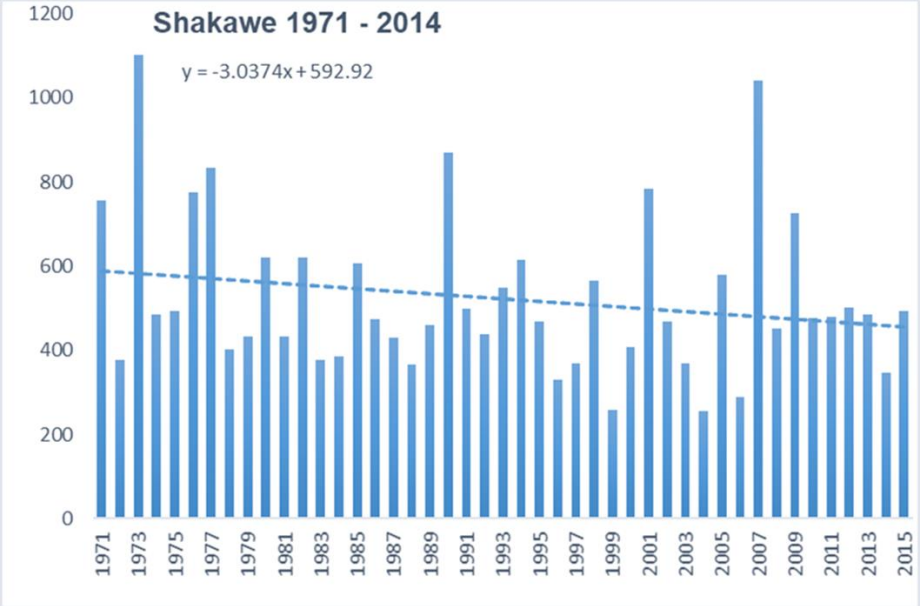

Figure 10: Rainfall data Shakawe

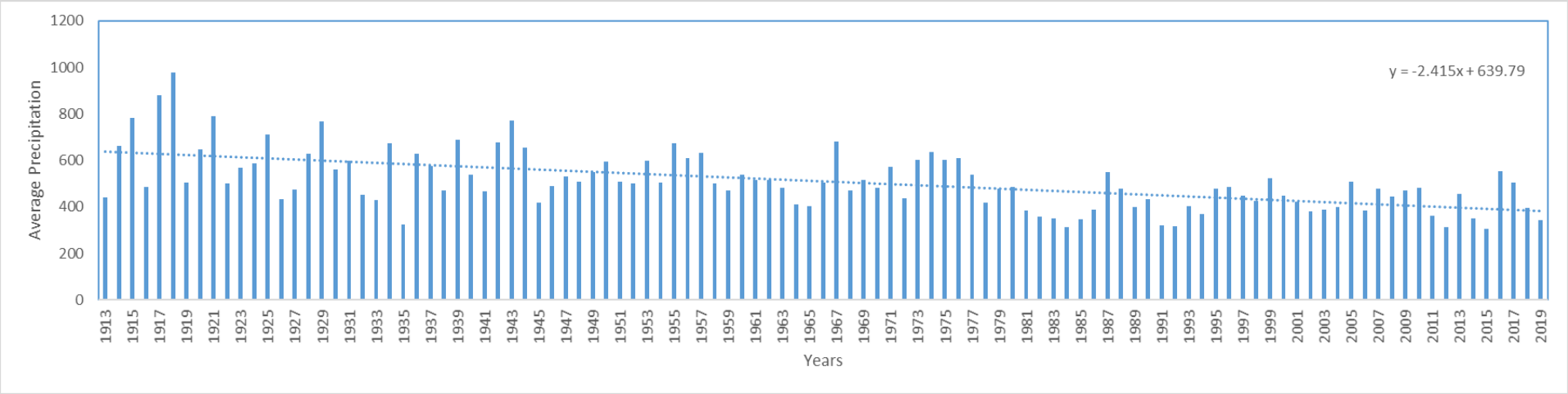

Figure 11: Average Precipitation 1913-2019

Table 4 shows the statistical results of the total annual precipitation, from the data one can deduce that 10 weather stations are statically significant at a 5% significance level. These stations include Lobatse Police Station, Ramatlabama Police Station, Serule, Mamumo, Mashunga, Bray Pol, Bulgerivier, Coligny, Buffeldoorns and, Severn Pol. Bray Pol located in the SW section of the study area, this station shows an increase in rainfall at a rate of 1.73, Mashunga another station found in the SE section of the study region shows a rate of change of 8.62.

The rest of the stations show a decrease in rainfall, these stations include, Buffeldoorns at a rate of change of (-1.83), Bulgerivier (-4.84), Coligny (-4.08), Lobatse police station (-4.52), Mamumo (-6.53), Ramatlabama police station (-3.06), Severn Pol (-2.30) and Serule (-7.51). These stations are located in various sections of the study region. Buffeldoorns, Bulgerivier, Coligny, Lobatse police station, and Ramatlabama are in the SE section. Mamumo in the NW, Severn Pol in the SW and Serule in the NE.

Table 4: Statistical results for the total annual precipitation

Stations	Data period	P-value	R-value	Coefficient of x
Bainesdrift	1980-2014	0.69	0.18	2.85
Bobonong	1980-2014	0.86	-0.08	-1.58
Bokspits	1980-2014	0.16	0.27	2.64
Bray Pol	1947-2019	**0.02**	-0.26	1.73
Buffeldoorns	1935-2019	**0.01**	-0.24	-1.83
Bulgerivier	1969-2019	**0.00**	-0.43	-4.84
Coligny	1968-2015	**0.04**	-0.30	-4.08
Delareyville	1927-2013	0.29	0.13	0.74
Dippenaarshoop	1980-2019	0.78	0.06	0.85
Francistown	1971-1999	0.96	-0.05	-1.21
Gaborone	1980-2015	0.98	-0.06	-0.96
Ghanzi Airport	1971-2014	0.82	-0.04	-0.59
Gumare	1980-2013	0.19	0.25	4.49
Hendrik Theron	1932-2017	0.68	-0.02	0.13
Hukuntsi	1983-2014	0.90	-0.01	-0.23
Jwaneng Airport	1988-2013	0.64	0.02	0.51
Kalamare	1980-2014	0.12	0.20	-3.42
Kalkfontein	1971-2011	0.52	-0.08	-1.01
Kang Agromentation	1981-2014	0.37	0.13	1.82

Stations	Data period	P-value	R-value	Coefficient of x
Klipfontein	1929-2017	0.25	0.11	0.73
Leeupoort	1913-2019	0.16	0.15	-1.83
Letlhakane Police Station	1979-2014	0.62	0.02	0.35
Lobatse Police Station	1971-2014	**0.04**	-0.34	-4.52
Mahalapye	1979 -2014	0.84	-0.05	-0.71
Mamumo	1971-2011	**0.00**	-0.45	-6.53
Mashunga	1980-2013	**0.01**	0.38	8.62
Matsiloje	1981-2012	0.53	0.03	0.54
Maun	1979-2013	0.11	0.23	3.09
Middlepits	1988-2012	0.96	0.01	0.26
Mochudi	1980-2014	0.85	-0.06	-1.11
Molepolole	1979-2014	0.53	0.06	1.08
Ncojane	1971-2012	0.71	0.09	0.99
Orapa	1968-2014	0.61	-0.08	-0.90
Palapye	1972-2013	0.79	-0.04	-0.59
Phitshane Molopo	1971-1999	0.29	-0.29	-5.69
Qangwa Primary School	1983-2013	0.30	-0.14	-3.78
Rakops Police Station	1971-2000	0.94	-0.01	0.71
Ramatlabama Police Station	1961-2014	**0.01**	-0.31	-3.06
Ramotswa	1971-2013	0.30	-0.15	-2.58
Schietfontein	1921-2018	0.54	-0.06	0.05
Sebina Store	1971-2013	0.07	-0.34	-5.07
Sehitwa	1970-2013	0.08	-0.28	-3.24
Serongwa	1978-2012	0.93	0.00	0.03
Serowe	1971-2015	0.39	-0.12	1.93
Serule	1986-2014	**0.01**	-0.37	-7.51
Severn Pol	1967-2019	**0.00**	-0.34	-2.30
Shakawe	1971-2011	0.26	-0.21	-3.03
Sir Seretse	1985-2013	0.34	-0.10	-2.07
Thamaga	1986-2013	0.77	-0.04	-0.96
Tlokweng Border	1980-2012	0.80	0.08	1.38
Tonota	1971-2013	0.07	-0.26	-4.03
Tsabong	1979-2014	0.46	0.12	1.33
Tshane	1979-2014	0.68	-0.13	-1.61
Vaalharts	1935-2019	0.63	0.06	0.40
Vryburg	1987-2019	0.95	0.00	0.10
Zeerust	1940-2019	0.23	-0.15	1.22

Table 5: Weather Stations showing the occurrence of Wet and Dry drought conditions during the occurrence of El Niño (Cherian *et al*., 2021; de Fátima Bomfim *et al.,* 2021; Golden gate weather services, 2021; Tyrrell *et al.,* 2021)

	Number of Station which calculated dry drought conditions	**Number of Station which calculated wet drought conditions**		**Number of Station which calculated dry drought conditions**	**Number of Station which calculated wet drought conditions**		**Number of Station which recorded dry drought conditions**	**Number of Station which calculated wet drought conditions**		**Number of Station which recorded dry drought conditions**	**Number of Station which calculated wet drought conditions**
Weak - 11			**Moderate - 7**			**Strong - 5**			**Very Strong - 3**		
1952-53	1	1	1951-52	0	2	1957-58	0	1	1982-83	16	2
1953-54	1	2	1963-64	2	1	1965-66	11	1	1997-98	5	11
1958-59	2	2	1968-69	0	0	1972-73	2	7	2015-16	9	0
1969-70	3	0	1986-87	12	14	1987-88	2	32			
1976-77	0	20	1994-95	10	5	1991-92	22	1			
1977-78	1	13	2002-03	5	7						
1979-80	3	8	2009-10	4	19						
2004-05	0	21									
2006-07	0	13									
2014-15	11	1									
2018-19	7	0									

Table 6: Weather Stations showing the occurrence of Wet and Dry drought conditions during the occurrence of La Niña (Cherian *et al.,* 2021; de Fátima Bomfim *et al.,* 2021; Golden gate weather services, 2021; Tyrrell *et al.,* 2021)

	Number of Station which calculated dry drought conditions	**Number of Station which calculated wet drought conditions**		**Number of Station which calculated dry drought conditions**	**Number of Station which calculated wet drought conditions**		**Number of Station which calculated dry drought conditions**	**Number of Station which calculated wet drought conditions**
La Niña - 23								
Weak - 11			**Moderate - 5**			**Strong - 7**		
1954-55	0	3	1955-56	4	4	1973-74	2	0
1964-65	0	0	1970-71	0	3	1975-76	0	23
1971-72	0	3	1995-96	0	21	1988-89	1	24
1974-75	0	29	2011-12	16	6	1998-99	0	25
1983-84	20	1	2020-21			1999-00	3	42
1984-85	10	1				2007-08	4	25
2000-01	0	21				2010-11	0	2
2005-06	10	27						
2008-09	0	28						
2016-17	0	2						
2017-18	4	2						

4.5. Conclusion

The results of this study indicate that this region is characterised by the occurrence of both droughts and floods over certain periods. The extreme weather events in the region are influenced by the occurrence of both La Niña and El Niño events. In the 1970s the area calculated the occurrence of floods, and this was seen in various weather stations. In the 1980s the area showed the occurrence of dry drought conditions however at the end of the 1980s the area showed both the occurrence of droughts and floods, this was also seen at the end of the 1990s were several stations recorded the occurrence of wet drought conditions. The area seldom experienced the occurrence of extremely wet and dry drought conditions. Based on the results obtained from the IDW and Ok interpolation method the region is affected by normal drought conditions, however, the northern region of the study region computed the occurrence of moderate to severe dry drought conditions. The region further showed a decrease in the occurrence of rainfall at the rate of -2.42. However, some stations have shown an increase in the occurrence of rainfall and these stations include Bray Pol and Mashunga with rates of 1.73 and 8.62, respectively.

Chapter 5: DISCUSSION

The primary focus of this study was to assess the spatiotemporal variation in extreme precipitation events in the central portion of southern Africa. The results of this study indicate that there are temporal variations across time scales at the same locations.

5.1. Temporal frequency of droughts

The declaration of droughts in Botswana is attributed to the amount of precipitation, and factors such as crop performance, rangeland conditions and the physical conditions of livestock (Mosalagae and Mogotsi, 2013; Mogotsi *et al.,* 2013). Studies conducted in Botswana indicated that there was an occurrence of droughts in the 1960s, good rains occurred in the 1970s, followed by droughts in the 1980s (Mogotsi *et al.,* 2013; Masih *et al.,* 2014; Byakatonda *et al.,* 2018). As noted in this study (Figure 4; Table 5; Table 6), fewer stations showed the occurrence of droughts in the 1970s, the intensity and frequency of droughts increased in the 1980s and 1990s.

Mogotsi *et al.,* (2013) noted that the community members in Kgalagadi North and Bobonong Sub-districts could recall some of the droughts which occurred in the 1930s, however, due to limited meteorological data, the results of this research could not note most of those droughts. Some of the South African weather stations where data existed in the 1930s, recorded the occurrence of dry drought conditions. In 1933, four weather stations recorded the occurrence of droughts (Delareyville, Leeupoort, Hendrik Theron, Klipfontein), 1934 (Leeupoort), 1935 (Buffeldoorns, Leeupoort), Leeupoort was the only station which experienced the occurrence of droughts from 1933-1935. Following a drought period from 1933 to 1935, a period of good rainfall followed (Hitchcock, 1979; Mogotsi *et al.,* 2013). Figure 4 demonstrates that after 1935

the frequency of droughts decreased. More drought occurrences were recorded in the years 1968/1970, 1974/1975, 1979/1980, 1981/1982, and 1990/1992 (Parry, 1989; Fako and Molamu, 1995; Mogotsi *et al.,* 2013). These droughts have been found to coincide with the results of the study, however, no weather station showed the occurrence of droughts in 1974/75. The 1981 to 1987 drought increased the proportion of households with food insecurity (Parry, 1989; Seekings, 2017). Droughts occur fairly regularly in the North West province, however in the period between 1985 and 2015 the intensity and frequency of droughts have increased (Serumaga-Zake, 2020). Figure 4, shows that from 1981 to 1988 the occurrence of droughts was at least calculated by one or more weather stations.

Byakatonda *et al.,* (2018) indicated that Botswana recorded droughts between the years, 1991-1999, 2001-2005, 2009-2013 and 2014-2016. In the North West Province extreme droughts were recorded in 1985-2015, severe droughts in 1995-2004 and 2005-2015, moderate droughts in 1985-1994 and 1995-2004, and mild droughts in 2005-2015 (Botai *et al.,* 2016; Serumaga-Zake, 2020). The results of the study indicate an increased frequency of droughts in the years 1991-1992, where in the year 1991, 13 stations calculated the occurrence of droughts. In the year 1992, 19 stations recorded the occurrence of dry drought conditions. The effects of the droughts on hydrological systems can only be identified where drought occurrence is at longer timescales (Awange *et al.,* 2016; Homdee *et al.,* 2016; Zhu *et al.,* 2016; Byakatonda *et al.,* 2018).

The La Niña years 1967/1968, 1973/1974, 1999/2000, 2010/2011 are periods which were humid in this region (Byakatonda *et al.,* 2020). However, in the study region

results indicate that in 1973/1974 two stations recorded the occurrence of dry drought conditions, two stations in 1999/2000 and five stations in 2010/2011. Some of the droughts coincided with the El Niño years, 1963/1964, 1982/1983, 1994/1995, 2002/2003, 2004/2005, 2006/2007 and the most recent 2015/2016. The 2015/2016 drought has been identified as the year with the strongest El Niño in 100 years (Hassen *et al.,* 2016; Byakatonda *et al.,* 2018). These extreme dry conditions in 2014/15 and 2015/16 resulted in crop failure, food shortages, and economic crises (Hoell and Cheng, 2018). Wet conditions which followed in 2016/17 further resulted in flooding, crop destruction and displacement of people (Hoell and Cheng, 2018).

5.2. Spatial frequency of droughts

Kruger and Nxumalo, (2017) and Marumbwa *et al.,* (2019) indicated that there have been declining rainfall trends over SW parts of southern Africa and increasing trends in the northern parts of Mozambique, Zambia, and Malawi. Studies conducted by Marumbwa *et al.,* (2019) indicate that annual rainfall totals in the north (Maun and Shakawe) are explained by the number of days with rains, more intense events in the southwest (Ghanzi and Tsabong) and in Serowe and Mochudi in the southeast, the annual rainfall is explained by a balance between the number of days with rain and intense events (Marumbwa *et al.,* 2019).

Results of the study indicate Shakawe, and Maun as being characterised by the frequent occurrence of drought conditions, Shakawe station calculated the occurrence of moderate to severe dry drought conditions. Batisani, (2011) indicates that Francistown (Northeast), Ghanzi (West), Kasane (North), Lobatse (South), Maun (Northwest), and Tsabong (South), these areas are characterised by the occurrence

of normal drought conditions. However, Lobatse and Maun have greater than 30% of moderate dry drought conditions (Batisani, 2011). These results coincide with the results obtained in this study which indicate that the study region is characterised by normal drought conditions. Shakawe located in the northern section of the study region calculated the occurrence of moderate to severe dry drought conditions, using both OK and IDW interpolation methods. The results of the study conducted by Nkemeleng *et al.,* (2018) suggest that climate change affects Botswana through a decrease in rainfall. The drought-prone areas are located in the western portion of the study region, these areas include Shakawe, Ghanzi, Tsabong, Ncojane, Tshane, Middlepits, Bokspits, and they are in proximity to the Kalahari Desert. The main drivers of these changes are the effects of ENSO, TTT, movement of the ITCZ and the Angola low (Reason, and Smart, 2015; Manatsa *et al.*, 2017; Howard and Washington, 2018; Maruatona and Moses, 2021). The western region of Southern Africa has been identified to be drier than the other regions (Blamey *et al.,* 2018).

5.3. Contemporary issues related to droughts

A range of studies have indicated that the occurrence of droughts in Botswana are linked to the Pacific ENSO episodes, hence the area experiences severe drought conditions (Nicolson *et al.,* 2011). The climate of Botswana is also largely influenced by the shifting of the ITCZ, westerlies and easterlies (Byakatonda *et al.,* 2018). The Kalahari Desert in the west and the Okavango basin in the North, and the Limpopo basis in the SE are physical features that play a role in moderating the local climate (Mukwada, 2018; Byakatonda *et al.,* 2018). This further explains the distribution of dry drought conditions around the study region, as per the SPI plots areas in the western and northern regions experience more droughts as compared to areas in the east.

Semi-arid areas show high climate variability and over the years this variability has increased (Ahmed *et al.,* 2018; Mohammed and Scholz, 2019). This variability has a great influence on the spatiotemporal characteristics of droughts (Ahmed *et al.,* 2018; Mohammed and Scholz, 2019). Across the study region, one can identify that both spatially and temporally, precipitation patterns vary, this can be observed from both the SPI and annual rainfall plots. Droughts that have occurred in the years, 1961/62,1965/66,1980/81,1986/87, 1991/1992, 2001/02, 2005/06, 2009/10, 2012/13, 2014/15, 2015/16, have coincided with the El Niño years (Byakatonda *et al.,* 2018).

Studies conducted by Pachauri and Reisinger, (2007) and Stocker *et al.,* (2013) indicate that climate change is likely associated with the shift in the atmospheric circulation with dry locations getting drier. As a result of these shifts, these locations may degenerate into hyper-arid areas (Byakatonda *et al.,* 2019). According to the results of Byakatonda *et al.* (2019), Botswana is vulnerable to two drought categories which are severe and moderate dry drought conditions. A study by Batisani *et al.,* (2011) indicated that Botswana is prone to moderate dry droughts, and this aligns with the results obtained in this study which indicated that the study region is prone to normal drought conditions to moderate dry drought conditions.

The occurrence of below-average rainfall at the beginning of the crop season (sowing) 2013/2014, 2014/2015, 2016/2017 has been linked to the strong episode of El Niño, since March 2015 which continued into the early 2016 and its impact persisted well into 2017 (Cunha *et al.,* 2019; Byakatonda *et al.,* 2020). Rainfall has been decreasing on both annual and monthly bases as per the average precipitation plot (Figure 11) and these results are found to be consistent with the results obtained by Batisani and

Yarnal, (2010). ENSO influences southern Africa through extra-tropical teleconnections (Pomposi *et al.,* 2018; Monerie *et al.,* 2019). As a result of alternating Rossby wave trains of pressure and height anomalies that originate from the tropics during ENSO events, the Southeast Atlantic and southern African regions experience significant atmosphere circulation and SST (Blamey *et al.,* 2018). A Rossby wave train (RWT) is a coherent envelope of baroclinic waves propagating along a waveguide at mid-latitudes and can produce downstream development (Thornton, 2014).

During the year 1997/1998, tropical Africa experienced excess moisture due to a combination of eastward moisture from the enhanced Angola low and a westward flux of moisture from the warm tropical Indian Ocean (Reason, and Smart, 2015; Crétat *et al.,* 2019; Pascale *et al.,* 2019; Rapolaki *et al.,* 2021). In 1997/1998, the increase in rainfall in eastern Africa was attributed to the presence of anticyclonic anomalies in the tropical Indian Ocean that developed during an El Niño event. (Crétat *et al.,* 2019; Taschetto *et al.,* 2020). During this El Niño event, five weather stations recorded the occurrence of dry drought conditions and 11 computed wet drought conditions (Table 5). As a result of the strong anticyclonic anomaly over the west of southern Africa and extending into central Africa, moisture flux anomalies were observed over Tanzania and northern Mozambique, resulting in less atmospheric moisture transport from the Indian Ocean to southern Africa than would be expected (Reason, and Smart, 2015).

The lack of moisture over southern Africa has led to a decrease in precipitation, fuelling the occurrence of drought conditions (Figure 7; Figure 8). The average precipitation plot (Figure 11), shows a decline in precipitation from 1913 to 2019, at a rate of change of -2.41. During the 2015/2016 drought event, the Botswana High exerted a significant

influence over rainfall in southern Africa during October, November, and December. (Driver and Reason, 2017; Nonjinge, 2018; Wilson and Mohanakumar, 2021). The 2015/2016 drought was recorded by seven weather stations in 2015 (Bray Pol, Bulgerivier, Dippenaarshoop, Vaalharts, and Coligny), 2016 (Zeerust, Bray Pol, Vryburg, and Bulgerivier), none of the weather stations computed the occurrence of wet drought conditions (Table 5).

The Angolan low-pressure system forms on the plateau region to the east of the Angolan and the Namibian highlands (Munday and Washington, 2017). The intensity of the Angolan low is associated with enhanced local convection, increased westerly moisture transport from the southeast Atlantic and the penetration of moisture-bearing north easterlies deep into the subtropics (Mundy and Washington, 2017). Stronger Botswana high and weak Angola low coincides with dry conditions experienced during January, February, and March. This has likely contributed to southern Africa's lower atmospheric stability by transporting drier and cooler South Atlantic air over the continent (Blamey *et al.,* 2018).

5.4. Limitations of the study

The study was computed for the proposed period however, some limitations arose, and these limitations include differences in meteorological station equipment used in the weather stations in Botswana and South Africa. Limited data from the meteorological offices, which means more time was needed to clean the data available to make the data user friendly. The results of this study have highlighted that this region shows spatial heterogeneity wherein weather stations that are closer to one

another yield highly varying results. This poses a limitation on the results obtained as areas that are far apart will show high variability.

Methods used also have different limitations, where IDW is not a very good interpolation method for mountainous areas, however, this method is good for estimating changes in terrain, e.g., cliffs and fault lines, to be able to overcome this limitation, OK was chosen as another method for interpolation. The other limitation arose from the completeness of data. Some weather stations did not have complete precipitation data, with others having data from the 1920s and others having data starting from the 1960s, hence the study period was chosen to be from 1970 to 2019 as this is the period where most stations had complete precipitation records.

Chapter 6: CONCLUSION

This study has provided new insights into the drought distribution in the study region. It has further indicated that in various regions of the study, there are varying ways in which drought conditions affect the area. The western and northern regions of the study have been identified as the regions which are prone to the occurrence of moderate to severe dry drought conditions. The 12-month SPI has been used to analyse the occurrence of drought conditions as it compares 12 consecutive months in the area of the study as compared to the 1,3, 6 timescales that might be affected by seasonality. The two interpolation methods used in the study which are OK and IDW have differing results in terms of the type of droughts that are dominant in the study region.

IDW was found to be a better interpolation method as it could show the varying drought types. The study further concluded that in the years there has been an increase in the occurrence of droughts across the study region which might lead to changes in the livelihoods of various communities. The results indicate modest spatial trends but strong and coherent temporal trends in the rainfall data in the study region. The results of this study indicate that normal drought conditions are more prevalent drought conditions with the frequency of severe dry drought conditions and extremely dry drought conditions being low in all regions of the study.

6.1. Achievement of Aims and Objectives

The primary aim of the research is to assess contemporary spatiotemporal variation in extreme precipitation events in the central part of southern Africa from 1970 to 2019. The aim of the study was achieved as the spatiotemporal variations of extreme precipitation events were computed using the SPI to determine both drought and flood events in the study region. The results of the SPI computation were used to create maps across the study region using both the OK and IDW interpolation methods.

The objectives include:

- Calculating the standardized precipitation index (SPI) over the past 50 years for each meteorological station in the study region.

  The SPI of the area was computed for each of the weather stations however the period depended on the available data whereas in some stations data was available for shorter periods. However, in other areas, meteorological data were available for longer periods. The results are found in section 8.2. SPI Results, where SPI plots for all the weather stations were computed.

- Visualising spatiotemporal trends via the use of two different spatial interpolation methods and assessing their accuracy,

  The spatiotemporal trends were computed using IDW and OK. The yearly maps were computed from 1970 to 2019, and the average SPI maps were computed for both interpolation methods.

6.2. Areas for future study

This research was aimed at calculating the 12-month SPI and using two interpolation methods to map out the spatial distribution of precipitation in the study region. Time constraints and the scale of this research allowed for the usage of one time period and two interpolation methods. Future studies can explore the study region using remote sensing phenology data which uses data obtained by satellite sensors that measure wavelengths of light absorbed and reflected by green plants. Remote sensing data can integrate for instance Normalized Difference Vegetation Index (NDVI) and Normalized Difference Water Index (NDWI) data. NDVI data can be used to identify whether vegetation in the study region is moisture stressed or there is excess moisture. Low NDVI values indicate moisture stressed vegetation and high values indicate high-density green vegetation and this can be used to identify whether in a certain period the area was experiencing low or excess precipitation. NDWI can also be used to determine the presence of moisture in vegetation cover. Regional climate models (RCMs) can be used to model rainfall variability for the Tswana urbanism and into the future. RCMs are used to gain high-resolution climate information and are also used as dynamically downscaling tools. The advantage of these methods is that they can improve the representation of smaller-scale factors as compared to the General Circulation Models (GCMs). Historical records such as documents and journals can be integrated with the climate data to assist in identifying the occurrence of extreme weather events in the study region.

6.3. Significance of the study

The study was conducted in an area with fewer climate studies, particularly studies which focus on the spatial distribution of extreme rainfall events. This area has been reported as having a decrease in precipitation events. The significance of this study is that it identifies areas that are prone to the occurrence of both drought and flood events and those areas that have shown no changes in the occurrence of extreme rainfall events.

Chapter 7: REFERENCES

Abolverdi, J. and Khalili, D., 2010. Probabilistic analysis of extreme regional meteorological droughts by L-moments in a semi-arid environment. *Theoretical and Applied Climatology*, *102*(3-4), 351-366.

Acevedo, W. and Masuoka, P., 1997. Time-series animation techniques for visualizing urban growth. *Computers and Geosciences*, *23*(4), 423-435.

Adames, Á.F., Patoux, J. and Foster, R.C., 2014. The contribution of extratropical waves to the MJO wind field. *Journal of Atmospheric Sciences*, *71*(1), 155-176.

Adeel, Z., Alarcón, A.M., Bakkensen, L., Franco, E., Garfin, G.M., McPherson, R.A., Méndez, K., Roudaut, M.B., Saffari, H. and Wen, X., 2020. Developing a comprehensive methodology for evaluating economic impacts of floods in Canada, Mexico and the United States. *International Journal of Disaster Risk Reduction*, *50*, 1-13.

Adhikary, S.K., Muttil, N. and Yilmaz, A.G., 2017. Cokriging for enhanced spatial interpolation of rainfall in two Australian catchments. *Hydrological Processes*, *31*(12), 2143-2161.

Adisa, O.M., Masinde, M. and Botai, J.O., 2021. Assessment of the Dissimilarities of EDI and SPI Measures for Drought Determination in South Africa. *Water, 13*(1), 1-17.

Aggarwal, S. and Li, J., 2009. Response of hydrological processes to land-cover and climate changes in Kejie watershed, south-west China. *Hydrological Processes: An International Journal*, *23*(8), 1179-1191.

Ahmed, K., Shahid, S. and Nawaz, N., 2018. Impacts of climate variability and change on seasonal drought characteristics of Pakistan. *Atmospheric Research*, *214*, 364-374.

Akinyemi, F.O., 2017. Climate change and variability in Semiarid Palapye, Eastern Botswana: An assessment from smallholder farmers' perspective. *Weather, Climate, and Society*, *9*(3), 349-365.

Al-Quraishi, A.M.F., Qader, S.H. and Wu, W., 2020. Drought monitoring using spectral and meteorological based indices combination: a case study in Sulaimaniyah, Kurdistan Region of Iraq. In *Environmental Remote Sensing and GIS in Iraq*, 377-393.

Alvarez-Garreton, C., Boisier, J.P., Garreaud, R., Seibert, J. and Vis, M., 2021. Progressive water deficits during multiyear droughts in basins with long hydrological memory in Chile. *Hydrology and Earth System Sciences*, *25*(1), 429-446.

Amini, M.A., Torkan, G., Eslamian, S., Zareian, M.J. and Adamowski, J.F., 2019. Analysis of deterministic and geostatistical interpolation techniques for mapping meteorological variables at large watershed scales. *Acta Geophysica*, *67*(1), 191-203.

Anderson, W., Muñoz, Á.G., Goddard, L., Baethgen, W. and Chourio, X., 2020. MJO teleconnections to crop growing seasons. *Climate Dynamics*, 54, 1-17.

Anim, F.D.K., Raphala, S.B. and Mandleni, B., 2008. Contract farming: A case study of small-scale sunflower farmers in Bojanala district of North West Province. *Journal of Agricultural Research*, *46*(2), 187-202.

Anstey, J.A. and Shepherd, T.G., 2014. High-latitude influence of the quasi-biennial oscillation. *Quarterly Journal of the Royal Meteorological Society*, *140*(678), 1-21.

Antal, A., Guerreiro, P.M. and Cheval, S., 2021. Comparison of spatial interpolation methods for estimating the precipitation distribution in Portugal. *Theoretical and Applied Climatology*, 1-14.

Apaydin, H., Sonmez, F.K. and Yildirim, Y.E., 2004. Spatial interpolation techniques for climate data in the GAP region in Turkey. *Climate Research*, *28*(1), 31-40.

Arcari, P. and Tapper, N., 2017. The variable impact of ENSO events on regional dengue/DHF in Indonesia. *Singapore Journal of Tropical Geography*, 38(1), 5-24.

Ash, K.D. and Matyas, C.J., 2012. The influences of ENSO and the subtropical Indian Ocean Dipole on tropical cyclone trajectories in the southwestern Indian Ocean. *International Journal of Climatology*, *32*(1), 41-56.

Ashley, S.T. and Ashley, W.S., 2008. Flood fatalities in the United States. *Journal of Applied Meteorology and Climatology*, *47*(3), 805-818.

Awange, J.L., Mpelasoka, F. and Goncalves, R.M., 2016. When every drop counts: Analysis of Droughts in Brazil for the 1901-2013 period. *Science of the Total Environment*, *566*, 1472-1488.

Aziz, M.K.B.M., Yusof, F., Daud, Z.M., Yusop, Z. and Kasno, M.A., 2019. Comparison of Semivariogram Models in Rain Gauge Network Design. *Matematika*, *35*(2), 157-170.

Banholzer, S., Kossin, J. and Donner, S., 2014. The impact of climate change on natural disasters. In *Reducing disaster: Early Warning Systems for Climate Change*, 21-49.

Banze, F., Guo, J. and Xiaotao, S., 2018. Variability and trends of rainfall, precipitation, and discharges over the Zambezi River basin, southern Africa: a review. *International Journal of Hydrology,* 2, 132-135.

Barnard, P.L., Hoover, D., Hubbard, D.M., Snyder, A., Ludka, B.C., Allan, J., Kaminsky, G.M., Ruggiero, P., Gallien, T.W., Gabel, L. and McCandless, D., 2017. Extreme oceanographic forcing and coastal response due to the 2015–2016 El Niño. *Nature Communications*, *8(1),* 1-8.

Batisani, N. and Yarnal, B., 2010. Rainfall variability and trends in semi-arid Botswana: implications for climate change adaptation policy. *Applied Geography*, *30*(4), 483-489.

Batisani, N., 2011. The spatiotemporal-severity dynamics of drought in Botswana. *Journal of Environmental Protection*, *2*(06), 803-816.

Batisani, N., 2012. Climate variability, yield instability and global recession: the multi-stressor to food security in Botswana. *Climate and Development*, *4*(2), 129-140.

Battisti, D.S., Vimont, D.J. and Kirtman, B.P., 2019. 100 Years of Progress in Understanding the Dynamics of Coupled Atmosphere–Ocean Variability. *Meteorological Monographs*, 59, 1-8.

Beraki, A.F., Morioka, Y., Engelbrecht, F.A., Nonaka, M., Thatcher, M., Kobo, N. and Behera, S., 2020. Examining the impact of multiple climate forcings on simulated southern Hemisphere climate variability. *Climate Dynamics*, *54*(11), 4775-4792.

Berhane, F., Zaitchik, B. and Badr, H.S., 2015. The Madden–Julian oscillation's influence on spring rainy season precipitation over equatorial West Africa. *Journal of Climate*, *28*(22), 8653-8672.

Berndt, C. and Haberlandt, U., 2018. Spatial interpolation of climate variables in Northern Germany—Influence of temporal resolution and network density. *Journal of Hydrology: Regional Studies*, *15*, 184-202.

Bhaga, T.D., Dube, T., Shekede, M.D. and Shoko, C., 2020. Impacts of Climate Variability and Drought on Surface Water Resources in Sub-Saharan Africa Using Remote Sensing: A Review. *Remote Sensing*, *12*(24), 1-36.

Bhatti, A.S., Wang, G., Ullah, W., Ullah, S., Fiifi Tawia Hagan, D., Kwesi Nooni, I., Lou, D. and Ullah, I., 2020. Trend in extreme precipitation indices based on long term in situ precipitation records over Pakistan. *Water*, *12*(3), 1-19.

Blamey, R.C., Kolusu, S.R., Mahlalela, P., Todd, M.C. and Reason, C.J.C., 2018. The role of regional circulation features in regulating El Niño climate impacts over southern Africa: A comparison of the 2015/2016 drought with previous events. *International Journal of Climatology*, *38*(11), 4276-4295.

Blamey, R.C., Middleton, C., Lennard, C., and Reason, C.J.C., 2017. A climatology of potential severe convective environments across South Africa. *Climate Dynamics*, 49(5-6), 2161-2178.

Borgomeo, E., Pflug, G., Hall, J.W. and Hochrainer-Stigler, S., 2015. Assessing water resource system vulnerability to unprecedented hydrological drought using copulas to characterize drought duration and deficit. *Water Resources Research*, *51*(11), 8927-8948.

Botai, C.M., Botai, J.O., Dlamini, L.C., Zwane, N.S. and Phaduli, E., 2016. Characteristics of droughts in South Africa: a case study of Free State and North West Provinces. *Water*, *8*(10), 1-23.

Boyd, M., Porth, B., Porth, L. and Turenne, D., 2019. The impact of spatial interpolation techniques on spatial basis risk for weather insurance: an application to forage crops. *North American Actuarial Journal*, *23*(3), 412-433.

Bramer, I., Anderson, B.J., Bennie, J., Bladon, A.J., De Frenne, P., Hemming, D., Hill, R.A., Kearney, M.R., Körner, C., Korstjens, A.H. and Lenoir, J., 2018. Advances in monitoring and modelling climate at ecologically relevant scales. In *Advances in Ecological Research*, 58, 101-161.

Brönnimann, S., Malik, A., Stickler, A., Wegmann, M., Raible, C.C., Muthers, S., Anet, J., Rozanov, E. and Schmutz, W., 2016. Multidecadal variations of the effects of the Quasi-Biennial Oscillation on the climate system. *Atmospheric Chemistry and Physics*, *16*(24), 15529-15543.

Byakatonda, J., Parida, B.P., Kenabatho, P.K. and Moalafhi, D.B., 2016. Modeling dryness severity using artificial neural network at the Okavango Delta, Botswana. *Glob Nest J*, *18*, 463-481.

Byakatonda, J., Parida, B.P., Kenabatho, P.K. and Moalafhi, D.B., 2019. Prediction of onset and cessation of austral summer rainfall and dry spell frequency analysis in semiarid Botswana. *Theoretical and Applied Climatology*, *135(1-2),* 101-117.

Byakatonda, J., Parida, B.P., Moalafhi, D.B. and Kenabatho, P.K., 2018. Analysis of long-term drought severity characteristics and trends across semiarid Botswana using two drought indices. *Atmospheric Research*, *213*, 492-508.

Byakatonda, J., Parida, B.P., Moalafhi, D.B., Kenabatho, P.K. and Lesolle, D., 2020. Investigating relationship between drought severity in Botswana and ENSO. *Natural Hazards*, *100(1),* 255-278.

Chen, T., Ren, L., Yuan, F., Yang, X., Jiang, S., Tang, T., Liu, Y., Zhao, C. and Zhang, L., 2017. Comparison of spatial interpolation schemes for rainfall data and application in hydrological modelling. *Water*, *9(5),* 1-18.

Cheng, K.S., Lin, Y.C. and Liou, J.J., 2008. Rain-gauge network evaluation and augmentation using geostatistics. *Hydrological Processes: An International Journal*, *22*(14), 2554-2564.

Cherian, S., Sridhara, S., Manoj, K.N., Gopakkali, P., Ramesh, N., Alrajhi, A.A., Dewidar, A.Z. and Mattar, M.A., 2021. Impact of El Niño Southern Oscillation on Rainfall and Rice Production: A Micro-Level Analysis. *Agronomy*, *11*(6), 1-13.

Childs, C., 2004. Interpolating surfaces in ArcGIS spatial analyst. *ArcUser, July-September*, *3235*, 1-4.

Chonabayashi, S., Jithitikulchai, T. and Qu, Y., 2020. Does agricultural diversification build economic resilience to drought and flood? Evidence from poor households in Zambia. *African Journal of Agricultural and Resource Economics*, *15*(311-2020-1781), 65-80.

Chowdhury, S. and Jahan, N., 2019. Application of CORDEX data to Assess Meteorological Droughts of Rajshahi using Standard Precipitation Index (SPI). In *2nd International Conference on Water and Environmental Engineering (iCWEE-2019, Dhaka)*, *19,* 1-15.

Clem, K.R., Renwick, J.A. and McGregor, J., 2017. Relationship between eastern tropical Pacific cooling and recent trends in the southern Hemisphere zonal-mean circulation. *Climate Dynamics, 49(1-2),* 113-129.

Cook, C., Reason, C.J. and Hewitson, B.C., 2004. Wet and dry spells within particularly wet and dry summers in the South African summer rainfall region. *Climate Research*, *26(1),* 17-31.

Crétat, J., Pohl, B., Dieppois, B., Berthou, S. and Pergaud, J., 2019. The Angola Low: relationship with southern African rainfall and ENSO. *Climate Dynamics*, *52(3),* 1783-1803.

Cui, J., Tang, W., Jin, L., Deng, C., Zou, X. and Gu, S., 2018. An improved ionosphere interpolation algorithm for network RTK in low-latitude regions. *GPS Solutions*, *22(4)*, 1-11.

Cunha, A.P., Zeri, M., Deusdará Leal, K., Costa, L., Cuartas, L.A., Marengo, J.A., Tomasella, J., Vieira, R.M., Barbosa, A.A., Cunningham, C. and Cal Garcia, J.V., 2019. Extreme drought events over Brazil from 2011 to 2019. *Atmosphere*, *10(11),* 1-20.

Dai, A., 2011. Characteristics and trends in various forms of the Palmer Drought Severity Index during 1900–2008. *Journal of Geophysical Research: Atmospheres*, *116*(D12), 1-26.

Daly, C., 2006. Guidelines for assessing the suitability of spatial climate data sets. *International Journal of Climatology: A Journal of the Royal Meteorological Society*, 26(6), 707-721.

Daly, C., Gibson, W.P., Taylor, G.H., Johnson, G.L. and Pasteris, P., 2002. A knowledge-based approach to the statistical mapping of climate. *Climate Research*, 22(2), 99-113.

Daron, J., Burgin, L., Janes, T., Jones, R.G. and Jack, C., 2019. Climate process chains: Examples from southern Africa. *International Journal of Climatology*, *39(12),* 4784-4797.

Das, S., 2021. Extreme rainfall estimation at ungauged locations: Information that needs to be included in low-lying monsoon climate regions like Bangladesh. *Journal of Hydrology*, *601*, 1-12.

Dätwyler, C., Neukom, R., Abram, N.J., Gallant, A.J., Grosjean, M., Jacques-Coper, M., Karoly, D.J. and Villalba, R., 2018. Teleconnection stationarity, variability and trends of the southern Annular Mode (SAM) during the last millennium. *Climate Dynamics,* 51(5-6), 2321-2339.

Davis, C.L. and Vincent, K., 2017. Climate risk and vulnerability: Socio Economic Impacts of extreme weather events in South Africa, *A handbook for Southern Africa,* 30-46.

de Amorim Borges, P., Franke, J., da Anunciação, Y.M.T., Weiss, H. and Bernhofer, C., 2016. Comparison of spatial interpolation methods for the estimation of precipitation distribution in Distrito Federal, Brazil. *Theoretical and Applied Climatology*, *123*(1-2), 335-348.

de Fátima Bomfim, F., Lansac-Tôha, F.M., Bonecker, C.C. and Lansac-Tôha, F.A., 2021. Determinants of zooplankton functional dissimilarity during years of El Niño and La Niña in floodplain shallow lakes. *Aquatic Sciences,* 83(2), 1-13.

De Silva, M.M.G.T. and Kawasaki, A., 2018. Socioeconomic vulnerability to disaster risk: a case study of flood and drought impact in a rural Sri Lankan community. *Ecological Economics*, *152*, 131-140.

De Wandelgek, 2019. Botswana – Wondelgem.Nl. [Online] Available at: <http://www.wandelgek.nl/?page_id=25729> [Accessed 8 May 2020].

Depsky, N. and Pons, D., 2020. Meteorological droughts are projected to worsen in Central America's Dry Corridor throughout the 21st century. *Environmental Research Letters*, *16*(1), 1-15.

Di Capua, G., Kretschmer, M., Donner, R.V., van den Hurk, B., Vellore, R., Krishnan, R. and Coumou, D., 2020. Tropical and mid-latitude teleconnections interacting with the Indian summer monsoon rainfall: a theory-guided causal effect network approach. *Earth System Dynamics,* 11(1), 17-34.

Dirks, K.N., Hay, J.E., Stow, C.D. and Harris, D., 1998. High-resolution studies of rainfall on Norfolk Island: Part II: Interpolation of rainfall data. *Journal of Hydrology*, *208*(3-4), 187-193.

Domeisen, D.I., Garfinkel, C.I. and Butler, A.H., 2019. The teleconnection of El Niño Southern Oscillation to the stratosphere. *Reviews of Geophysics, 57(1),* 5-47.

Dougherty, J.P., Flatnes, J.E., Gallenstein, R.A., Miranda, M.J. and Sam, A.G., 2020. Climate change and index insurance demand: Evidence from a framed field experiment in Tanzania. *Journal of Economic Behavior & Organization*, *175*, 155-184.

Driver, P. and Reason, C.J.C., 2017. Variability in the Botswana High and its relationships with rainfall and temperature characteristics over southern Africa. *International Journal of Climatology*, *37*, 570-581.

Driver, P., Abiodun, B. and Reason, C.J.C., 2019. Modelling the precipitation response over southern Africa to the 2009–2010 El Niño using a stretched grid global atmospheric model. *Climate Dynamics,* 52(7-8), 3929-3949.

Du, L., Mikle, N., Zou, Z., Huang, Y., Shi, Z., Jiang, L., McCarthy, H.R., Liang, J. and Luo, Y., 2018. Global patterns of extreme drought-induced loss in land primary production: Identifying ecological extremes from rain-use efficiency. *Science of the Total Environment*, *628*, 611-620.

Dunleavy, B., 2021. *Analysis: 99.9% of climate studies agree that humans are causing climate change*. [online] UPI. Available at: <https://www.upi.com/Science_News/2021/10/19/climate-change-scientists-agree-humans-study/2671634660959/> [Accessed 19 February 2022].

Elumalai, V., Brindha, K., Sithole, B. and Lakshmanan, E., 2017. Spatial interpolation methods and geostatistics for mapping groundwater contamination in a coastal area. *Environmental Science and Pollution Research*, *24*(12), 11601-11617.

Fako, T.T. and Molamu, L., 1995. The seven-year drought, household food security and vulnerable groups in Botswana. *Pula: Botswana Journal of African Studies*, *9*(2), 48-70.

Fanta, V., Šálek, M. and Sklenicka, P., 2019. How long do floods throughout the millennium remain in the collective memory? *Nature Communications*, *10*(1), 1-9.

Feidas, H., Karagiannidis, A., Keppas, S., Vaitis, M., Kontos, T., Zanis, P., Melas, D. and Anadranistakis, E., 2014. Modeling and mapping temperature and precipitation climate data in Greece using topographical and geographical parameters. *Theoretical and Applied Climatology*, *118*(1-2), 133-146.

Feng, P.N. and Lin, H., 2019. Modulation of the MJO-Related Teleconnections by the QBO. *Journal of Geophysical Research: Atmospheres*, *124(22*), 12022-12033.

Foehn, A., Hernández, J.G., Schaefli, B. and De Cesare, G., 2018. Spatial interpolation of precipitation from multiple rain gauge networks and weather radar data for operational applications in Alpine catchments. *Journal of Hydrology*, *563*, 1092-1110.

Frei, C. and Isotta, F.A., 2019. Ensemble spatial precipitation analysis from rain gauge data: methodology and application in the European Alps. *Journal of Geophysical Research: Atmospheres*, *124*(11), 5757-5778.

Fréjaville, T. and Benito Garzón, M., 2018. The EuMedClim database: Yearly climate data (1901–2014) of 1 km resolution grids for Europe and the Mediterranean basin. *Frontiers in Ecology and Evolution*, *6*, 1-5.

Freychet, N., Sparrow, S., Tett, S.F.B., Mineter, M.J., Hegerl, G.C. and Wallom, D.C.H., 2018. Impacts of anthropogenic forcings and El Niño on Chinese extreme temperatures. *Advances in Atmospheric Sciences,* 35(8), 994-1002.

Gaughan, A.E., Staub, C.G., Hoell, A., Weaver, A. and Waylen, P.R., 2016. Inter-and Intra-annual precipitation variability and associated relationships to ENSO and the IOD in southern Africa. *International Journal of Climatology,* 36(4), 1643-1656.

Gershunov, A. and Barnett, T.P., 1998. Interdecadal modulation of ENSO teleconnections. *Bulletin of the American Meteorological Society*, *79*(12), 2715-2726.

Giorgi, F., Raffaele, F. and Coppola, E., 2019. The response of precipitation characteristics to global warming from climate projections. *Earth System Dynamics*, *10*(1), 73-89.

Gizaw, M.S. and Gan, T.Y., 2017. Impact of climate change and El Niño episodes on droughts in sub-Saharan Africa. *Climate Dynamics, 49(1-2),* 665-682.

Golden gate weather services. 2021. *El Niño and La Niña Years and Intensities*. [online] Available at: <https://ggweather.com/enso/oni.htm> [Accessed 7 November 2021].

Gong, H., Zhou, W., Chen, W., Wang, L., Leung, M.Y.T., Cheung, P.K.Y. and Zhang, Y., 2019. Modulation of the southern Indian Ocean dipole on the impact of El Niño–Southern Oscillation on Australian summer rainfall. *International Journal of Climatology*, *39*(4), 2484-2490.

Goovaerts, P., 2000. Geostatistical approaches for incorporating elevation into the spatial interpolation of rainfall. *Journal of hydrology*, *228*(1-2), 113-129.

Goulden, M.L. and Bales, R.C., 2019. California forest die-off linked to multi-year deep soil drying in 2012–2015 drought. *Nature Geoscience*, *12*(8), 632-637.

Güner Bacanli, Ü, 2017. Trend analysis of precipitation and drought in the Aegean region, Turkey. *Meteorological Applications*, *24*(2), 239-249.

Guo, E., Zhang, J., Wang, Y., Quan, L., Zhang, R., Zhang, F. and Zhou, M., 2019. Spatiotemporal variations of extreme climate events in Northeast China during 1960–2014. *Ecological Indicators*, *96*, 669-683.

Gutiérrez, A.P.A., Engle, N.L., De Nys, E., Molejón, C. and Martins, E.S., 2014. Drought preparedness in Brazil. *Weather and Climate Extremes*, *3*, 95-106.

Hadi, M. P., Suprayogi, S., & Herumurti, S. (2020). Impact of rainfall intensity, monsoon and MJO to rainfall merging in the Indonesian maritime continent. *Journal of Earth System Science*, 129(1), 1-20.

Haertel, P., 2018. Sensitivity of the Madden Julian oscillation to ocean warming in a Lagrangian atmospheric model. *Climate*, *6*(2), 1-19.

Haile, G.G., Tang, Q., Li, W., Liu, X. and Zhang, X., 2020. Drought: Progress in broadening its understanding. *Wiley Interdisciplinary Reviews: Water*, *7*(2), 1-25.

Han, W., Meehl, G.A., Hu, A., Zheng, J., Kenigson, J., Vialard, J., Rajagopalan, B. and Yanto, 2017. Decadal variability of the Indian and Pacific Walker cells since the 1960s: Do they covary on decadal time scales? *Journal of Climate*, 30(21), 8447-8468.

Hanel, M., Rakovec, O., Markonis, Y., Máca, P., Samaniego, L., Kyselý, J. and Kumar, R., 2018. Revisiting the recent European droughts from a long-term perspective. *Scientific reports*, *8*(1), 1-11.

Hannaford, M.J., Bigg, G.R., Jones, J.M., Phimister, I. and Staub, M., 2014. Climate variability and societal dynamics in pre-colonial southern African history (AD 900-1840): A synthesis and critique. *Environment and History*, *20*(3), 411-445.

Hansen, J., Sato, M., Ruedy, R., Schmidt, G.A., Lo, K. and Persin, A., 2016. Global temperature in 2015. *GISS, NASA, NY. URL: http://data. giss. nasa. Gov*, 1-6.

Hasanean, H. and Almazroui, M., 2015. Rainfall: features and variations over Saudi Arabia, a review. *Climate*, *3*(3), 578-626.

Hengl, T., 2009. A practical guide to geostatistical mapping. 1-258.

Hessl, A., Allen, K.J., Vance, T., Abram, N.J. and Saunders, K.M., 2017. Reconstructions of the southern annular mode (SAM) during the last millennium. *Progress in Physical Geography,* 41(6), 834-849.

Hodam, S., Sarkar, S., Marak, A.G., Bandyopadhyay, A. and Bhadra, A., 2017. Spatial interpolation of reference evapotranspiration in India: comparison of IDW and Kriging Methods. *Journal of the Institution of Engineers (India): Series A*, *98(4),* 511-524.

Hoell, A. and Cheng, L., 2018. Austral summer southern Africa precipitation extremes forced by the El Niño-Southern oscillation and the subtropical Indian Ocean dipole. *Climate Dynamics, 50(9-10),* 3219-3236.

Hoell, A., Funk, C., Zinke, J. and Harrison, L., 2017. Modulation of the southern Africa precipitation response to the El Niño Southern Oscillation by the subtropical Indian Ocean dipole. *Climate Dynamics, 48(7-8),* 2529-2540.

Hofstra, N., Haylock, M., New, M., Jones, P. and Frei, C., 2008. Comparison of six methods for the interpolation of daily, European climate data. *Journal of Geophysical Research: Atmospheres, 113(D21*), 1-19.

Homdee, T., Pongput, K. and Kanae, S., 2016. A comparative performance analysis of three standardized climatic drought indices in the Chi River basin, Thailand. *Agriculture and Natural Resources*, *50*(3), 211-219.

Hood, L.L., Redman, M.A., Johnson, W.L. and Galarneau Jr, T.J., 2020. Stratospheric Influences on the MJO-Induced Rossby Wave Train: Effects on Intraseasonal Climate. *Journal of Climate,* 33(1), 365-389.

Howard, E. and Washington, R., 2018. Characterizing the synoptic expression of the Angola low. *Journal of Climate*, *31*(17), 7147-7165.

Hsu, C.W. and Yin, J., 2019. How likely is an El Niño to break the global mean surface temperature record during the 21st century? *Environmental Research Letters*, *14*(9), 1-10.

Huang, B., Jiang, B. and Li, H., 2001. An integration of GIS, virtual reality and the Internet for visualization, analysis and exploration of spatial data. *International Journal of Geographical Information Science*, *15*(5), 439-456.

Huang, D., Dai, A., Yang, B., Yan, P., Zhu, J. and Zhang, Y., 2019. Contributions of different combinations of the IPO and AMO to recent changes in winter East Asian jets. *Journal of Climate, 3*2(5), 1607-1626.

Hudson, J.W., 2002. Responses to climate variability of the livestock sector in the North-West Province, South Africa (Doctoral dissertation, Colorado State University. Libraries).

Ikechukwu, M.N., Ebinne, E., Idorenyin, U. and Raphael, N.I., 2017. Accuracy assessment and comparative analysis of IDW, spline and kriging in spatial interpolation of landform (Topography): An experimental study. *Journal of Geographic Information System*, *9*(3), 354-371.

Imbol Koungue, R.A., Rouault, M., Illig, S., Brandt, P. and Jouanno, J., 2019. Benguela Niños and Benguela Niñas in forced ocean simulation from 1958 to 2015. *Journal of Geophysical Research: Oceans*, *124*(8), 5923-5951.

Iqbal, F. and Chand, S., 2014. Modelling the Monthly and Annual Temperature Series of Quetta, Pakistan. *Pakistan Journal of Statistics & Operation Research,* 10(4), 1-10.

Islam, A.R.M.T., Ahmed, N., Bodrud-Doza, M. and Chu, R., 2017. Characterizing groundwater quality ranks for drinking purposes in Sylhet district, Bangladesh, using entropy method, spatial

autocorrelation index, and geostatistics. *Environmental Science and Pollution Research*, *24*(34), 26350-26374.

Jain, V.K., Pandey, R.P., Jain, M.K. and Byun, H.R., 2015. Comparison of drought indices for appraisal of drought characteristics in the Ken River Basin. *Weather and Climate Extremes*, *8*, 1-11.

Jalali, M., Karami, S. and Marj, A.F., 2016. Geostatistical evaluation of spatial variation related to groundwater quality database: case study for Arak plain aquifer, Iran. *Environmental Modelling & Assessment*, *21*(6), 707-719.

Jeffrey, S.J., Carter, J.O., Moodie, K.B. and Beswick, A.R., 2001. Using spatial interpolation to construct a comprehensive archive of Australian climate data. *Environmental Modelling & Software*, *16*(4), 309-330.

Jin, D., Guan, Z., Huo, L. and Wang, X., 2017. Possible impacts of Spring Sea surface temperature anomalies over South Indian Ocean on summer rainfall in Guangdong-Guangxi region of China. *Climate Dynamics*, *49*(9-10), 3075-3090.

Jones, L. and Tanner, T., 2017. 'Subjective resilience': using perceptions to quantify household resilience to climate extremes and disasters. *Regional Environmental Change*, *17*(1), 229-243.

Kane, R.P., 2009. Periodicities, ENSO effects and trends of some South African rainfall series: an update. *South African Journal of Science*, *105*(5-6), 199-207.

Keskin, M., Dalgin, S. and Dogru, A.O., 2017. EVALUATING THE EFFECT OF TOPOGRAPHY ON SPATIAL INTERPOLATION OF METEOROLOGICAL DATA. *FRESENIUS ENVIRONMENTAL BULLETIN*, *26(1),* 64-68.

Keskiner, A.D., Çetin, M. and Nagano, T., 2019. Mapping spatio-temporal tendencies of climate types in Geographic Information Systems (GIS) media: A case study in Şanlıurfa and its environs. *Mustafa Kemal Üniversitesi Tarım Bilimleri Dergisi*, *24*, 232-240.

Khalafzai, M.A.K., McGee, T.K. and Parlee, B., 2019. Flooding in the James Bay region of Northern Ontario, Canada: Learning from traditional knowledge of Kashechewan First Nation. *International Journal of Disaster Risk Reduction*, *36*, 1-17.

Khan, M.Z.K., Rahman, A., Rahman, M.A. and Renzaho, A.M., 2021. Impact of droughts on child mortality: a case study in southern African countries. *Natural Hazards*, 1-14.

Khodri, M., Izumo, T., Vialard, J., Janicot, S., Cassou, C., Lengaigne, M., Mignot, J., Gastineau, G., Guilyardi, E., Lebas, N. and Robock, A., 2017. Tropical explosive volcanic eruptions can trigger El Niño by cooling tropical Africa. *Nature Communications,* 8(1), 1-13.

Khosravi, Y., Zamani, A.A., Parizanganeh, A.H. and Yaftian, M.R., 2018. Assessment of spatial distribution pattern of heavy metals surrounding a lead and zinc production plant in Zanjan Province, Iran. *Geoderma Regional*, *12*, 10-17.

Kikuchi, K., 2020. Extension of the bimodal intraseasonal oscillation index using JRA-55 reanalysis. *Climate Dynamics*, *54*(1), 919-933.

Klotzbach, P.J. and Oliver, E.C., 2015. Modulation of Atlantic basin tropical cyclone activity by the Madden–Julian oscillation (MJO) from 1905 to 2011. *Journal of Climate*, *28*(1), 204-217.

Kolusu, S.R., Shamsudduha, M., Todd, M.C., Taylor, R.G., Seddon, D., Kashaigili, J.J., Ebrahim, G.Y., Cuthbert, M.O., Sorensen, J.P., Villholth, K.G. and MacDonald, A.M., 2019. The El Niño event of 2015–2016: climate anomalies and their impact on groundwater resources in East and southern Africa. *Hydrology and Earth System Sciences*, *23*(3), 1751-1762.

Koplitz, S.N., Mickley, L.J., Jacob, D.J., Marlier, M.E., DeFries, R.S., Gaveau, D.L., Locatelli, B., Reid, J.S., Xian, P. and Myers, S.S., 2018. Role of the Madden-Julian Oscillation in the transport of smoke from Sumatra to the Malay Peninsula during severe non-El Nino haze events. *Journal of Geophysical Research: Atmospheres*, *123*(11), 6282-6294.

Krivoruchko, K. and Gotay, C.A., 2003, July. Using spatial statistics in GIS. *In International Congress on Modelling and Simulation,* 713-736.

Kruger, A.C. and Nxumalo, M.P., 2017. Historical rainfall trends in South Africa: 1921–2015. *Water SA*, *43*(2), 285-297.

Kumar, P.R. and Kamra, A.K., 2012. Variability of lightning activity in South/Southeast Asia during 1997–98 and 2002–03 El Nino/La Nina events. *Atmospheric Research*, *118*, 84-102.

Kumar, U., Singh, S., Bisht, J.K. and Kant, L., 2021. Use of meteorological data for identification of agricultural drought in Kumaon region of Uttarakhand. *Journal of Earth System Science*, *130*(3), 1-13.

Kundu, A. and Dutta, D., 2011. Monitoring desertification risk through climate change and human interference using remote sensing and GIS techniques. *International Journal of Geomatics and Geosciences*, *2*(1), 21-33.

Kuroda, Y., 2018. On the origin of the solar cycle modulation of the Southern Annular Mode. *Journal of Geophysical Research: Atmospheres*, *123*(4), 1959-1969.

Kusangaya, S., Mazvimavi, D., Shekede, M.D., Masunga, B., Kunedzimwe, F. and Manatsa, D., 2021. Climate Change Impact on Hydrological Regimes and Extreme Events in Southern Africa. *Climate Change and Water Resources in Africa: Perspectives and Solutions Towards an Imminent Water Crisis*, 87-129.

Kusangaya, S., Warburton, M.L., Van Garderen, E.A. and Jewitt, G.P., 2014. Impacts of climate change on water resources in southern Africa: A review. *Physics and Chemistry of the Earth, Parts A/B/C*, *67*, 47-54.

Lakhraj-Govender, R. and Grab, S.W., 2019. Assessing the impact of El Niño–Southern Oscillation on South African temperatures during austral summer. *International Journal of Climatology*, *39*(1), 143-156.

Latimer, C.E. and Zuckerberg, B., 2019. How extreme is extreme? Demographic approaches inform the occurrence and ecological relevance of extreme events. *Ecological Monographs*, *89*(4), 1-15.

Lekprichakul, T., 2008. Impact of 2004/2005 Drought on Zambia's Agricultural Production: Preliminary Results, 2008(002), 1-26.

Lenton, T.M., Rockström, J., Gaffney, O., Rahmstorf, S., Richardson, K., Steffen, W. and Schellnhuber, H.J., 2019. Climate tipping points—too risky to bet against, *Nature*, 1-5.

Li, J.P., and Wang, J.X., 2016. Impacts of annular modes on extreme climate events over the East Asian monsoon region. *Dynamics and Predictability of Large-Scale, High-Impact Weather and Climate Events,* 2, 343-353.

Li, X. and Hu, Q., 2019. Spatiotemporal changes in extreme precipitation and its dependence on topography over the Poyang Lake basin, China. *Advances in Meteorology*, *2019*, 1-15.

Li, X., Zhang, K., Gu, P., Feng, H., Yin, Y., Chen, W. and Cheng, B., 2021. Changes in precipitation extremes in the Yangtze River Basin during 1960–2019 and the association with global warming, ENSO, and local effects. *Science of the Total Environment*, *760*, 1-13.

Li, Y., Han, W., Hu, A., Meehl, G.A. and Wang, F., 2018. Multidecadal changes of the upper Indian Ocean heat content during 1965–2016. *Journal of Climate,* 31(19), 7863-7884.

Lian, T., Chen, D., Ying, J., Huang, P. and Tang, Y., 2018. Tropical Pacific trends under global warming: El Niño-like or La Niña-like? *National Science Review,* 5(6), 810-812.

Liang, L. and Gong, P., 2017. Climate change and human infectious diseases: A synthesis of research findings from global and spatio-temporal perspectives. *Environment international*, 103, 99-108.

Libanda, B., Zheng, M. and Ngonga, C., 2019. Spatial and temporal patterns of drought in Zambia. *Journal of Arid Land*, *11*(2), 180-191.

Lim, E.P., Hendon, H.H., Hope, P., Chung, C., Delage, F. and McPhaden, M.J., 2019. Continuation of tropical Pacific Ocean temperature trend may weaken extreme El Niño and its linkage to the Southern Annular Mode. *Scientific Reports,* 9(1), 1-15.

Lin, I.I., Camargo, S.J., Patricola, C.M., Boucharel, J., Chand, S., Klotzbach, P., Chan, J.C., Wang, B., Chang, P., Li, T. and Jin, F.F., 2020. ENSO and tropical cyclones. *El Niño Southern Oscillation in a Changing Climate*, 377-408.

Logan, R. and Silberbauer, B.G., 2019. Kalahari Desert | Map & Facts. [Online] Encyclopaedia Britannica. Available at: <https://www.britannica.com/place/Kalahari-Desert> [Accessed 8 May 2020].

Lotha, G., 2020. Limpopo | Province, South Africa. [Online] Encyclopaedia Britannica. Available at: <https://www.britannica.com/place/Limpopo> [Accessed 28 June 2020].

Lovino, M.A., Müller, O.V., Berbery, E.H. and Müller, G.V., 2018. How have daily climate extremes changed in the recent past over north-eastern Argentina? *Global and planetary change,* 168, 78-97.

Lüdecke, H.J., Müller-Plath, G., Wallace, M.G. and Lüning, S., 2021. Decadal and multidecadal natural variability of African rainfall. *Journal of Hydrology: Regional Studies*, *34*, 1-23.

Luo, W., Taylor, M.C. and Parker, S.R., 2008. A comparison of spatial interpolation methods to estimate continuous wind speed surfaces using irregularly distributed data from England and Wales. *International Journal of Climatology: A Journal of the Royal Meteorological Society*, *28*(7), 947-959.

Ly, S., Charles, C. and Degre, A., 2011. Geostatistical interpolation of daily rainfall at catchment scale: the use of several variogram models in the Ourthe and Ambleve catchments, Belgium. *Hydrology and Earth System Sciences*, *15*(7), 2259-2274.

Ly, S., Charles, C. and Degré, A., 2013. Different methods for spatial interpolation of rainfall data for operational hydrology and hydrological modeling at watershed scale: a review. *Biotechnologie, Agronomie, Société et Environnement*, *17*(2), 392-406.

Lynas, M., Houlton, B.Z. and Perry, S., 2021. Greater than 99% consensus on human caused climate change in the peer-reviewed scientific literature. *Environmental Research Letters*, *16*(11), 1-8.

Lyra, G.B., Correia, T.P., de Oliveira-Júnior, J.F. and Zeri, M., 2018. Evaluation of methods of spatial interpolation for monthly rainfall data over the state of Rio de Janeiro, Brazil. *Theoretical and Applied Climatology*, *134*(3), 955-965.

Lyu, K., Zhang, X., Church, J.A., Hu, J. and Yu, J.Y., 2017. Distinguishing the quasi-decadal and multidecadal sea level and climate variations in the Pacific: implications for the ENSO-like low-frequency variability. *Journal of Climate,* 30(13), 5097-5117.

Ma, Z., Xie, J., Li, H., Sun, Q., Si, Z., Zhang, J. and Guo, J., 2017. The role of data analysis in the development of intelligent energy networks. *IEEE Network*, *31*(5), 88-95.

Machiwal, D., Cloutier, V., Güler, C. and Kazakis, N., 2018. A review of GIS-integrated statistical techniques for groundwater quality evaluation and protection. *Environmental Earth Sciences*, *77*(19), 1-30.

Madsen, H., Lawrence, D., Lang, M., Martinkova, M. and Kjeldsen, T.R., 2014. Review of trend analysis and climate change projections of extreme precipitation and floods in Europe. *Journal of Hydrology*, *519*, 3634-3650.

Madzudzo, R., Toteng, E. and Mulalu, M., 2018. FLOOD DISASTER VULNERABILITY ASSESSMENT OF PHYSICAL AND ENVIRONMENTAL FACTORS IN RAMOTSWA AND TAUNG VILLAGES, BOTSWANA. *Botswana Journal of Technology*, *23*(1), 97-119.

Makondo, C.C. and Thomas, D.S., 2020. Seasonal and intra-seasonal rainfall and drought characteristics as indicators of climate change and variability in southern Africa: a focus on Kabwe and Livingstone in Zambia. *Theoretical and Applied Climatology*, 1-14.

Malherbe, J., Dieppois, B., Maluleke, P., Van Staden, M. and Pillay, D.L., 2016. South African droughts and decadal variability. *Natural Hazards*, 80(1), 657-681.

Malherbe, J., Smit, I.P., Wessels, K.J. and Beukes, P.J., 2020. Recent droughts in the Kruger National Park as reflected in the extreme climate index. *African Journal of Range & Forage Science*, *37*(1), 1-17.

Maloney, E.D., Adames, Á.F. and Bui, H.X., 2019. Madden–Julian oscillation changes under anthropogenic warming. *Nature Climate Change*, *9*(1), 26-33.

Manatsa, D. and Reason, C., 2017. ENSO–Kalahari Desert linkages on southern Africa summer surface air temperature variability. *International Journal of Climatology,* 37(4), 1728-1745.

Manatsa, D., Matarira, C.H. and Mukwada, G., 2011. Relative impacts of ENSO and Indian Ocean dipole/zonal mode on east SADC rainfall. *International Journal of Climatology*, *31*(4), 558-577.

Manatsa, D., Mushore, T. and Lenouo, A., 2017. Improved predictability of droughts over southern Africa using the standardized precipitation evapotranspiration index and ENSO. *Theoretical and Applied Climatology*, 127(1-2), 259-274.

Manhique, A.J., Reason, C.J.C., Silinto, B., Zucula, J., Raiva, I., Congolo, F. and Mavume, A.F., 2015. Extreme rainfall and floods in southern Africa in January 2013 and associated circulation patterns. *Natural Hazards*, *77*(2), 679-691.

Maracchi, G., Pérarnaud, V. and Kleschenko, A.D., 2000. Applications of geographical information systems and remote sensing in agrometeorology. *Agricultural and Forest Meteorology*, *103*(1-2), 119-136.

Mariano, D.A., dos Santos, C.A., Wardlow, B.D., Anderson, M.C., Schiltmeyer, A.V., Tadesse, T. and Svoboda, M.D., 2018. Use of remote sensing indicators to assess effects of drought and human-induced land degradation on ecosystem health in North-eastern Brazil. *Remote Sensing of Environment,* 213, 129-143.

Marshall, J., Kushnir, Y., Battisti, D., Chang, P., Czaja, A., Dickson, R., Hurrell, J., McCARTNEY, M.I.C.H.A.E.L., Saravanan, R. and Visbeck, M., 2001. North Atlantic climate variability: phenomena, impacts and mechanisms. *International Journal of Climatology: A Journal of the Royal Meteorological Society*, *21*(15), 1863-1898.

Maruatona, P.B. and Moses, O., 2021. Assessment of the onset, cessation, and duration of rainfall season over Botswana. *Modelling Earth Systems and Environment*, 1-12.

Marumbwa, F.M., Cho, M.A. and Chirwa, P.W., 2019. Analysis of spatio-temporal rainfall trends across southern African biomes between 1981 and 2016. *Physics and Chemistry of the Earth, Parts A/B/C*, *114*, 1-9.

Masih, I., Maskey, S., Mussá, F.E.F. and Trambauer, P., 2014. A review of droughts on the African continent: a geospatial and long-term perspective. *Hydrology and Earth System Sciences*, *18*(9), 3635-3649.

Mathbout, S., Lopez-Bustins, J.A., Martin-Vide, J., Bech, J. and Rodrigo, F.S., 2018. Spatial and temporal analysis of drought variability at several time scales in Syria during 1961–2012. *Atmospheric Research*, *200*, 153-168.

Maúre, G., Pinto, I., Ndebele-Murisa, M., Muthige, M., Lennard, C., Nikulin, G., Dosio, A. and Meque, A., 2018. The southern African climate under 1.5 C and 2 C of global warming as simulated by CORDEX regional climate models. *Environmental Research Letters*, *13*(6), 1-10.

Mazibuko, S.M., Mukwada, G. and Moeletsi, M.E., 2021. Assessing the frequency of drought/flood severity in the Luvuvhu River catchment, Limpopo Province, South Africa. *Water SA*, *47(2),* 172-184.

Mazvimavi, D., 2010. Investigating changes over time of annual rainfall in Zimbabwe. *Hydrology and Earth System Sciences*, *14*(12), 2671-2679.

Mberego, S., 2017. Temporal patterns of precipitation and vegetation variability over Botswana during extreme dry and wet rainfall seasons. *International Journal of Climatology,* 37(6), 2947-2960.

Mbokodo, I., Bopape, M.J., Chikoore, H., Engelbrecht, F. and Nethengwe, N., 2020. Heatwaves in the future warmer climate of South Africa. *Atmosphere*, *11*(7), 1-18.

McKee, J.L. and Binns, A.D., 2016. A review of gauge–radar merging methods for quantitative precipitation estimation in hydrology. *Canadian Water Resources Journal*, *41*(1-2), 186-203.

McKee, T.B., Doesken, N.J. and Kleist, J., 1993, January. The relationship of drought frequency and duration to time scales. In *Proceedings of the 8th Conference on Applied Climatology*, 17(22), 179-183.

McKenna, A., 2019. North West | Province, South Africa. [Online] Encyclopaedia Britannica. Available at: <https://www.britannica.com/place/North-West-province-South-Africa> [Accessed 8 May 2020].

McKenna, A., 2020. Gauteng | Province, South Africa. [Online] Encyclopaedia Britannica. Available at: <https://www.britannica.com/place/Gauteng> [Accessed 28 June 2020].

McKenna, A., 2020. Gauteng | Province, South Africa. [Online] Encyclopaedia Britannica. Available at: <https://www.britannica.com/place/Gauteng> [Accessed 28 June 2020].

Middleton, N., 2019. Variability and trends in dust storm frequency on decadal timescales: Climatic drivers and human impacts. *Geosciences*, *9*(6), 1-12.

Mind'je, R., Li, L., Amanambu, A.C., Nahayo, L., Nsengiyumva, J.B., Gasirabo, A. and Mindje, M., 2019. Flood susceptibility modelling and hazard perception in Rwanda. *International Journal of Disaster Risk Reduction*, *38*, 1-12.

Mishra, A.K. and Singh, V.P., 2010. A review of drought concepts. *Journal of hydrology*, *391*(1-2), 202-216.

Misra, A.K., 2014. Climate change and challenges of water and food security. *International Journal of Sustainable Built Environment*, *3*(1), 153-165.

Mlenga, D.H., Jordaan, A.J. and Mandebvu, B., 2019. Monitoring droughts in Eswatini: A spatiotemporal variability analysis using the Standard Precipitation Index. *Jàmbá: Journal of Disaster Risk Studies*, *11*(1), 1-11.

Moghbeli, A., Delbari, M. and Amiri, M., 2020. Application of a standardized precipitation index for mapping drought severity in an arid climate region, south-eastern Iran. *Arabian Journal of Geosciences*, *13*(5), 1-16.

Mogotsi, K., Nyangito, M.M. and Nyariki, D.M., 2013. The role of drought among agro-pastoral communities in a semi-arid environment: the case of Botswana. *Journal of Arid Environments*, *91*, 38-44.

Mohammed, R. and Scholz, M., 2019. Climate variability impact on the spatiotemporal characteristics of drought and Arid ityin arid and semi-arid regions. *Water Resources Management*, *33*(15), 5015-5033.

Mokarram, M. and Hojati, M., 2017. Using ordered weight averaging (OWA) aggregation for multi-criteria soil fertility evaluation by GIS (case study: southeast Iran). *Computers and Electronics in Agriculture*, *132*, 1-13.

Mondol, M., Haque, A., Ara, I. and Das, S.C., 2017. Meteorological drought index mapping in Bangladesh using standardized precipitation index during 1981–2010. *Advances in Meteorology*, *2017*, 1-18.

Monerie, P.A., Robson, J., Dong, B., Dieppois, B., Pohl, B. and Dunstone, N., 2019. Predicting the seasonal evolution of southern African summer precipitation in the DePreSys3 prediction system. *Climate Dynamics*, *52*(11), 6491-6510.

Montazerolghaem, M., Vervoort, W., Minasny, B. and McBratney, A., 2016. Long-term variability of the leading seasonal modes of rainfall in south-eastern Australia. *Weather and Climate Extremes,* 13, 1-14.

Morioka, Y., Tozuka, T. and Yamagata, T., 2011. On the growth and decay of the subtropical dipole mode in the South Atlantic. *Journal of Climate*, *24*(21), 5538-5554.

Moron, V., Robertson, A.W., Qian, J.H. and Ghil, M., 2015. Weather types across the Maritime Continent: From the diurnal cycle to interannual variations. *Frontiers in Environmental Science*, *2*, 65-73.

Mosalagae, D. and Mogotsi, K., 2013. Caught in a sandstorm: an assessment of pressures on communal pastoral livelihoods in the Kalahari Desert of Botswana. *Pastoralism: Research, Policy and Practice*, *3*(1), 1-20.

Moses, O. and Ramotonto, S., 2018. Assessing forecasting models on prediction of the tropical cyclone Dineo and the associated rainfall over Botswana. *Weather and Climate Extremes*, *21*, 102-109.

Moses, O., 2019. Weather systems influencing Botswana rainfall: the case of 9 December 2018 storm in Mahalapye, Botswana. *Modelling Earth Systems and Environment*, *5*(4), 1473-1480.

Mtilatila, L., Bronstert, A., Bürger, G. and Vormoor, K., 2020. Meteorological and hydrological drought assessment in Lake Malawi and Shire River basins (1970–2013). *Hydrological Sciences Journal*, *65*(16), 2750-2764.

Mukwada, G., 2018. Savanna ecosystems of southern Africa. *In Southern African Landscapes and Environmental Change*, 181-201.

Mulenga, H.M., Rouault, M. and Reason, C.J.C., 2003. Dry summers over northeastern South Africa and associated circulation anomalies. *Climate Research*, *25*(1), 29-41.

Munawar, H.S., 2020. Flood disaster management: Risks, technologies, and future directions. *Machine Vision Inspection Systems: Image Processing, Concepts, Methodologies and Applications*, *1*, 115-146.

Munday, C. and Washington, R., 2017. Circulation controls on southern African precipitation in coupled models: The role of the Angola low. *Journal of Geophysical Research: Atmospheres*, *122*(2), 861-877.

Muthusamy, M., Schellart, A., Tait, S. and Heuvelink, G.B., 2017. Geostatistical upscaling of rain gauge data to support uncertainty analysis of lumped urban hydrological models. *Hydrology and Earth System Sciences*, *21*(2), 1077-1091.

Mutiibwa, D., Vavrus, S.J., McAfee, S.A. and Albright, T.P., 2015. Recent spatiotemporal patterns in temperature extremes across conterminous United States. *Journal of Geophysical Research: Atmospheres*, *120*(15), 7378-7392.

Nangombe, S., Madyiwa, S. and Wang, J., 2018. Precursor conditions related to Zimbabwe's summer droughts. *Theoretical and Applied Climatology,* 131(1-2), 413-431.

Naoum, S. and Tsanis, I.K., 2004. Ranking spatial interpolation techniques using a GIS-based DSS. *Global Nest: The Int. J*, *6*(1), 1-20.

Nasirudeen, A.F., Kabo-bah, A.T., Amo-Boateng, M. and Karthikeyan, B., 2021. Analysis of drought patterns in the Tano river basin of Ghana. *Scientific African*, *13*, 1-13.

Negreiros, J., Painho, M., Aguilar, F. and Aguilar, M., 2010. Geographical information systems principles of ordinary kriging interpolator. *Journal of Applied Sciences*, *10*(11), 852-867.

Neukom, R., Nash, D.J., Endfield, G.H., Grab, S.W., Grove, C.A., Kelso, C., Vogel, C.H. and Zinke, J., 2014. Multi-proxy summer and winter precipitation reconstruction for southern Africa over the last 200 years. *Climate Dynamics*, *42*(9), 2713-2726.

Nash, D.J., Pribyl, K., Klein, J., Neukom, R., Endfield, G.H., Adamson, G.C. and Kniveton, D.R., 2016. Seasonal rainfall variability in southeast Africa during the nineteenth century reconstructed from documentary sources. *Climatic Change*, *134*(4), 605-619.

Ngongondo, C., Xu, C.Y., Gottschalk, L. and Alemaw, B., 2011. Evaluation of spatial and temporal characteristics of rainfall in Malawi: a case of data scarce region. *Theoretical and Applied Climatology*, *106*(1), 79-93.

Nicholson, S.E., 2017. Climate and climatic variability of rainfall over eastern Africa. *Reviews of Geophysics*, *55*(3), 590-635.

Nicholson, S.E., Leposo, D. and Grist, J., 2001. The relationship between El Niño and drought over Botswana. *Journal of Climate*, *14*(3), 323-335.

Niedzielski, T., 2014. El Niño/Southern Oscillation and selected environmental consequences. In *Advances in Geophysics*, 55, 77-122.

Nishimoto, E. and Yoden, S., 2017. Influence of the stratospheric quasi-biennial oscillation on the Madden–Julian oscillation during austral summer. *Journal of the Atmospheric Sciences,* 74(4), 1105-1125.

Njogu, H.W., 2021. Effects of floods on infrastructure users in Kenya. *Journal of Flood Risk Management*, 1-10.

Nkemelang, T., New, M. and Zaroug, M., 2018. Temperature and precipitation extremes under current, 1.5 C and 2.0 C global warming above pre-industrial levels over Botswana, and implications for climate change vulnerability. *Environmental Research Letters,* 13(6), 1-12.

Nobre, G.G., Muis, S., Veldkamp, T.I. and Ward, P.J., 2019. Achieving the reduction of disaster risk by better predicting impacts of El Niño and La Niña. *Progress in Disaster Science*, 1-6.

Nonjinge, G., 2018. Amidst drought, only half of Batswana are aware of climate change. *Afrobarometer Dispatch*, *264,* 1-10.

Notaro, M., 2018. Enhancement of vegetation-rainfall feedbacks on the Australian summer monsoon by the Madden–Julian Oscillation. *Climate Dynamics,* 51(7-8), 3093-3109.

Nowak, K., Hoerling, M., Rajagopalan, B. and Zagona, E., 2012. Colorado River basin hydro climatic variability. *Journal of Climate,* 25(12), 4389-4403.

Ogunrinde, A.T., Oguntunde, P.G., Olasehinde, D.A., Fasinmirin, J.T. and Akinwumiju, A.S., 2020. Drought spatiotemporal characterization using self-calibrating Palmer Drought Severity Index in the northern region of Nigeria. *Results in Engineering*, *5*, 1-12.

Ogwang, B.A., Ongoma, V., Shilenje, Z.W., Ramotubei, T.S., Letuma, M. and Ngaina, J.N., 2020. Influence of Indian Ocean dipole on rainfall variability and extremes over southern Africa. *MAUSAM*, *71*(4), 637-648.

Okumura, Y.M., Sun, T. and Wu, X., 2017. Asymmetric modulation of El Niño and La Niña and the linkage to tropical Pacific decadal variability. *Journal of Climate,* 30(12), 4705-4733.

Orti, M.V. and Negussie, K.G., 2019. Temporal statistical analysis and predictive modelling of drought and flood in Rundu–Namibia. *Climate Dynamics*, 53(3-4), 1247-1260.

Pachauri RK, Reisinger A, 2007 IPCC fourth assessment report. IPCC, Geneva, 1-73.

Paparrizos, S., Maris, F., Weiler, M. and Matzarakis, A., 2018. Analysis and mapping of present and future drought conditions over Greek areas with different climate conditions. *Theoretical and Applied Climatology*, *131*(1-2), 259-270.

Park, S., Kang, D., Yoo, C., Im, J. and Lee, M.I., 2020. Recent ENSO influence on East African drought during rainy seasons through the synergistic use of satellite and reanalysis data. *ISPRS Journal of Photogrammetry and Remote Sensing,* 162, 17-26.

Parry, D., 1989. Some effects of the 1981-87 drought on woody plants in Botswana. *Botswana Notes and Records*, *20*, 155-159.

Parsons, N., 2020. Botswana | History - Geography. [Online] Encyclopaedia Britannica. Available at: <https://www.britannica.com/place/Botswana> [Accessed 8 May 2020].

Pascale, S., Pohl, B., Kapnick, S.B. and Zhang, H., 2019. On the Angola low interannual variability and its role in modulating ENSO effects in southern Africa. *Journal of Climate*, *32*(15), 4783-4803.

Payab, A.H. and Türker, U., 2019. Comparison of standardized meteorological indices for drought monitoring at northern part of Cyprus. *Environmental Earth Sciences*, *78*(10), 1-19.

Pellicone, G., Caloiero, T., Modica, G. and Guagliardi, I., 2018. Application of several spatial interpolation techniques to monthly rainfall data in the Calabria region (southern Italy). *International Journal of Climatology*, *38*(9), 3651-3666.

Phillips, D.L., Dolph, J. and Marks, D., 1992. A comparison of geostatistical procedures for spatial analysis of precipitation in mountainous terrain. *Agricultural and Forest Meteorology*, *58*(1-2), 119-141.

Phora, K., 2018. *Inter-seasonal and intra-seasonal rainfall variability in the North West Province South Africa* (Doctoral dissertation, North-West University (South Africa)).

Pinto, I., Lennard, C., Tadross, M., Hewitson, B., Dosio, A., Nikulin, G., Panitz, H.J. and Shongwe, M.E., 2016. Evaluation and projections of extreme precipitation over southern Africa from two CORDEX models. *Climatic Change*, *135*(3-4), 655-668.

Pohl, B. and Fauchereau, N., 2012. The southern annular mode seen through weather regimes. *Journal of Climate,* 25(9), 3336-3354.

Pohl, B., Dieppois, B., Crétat, J., Lawler, D. and Rouault, M., 2018. From synoptic to interdecadal variability in southern African rainfall: toward a unified view across time scales. *Journal of Climate,* 31(15), 5845-5872.

Pohl, B., Richard, Y. and Fauchereau, N., 2007. Influence of the Madden–Julian oscillation on southern African summer rainfall. *Journal of Climate*, *20*(16), 4227-4242.

Pomposi, C., Funk, C., Shukla, S., Harrison, L. and Magadzire, T., 2018. Distinguishing southern Africa precipitation response by strength of El Niño events and implications for decision-making. *Environmental Research Letters*, *13*(7), 1-13.

Pourasghar, F., Tozuka, T., Ghaemi, H., Oettli, P., Jahanbakhsh, S. and Yamagata, T., 2015. Influences of the MJO on intraseasonal rainfall variability over southern Iran. *Atmospheric Science Letters*, *16*(2), 110-118.

Prakash, S., Seshadri, A., Srinivasan, J. and Pai, D.S., 2019. A new parameter to assess impact of rain gauge density on uncertainty in the estimate of monthly rainfall over India. *Journal of Hydrometeorology*, *20*(5), 821-832.

Pulwarty, R.S. and Melis, T.S., 2001. Climate extremes and adaptive management on the Colorado River: lessons from the 1997–1998 ENSO event. *Journal of Environmental Management,* 63(3), 307-324.

Qin, M., Dai, A., Li, D. and Hua, W., 2020. Understanding the inter-decadal variability of autumn precipitation over North Central China using model simulations. *International Journal of Climatology,* 40(2), 874-886.

Rao, J., Yu, Y., Guo, D., Shi, C., Chen, D. and Hu, D., 2019. Evaluating the Brewer–Dobson circulation and its responses to ENSO, QBO, and the solar cycle in different reanalyses. *Earth and Planetary Physics*, *3*(2), 166-181.

Raphaldini, B., Teruya, A.S., Leite da Silva Dias, P., Massaroppe, L. and Takahashi, D.Y., 2021. Stratospheric ozone and quasi-biennial oscillation (QBO) interaction with the tropical troposphere on intraseasonal and interannual timescales: a normal-mode perspective. *Earth System Dynamics*, *12*(1), 83-101.

Rapolaki, R.S., Blamey, R.C., Hermes, J.C. and Reason, C.J.C., 2020. Moisture sources associated with heavy rainfall over the Limpopo River Basin, southern Africa. *Climate Dynamics*, *55*(5), 1473-1487.

Rapolaki, R.S., Blamey, R.C., Hermes, J.C. and Reason, C.J.C., 2021. Moisture sources and transport during an extreme rainfall event over the Limpopo River Basin, southern Africa. *Atmospheric Research*, *264*, 1-17.

Rashid, H.A., 2020. Factors affecting ENSO predictability in a linear empirical model of tropical air-sea interactions. *Scientific Reports*, 10(1), 1-10.

Ratna, S.B., Behera, S., Ratnam, J.V., Takahashi, K. and Yamagata, T., 2013. An index for tropical temperate troughs over southern Africa. *Climate Dynamics,* 41(2), 421-441.

Reason, C.J. and Smart, S., 2015. Tropical southeast Atlantic warm events and associated rainfall anomalies over southern Africa. *Frontiers in Environmental Science*, *3*, 1-11.

Reason, C.J.C. and Rouault, M., 2002. ENSO-like decadal variability and South African rainfall. *Geophysical Research Letters,* 29(13), 1-16.

Reason, C.J.C., 2016. The Bolivian, Botswana, and Bilybara Highs and southern Hemisphere drought/floods. *Geophysical Research Letters,* 43(3), 1280-1286.

Reason, C.J.C., 2019. Low-frequency variability in the Botswana High and southern African regional climate. *Theoretical and Applied Climatology,* 137(1-2), 1321-1334.

Reddy, K.B. and Venkatramana, P., 2018. Comparison of different spatial interpolation techniques of field measurements to construct radio environment maps. *Int. J. Future Gener. Commun. Netw*, *11*, 21-31.

Riedel, F., Henderson, A.C., Heußner, K.U., Kaufmann, G., Kossler, A., Leipe, C., Shemang, E. and Taft, L., 2014. Dynamics of a Kalahari long-lived mega-lake system: hydromorphological and limnological changes in the Makgadikgadi Basin (Botswana) during the terminal 50 ka. *Hydrobiologia,* 739(1), 25-53.

Rogan, J. and Chen, D., 2004. Remote sensing technology for mapping and monitoring land-cover and land-use change. *Progress in Planning*, *61*(4), 301-325.

Rouault, M., Illig, S., Lübbecke, J. and Koungue, R.A.I., 2018. Origin, development and demise of the 2010–2011 Benguela Niño. *Journal of Marine Systems*, *188*, 39-48.

Ryazanova, A.A., Okladnikov, I.G. and Gordov, E.P., 2017, November. Integration of modern statistical tools for the analysis of climate extremes into the web-GIS “CLIMATE”. In *IOP Conference Series: Earth and Environmental Science*, 96(1), 1755-1307.

Salekin, S., Burgess, J.H., Morgenroth, J., Mason, E.G. and Meason, D.F., 2018. A comparative study of three non-geostatistical methods for optimising digital elevation model interpolation. *ISPRS International Journal of Eo-Information*, *7(8),* 1-15.

Salhi, A., Martin-Vide, J., Benhamrouche, A., Benabdelouahab, S., Himi, M., Benabdelouahab, T. and Ponsati, A.C., 2019. Rainfall distribution and trends of the daily precipitation concentration index in northern Morocco: a need for an adaptive environmental policy. *SN Applied Sciences*, *1*(3), 1-15.

Salinger, J., Hobday, A.J., Matear, R.J., O’Kane, T.J., Risbey, J.S., Dunstan, P., Eveson, J.P., Fulton, E.A., Feng, M., Plaganyi, E.E. and Poloczanska, E.S., 2016. Decadal-scale forecasting of climate drivers for marine applications. *In Advances in Marine Biology,* 74, 1-68.

Sangani, M.F., Khojasteh, D.N. and Owens, G., 2019. Dataset characteristics influence the performance of different interpolation methods for soil salinity spatial mapping. *Environmental Monitoring and Assessment*, *191*(11), 1-12.

Sa-venues.com. 2020. North West Province, South Africa. [Online] Available at: <https://www.sa-venues.com/north_west_province.htm> [Accessed 8 May 2020].

Schubert, S.D., Stewart, R.E., Wang, H., Barlow, M., Berbery, E.H., Cai, W., Hoerling, M.P., Kanikicharla, K.K., Koster, R.D., Lyon, B. and Mariotti, A., 2016. Global meteorological drought: A synthesis of current understanding with a focus on SST drivers of precipitation deficits. *Journal of Climate*, *29*(11), 3989-4019.

Schubert, S.D., Stewart, R.E., Wang, H., Barlow, M., Berbery, E.H., Cai, W., Hoerling, M.P., Kanikicharla, K.K., Koster, R.D., Lyon, B. and Mariotti, A., 2016. Global meteorological drought: a synthesis of current understanding with a focus on SST drivers of precipitation deficits. *Journal of Climate,* 29(11), 3989-4019.

Seekings, J., 2017. The discourse of dependency and the agrarian roots of welfare doctrines in Africa: The case of Botswana. *Sozialpolitik. ch*, *2*(2),2-4.

Seo, Y., Kim, S. and Singh, V.P., 2015. Estimating spatial precipitation using regression kriging and artificial neural network residual kriging (RKNNRK) hybrid approach. *Water Resources Management*, *29*(7), 2189-2204.

Serra, Y.L., Jiang, X., Tian, B., Amador-Astua, J., Maloney, E.D. and Kiladis, G.N., 2014. Tropical intraseasonal modes of the atmosphere. *Annual Review of Environment and Resources*, *39*, 189-215.

Serumaga-Zake, E., 2020. *The impact of rainfall variability on subsistence farmers in the North West Province, South Africa* (Doctoral dissertation, North-West University (South Africa)).

Shen, S.S., Dzikowski, P., Li, G. and Griffith, D., 2001. Interpolation of 1961–97 daily temperature and precipitation data onto Alberta polygons of ecodistrict and soil landscapes of Canada. *Journal of Applied Meteorology,* 40(12), 2162-2177.

Shinn, J.E., 2016. Adaptive environmental governance of changing social-ecological systems: Empirical insights from the Okavango Delta, Botswana. *Global Environmental Change,* 40, 50-59.

Shrestha, A.B., Bajracharya, S.R., Sharma, A.R., Duo, C. and Kulkarni, A., 2017. Observed trends and changes in daily temperature and precipitation extremes over the Koshi river basin 1975–2010. *International Journal of Climatology*, *37*(2), 1066-1083.

Siart, C., Bubenzer, O. and Eitel, B., 2009. Combining digital elevation data (SRTM/ASTER), high resolution satellite imagery (Quickbird) and GIS for geomorphological mapping: A multi-component case study on Mediterranean karst in Central Crete. *Geomorphology*, *112*(1-2), 106-121.

Sillmann, J., Thorarinsdottir, T., Keenlyside, N., Schaller, N., Alexander, L.V., Hegerl, G., Seneviratne, S.I., Vautard, R., Zhang, X. and Zwiers, F.W., 2017. Understanding, modelling and predicting weather and climate extremes: Challenges and opportunities. *Weather and climate extremes*, *18*, 65-74.

Singh, U. and Sharma, P.K., 2021. Drought forecasting using the stochastic model in the Betwa river basin, India. *Modeling Earth Systems and Environment*, 1-16.

Sithole, A. and Murewi, C.T., 2009. Climate variability and change over southern Africa: impacts and challenges. *African Journal of Ecology*, *47*, 17-20.

Sobral, B.S., de Oliveira-Júnior, J.F., de Gois, G., Pereira-Júnior, E.R., de Bodas Terassi, P.M., Muniz-Júnior, J.G.R., Lyra, G.B. and Zeri, M., 2019. Drought characterization for the state of Rio de Janeiro based on the annual SPI index: trends, statistical tests and its relation with ENSO. *Atmospheric research, 220*, 141-154.

Stan, C., Straus, D.M., Frederiksen, J.S., Lin, H., Maloney, E.D. and Schumacher, C., 2017. Review of tropical-extratropical teleconnections on Intraseasonal time scales. *Reviews of Geophysics*, *55*(4), 902-937.

Statistics Botswana. Botswana Environment Statistics: Natural Disaster Digest 2017; Ministry of Finance and Development Planning: Gaborone, Botswana, 2018, 10-44.

Stocker, T.F., D. Qin, G.-K. Plattner, M. Tignor, S.K. Allen, J. Boschung, A. Nauels, Y. Xia, V. Bex and P.M. Midgley, 2013. *Climate Change 2013: The Physical Science Basis. Contribution of Working Group I to the Fifth Assessment Report of the Intergovernmental Panel on Climate Change* Cambridge University Press, Cambridge, United Kingdom and New York, NY, USA.

Sun, F., Mejia, A., Zeng, P. and Che, Y., 2019. Projecting meteorological, hydrological and agricultural droughts for the Yangtze River basin. *Science of the Total Environment*, *696*, 1-15.

Sun, T. and Okumura, Y.M., 2020. Impact of ENSO-Like Tropical Pacific Decadal Variability on the Relative Frequency of El Niño and La Niña Events. *Geophysical Research Letters,* 47(3), 1-10.

Szatmári, G. and Pásztor, L., 2019. Comparison of various uncertainty modelling approaches based on geostatistics and machine learning algorithms. *Geoderma*, *337*, 1329-1340.

Székely, E., Giannakis, D. and Majda, A.J., 2016. Extraction and predictability of coherent intraseasonal signals in infrared brightness temperature data. *Climate Dynamics,* 46(5-6), 1473-1502.

Tabari, H., 2020. Climate change impact on flood and extreme precipitation increases with water availability. *Scientific reports*, *10*(1), 1-10.

Tabios III, G.Q. and Salas, J.D., 1985. A comparative analysis of techniques for spatial interpolation of precipitation 1. *JAWRA Journal of the American Water Resources Association*, *21*(3), 365-380.

Tadross, M., Engelbrecht, F.A., Jack, C., Wolski, P. and Davis, C.L., 2017. Projected climate change futures for southern Africa*. CSIR*, 1-11.

Takahashi, K. and Martínez, A.G., 2019. The very strong coastal El Niño in 1925 in the far-eastern Pacific. *Climate Dynamics,* 52(12), 7389-7415.

Tanyanyiwa, V.I. and Mufunda, E., 2020. Gendered impacts of climate change: The Zimbabwe perspective. *Climate Action*, 543-555.

Tapiador, F.J., Turk, F.J., Petersen, W., Hou, A.Y., García-Ortega, E., Machado, L.A., Angelis, C.F., Salio, P., Kidd, C., Huffman, G.J. and De Castro, M., 2012. Global precipitation measurement: Methods, datasets and applications. *Atmospheric Research*, *104*, 70-97.

Taschetto, A.S., Ummenhofer, C.C., Stuecker, M.F., Dommenget, D., Ashok, K., Rodrigues, R.R. and Yeh, S.W., 2020. ENSO atmospheric teleconnections. *El Niño Southern Oscillation in a Changing Climate*, 309-335.

Terray, P. and Dominiak, S., 2005. Indian Ocean sea surface temperature and El Niño–Southern Oscillation: A new perspective. *Journal of Climate,* 18(9), 1351-1368.

Thiessen, A.H., 1911. Precipitation averages for large areas. *Monthly Weather Review*, *39*(7).1082-1089.

Thomson, M.C., Muñoz, Á.G., Cousin, R. and Shumake-Guillemot, J., 2018. Climate drivers of vector-borne diseases in Africa and their relevance to control programmes. *Infectious Diseases of Poverty*, *7*(1), 1-22.

Thornton, C.L., 2014. *The relative frequency of Rossby wave train triggering mechanisms associated with downstream development over Europe*. NAVAL POSTGRADUATE SCHOOL MONTEREY CA, 1-139.

Todd, M. and Washington, R., 1999. Circulation anomalies associated with tropical-temperate troughs in southern Africa and the south West Indian Ocean. *Climate dynamics*, *15*(12), 937-951.

Todd, M.C., Washington, R. and Palmer, P.I., 2004. Water vapour transport associated with tropical–temperate trough systems over southern Africa and the southwest Indian Ocean. International Journal of Climatology: *A Journal of the Royal Meteorological Society,* 24(5), 555-568.

Toms, B.A., Barnes, E.A., Maloney, E.D. and van den Heever, S.C., 2020. The Global Teleconnection Signature of the Madden-Julian Oscillation and Its Modulation by the Quasi-Biennial Oscillation. *Journal of Geophysical Research: Atmospheres*, *125*(7), 1-23.

Trangmar, B.B., Yost, R.S. and Uehara, G., 1986. Application of geostatistics to spatial studies of soil properties. *Advances in agronomy*, *38*, 45-94.

Tshililo, F.P., 2017. *Rainy season characteristics with reference to maize production for the Luvuvhu river catchment, Limpopo Province, South Africa* (Doctoral dissertation, University of KwaZulu-Natal (South Africa).

Tudhope, A.W., Chilcott, C.P., McCulloch, M.T., Cook, E.R., Chappell, J., Ellam, R.M., Lea, D.W., Lough, J.M. and Shimmield, G.B., 2001. Variability in the El Niño-Southern Oscillation through a glacial-interglacial cycle. *Science*, *291*(5508), 1511-1517.

Tyrrell, N.L., Koskentausta, J.M. and Karpechko, A.Y., 2021. Sudden stratospheric warmings during El Niño and La Niña: sensitivity to model biases. *Weather and Climate Dynamics Discussions,* 1-20.

Ummenhofer, C.C. and Meehl, G.A., 2017. Extreme weather and climate events with ecological relevance: a review. *Philosophical Transactions of the Royal Society B: Biological Sciences*, *372*(1723), 1-13.

Ustrnul, Z. and Czekierda, D., 2005. Application of GIS for the development of climatological air temperature maps: an example from Poland. *Meteorological Applications*, *12*(1), 43-50.

Van Aalst, M.K., 2006. The impacts of climate change on the risk of natural disasters. *Disasters*, *30*(1), 5-18.

Van Loon, A.F., 2015. Hydrological drought explained. *Wiley Interdisciplinary Reviews: Water*, *2*(4), 359-392.

van Wilgen, N.J., Goodall, V., Holness, S., Chown, S.L. and McGeoch, M.A., 2016. Rising temperatures and changing rainfall patterns in South Africa's national parks. *International Journal of Climatology*, *36*(2), 706-721.

Vicente-Serrano, S.M., López-Moreno, J.I., Gimeno, L., Nieto, R., Morán-Tejeda, E., Lorenzo-Lacruz, J., Beguería, S. and Azorin-Molina, C., 2011. A multiscalar global evaluation of the impact of ENSO on droughts. *Journal of Geophysical Research: Atmospheres,* 116(D20), 1-23.

Vitart, F. and Robertson, A.W., 2018. The sub-seasonal to seasonal prediction project (S2S) and the prediction of extreme events. *Climate and Atmospheric Science*, *1*(1), 1-7.

Wang, C., 2019. Three-ocean interactions and climate variability: a review and perspective. *Climate Dynamics,* 53(7-8), 5119-5136.

Wang, T., Hamann, A., Spittlehouse, D. and Carroll, C., 2016. Locally downscaled and spatially customizable climate data for historical and future periods for North America. *PloS one*, *11*(6), 1-17.

Wang, W., Ertsen, M.W., Svoboda, M.D. and Hafeez, M., 2016. Propagation of drought: from meteorological drought to agricultural and hydrological drought, *Advances in Meteorology*, 1-6.

Washington, R. and Preston, A., 2006. Extreme wet years over southern Africa: Role of Indian Ocean sea surface temperatures. *Journal of Geophysical Research: Atmospheres,* 111(D15), 1-15.

Wei, Y., Ren, H.L., Mu, M. and Fu, J.X., 2020. Nonlinear optimal moisture perturbations as excitation of primary MJO events in a hybrid coupled climate model. *Climate Dynamics*, *54*(1), 675-699.

Wilson, S.S. and Mohanakumar, K., 2021. Influence of subtropical circulation systems on the changing El Niño-Indian summer monsoon relationship. *Atmospheric Research*, *252*, 1-17.

Wiston, M. and Mphale, K.M., 2019. Mesoscale convective systems: A case scenario of the 'heavy rainfall'event of 15–20 January 2013 over Southern Africa. *Climate*, *7*(6), 1-20.

Woodworth, P.L., Melet, A., Marcos, M., Ray, R.D., Wöppelmann, G., Sasaki, Y.N., Cirano, M., Hibbert, A., Huthnance, J.M., Monserrat, S. and Merrifield, M.A., 2019. Forcing factors affecting sea level changes at the coast. *Surveys in Geophysics*, 40(6), 1351-1397.

Wu, J., Miao, C., Zheng, H., Duan, Q., Lei, X. and Li, H., 2018. Meteorological and hydrological drought on the Loess Plateau, China: Evolutionary characteristics, impact, and propagation. *Journal of Geophysical Research: Atmospheres*, *123*(20), 11569-11584.

Wu, T. and Li, Y., 2013. Spatial interpolation of temperature in the United States using residual kriging. *Applied Geography*, *44*, 112-120.

Wu, X., Okumura, Y.M. and DiNezio, P.N., 2019. What Controls the Duration of El Niño and La Niña Events? *Journal of Climate*, 32(18), 5941-5965.

Xavier, A.C., King, C.W. and Scanlon, B.R., 2016. Daily gridded meteorological variables in Brazil (1980–2013). *International Journal of Climatology*, *36*(6), 2644-2659.

Xulu, N.G., Chikoore, H., Bopape, M.J.M. and Nethengwe, N.S., 2020. Climatology of the Mascarenes high and its influence on weather and climate over southern Africa. *Climate*, *8*(7), 1-11.

Yang, X., Xie, X., Liu, D.L., Ji, F. and Wang, L., 2015. Spatial interpolation of daily rainfall data for local climate impact assessment over the greater Sydney region. *Advances in Meteorology, 2015*, 1-12.

Yang, Y.M. and Wang, B., 2019. Improving MJO simulation by enhancing the interaction between boundary layer convergence and lower tropospheric heating. *Climate Dynamics*, *52*(7), 4671-4693.

Yeo, S.R. and Kim, K.Y., 2015. Decadal changes in the southern Hemisphere Sea surface temperature in association with El Niño–Southern Oscillation and Southern Annular Mode. *Climate Dynamics,* 45(11-12), 3227-3242.

Yoo, C. and Son, S.W., 2016. Modulation of the boreal wintertime Madden-Julian oscillation by the stratospheric quasi-biennial oscillation. *Geophysical Research Letters*, *43*(3), 1392-1398.

Yu, M., Li, Q., Hayes, M.J., Svoboda, M.D. and Heim, R.R., 2014. Are droughts becoming more frequent or severe in China based on the standardized precipitation evapotranspiration index: 1951–2010? *International Journal of Climatology*, *34*(3), 545-558.

Yuan, X. and Yonekura, E., 2011. Decadal variability in the southern Hemisphere. Journal of Geophysical Research: *Atmospheres*, 116(D19), 1-12.

Yuan, Xiaojun, Michael R. Kaplan, and Mark A. Cane. The interconnected global climate system—A review of tropical–polar teleconnections. *Journal of Climate,* 31(15), 5765-5792.

Zaitchik, B.F., 2017. Madden-Julian Oscillation impacts on tropical African precipitation. *Atmospheric Research*, *184*, 88-102.

Zhang, C., 2013. Madden–Julian oscillation: Bridging weather and climate. *Bulletin of the American Meteorological Society*, *94*(12), 1849-1870.

Zhang, L., Han, W., Li, Y. and Lovenduski, N.S., 2019. Variability of sea level and upper-ocean heat content in the Indian Ocean: Effects of subtropical Indian Ocean dipole and ENSO. *Journal of Climate*, *32*(21), 7227-7245.

Zhang, L., Kuczera, G., Kiem, A.S. and Willgoose, G., 2018. Using paleoclimate reconstructions to analyse hydrological epochs associated with Pacific decadal variability. *Hydrology and Earth System Sciences,* 22(12), 6399-6414.

Zhang, L.Y., Du, Y., Cai, W., Chen, Z., Tozuka, T. and Yu, J.Y., 2020. Triggering the Indian Ocean Dipole From the southern Hemisphere. *Geophysical Research Letters*, *47*(15), 1-25.

Zhang, N., Feng, M., Hendon, H.H., Hobday, A.J. and Zinke, J., 2017. Opposite polarities of ENSO drive distinct patterns of coral bleaching potentials in the southeast Indian Ocean. *Scientific Reports,* 7(1), 1-10.

Zhang, Q., Holmgren, K. and Sundqvist, H., 2015. Decadal rainfall dipole oscillation over southern Africa modulated by variation of austral summer Land–Sea contrast along the East Coast of Africa. *Journal of the Atmospheric Sciences*, *72*(5), 1827-1836.

Zhang, X., Lu, X. and Wang, X., 2016. Comparison of Spatial Interpolation Methods Based on Rain Gauges for Annual Precipitation on the Tibetan Plateau. *Polish Journal of Environmental Studies*, *25*(3), 1339-1345.

Zhang, X., Zwiers, F.W., Li, G., Wan, H. and Cannon, A.J., 2017. Complexity in estimating past and future extreme short-duration rainfall. *Nature Geoscience*, *10*(4), 255-259.

Zhao, H., Gao, G., An, W., Zou, X., Li, H. and Hou, M., 2017. Timescale differences between SC-PDSI and SPEI for drought monitoring in China. *Physics and Chemistry of the Earth, Parts A/B/C*, *102*, 48-58.

Zhao, Y. and Di Lorenzo, E., 2020. The impacts of extra-tropical ENSO Precursors on Tropical Pacific Decadal-scale Variability. *Scientific Reports,* 10(1), 1-12.

Zhu, Y., Liu, Y., Wang, W., Singh, V.P. and Ren, L., 2021. A global perspective on the probability of propagation of drought: From meteorological to soil moisture. *Journal of Hydrology*, *603*, 1-15.

Zhu, Y., Wang, W., Singh, V.P. and Liu, Y., 2016. Combined use of meteorological drought indices at multi-time scales for improving hydrological drought detection. *Science of the Total Environment*, *571*, 1058-1068.

Zinke, J., Dullo, W.C., Heiss, G.A. and Eisenhauer, A., 2004. ENSO and Indian Ocean subtropical dipole variability is recorded in a coral record off southwest Madagascar for the period 1659 to 1995. *Earth and Planetary Science Letters*, *228*(1-2), 177-194.

Chapter 8: APPENDICES

8.1. Annual Rainfall Plots

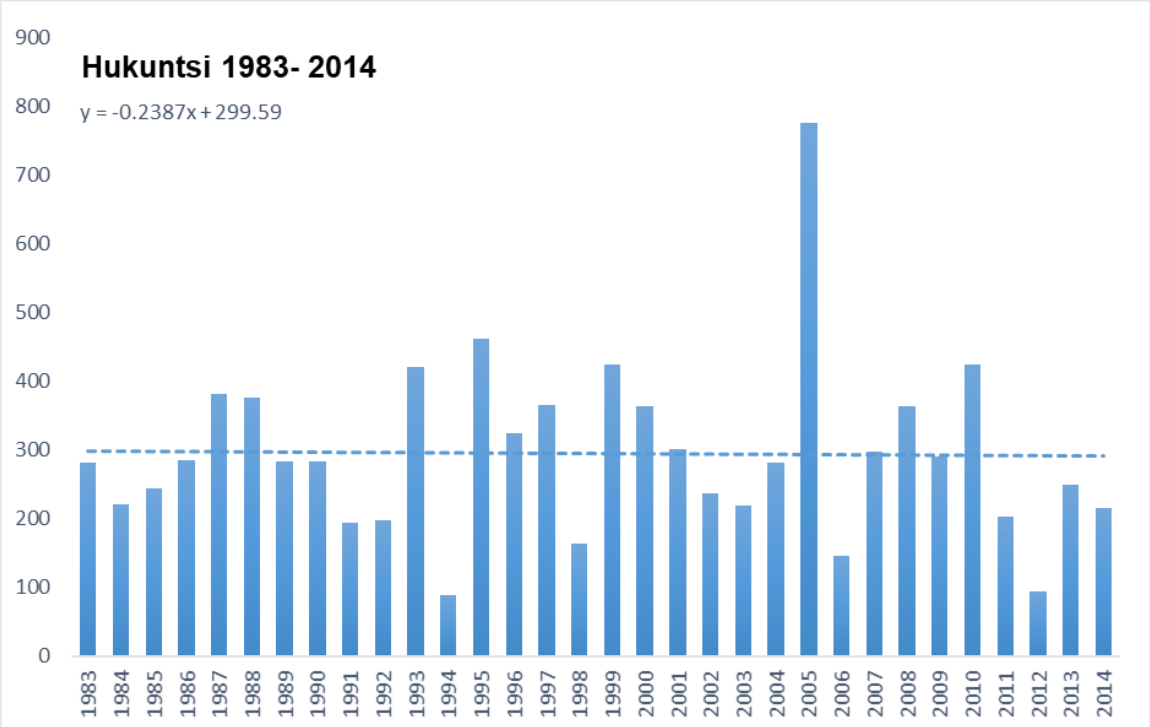

8.1a Rainfall data Hukuntsi

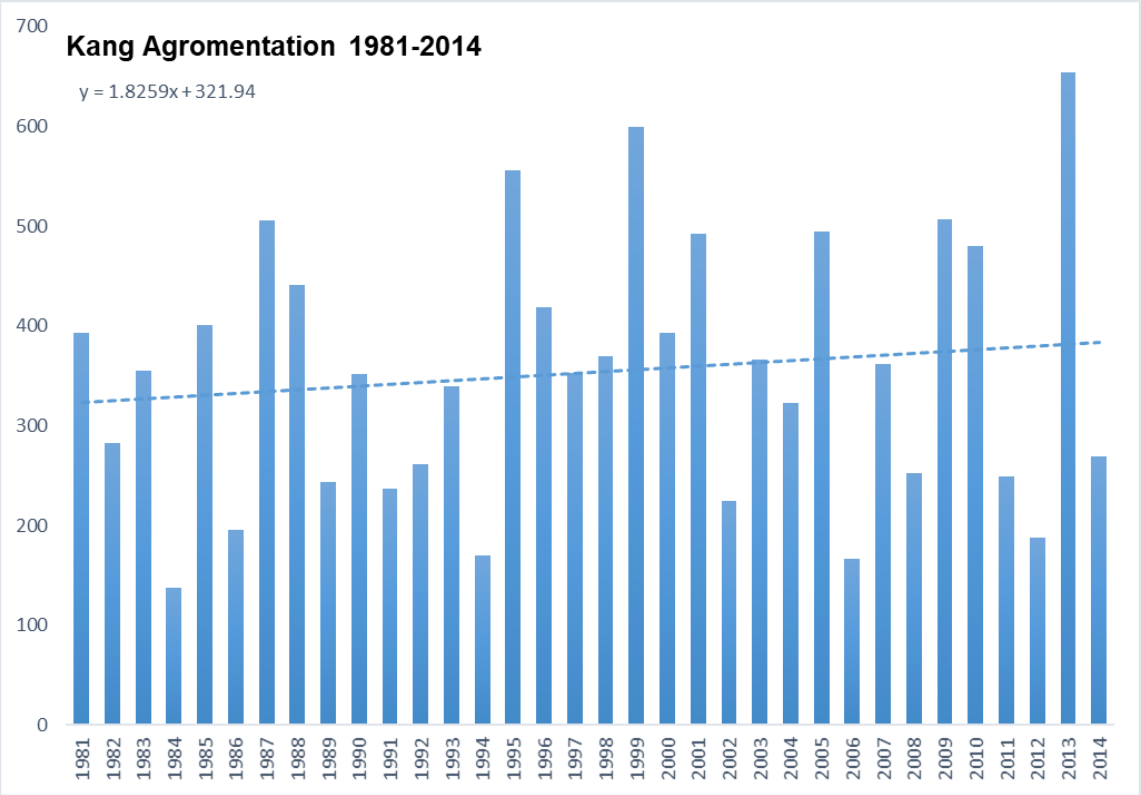

8.1b Rainfall data Kang Agromentation

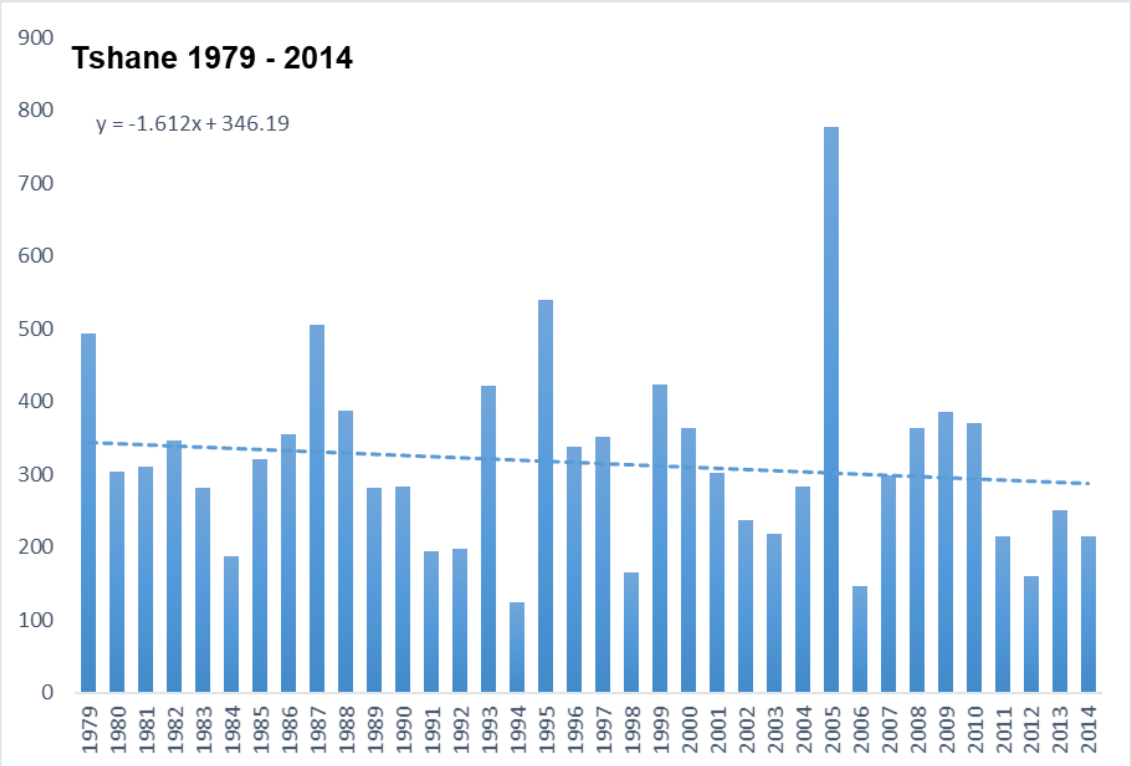

8.1c Rainfall data Tshane

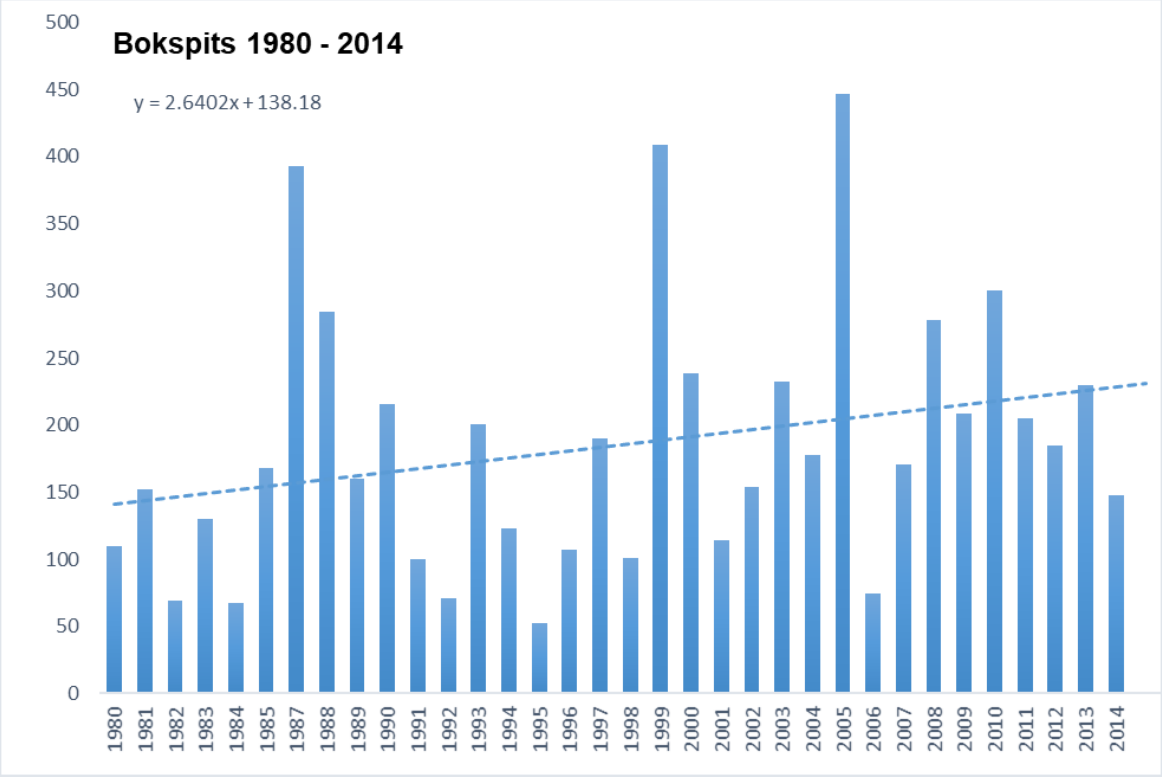

8.1d Rainfall data Bokspits

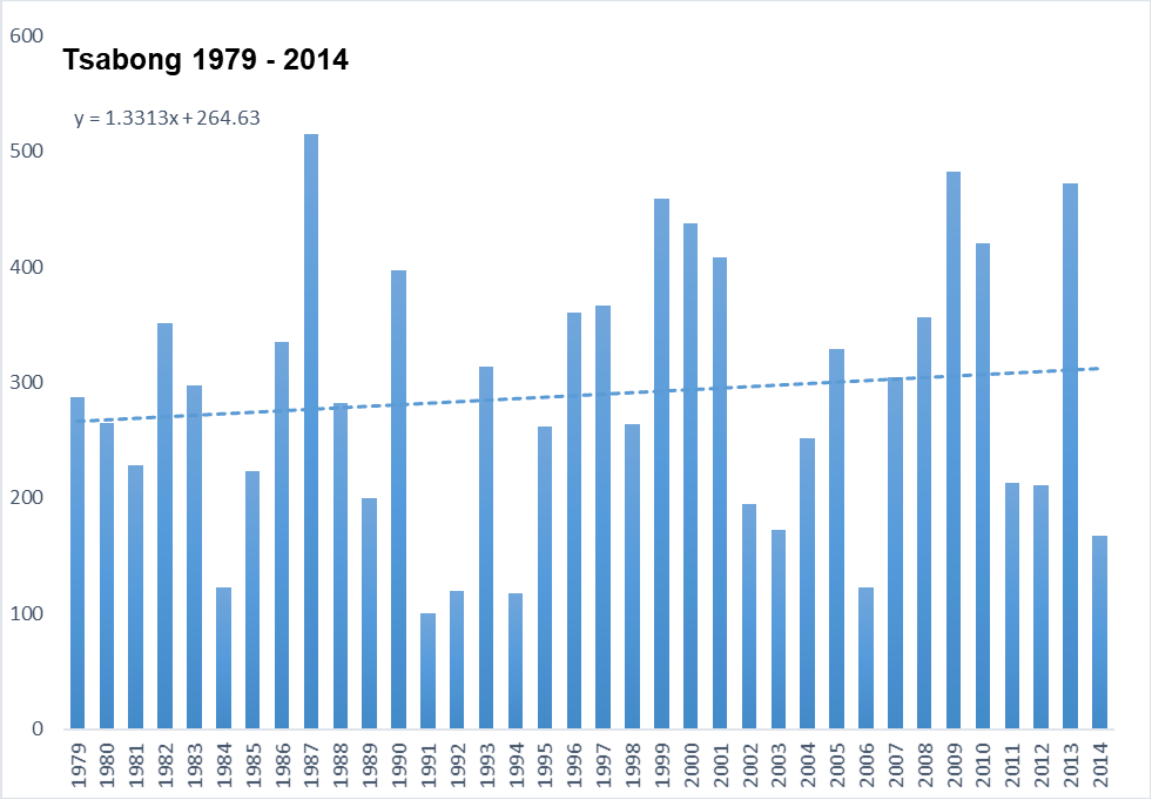

8.1e Rainfall data Tsabong

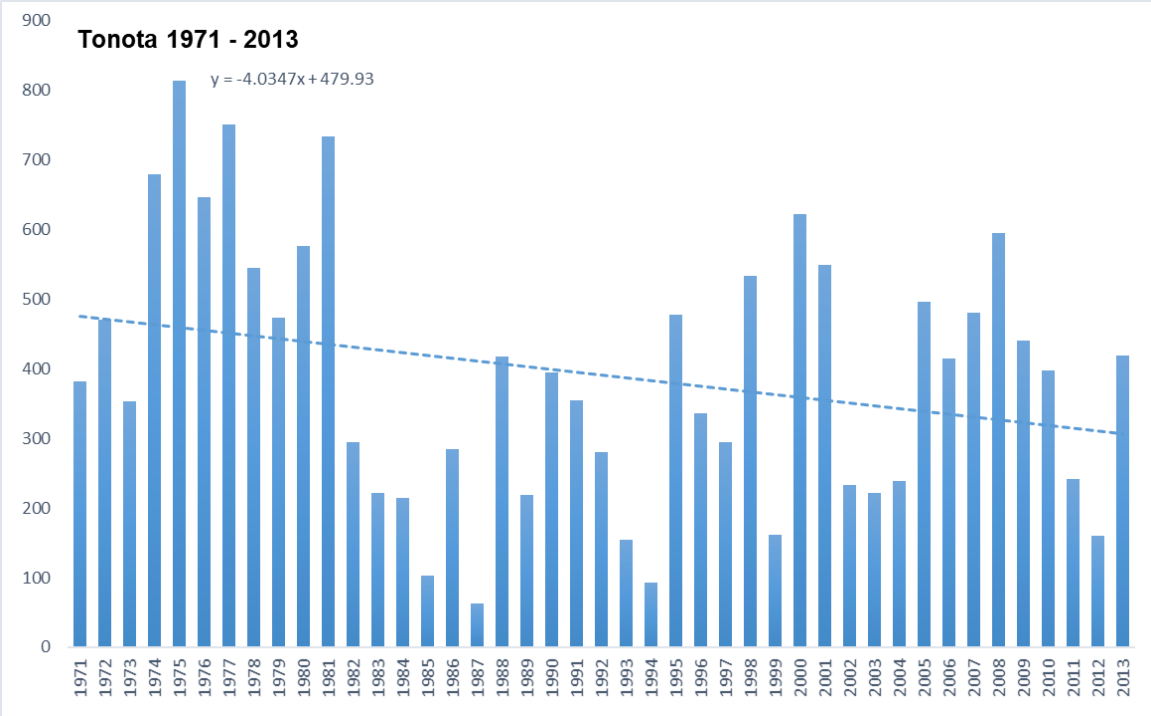

8.1f Rainfall data Tonota

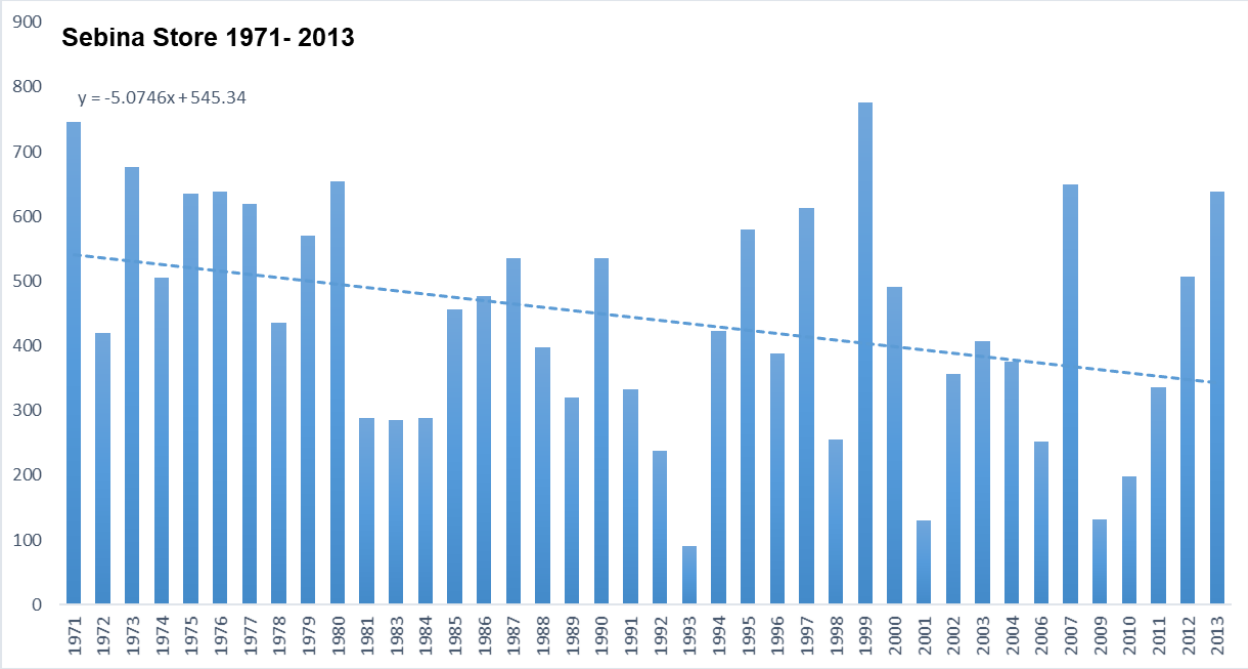

8.1g Rainfall data Sebina Store

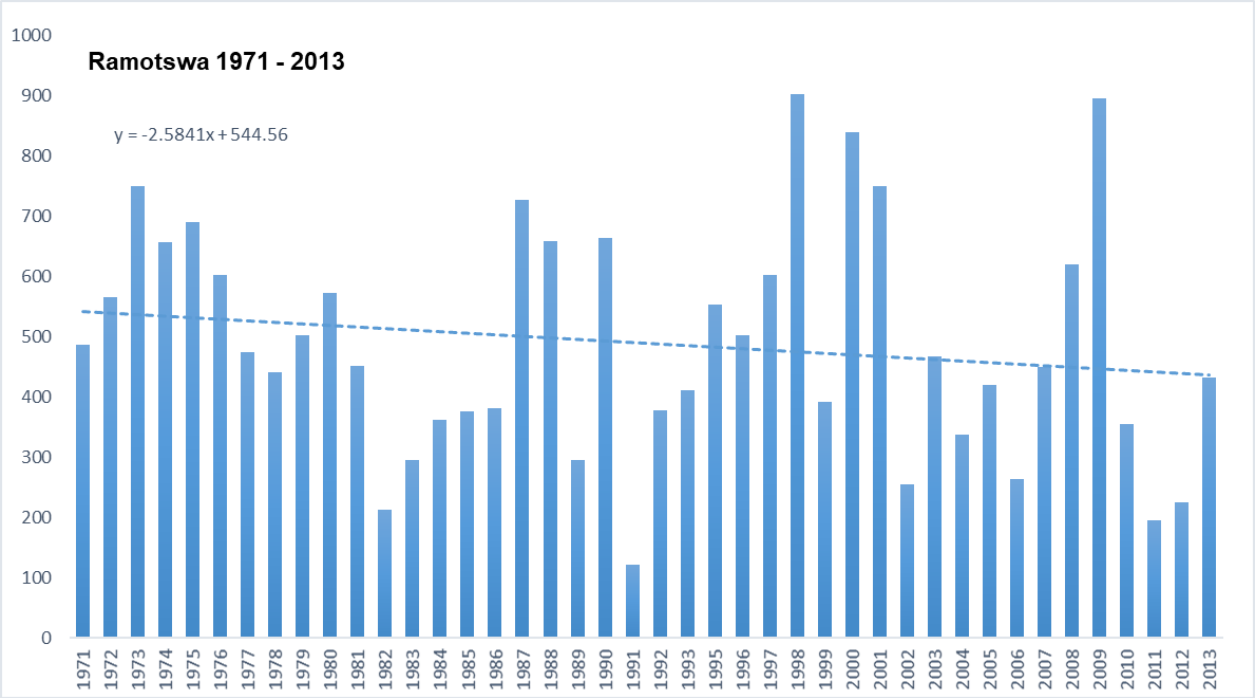

8.1h Rainfall data Ramotswa

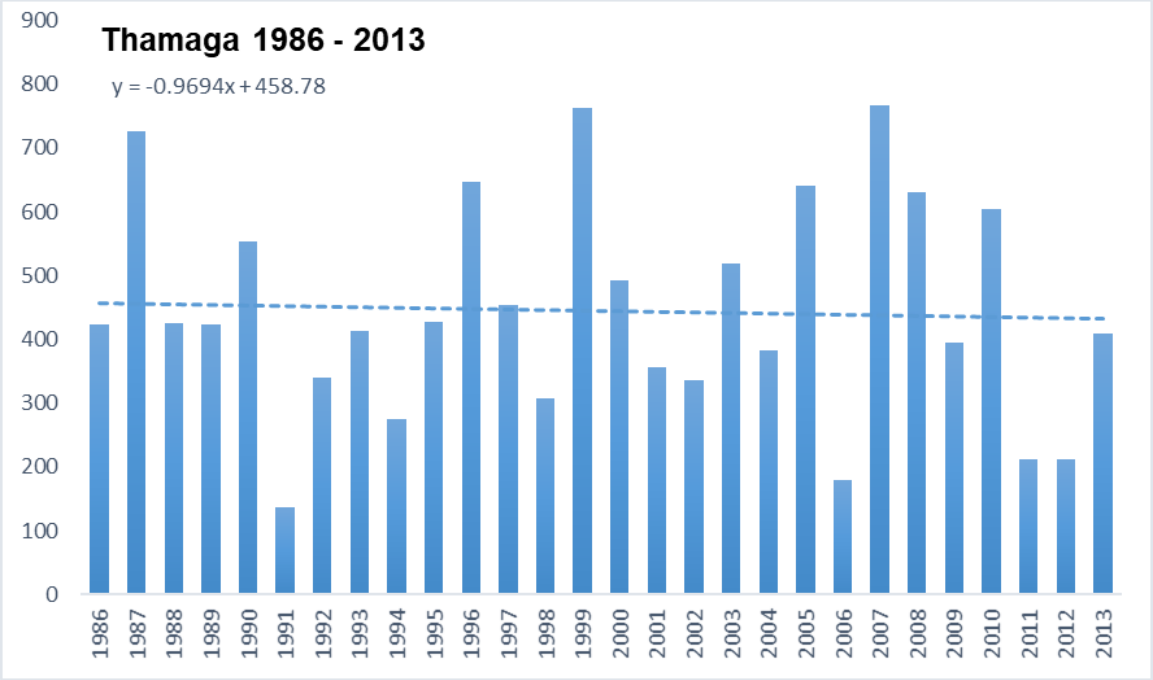

8.1i Rainfall data Thamaga

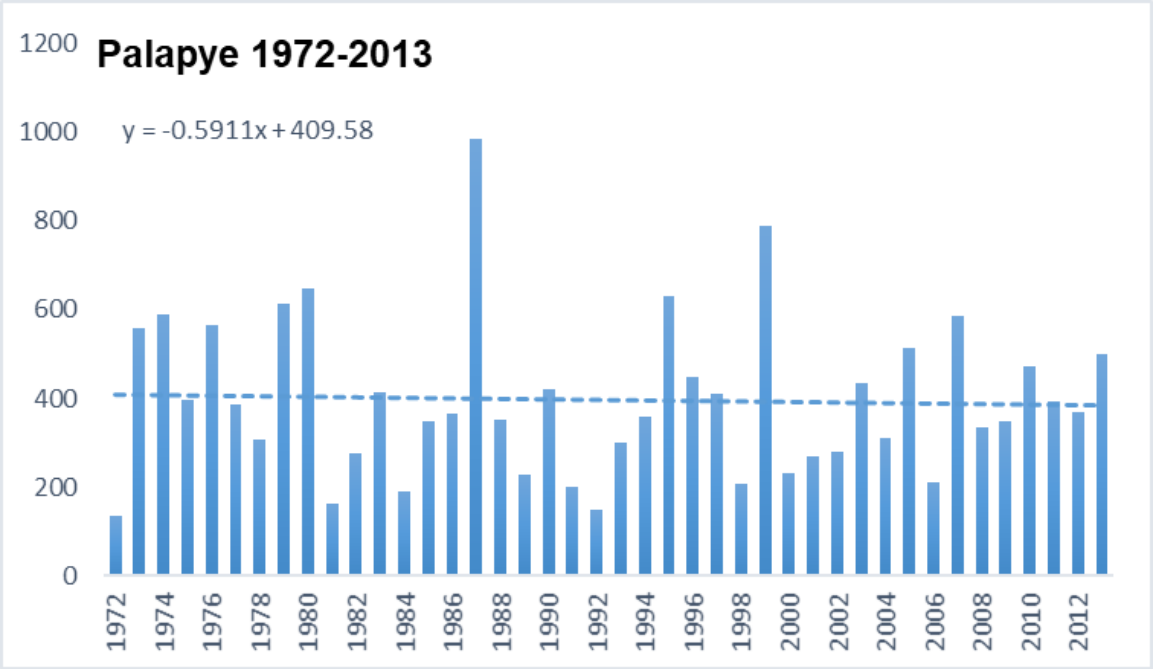

8.1j Rainfall data Palapye

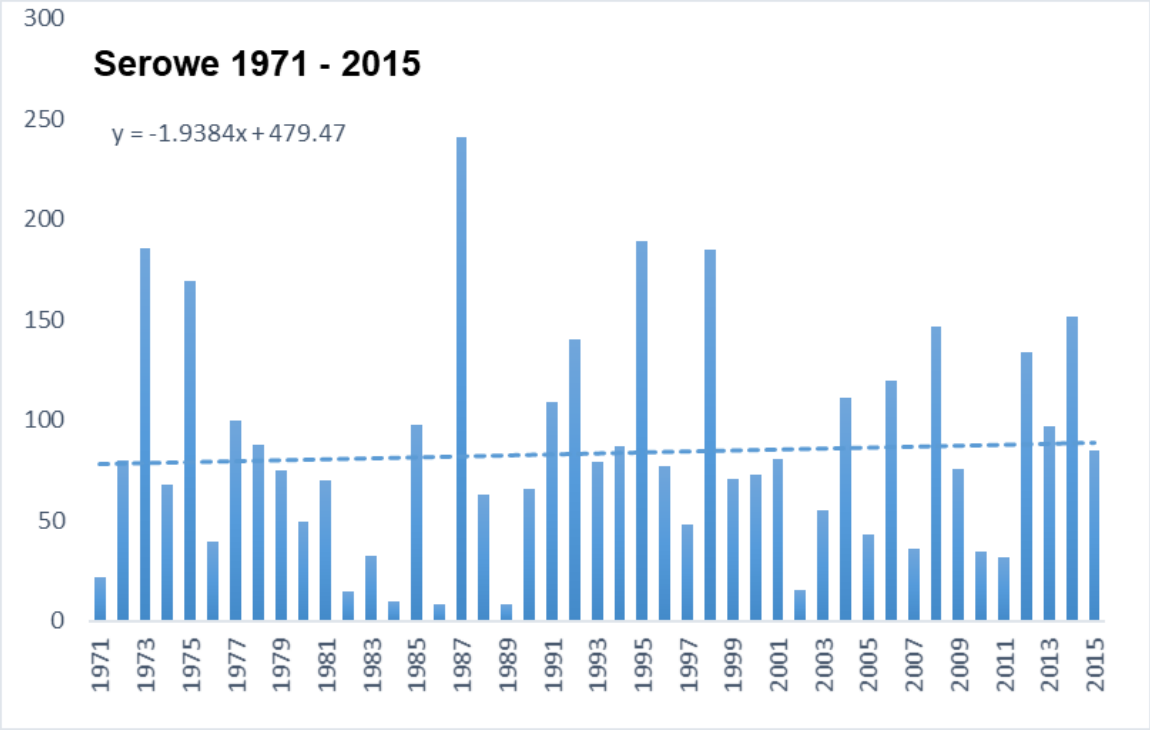

8.1k Rainfall data Serowe

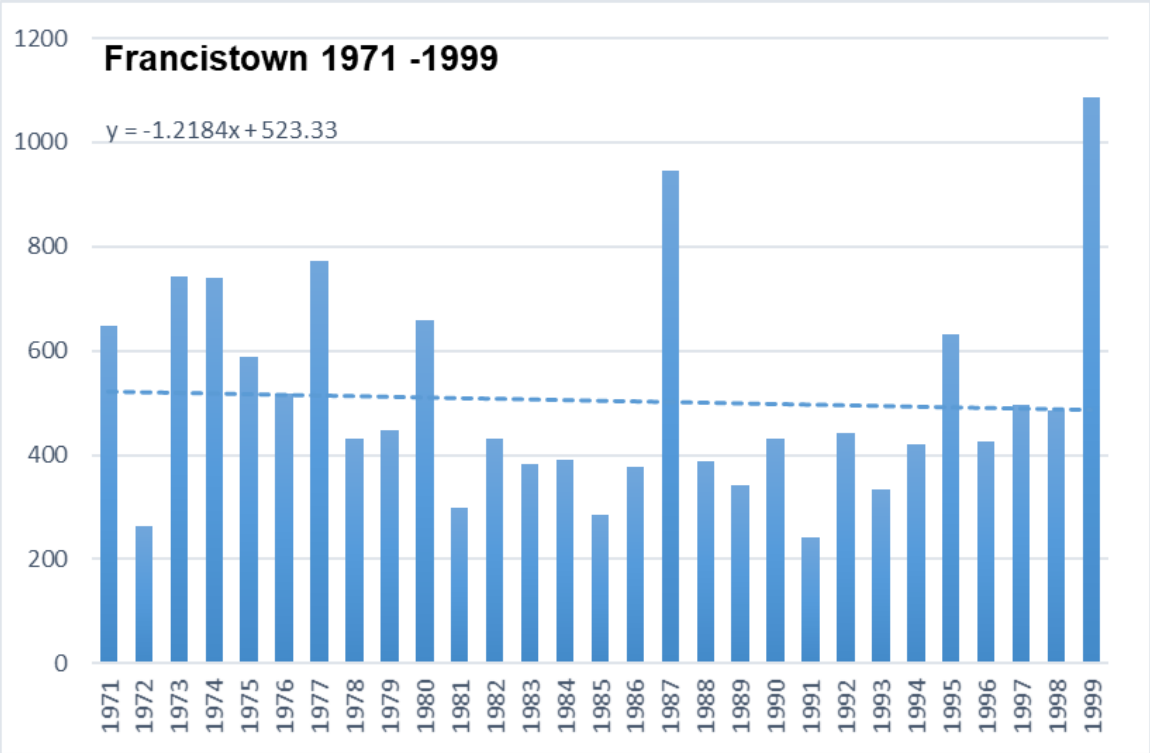

8.1l Rainfall data Hukuntsi

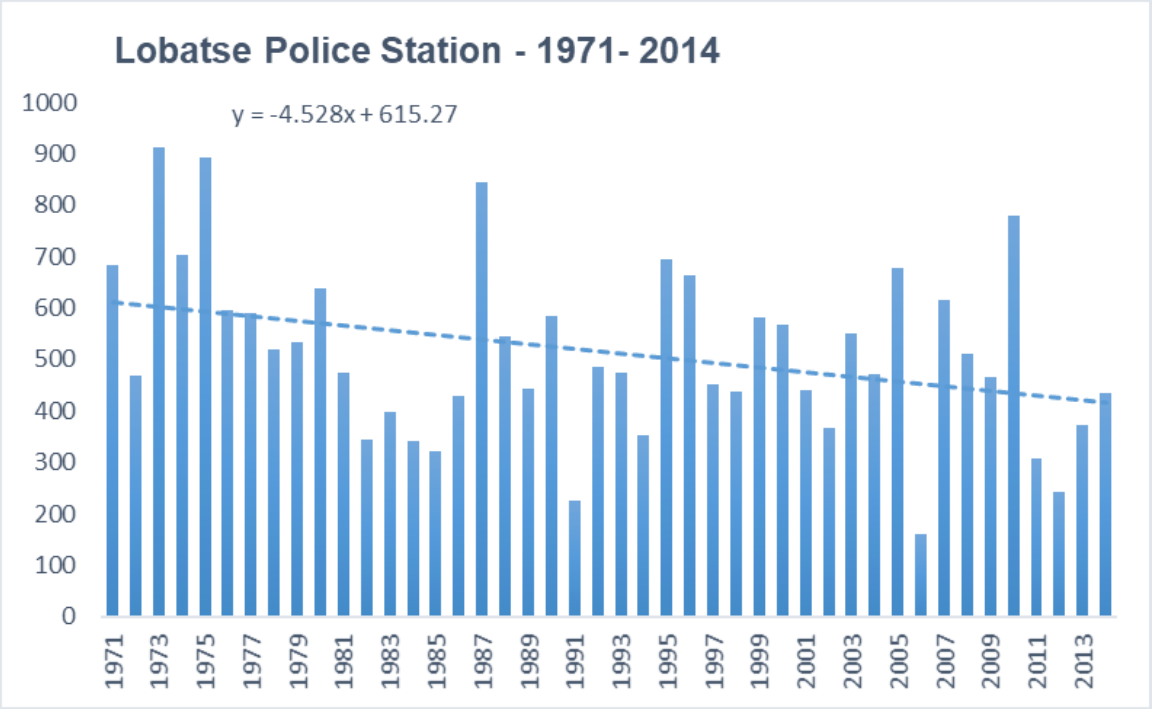

8.1m Rainfall data Lobatse Police Station

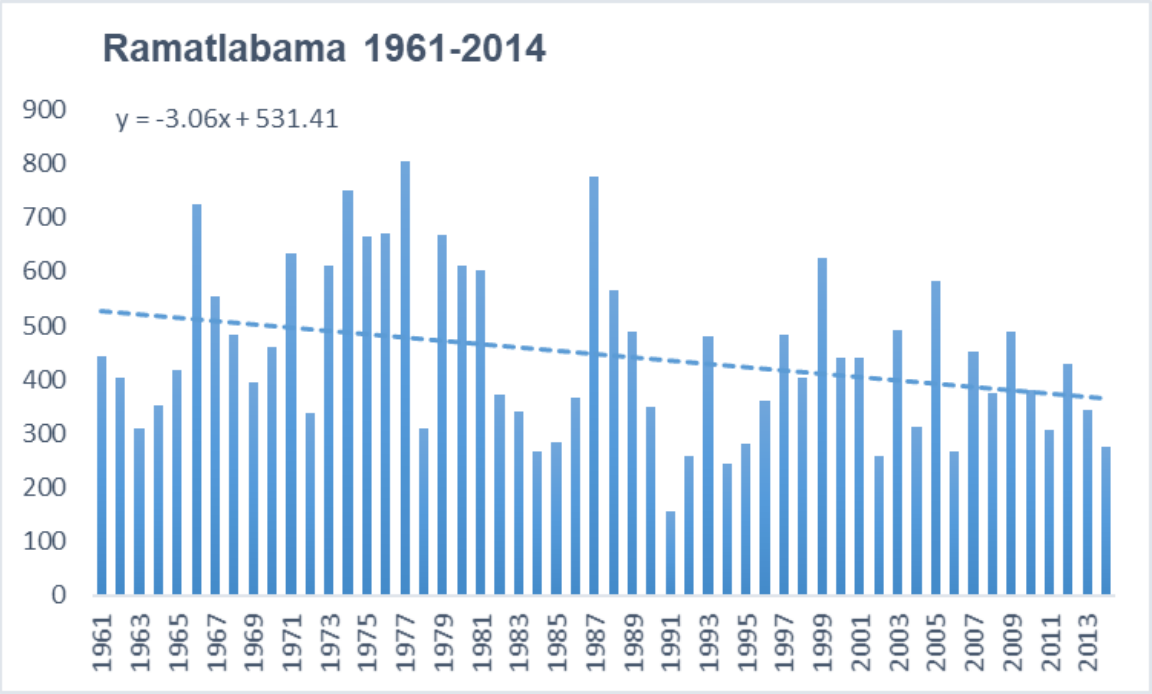

8.1n Rainfall data Ramatlabama

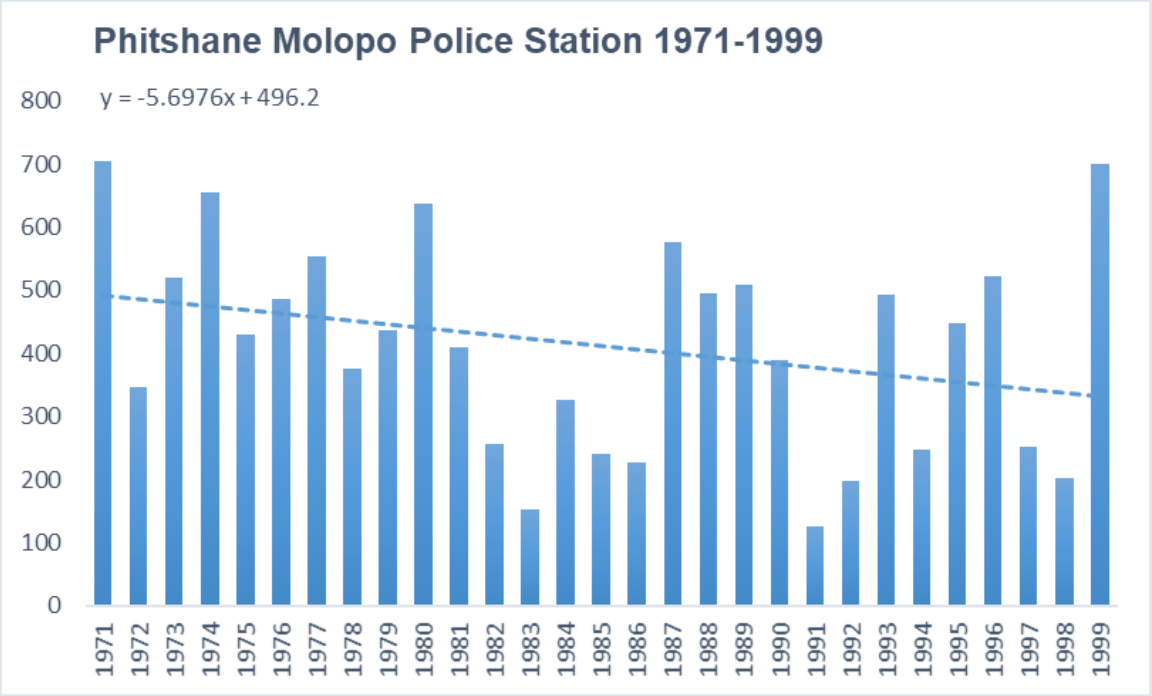

8.1o Rainfall data Phitshane Molopo Police Station

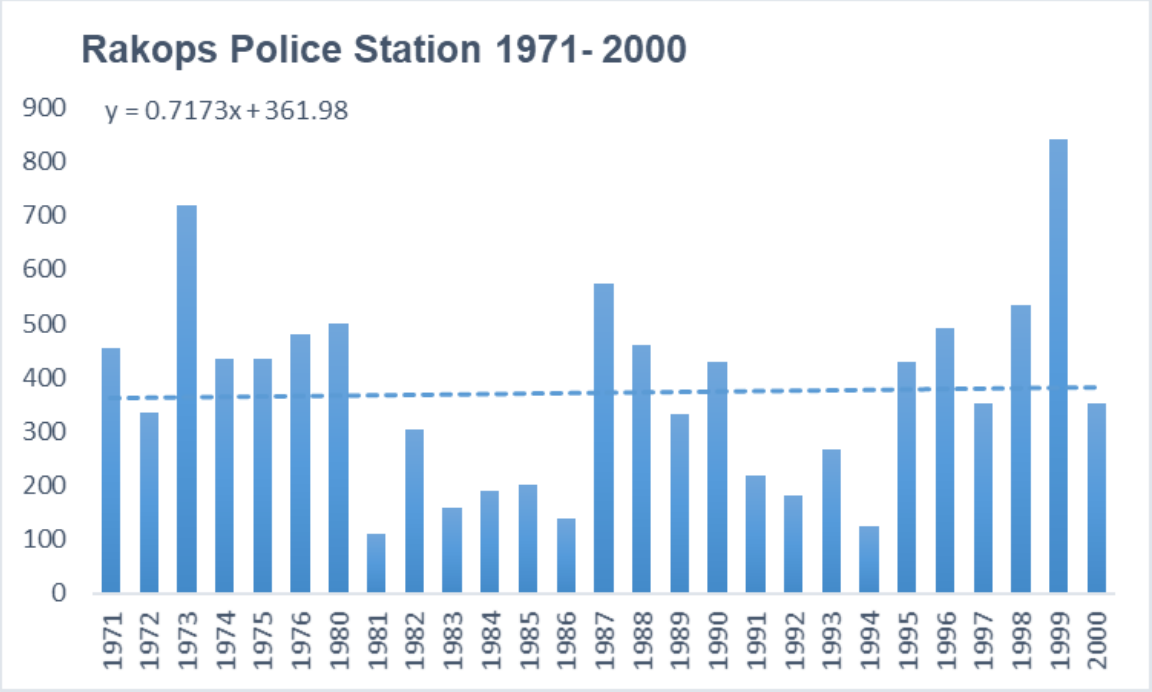

8.1p Rainfall data Rakops Police Station

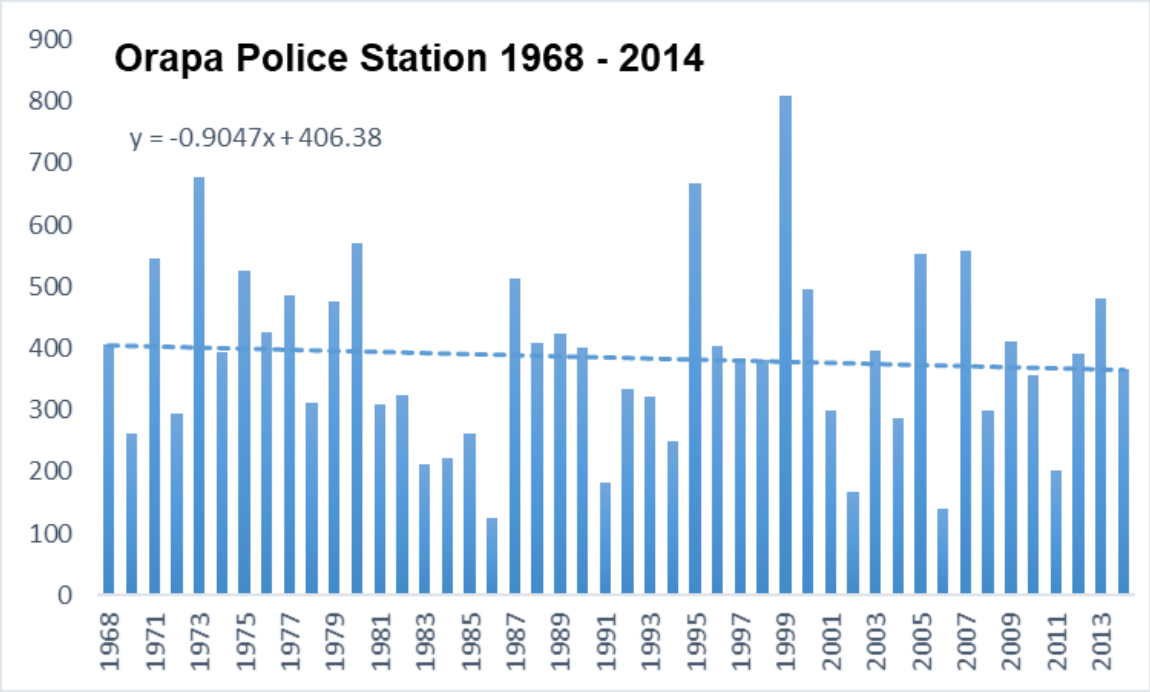

8.1q Rainfall data Orapa Police Station

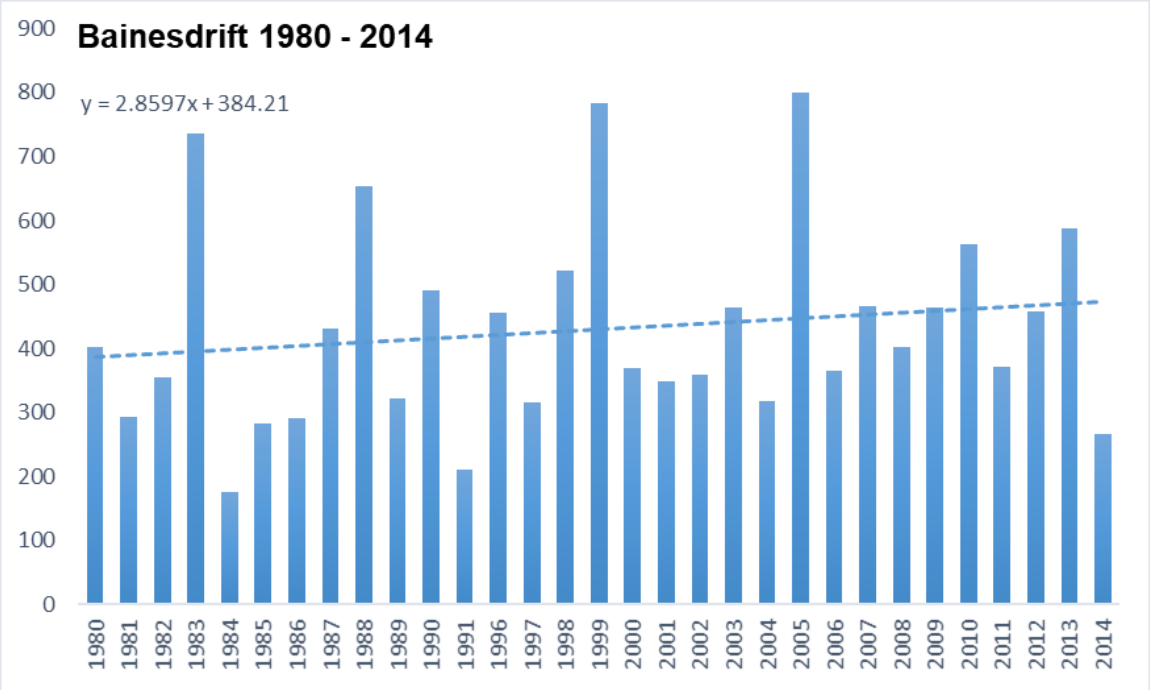

8.1r Rainfall data Bainesdrift

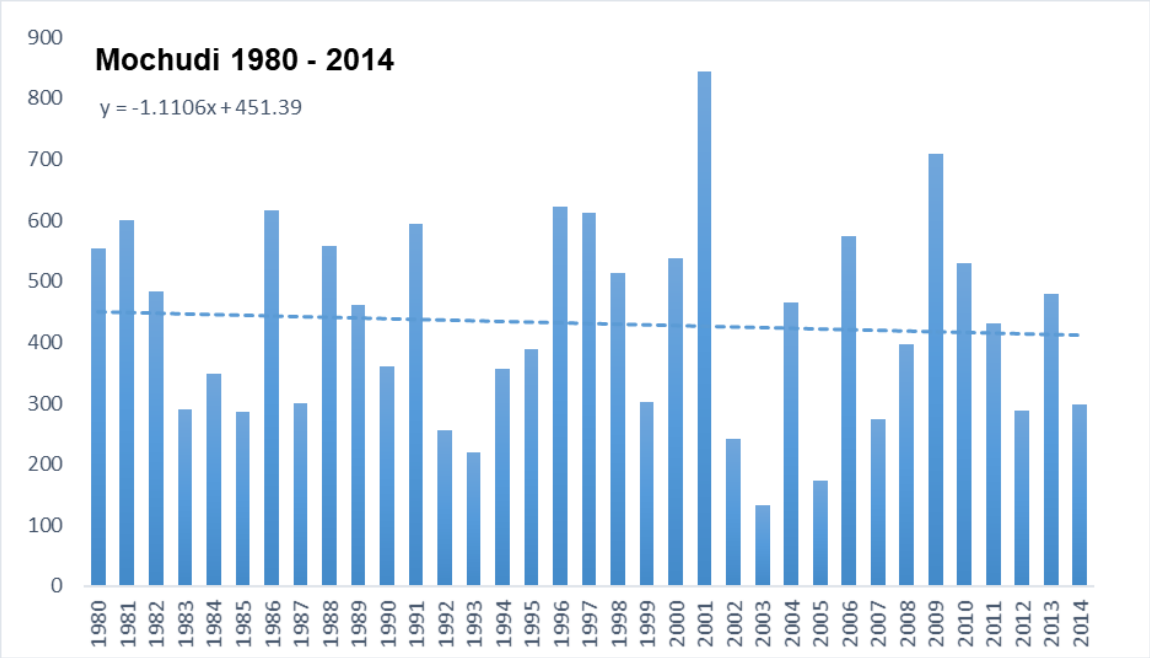

8.1s Rainfall data Mochudi

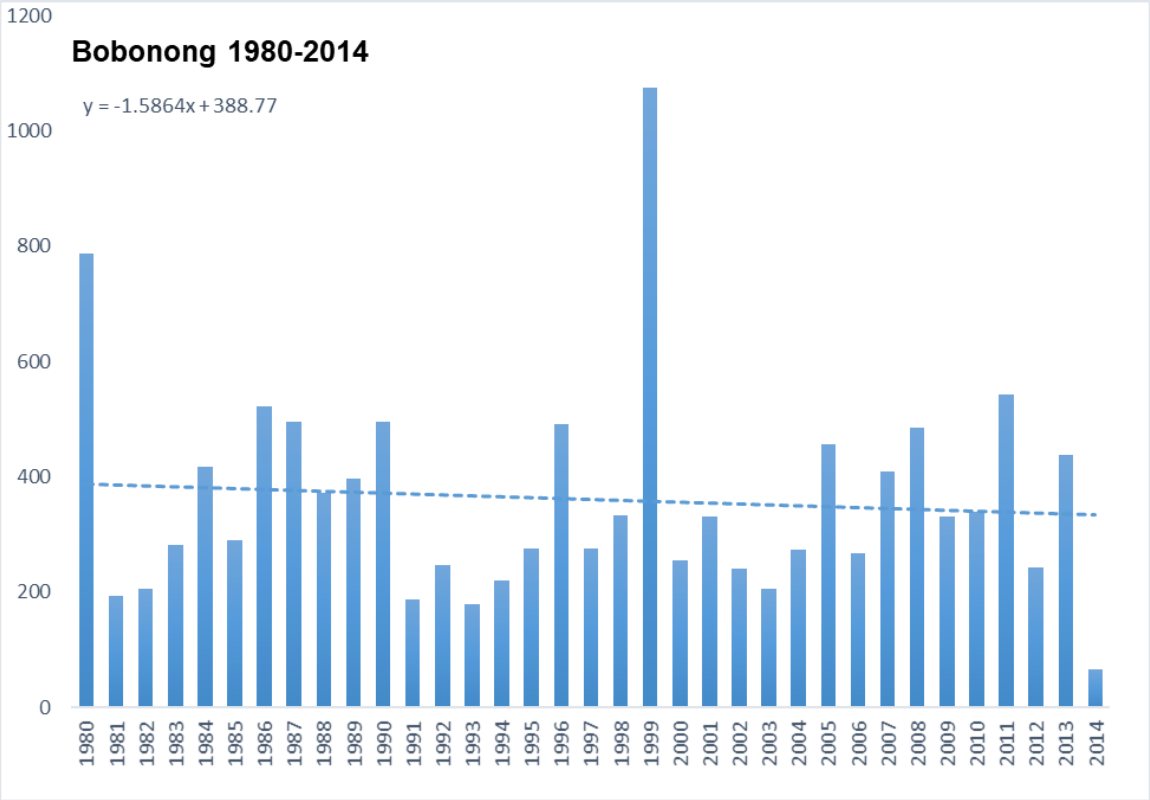

8.1t Rainfall data Bobonong

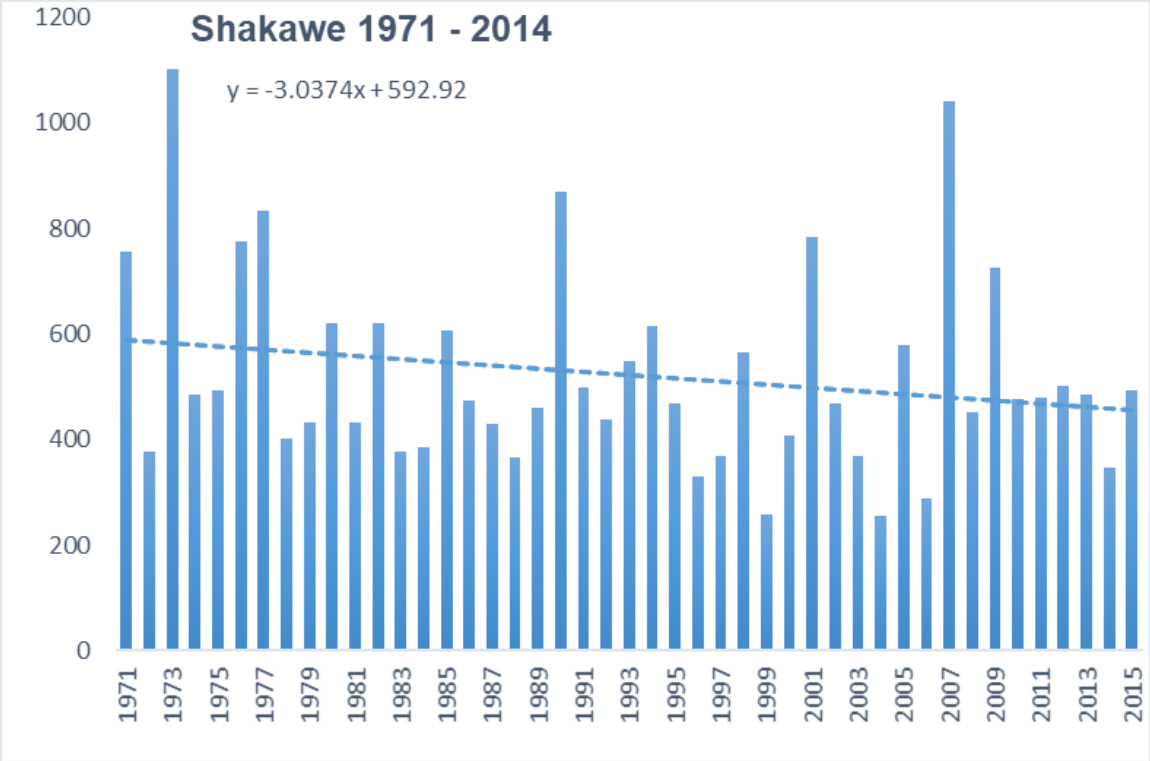

8.1u Rainfall data Shakawe

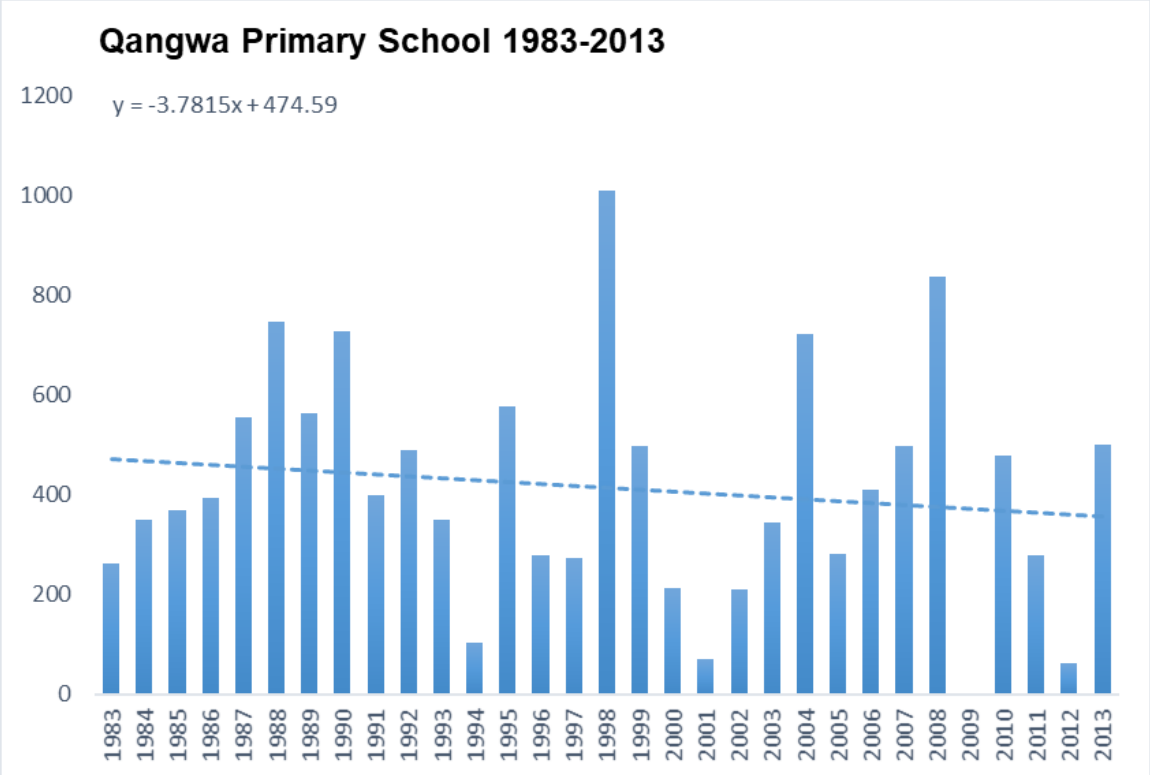

8.1v Rainfall data Qangwa Primary School

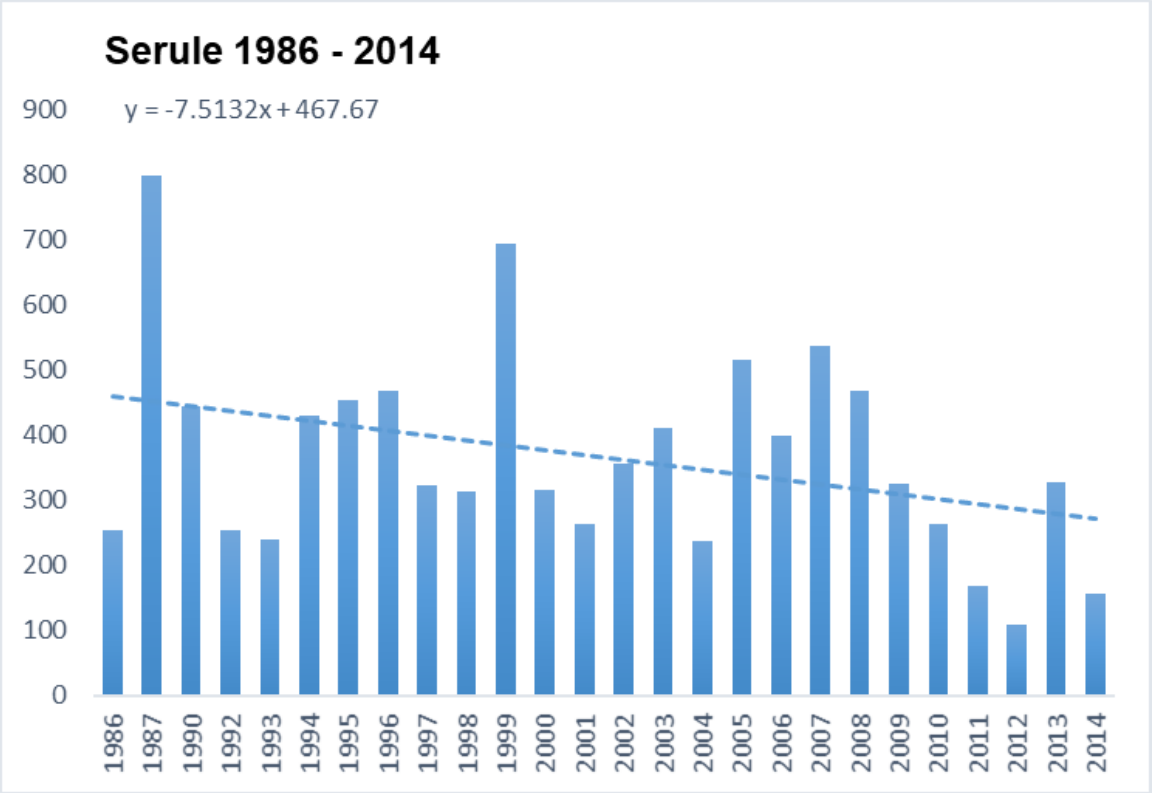

8.1w Rainfall data Serule

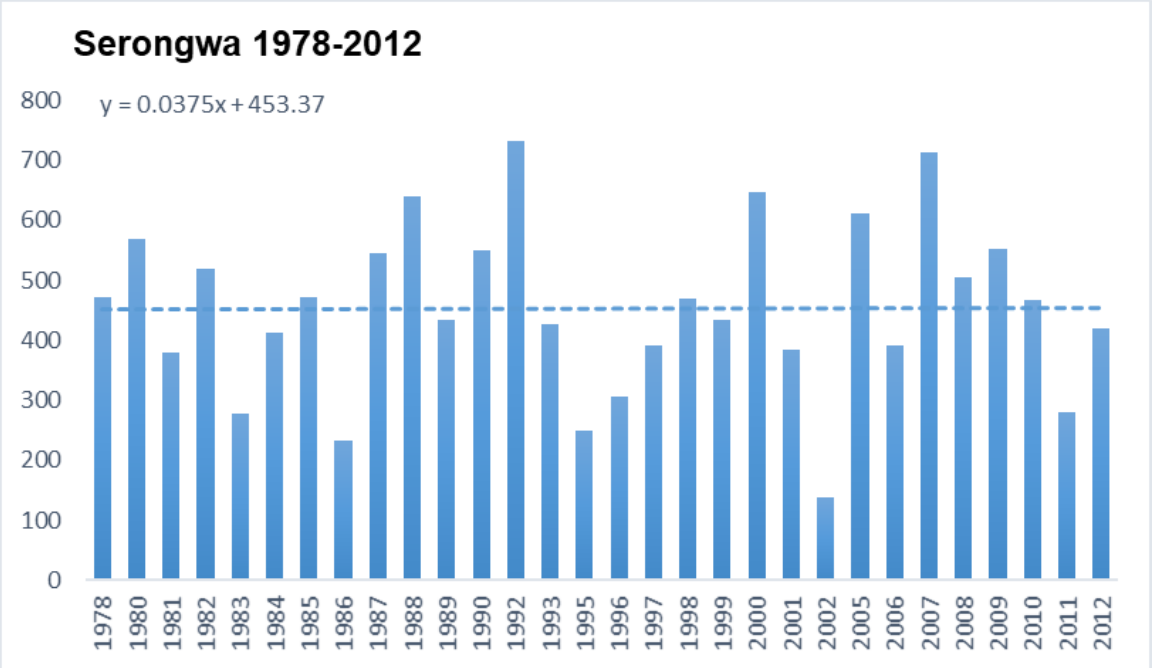

8.1x Rainfall data Serongwa

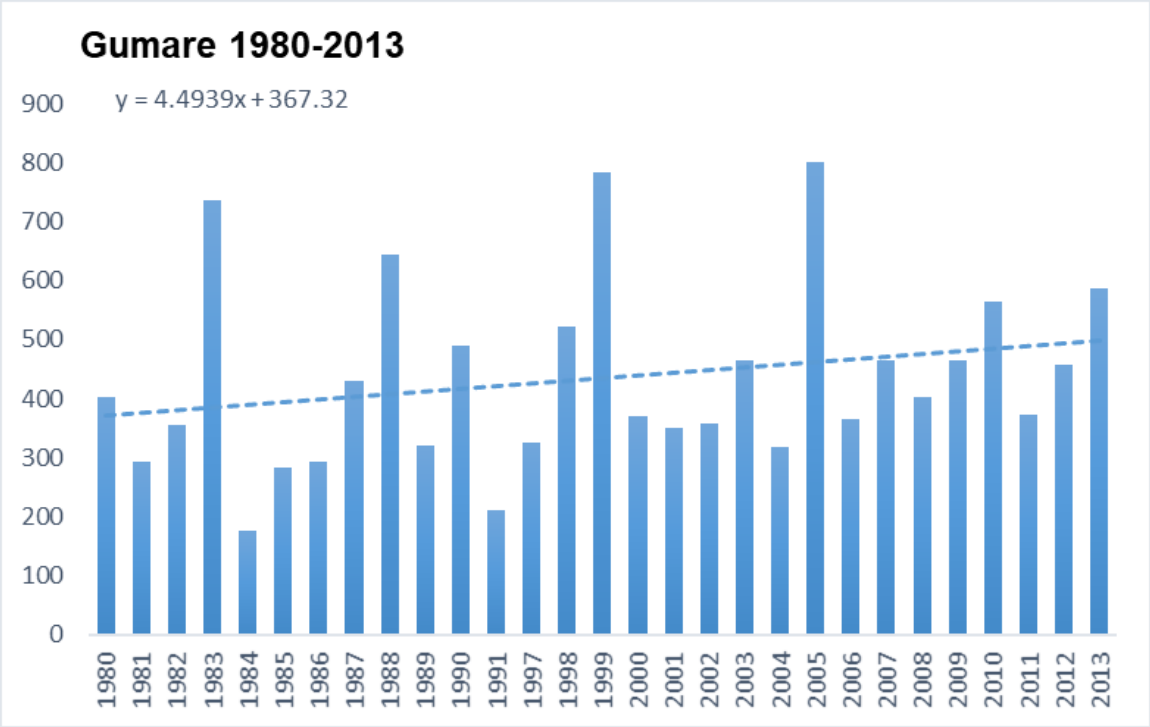

8.1y Rainfall data Gumare

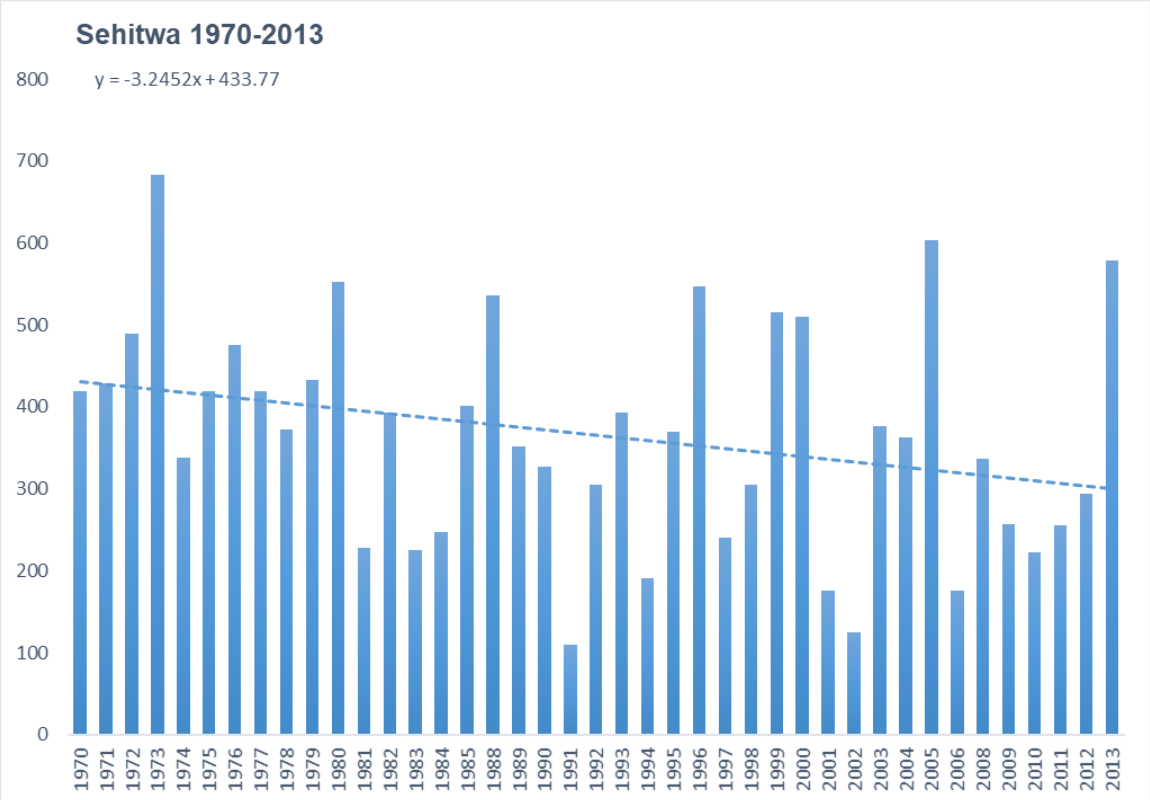

8.1z Rainfall data Sehitwa

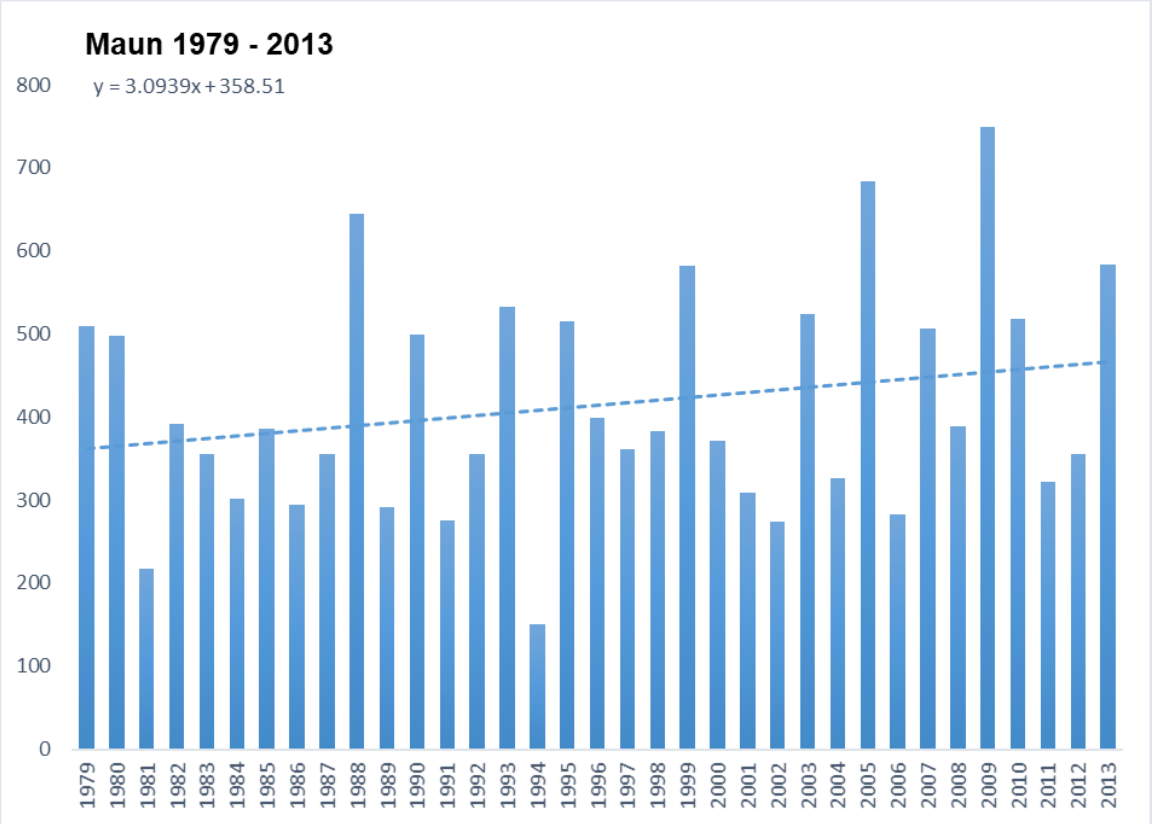

8.1aa Rainfall data Maun

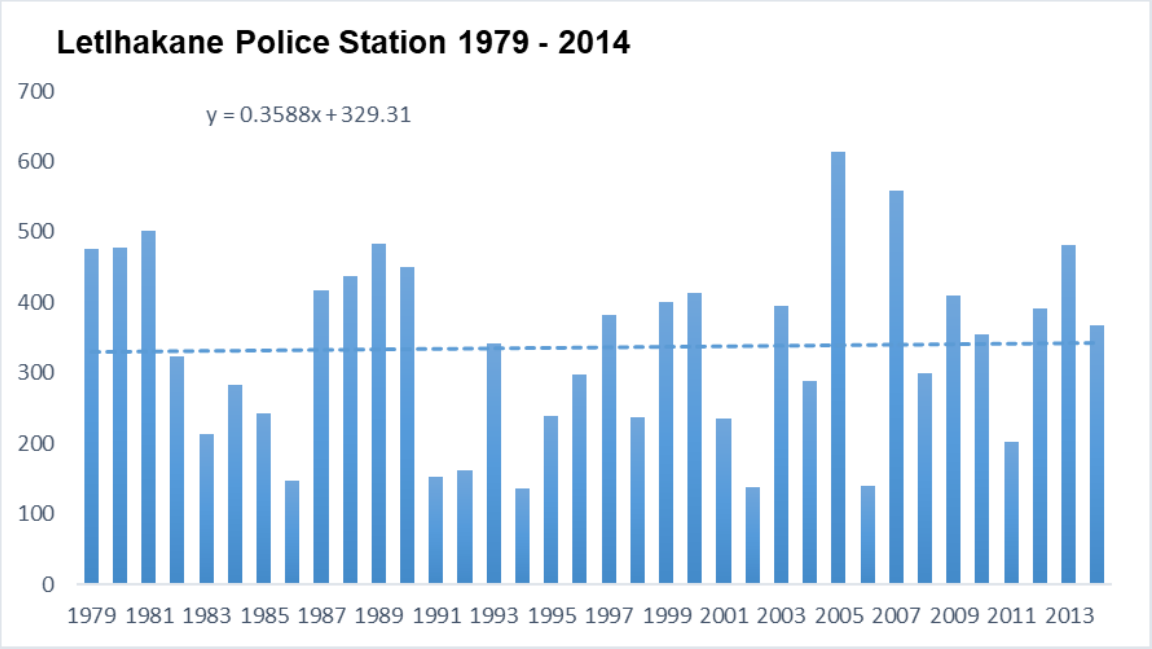

8.1ab Rainfall data Letlhakane Police Station

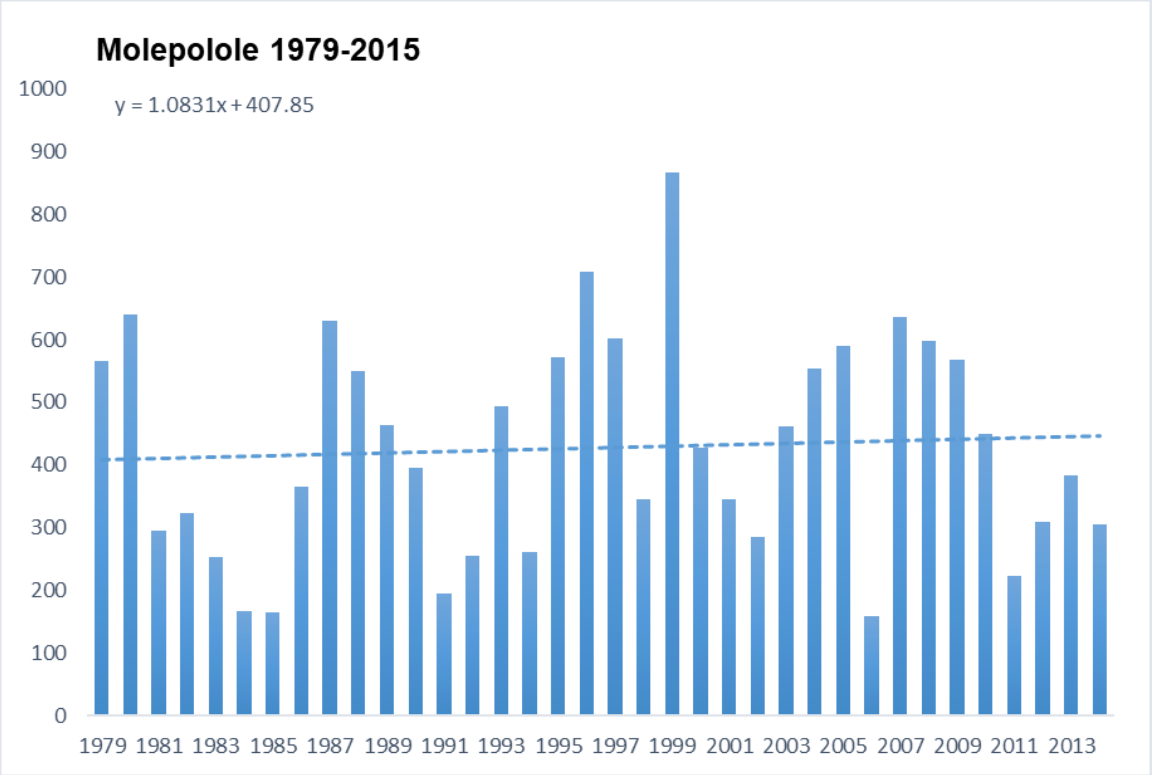

8.1ac Rainfall data Molepolole

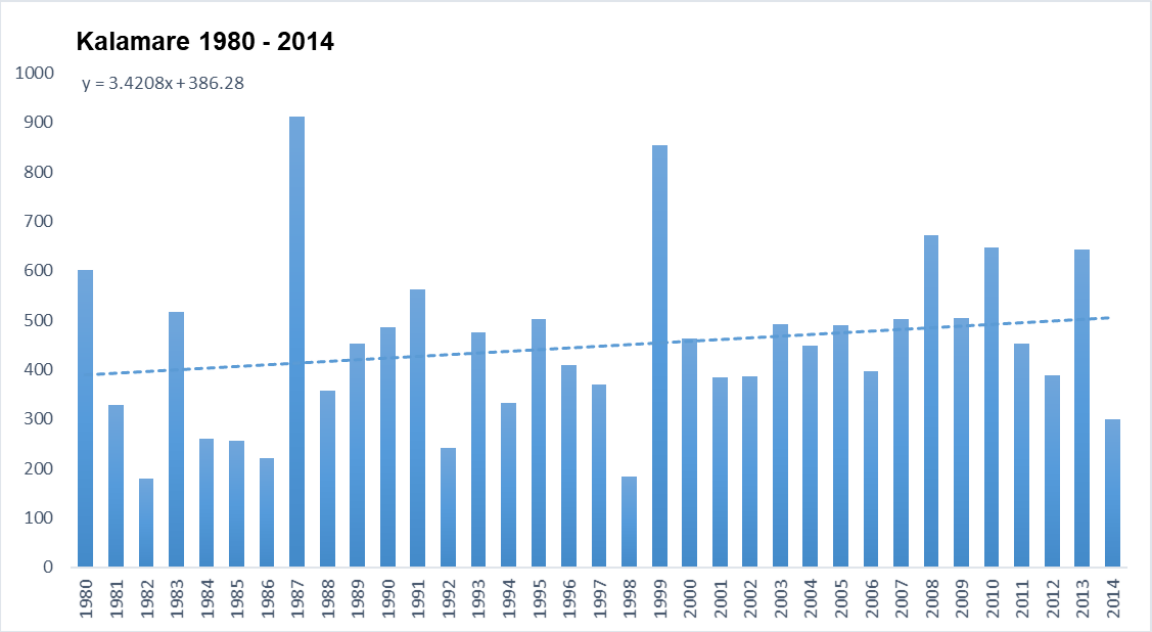

8.1ad Rainfall data Kalamare

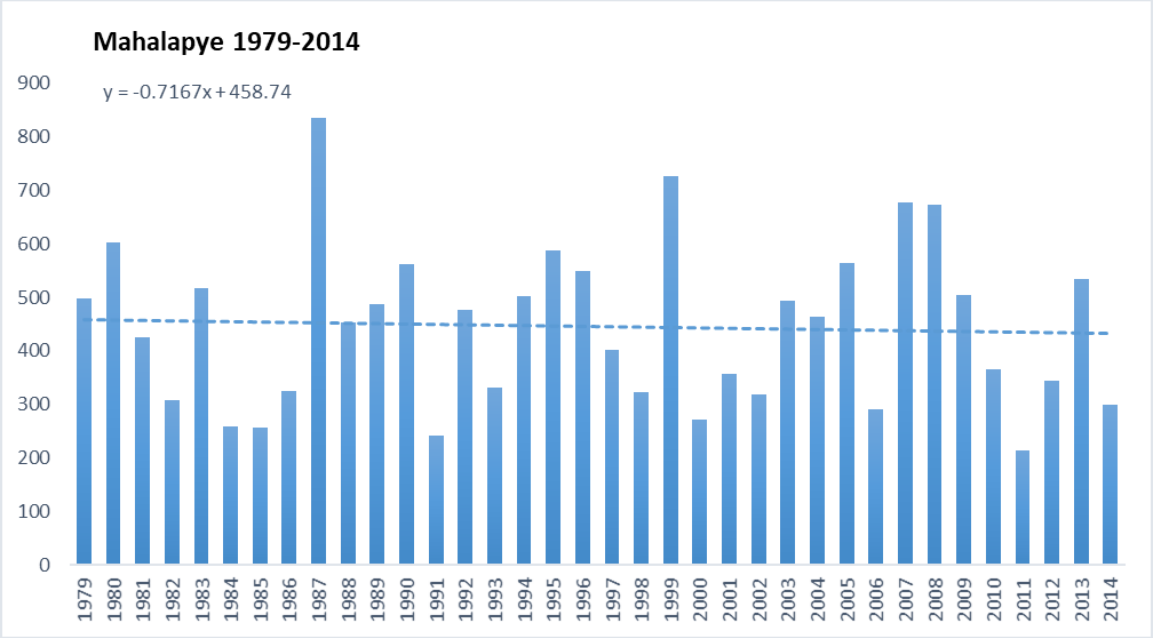

8.1ae Rainfall data Mahalapye

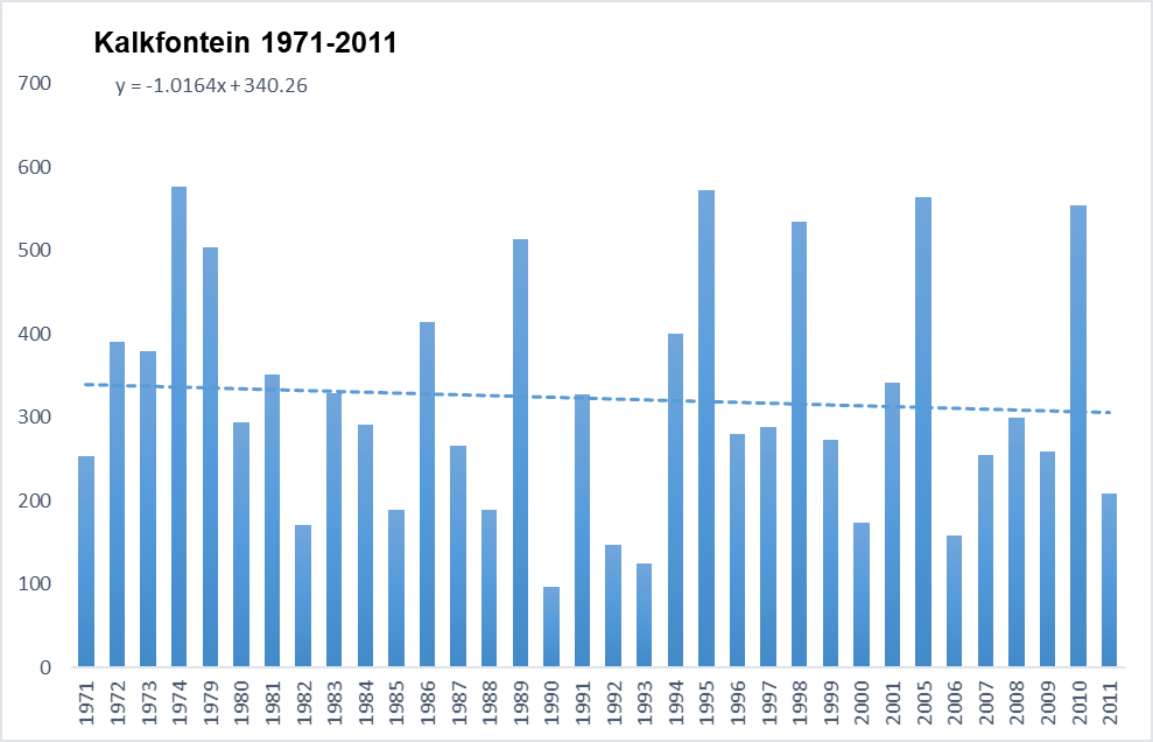

8.1af Rainfall data Kalkfontein

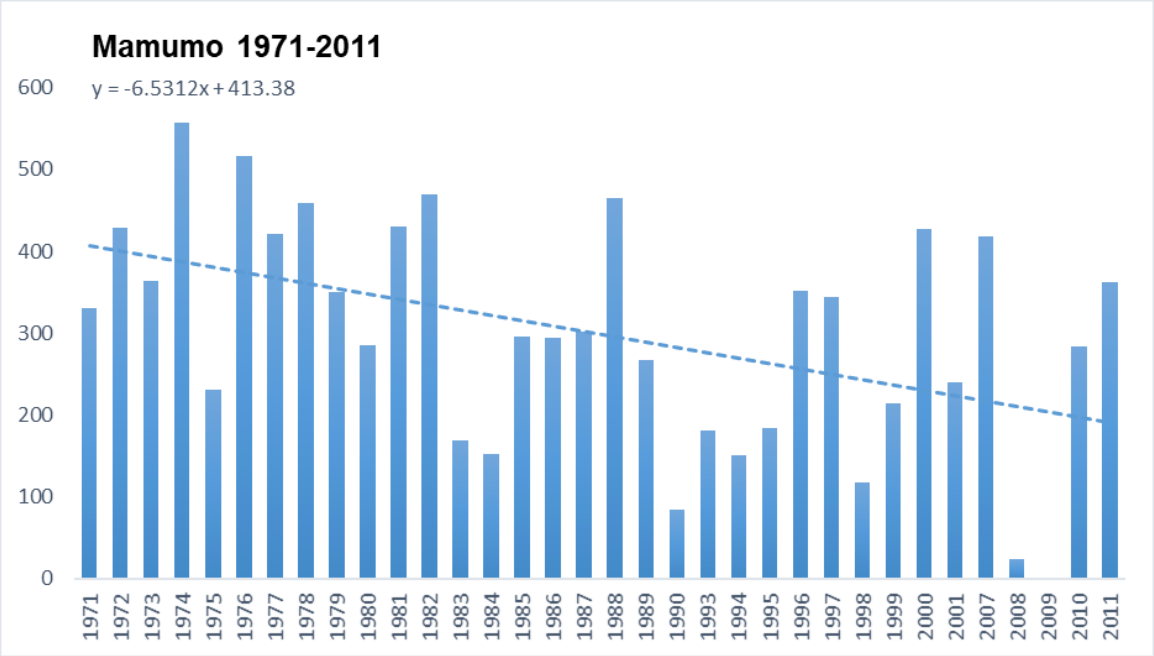

8.1ag Rainfall data Mamumo

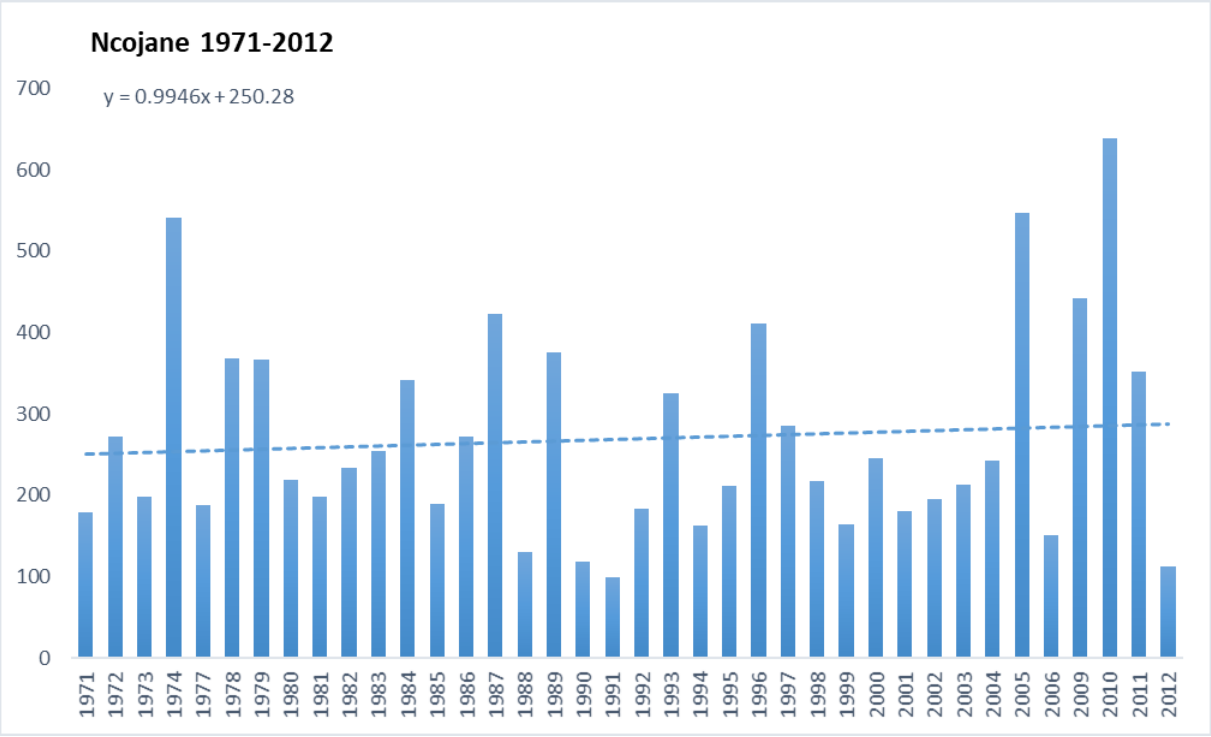

8.1ah Rainfall data Ncojane

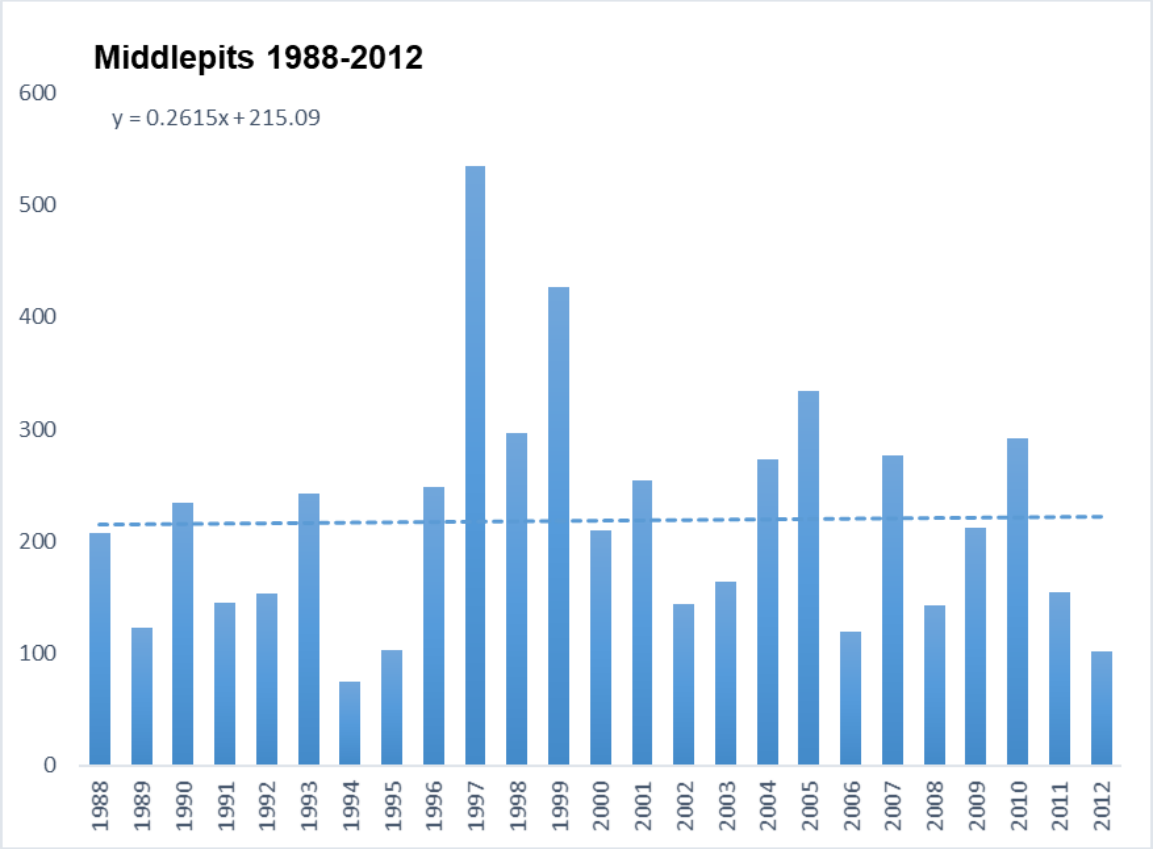

8.1ai Rainfall data Middlepits

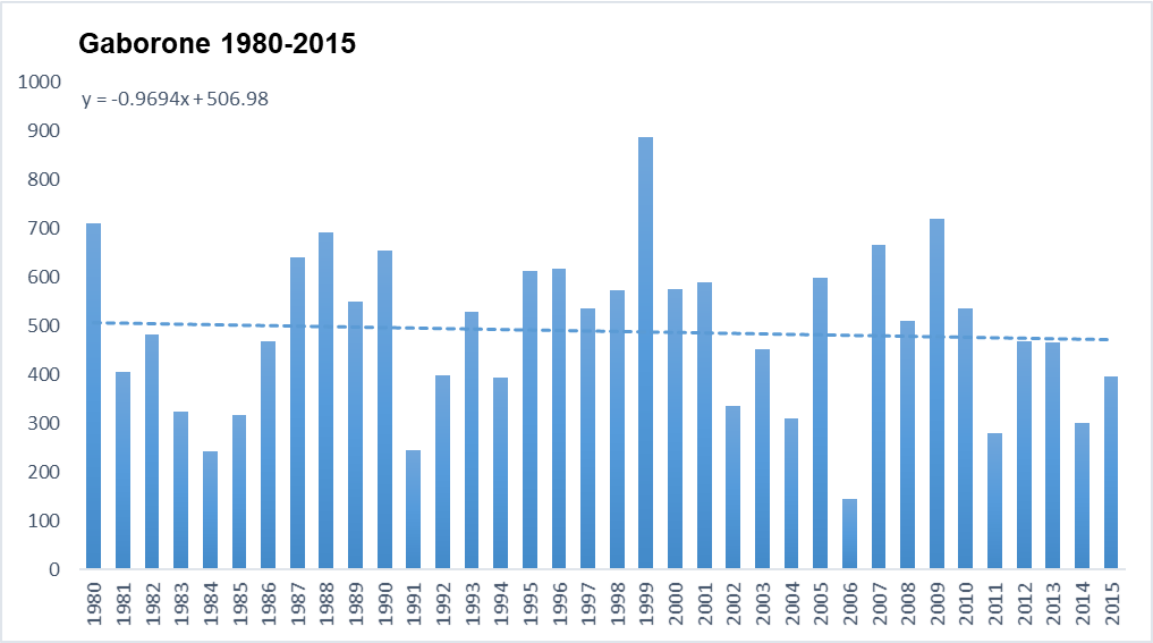

8.1aj Rainfall data Gaborone

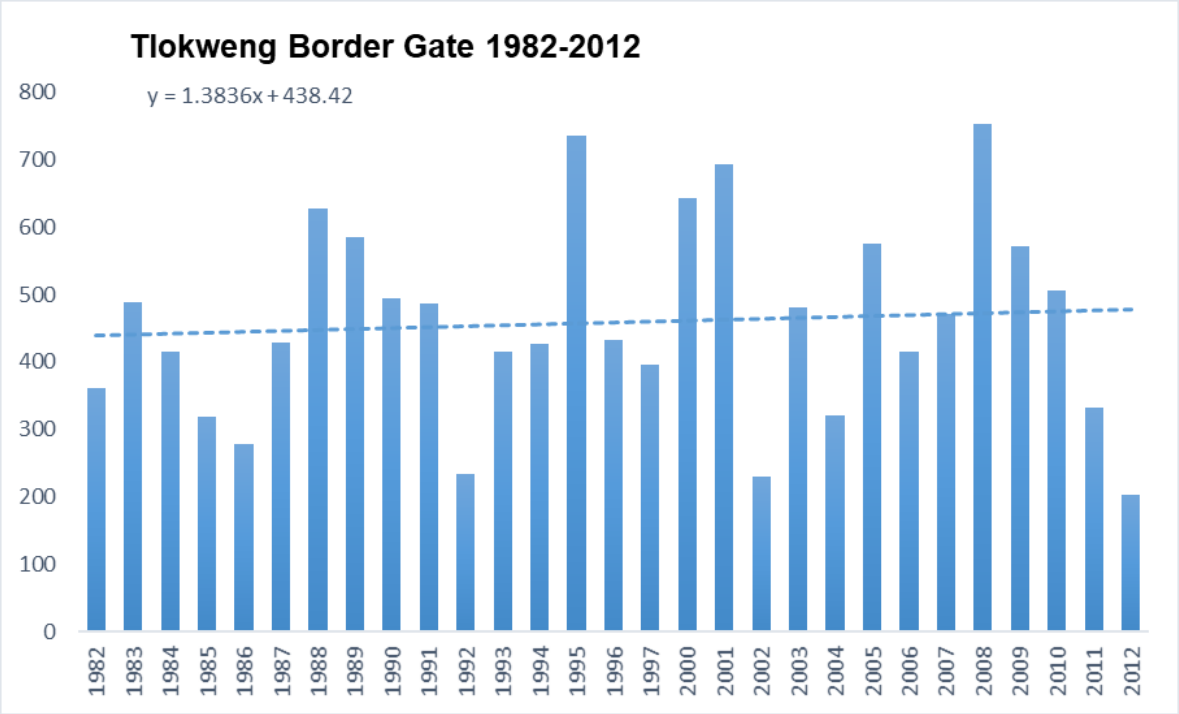

8.1ak Rainfall data Tlokweng border gate

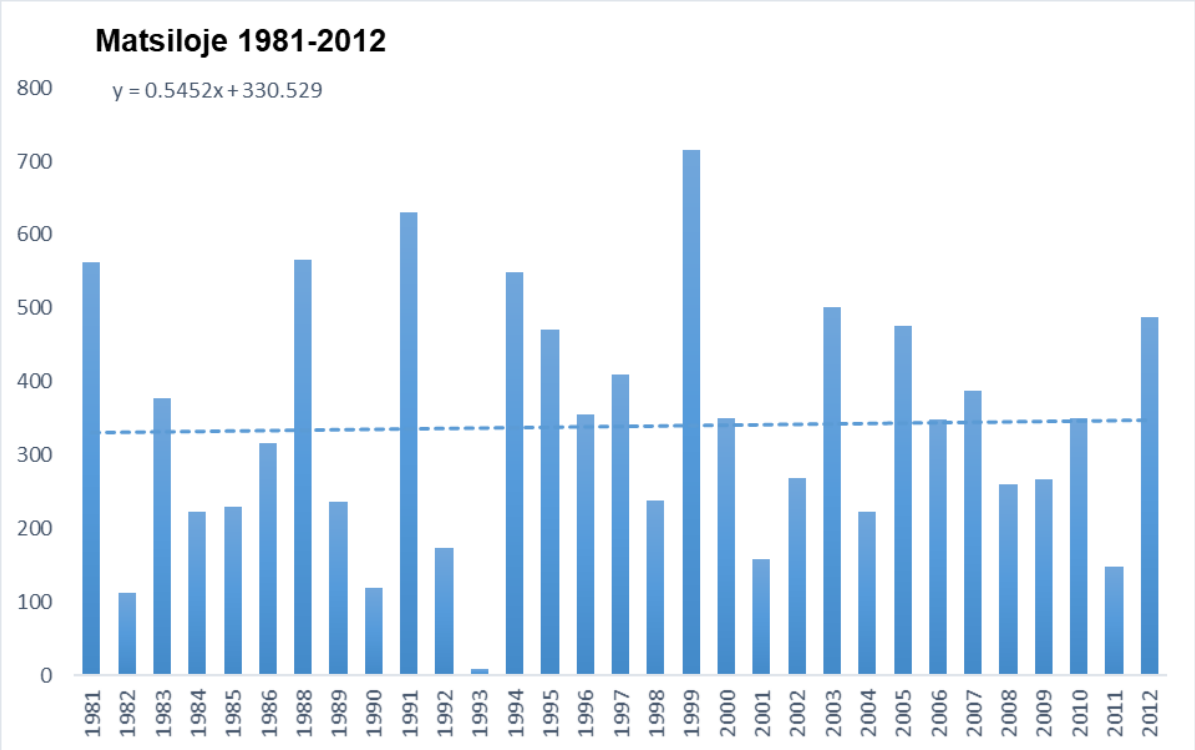

8.1al Rainfall data Matsiloje

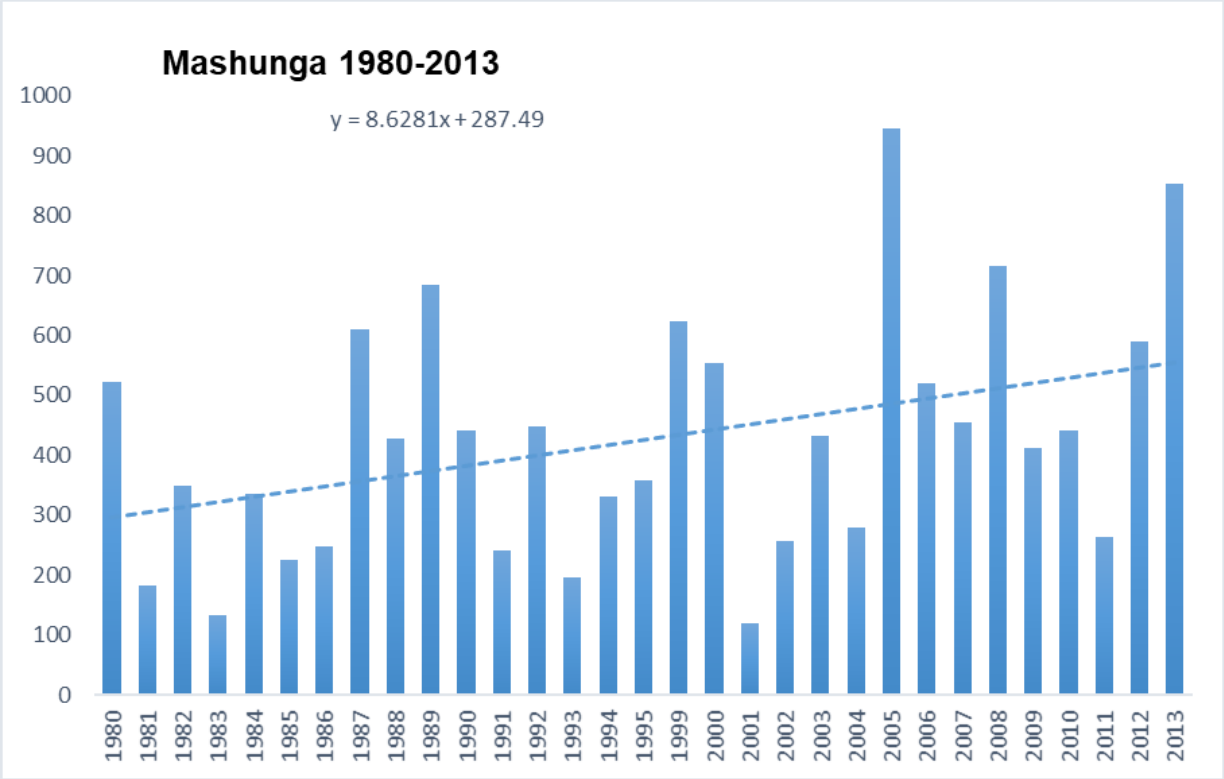

8.1am Rainfall data Mashunga

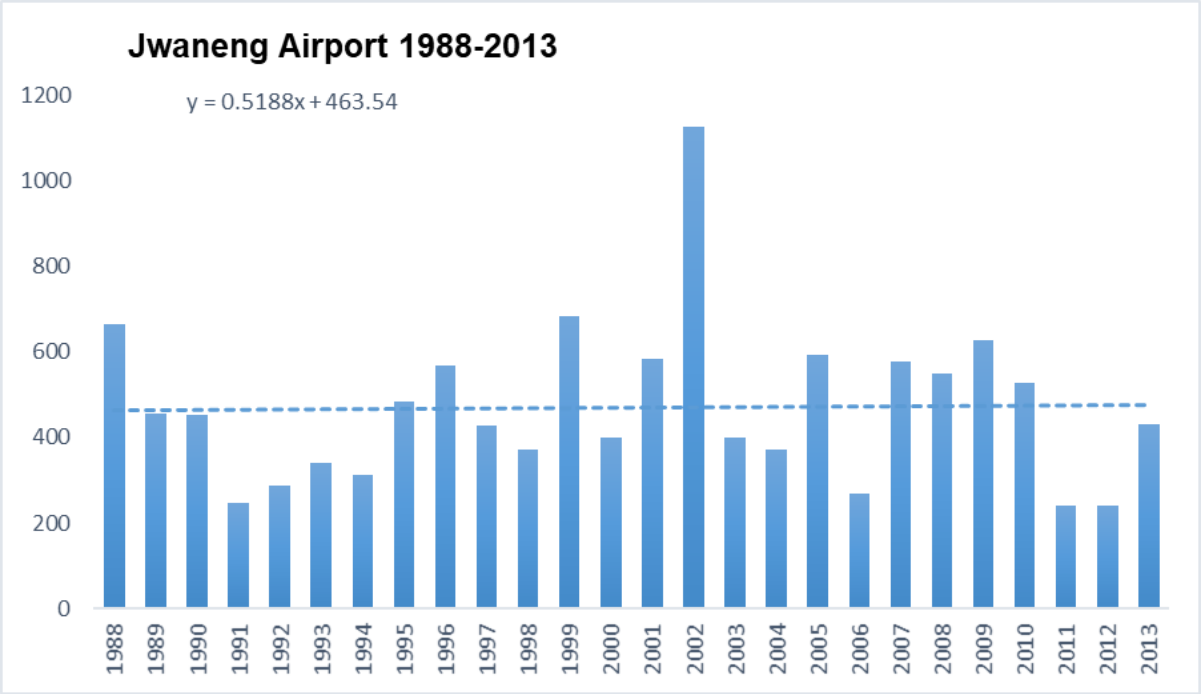

8.1an Rainfall data Jwaneng Airport

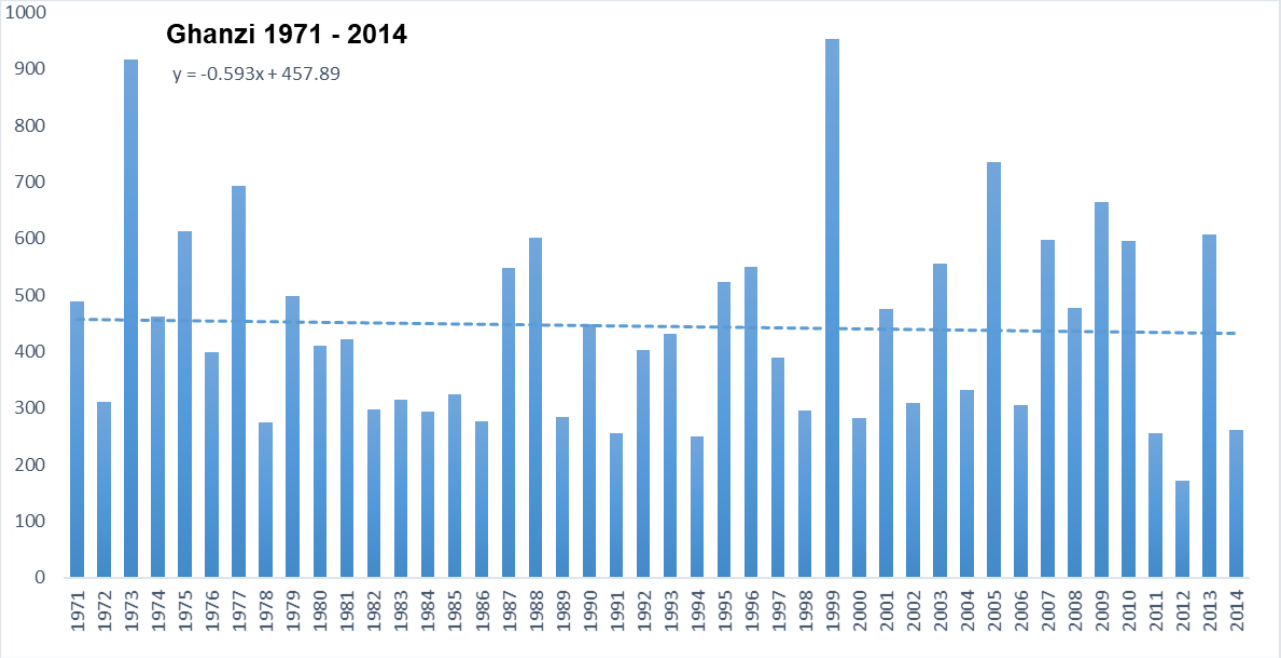

8.1ao Rainfall data Ghanzi

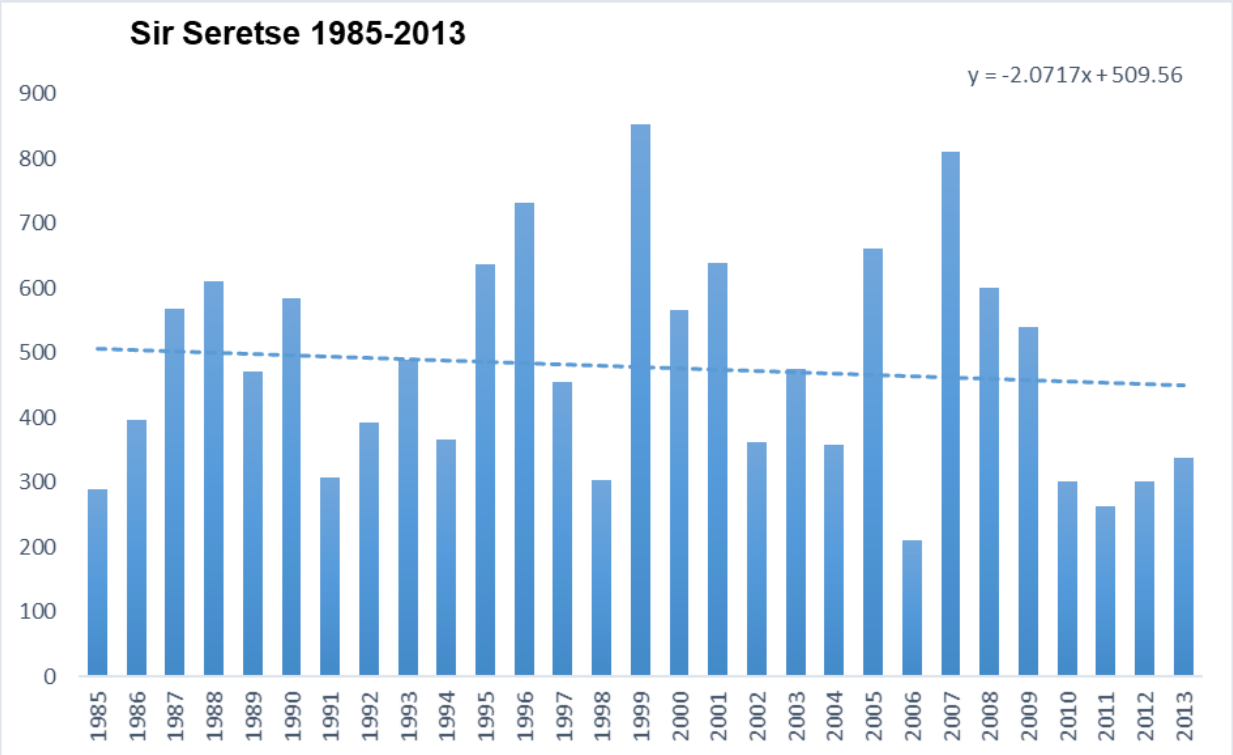

8.1ap Rainfall data Sir Seretse

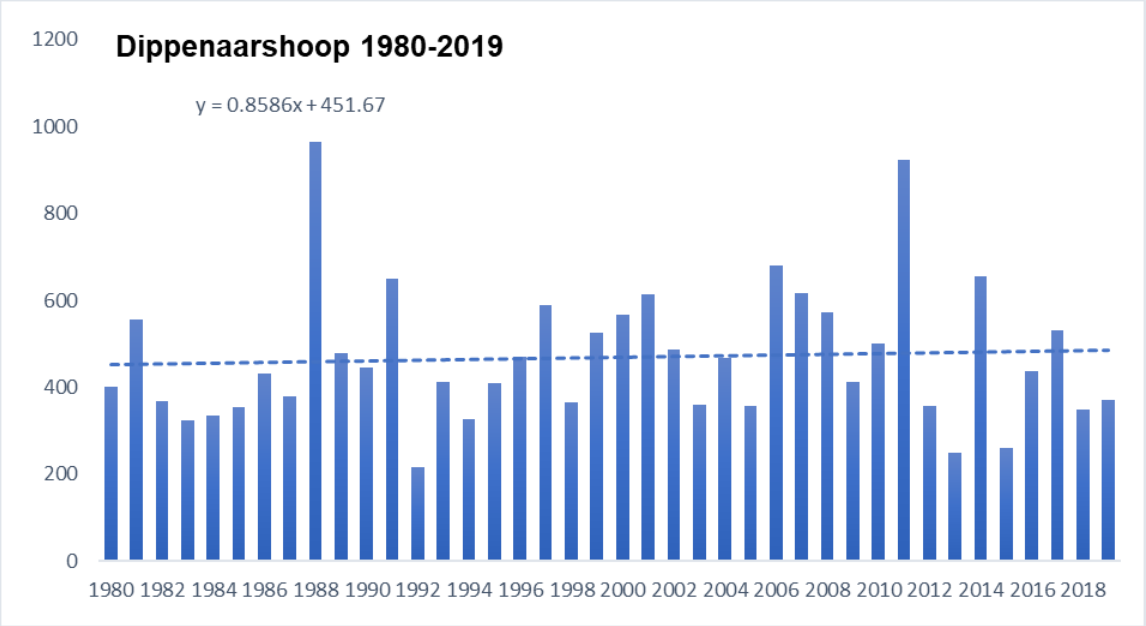

8.1aq Rainfall data Dippenaarshoop

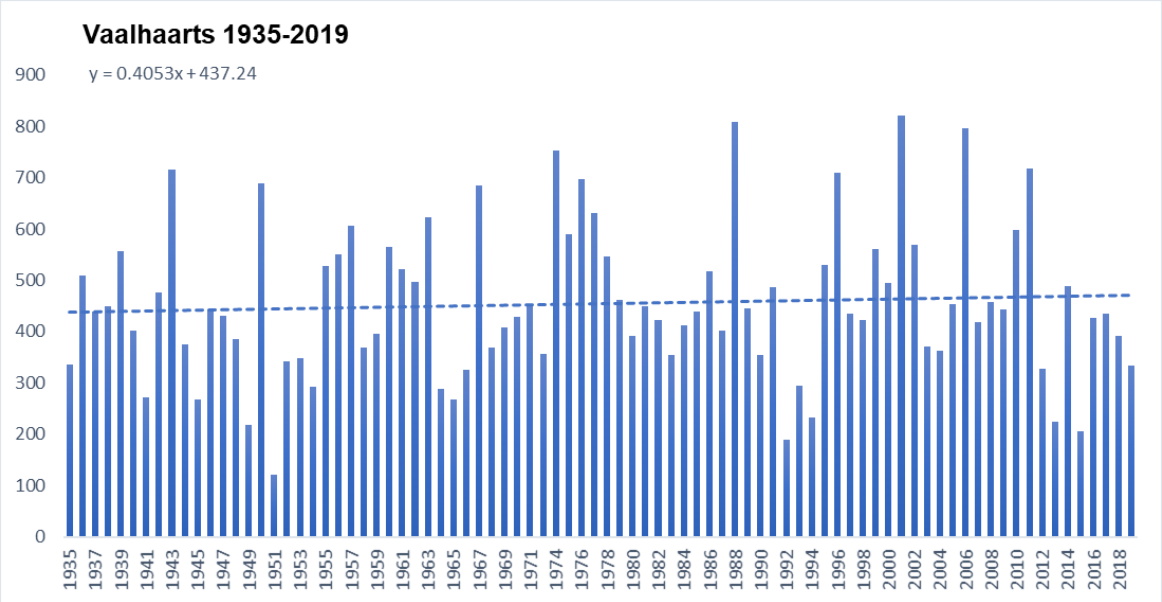

8.1ar Rainfall data Vaalharts

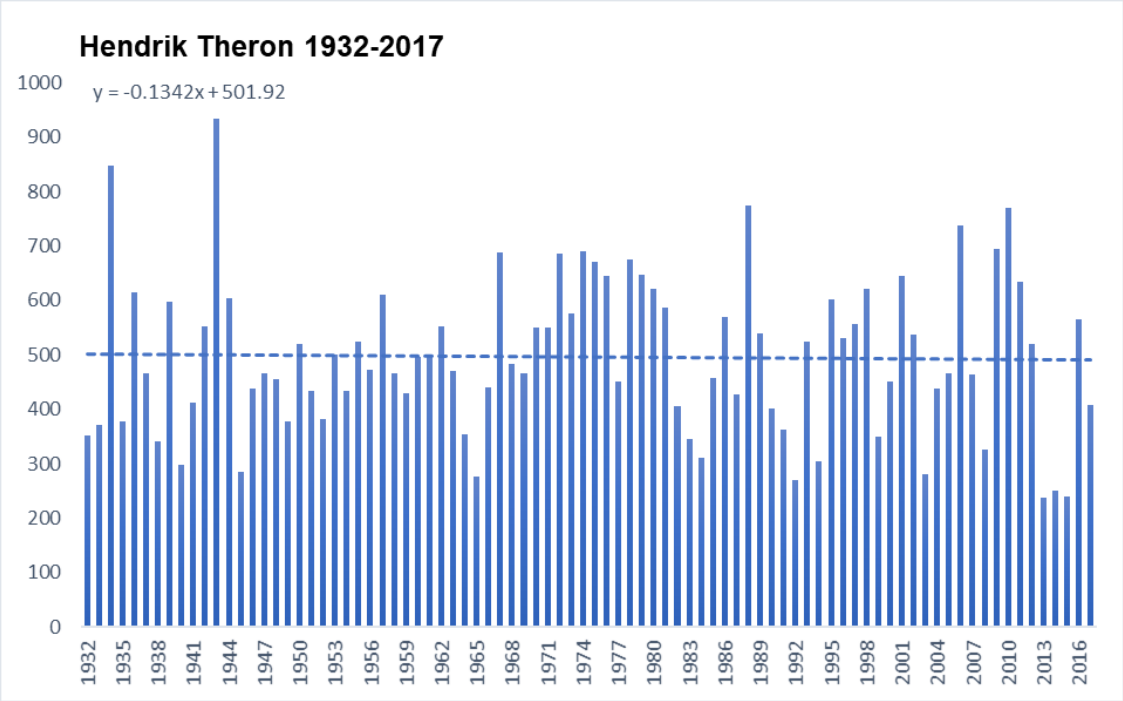

8.1as Rainfall data Hendrik Theron

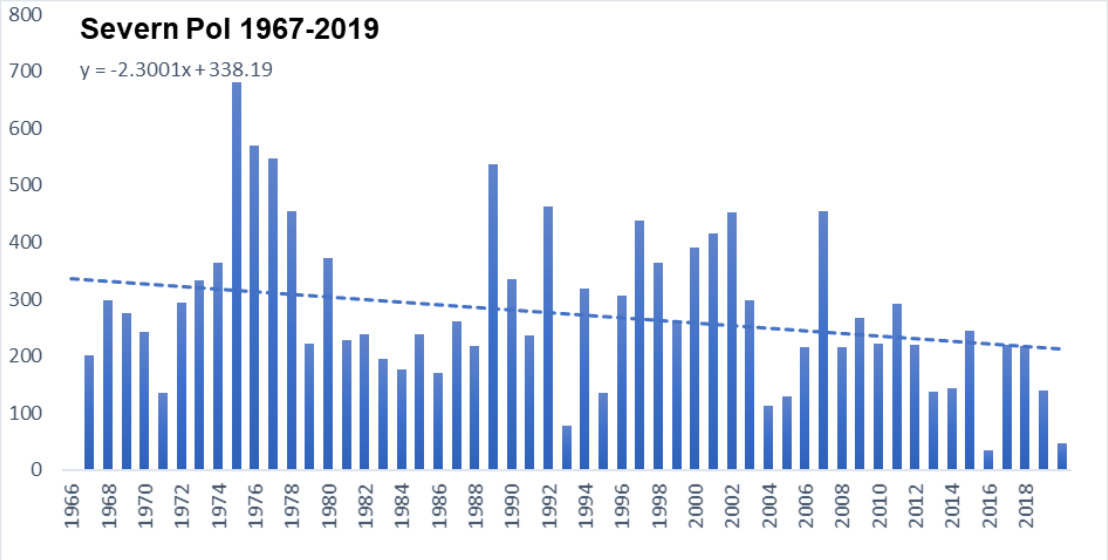

8.1at Rainfall data Severn Pol

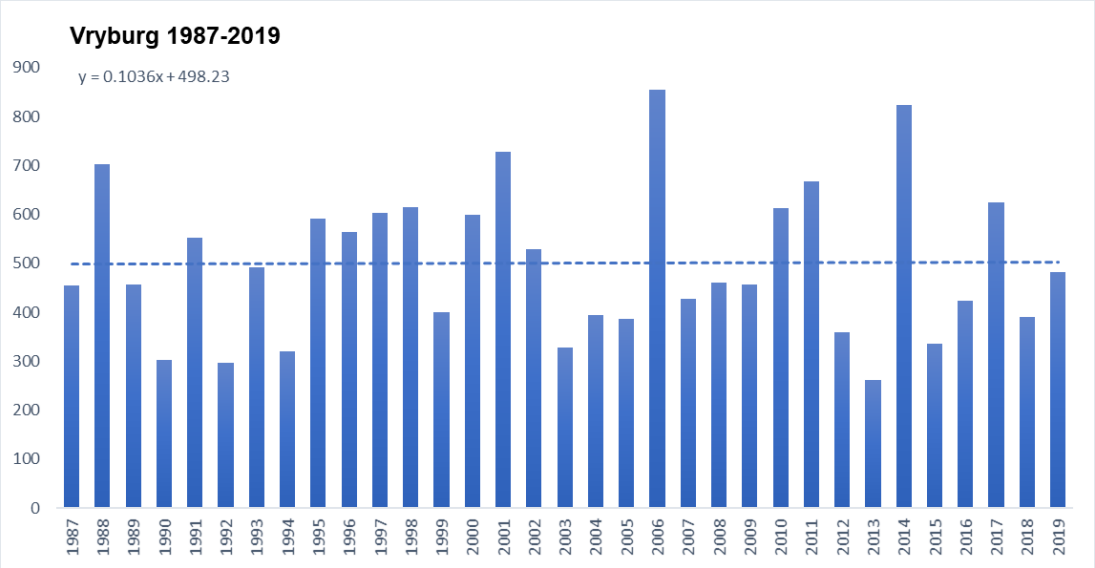

8.1au Rainfall data Vryburg

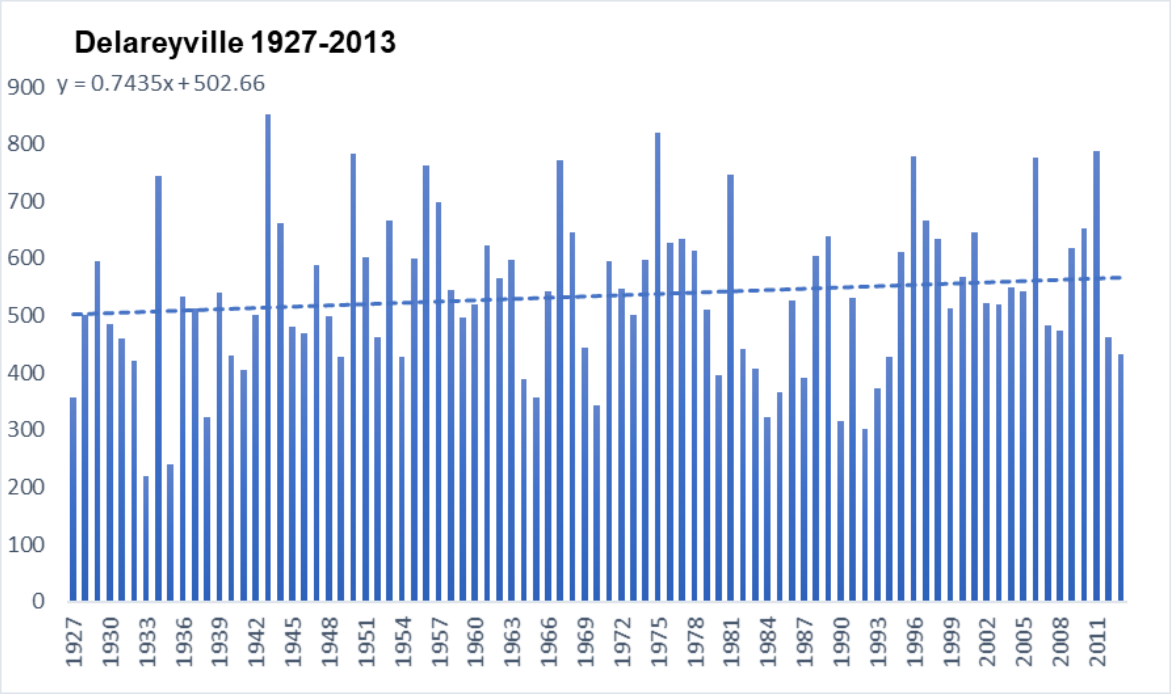

8.1av Rainfall data Delareyville

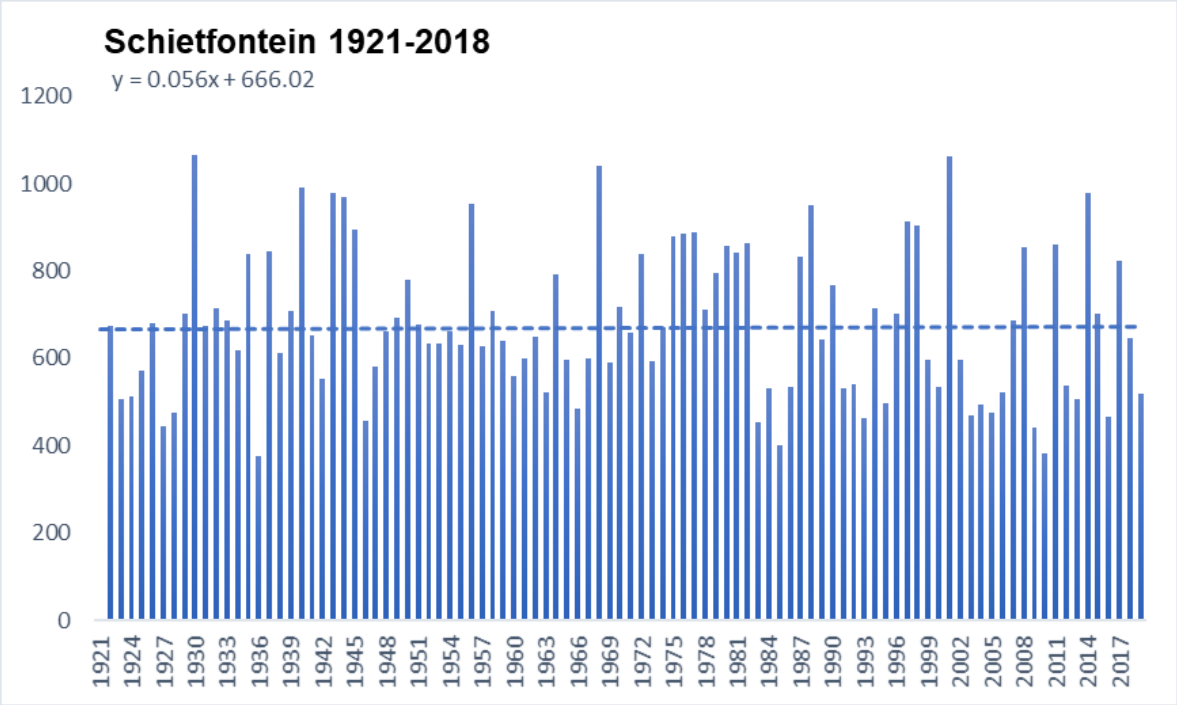

8.1aw Rainfall data Schietfontein

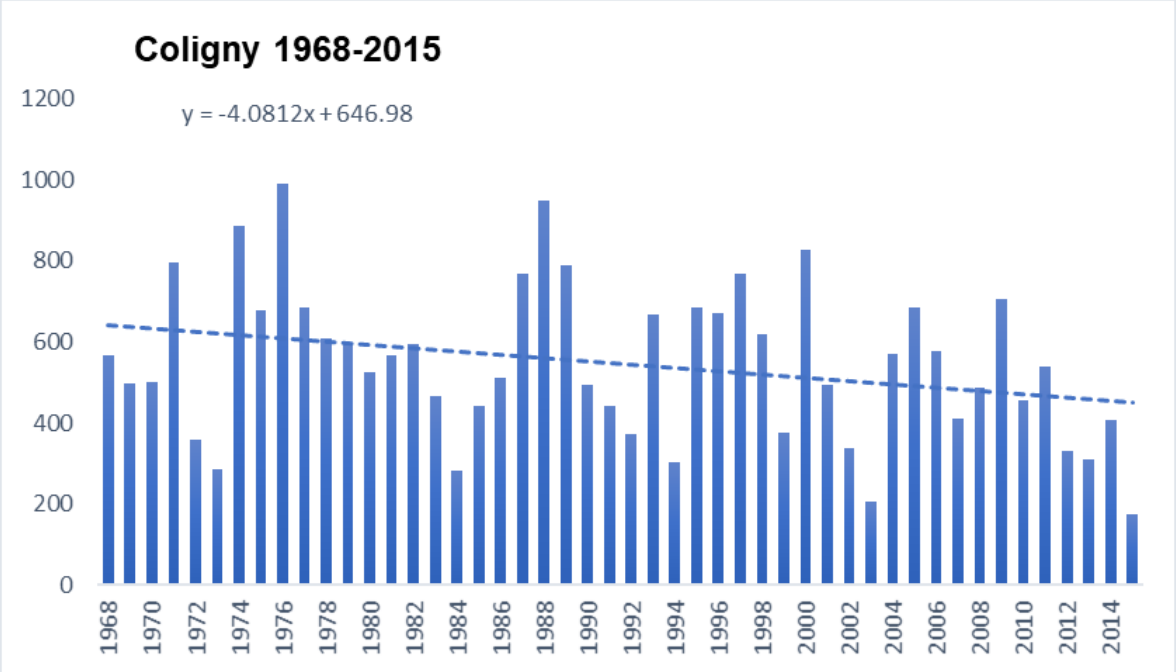

8.1ax Rainfall data Coligny

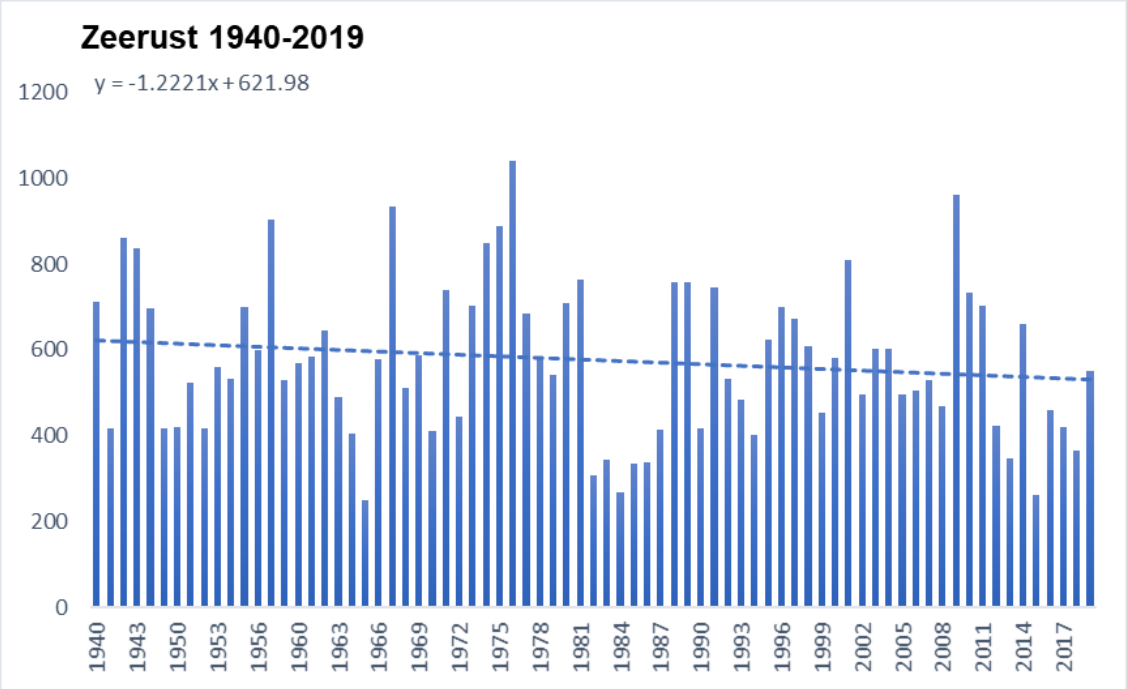

8.1ay Rainfall data Zeerust

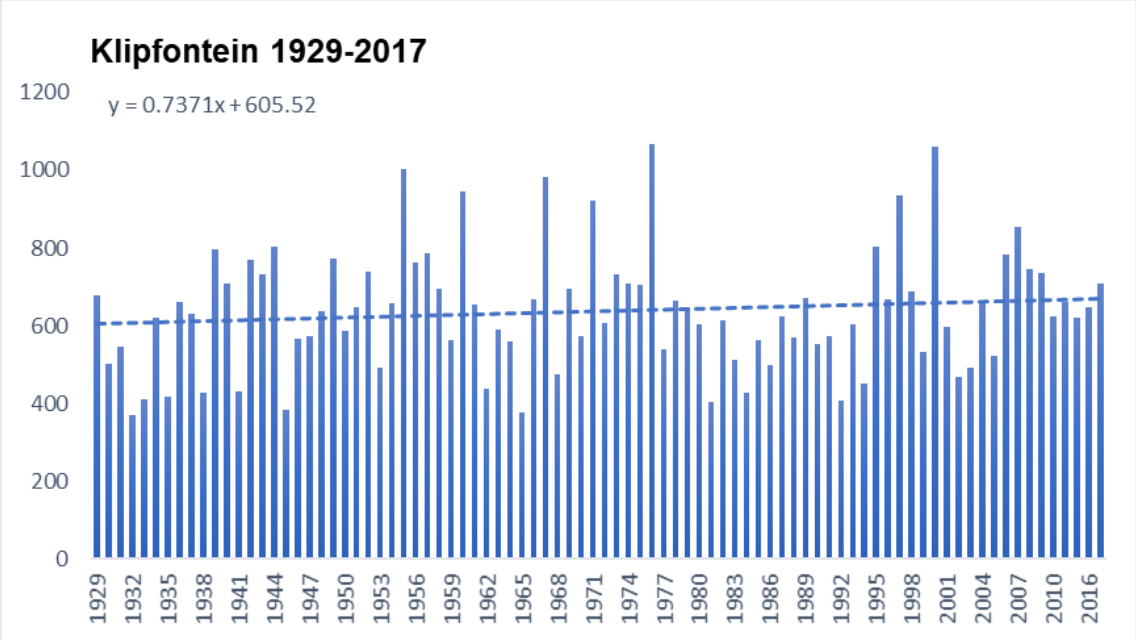

8.1az Rainfall data Klipfontein

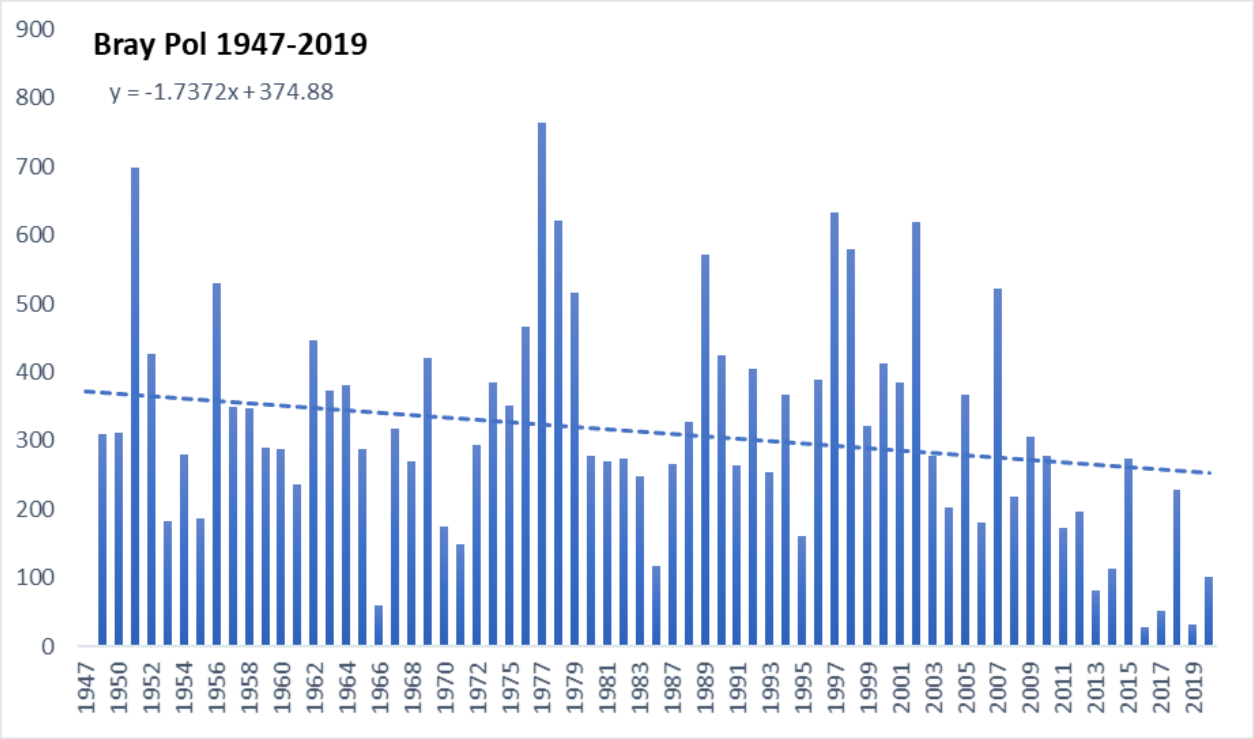

8.1ba Rainfall data Bray Pol

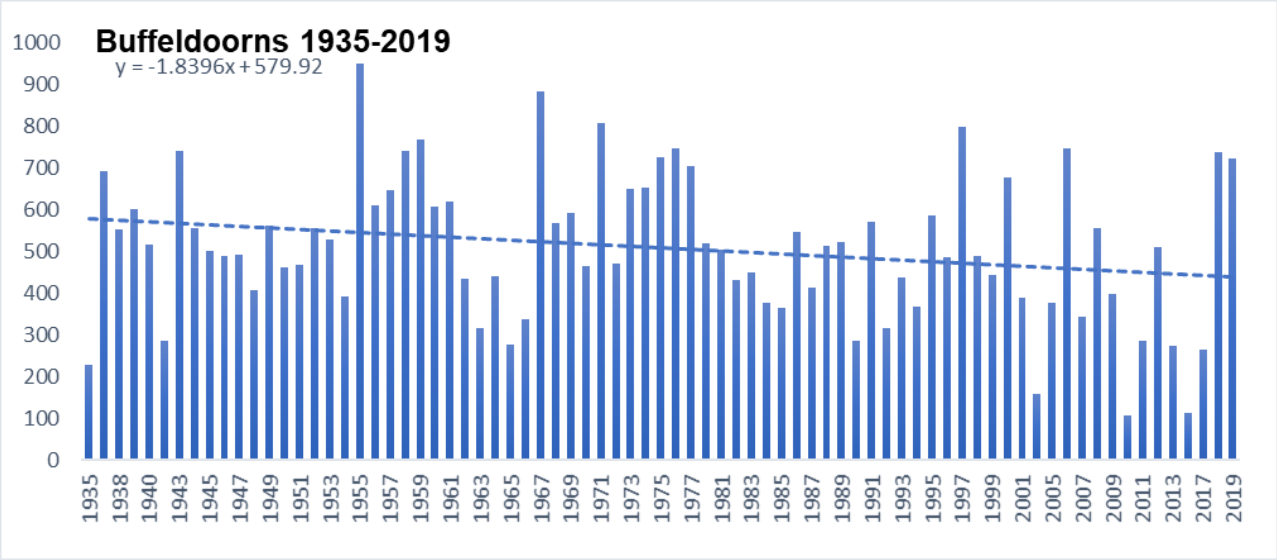

8.1bb Rainfall data Buffeldoorns

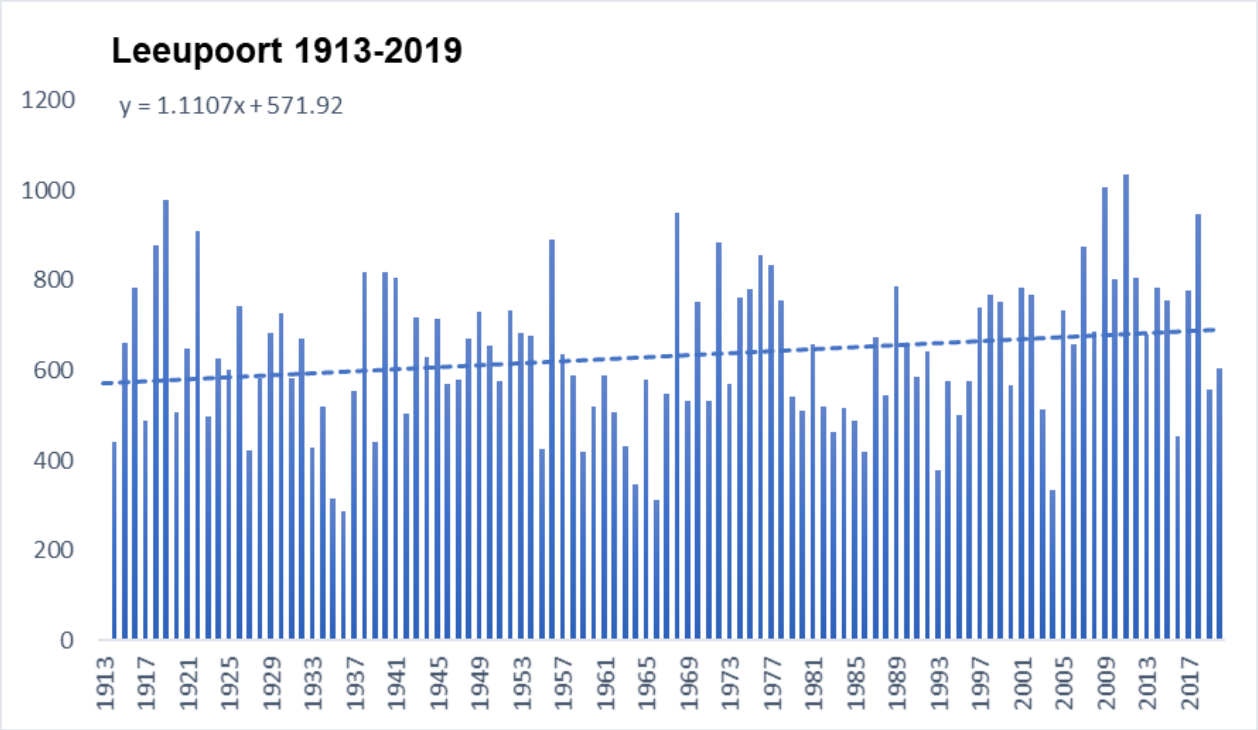

8.1bc Rainfall data Leeupoort

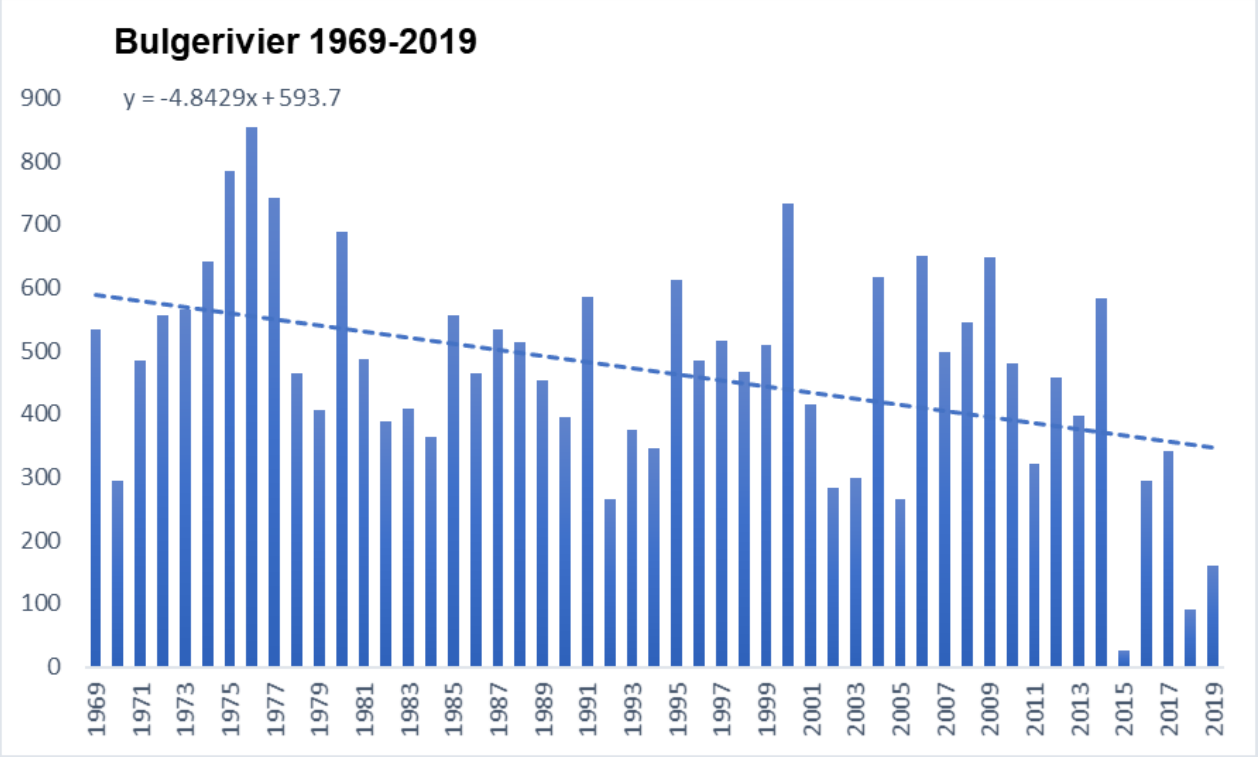

8.1bd Rainfall data Bulgerivier

8.2. SPI Results (The 12-month Standard Precipitation Index (SPI))

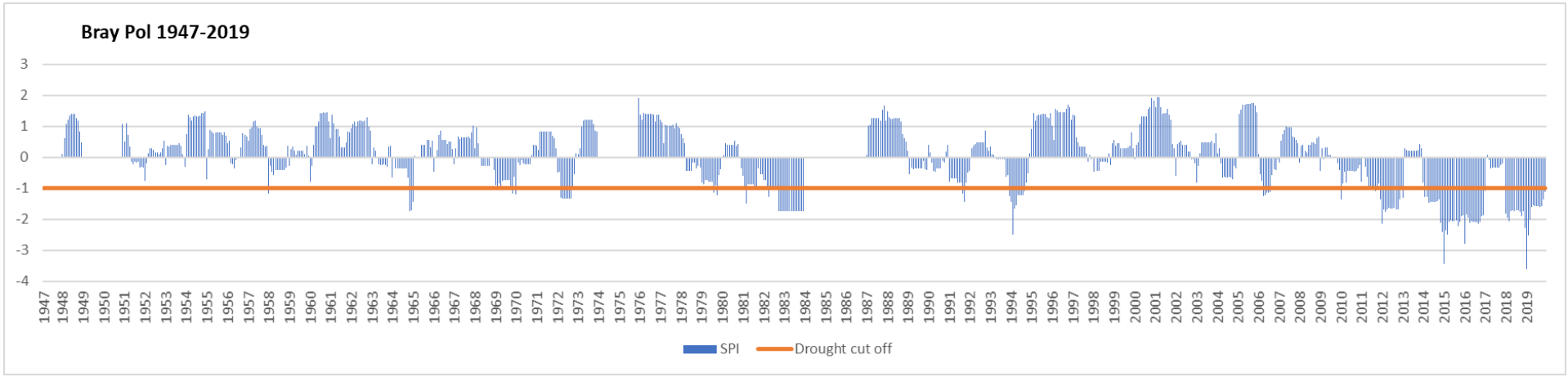

Figure 8.2a: The 12-month SPI for Bray Pol

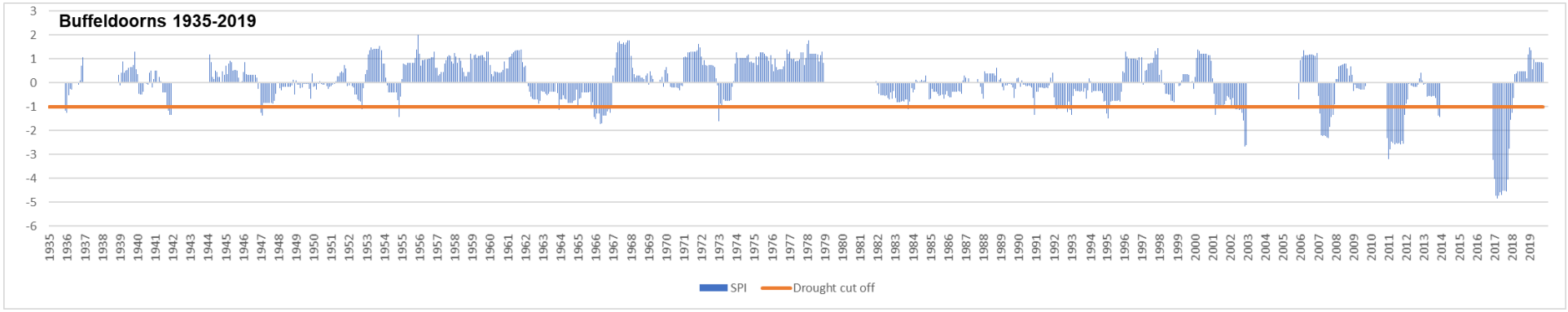

Figure 8.2b: The 12-month SPI for Buffeldoorns

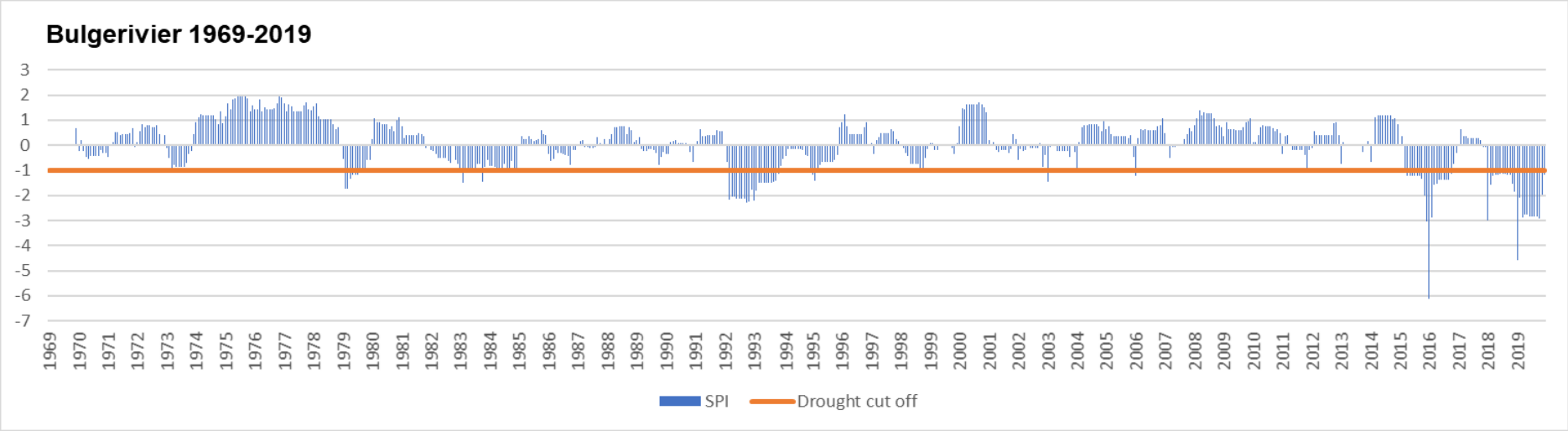

Figure 8.2c: The 12-month SPI for Bulgerivier

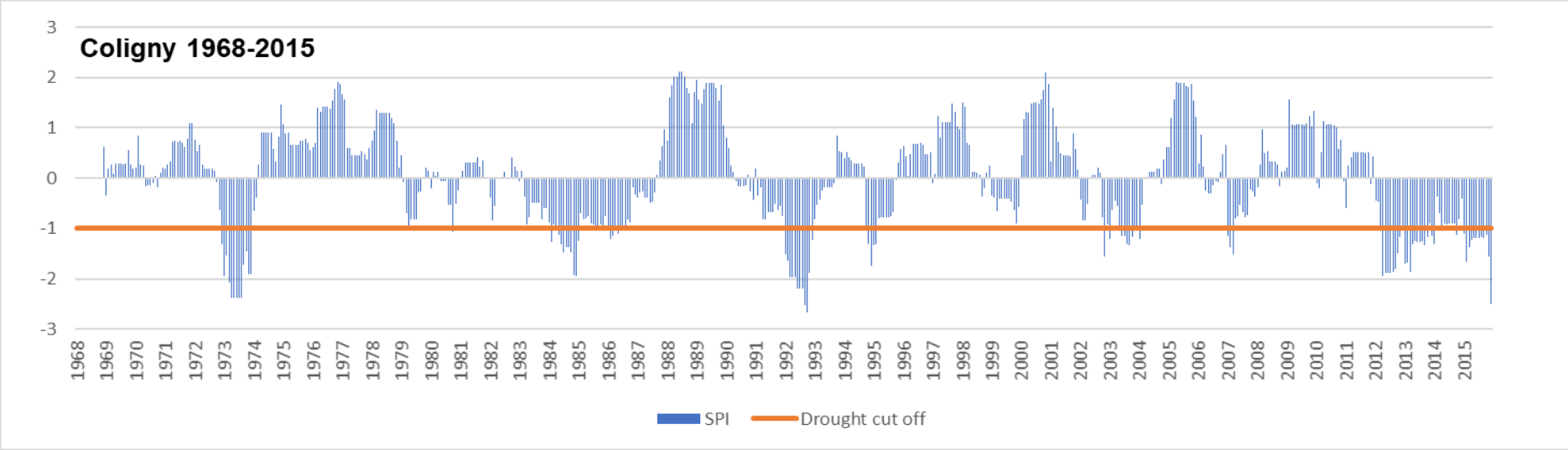

Figure 8.2d: The 12-month SPI for Coligny

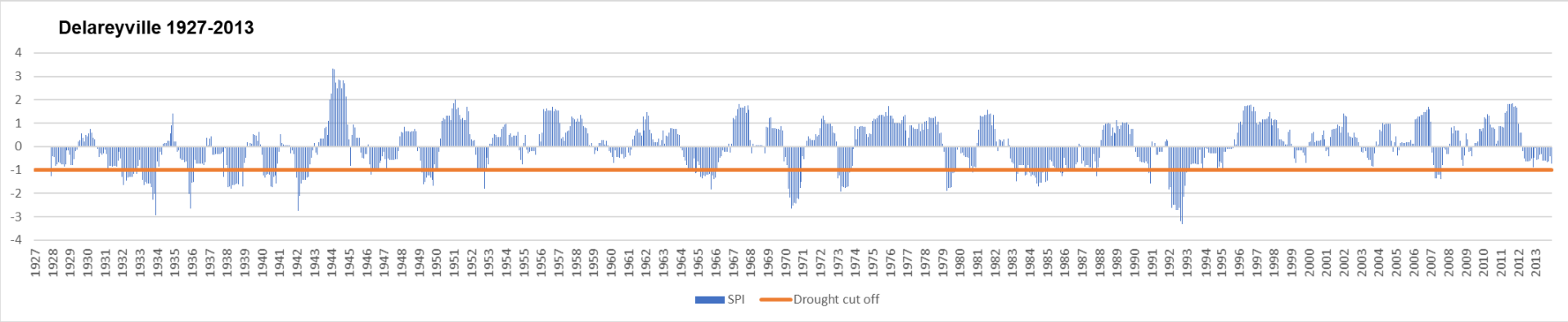

Figure 8.2e: The 12-month SPI for Delareyville

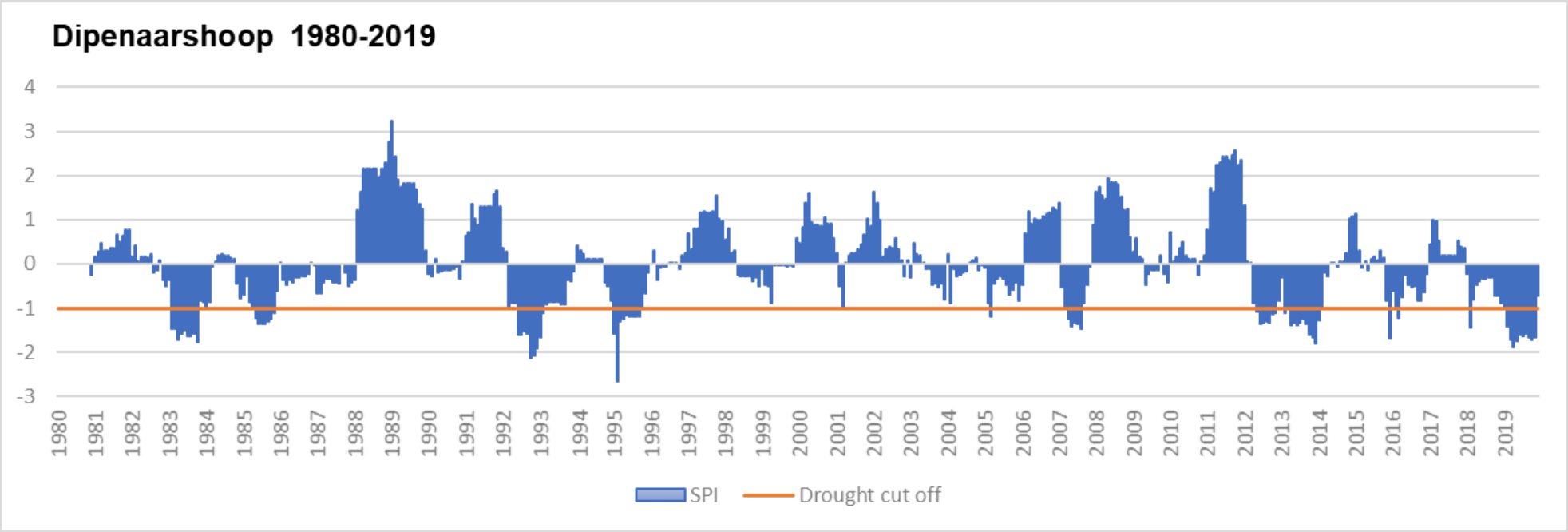

Figure 8.2f: The 12-month SPI for Dippenaarshoop

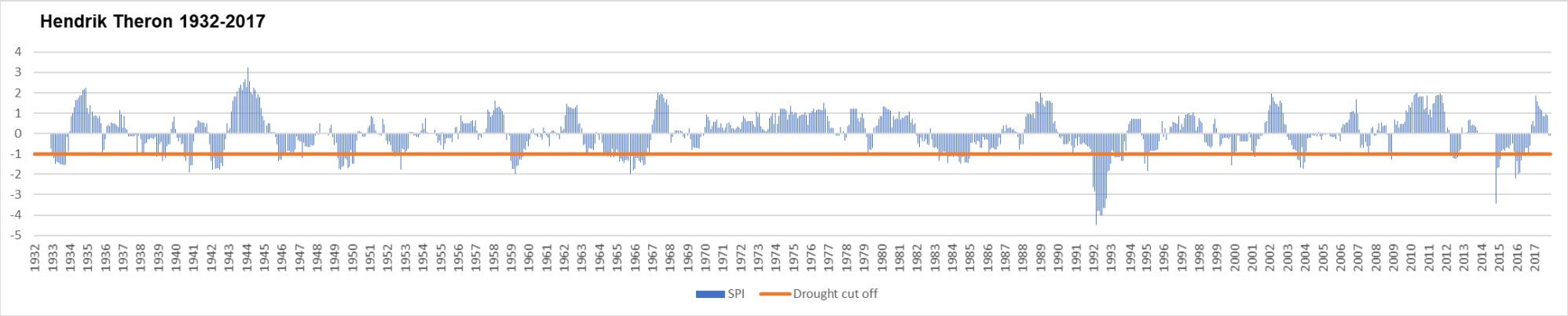

Figure 8.2g: The 12-month SPI for Hendrik Theron

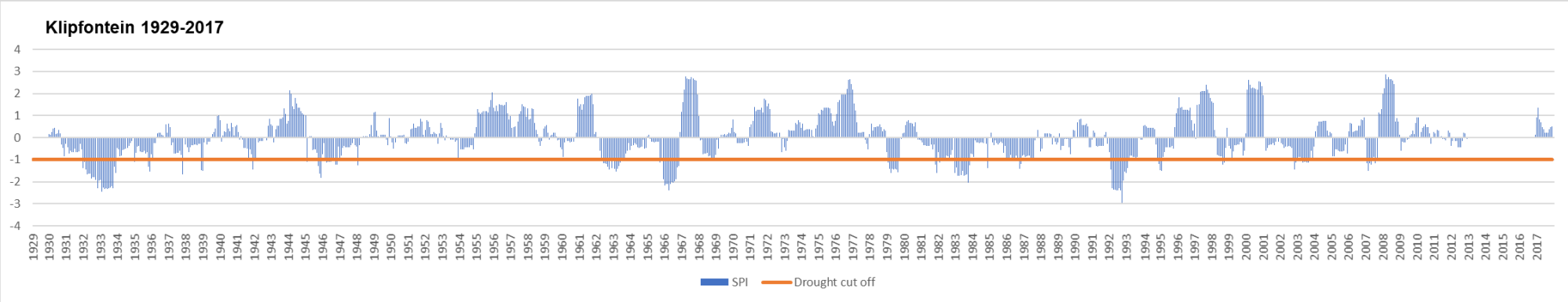

Figure 8.2h: The 12-month SPI for Klipfontein

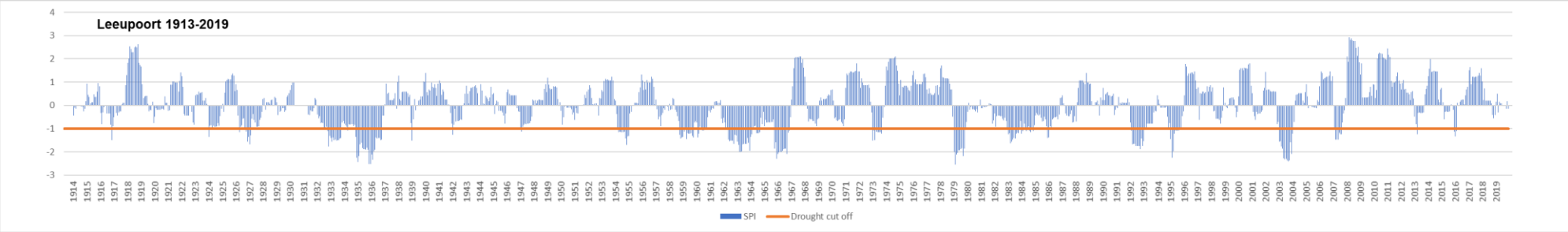

Figure 8.2i: The 12-month SPI for Leeupoort

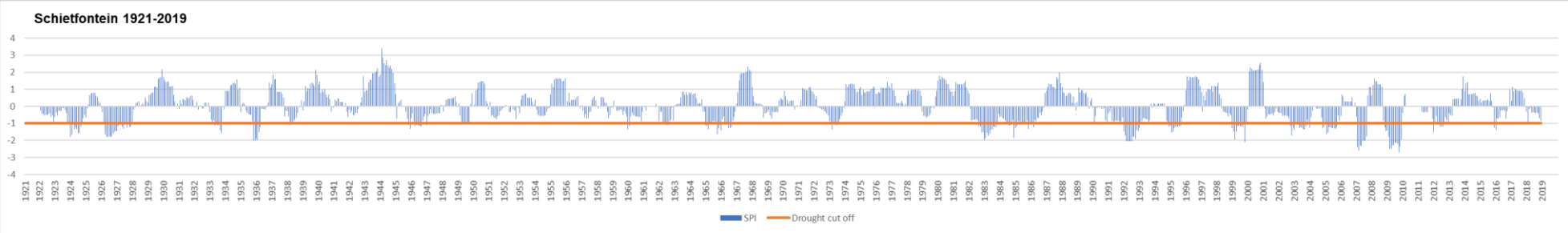

Figure 8.2j: The 12-month SPI for Schietfontein

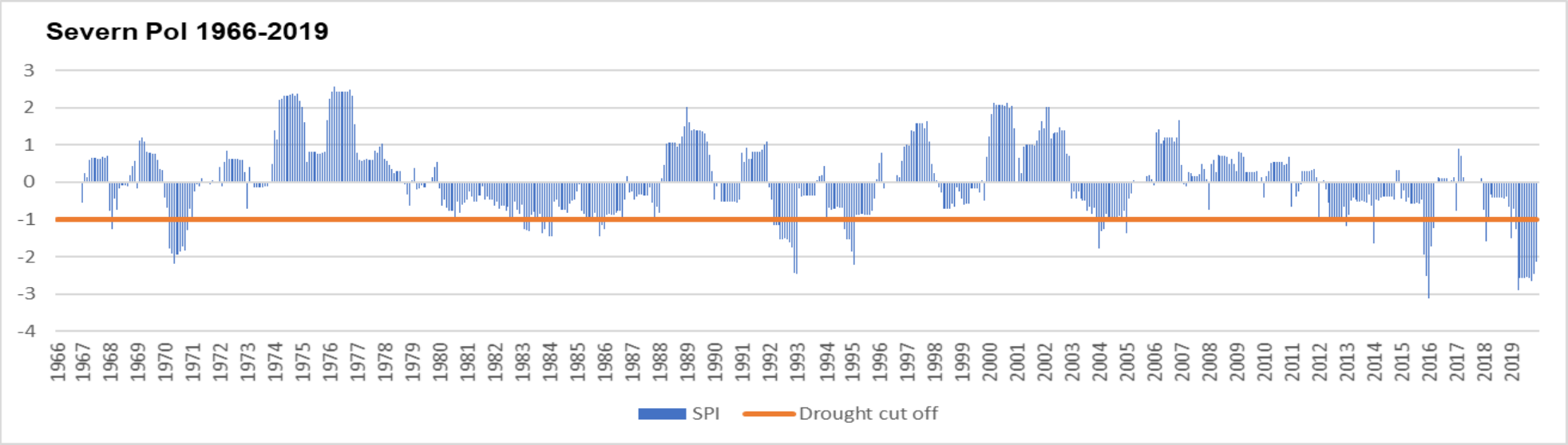

Figure 8.2k: The 12-month SPI for Severn Pol

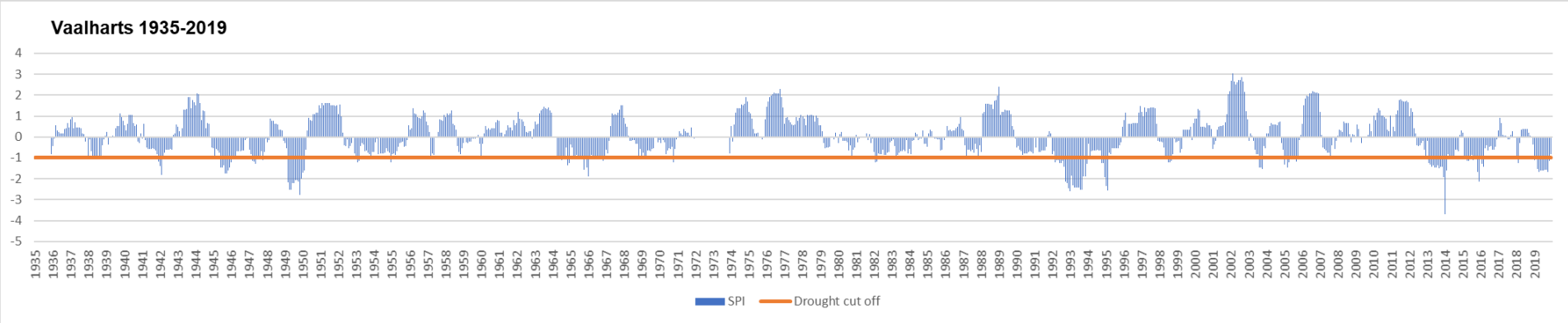

Figure 8.2m: The 12-month SPI for Vaalharts

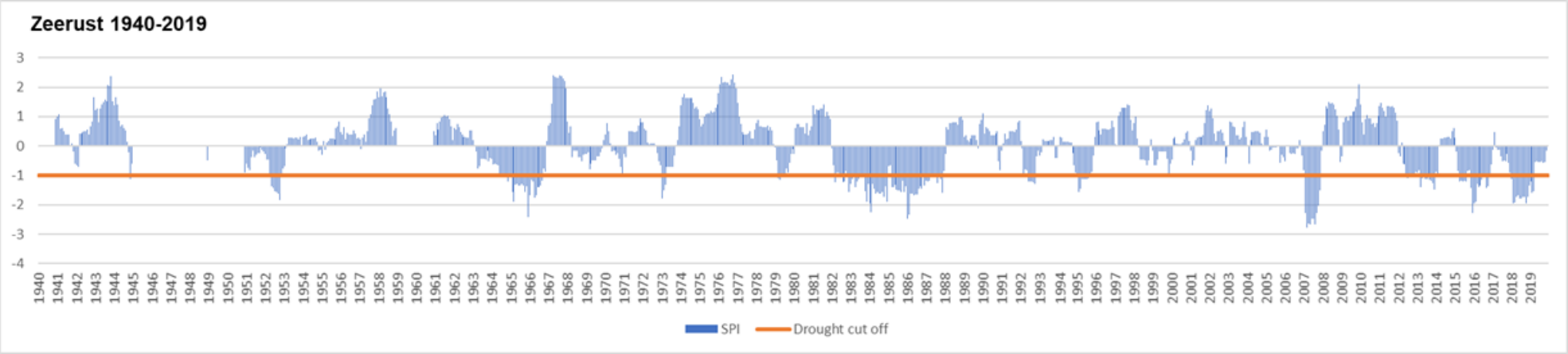

Figure 8.2n: The 12-month SPI for Zeerust

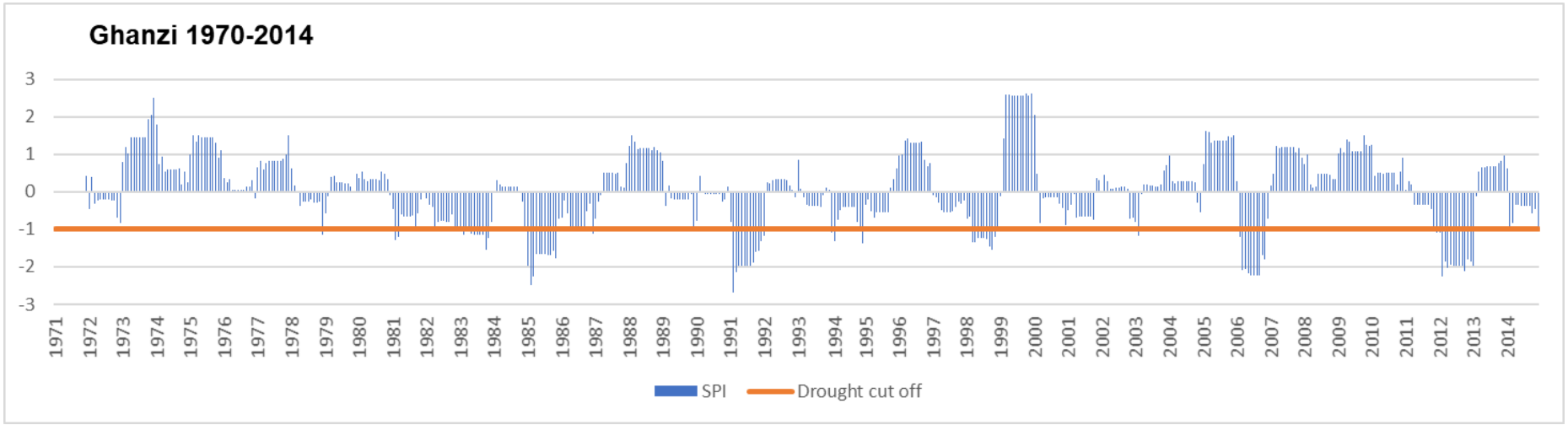

Figure 8.2o: The 12-month SPI for Ghanzi

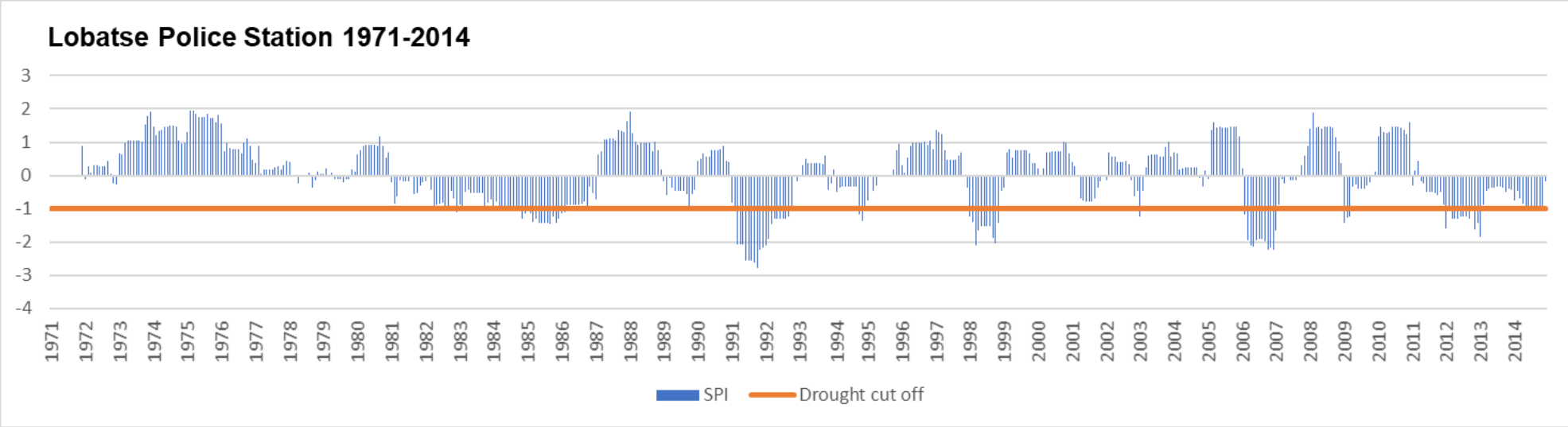

Figure 8.2o: The 12-month SPI for Lobatse Police Station

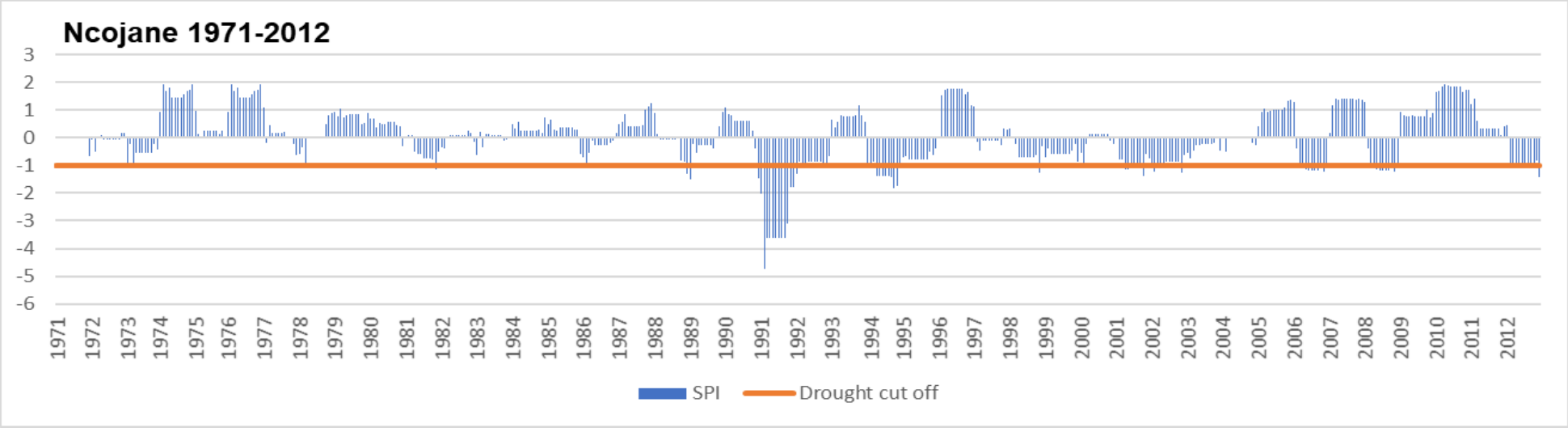

Figure 8.2p: The 12-month SPI for Ncojane

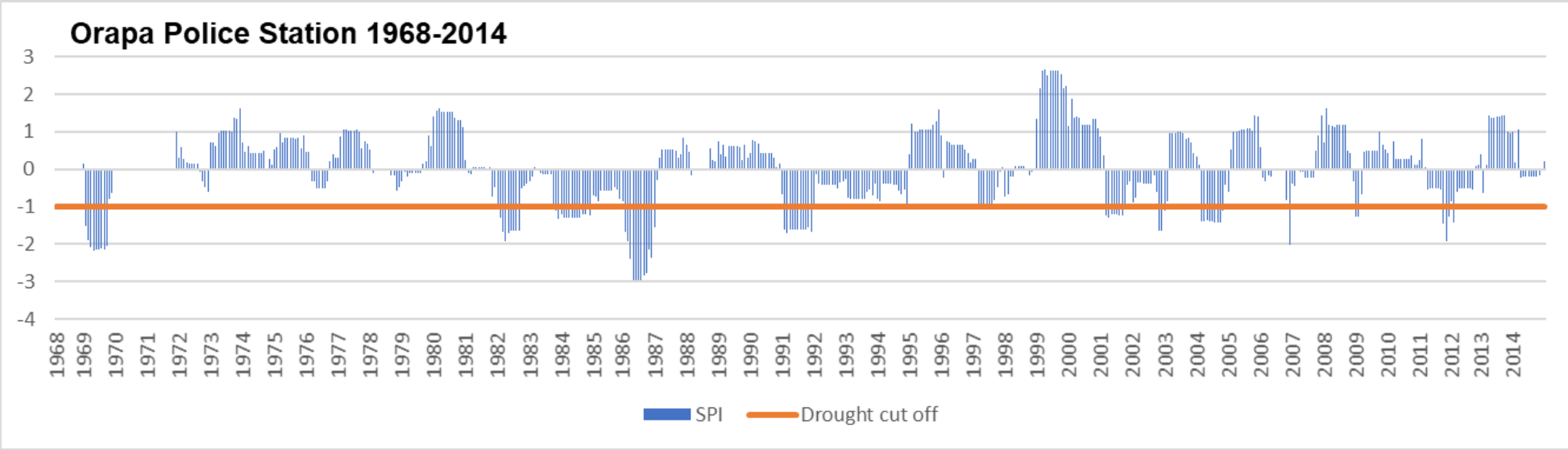

Figure 8.2q: The 12-month SPI for Orapa Police Station

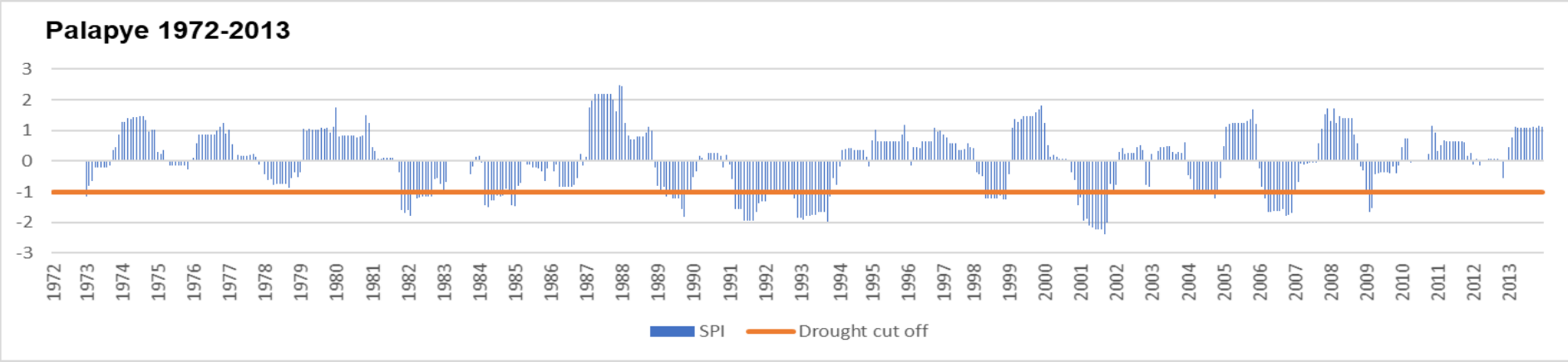

Figure 8.2r: The 12-month SPI for Palapye

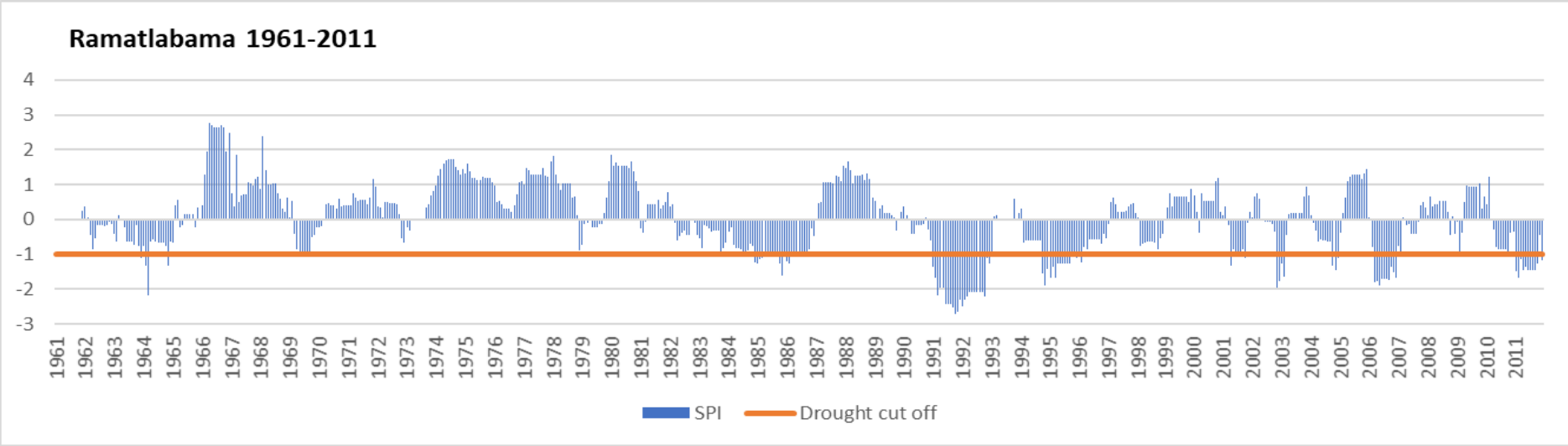

Figure 8.2s: The 12-month SPI for Ramatlabama

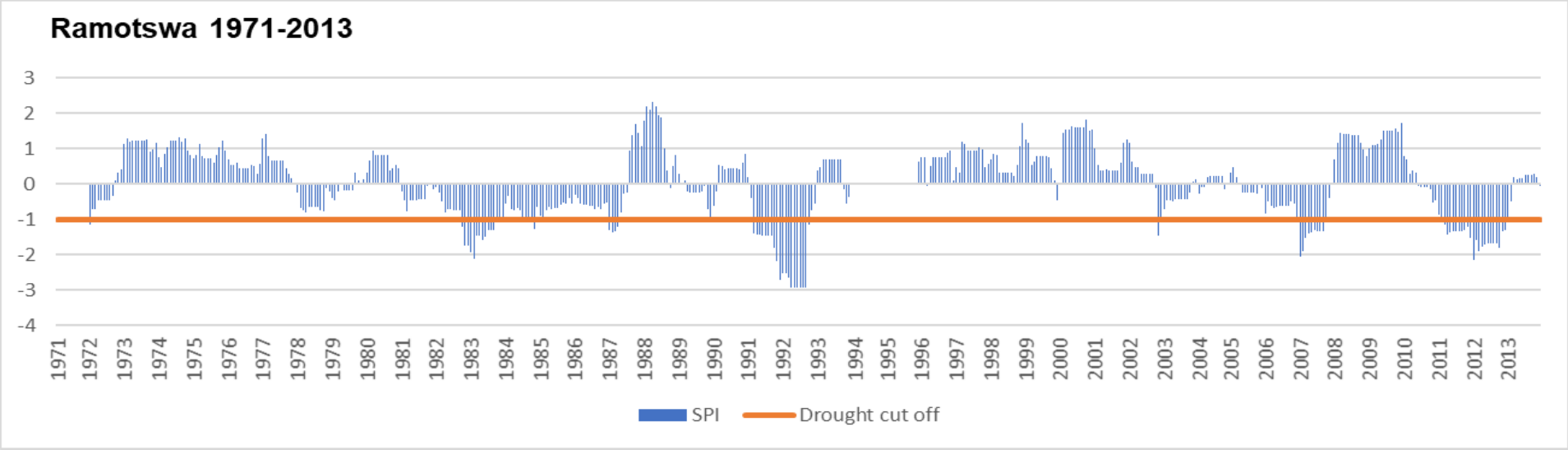

Figure 8.2t: The 12-month SPI for Ranotswa

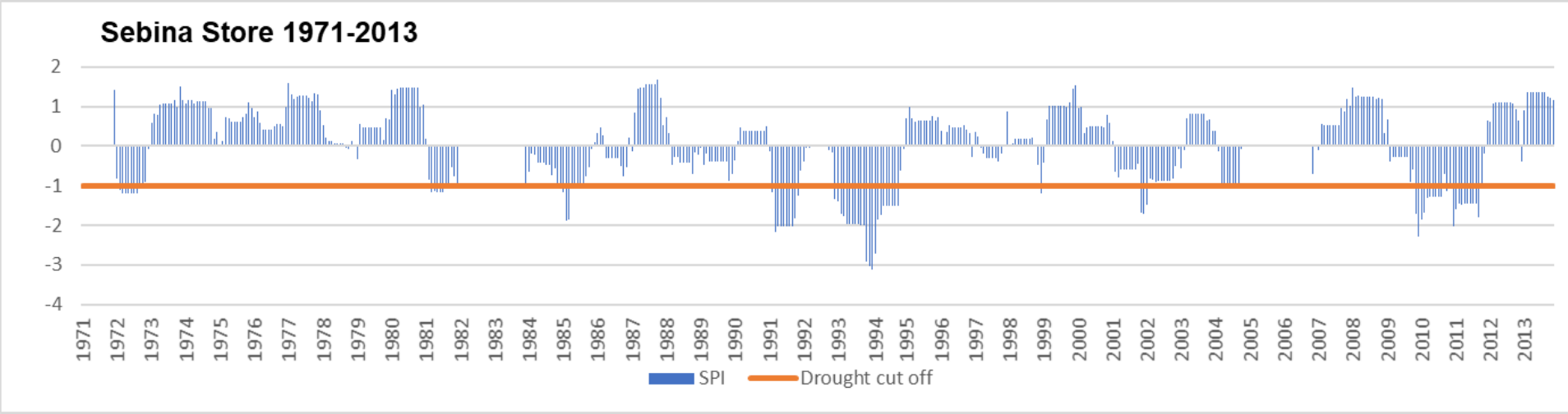

Figure 8.2u: The 12-month SPI for Sebina Store

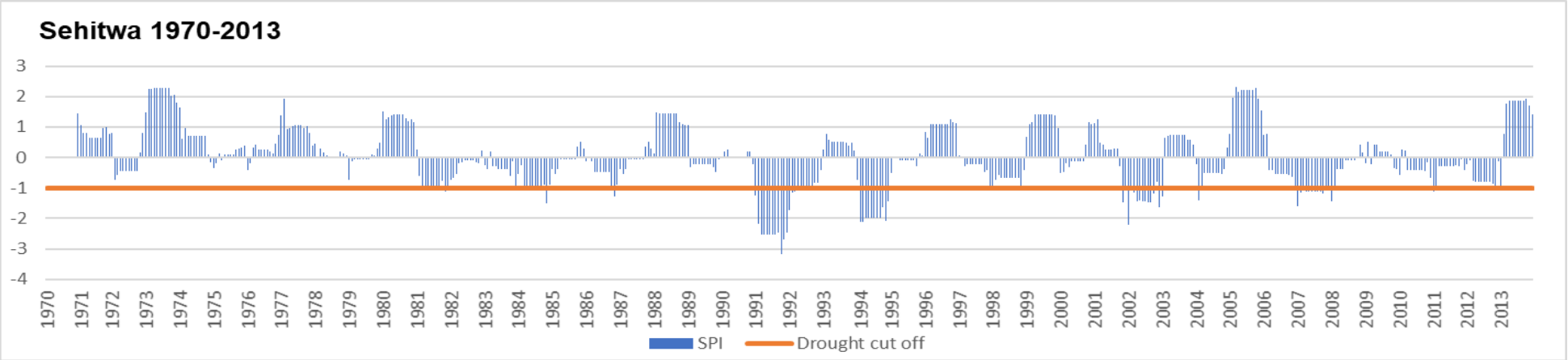

Figure 8.2v: The 12-month SPI for Sehitwa

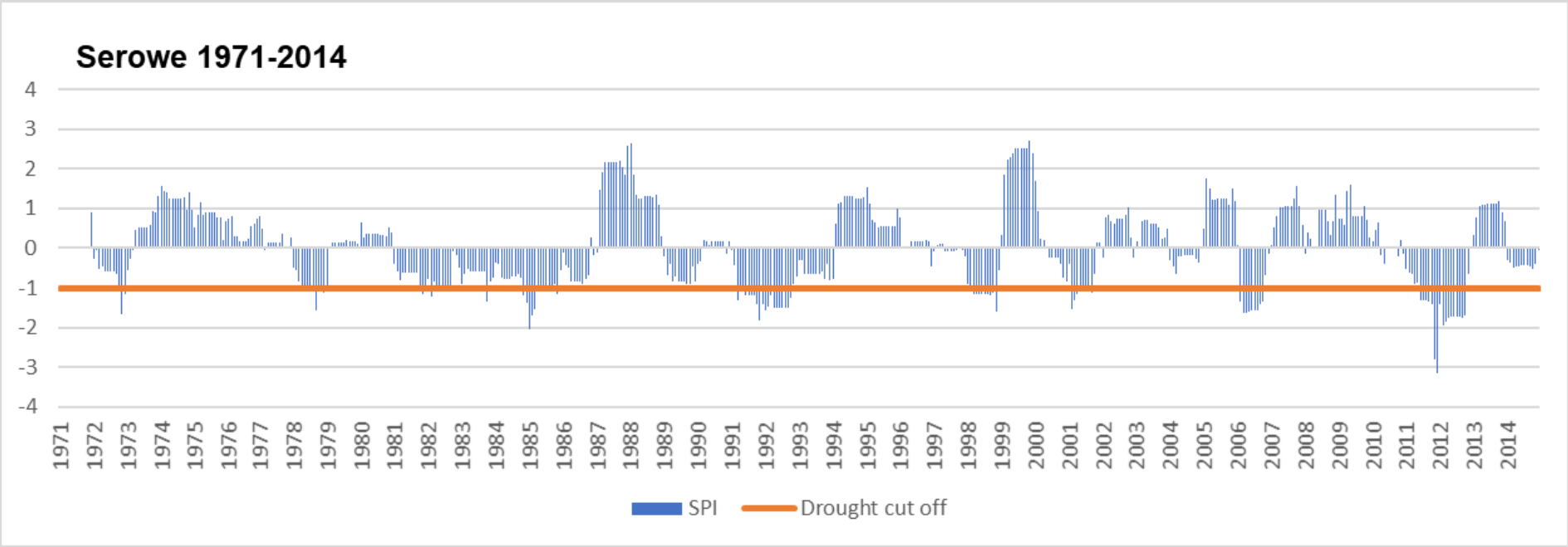

Figure 8.2w: The 12-month SPI for Serowe

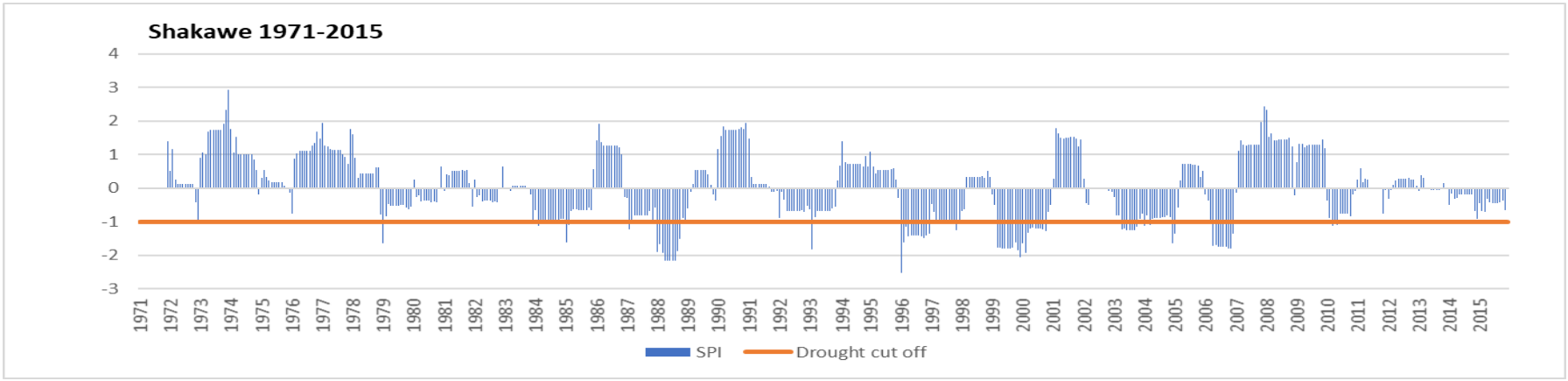

Figure 8.2x: The 12-month SPI for Shakawe

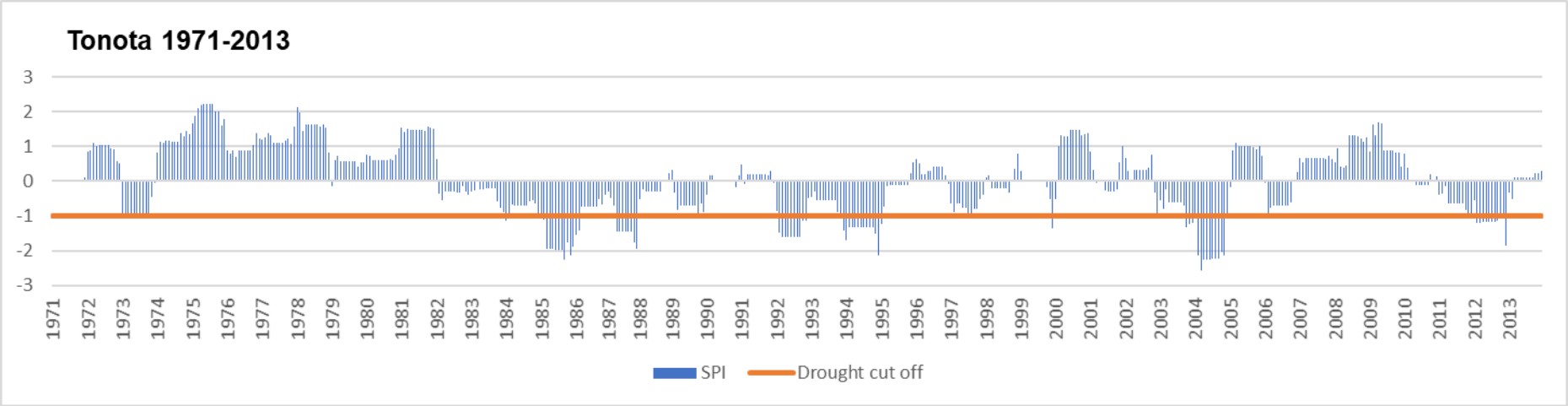

Figure 8.2y: The 12-month SPI for Tonota

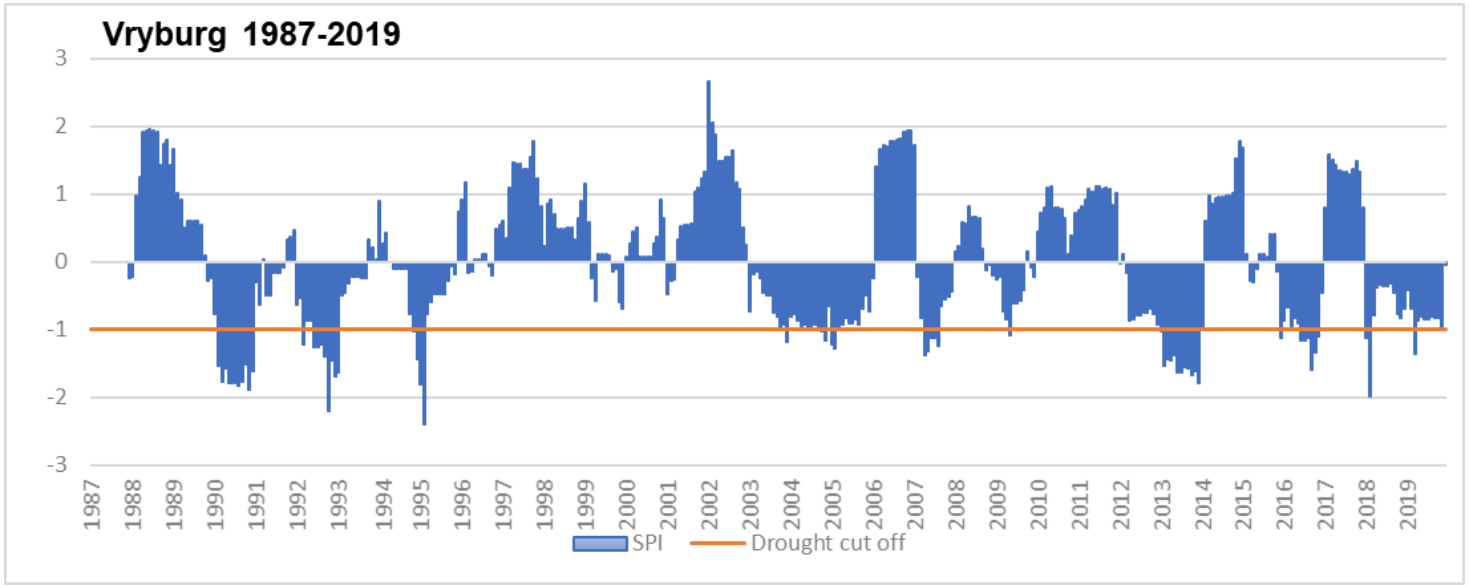

Figure 8.2z: The 12-month SPI for Vryburg

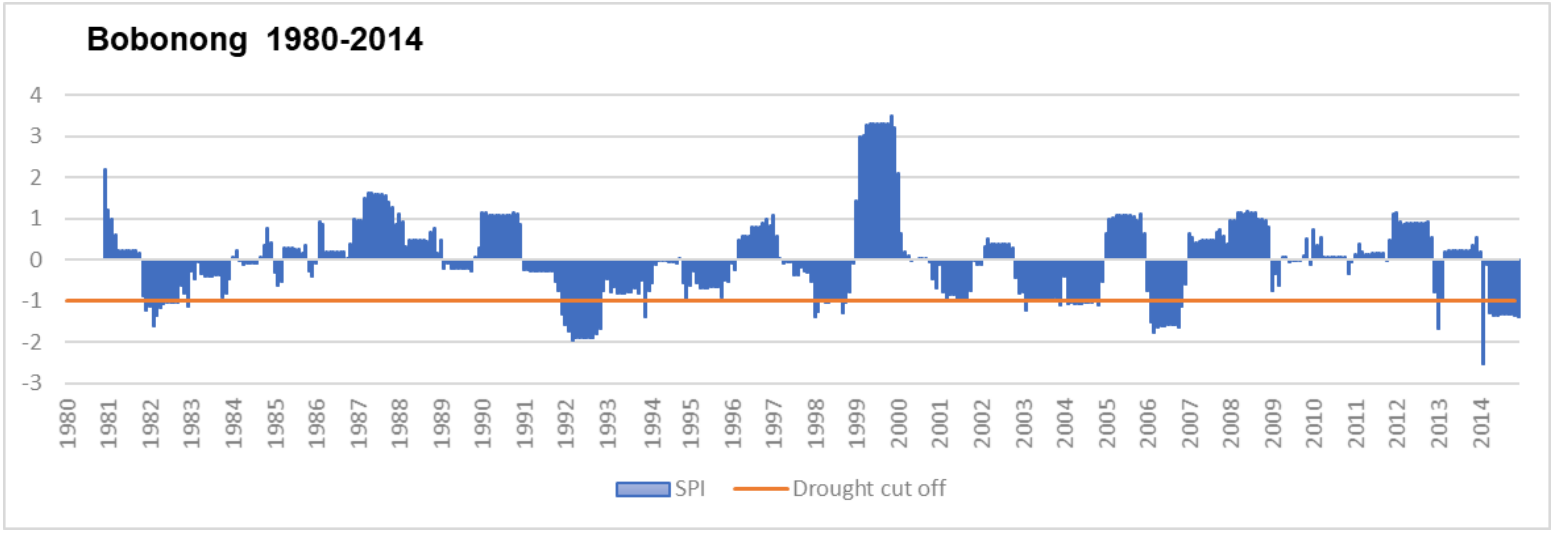

Figure 8.2aa: The 12-month SPI for Bobonong

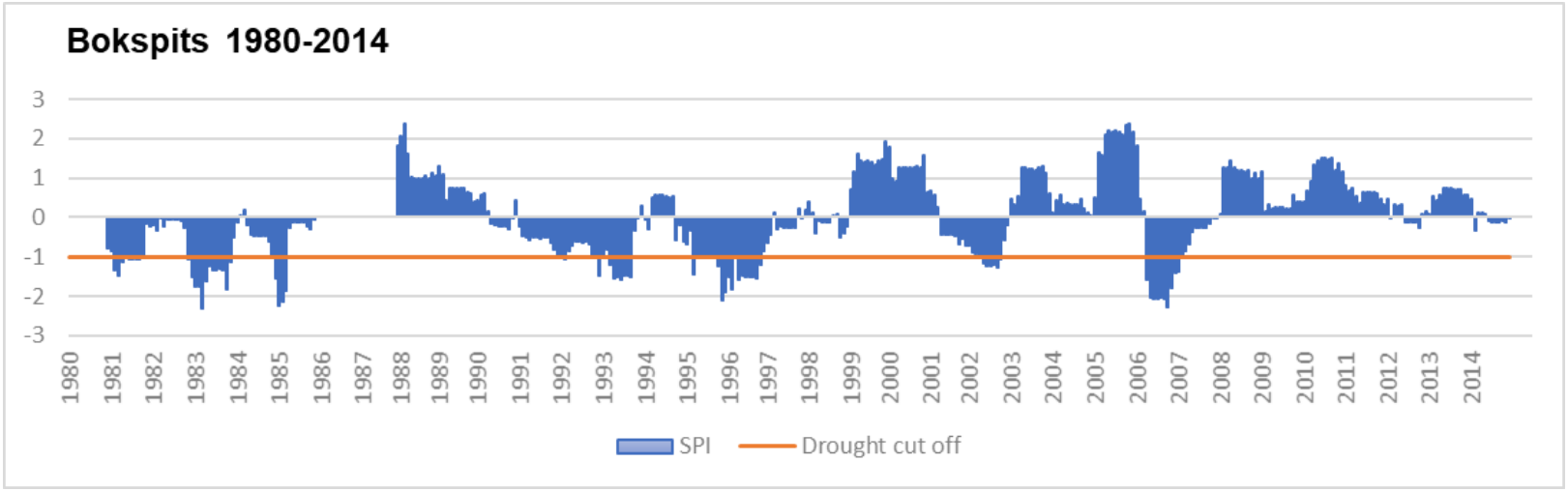

Figure 8.2ab: The 12-month SPI for Bokspits

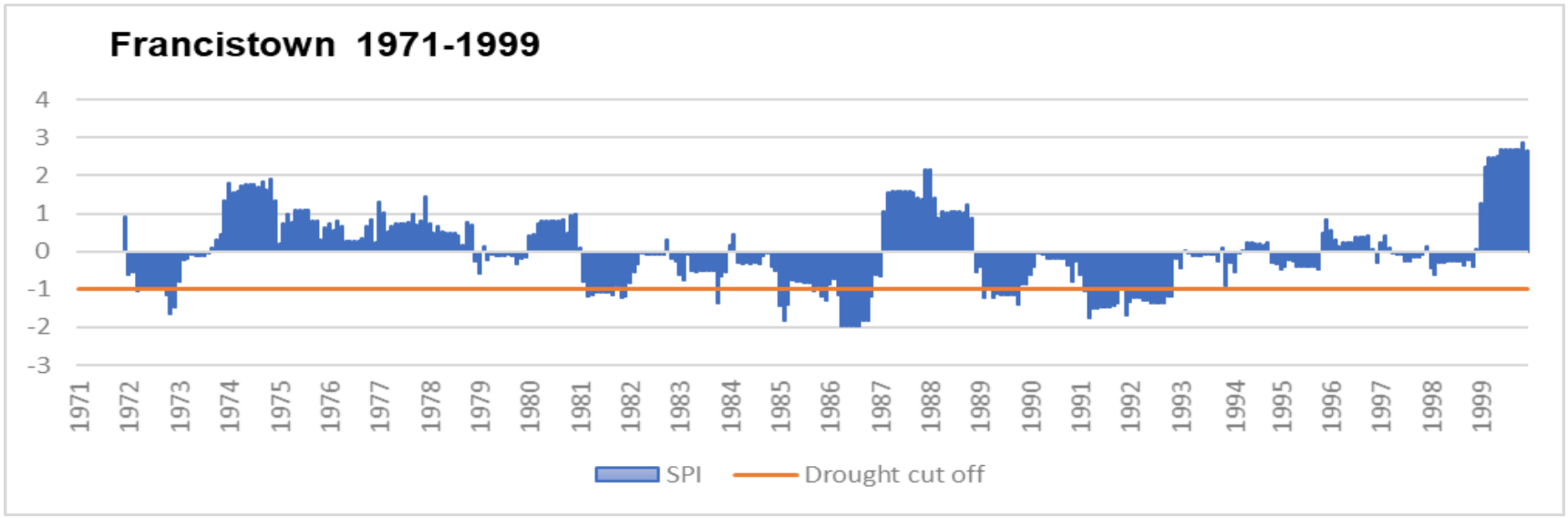

Figure 8.2ac: The 12-month SPI for Francistown

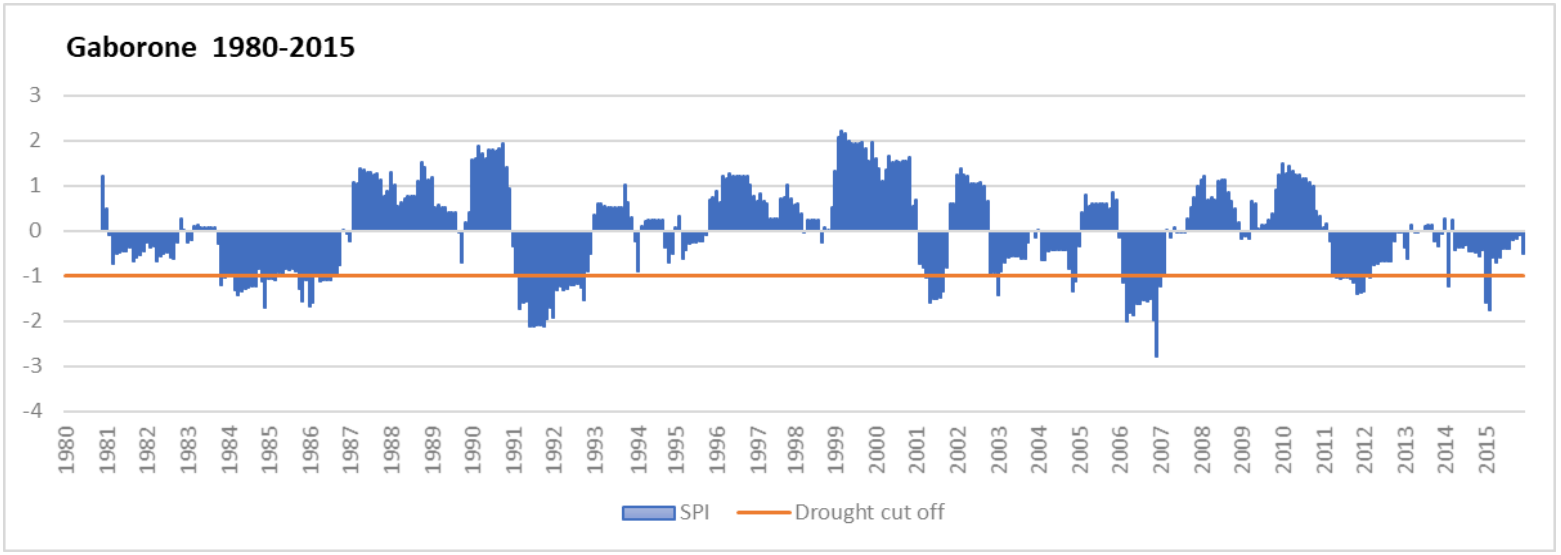

Figure 8.ad: The 12-month SPI for Gaborone

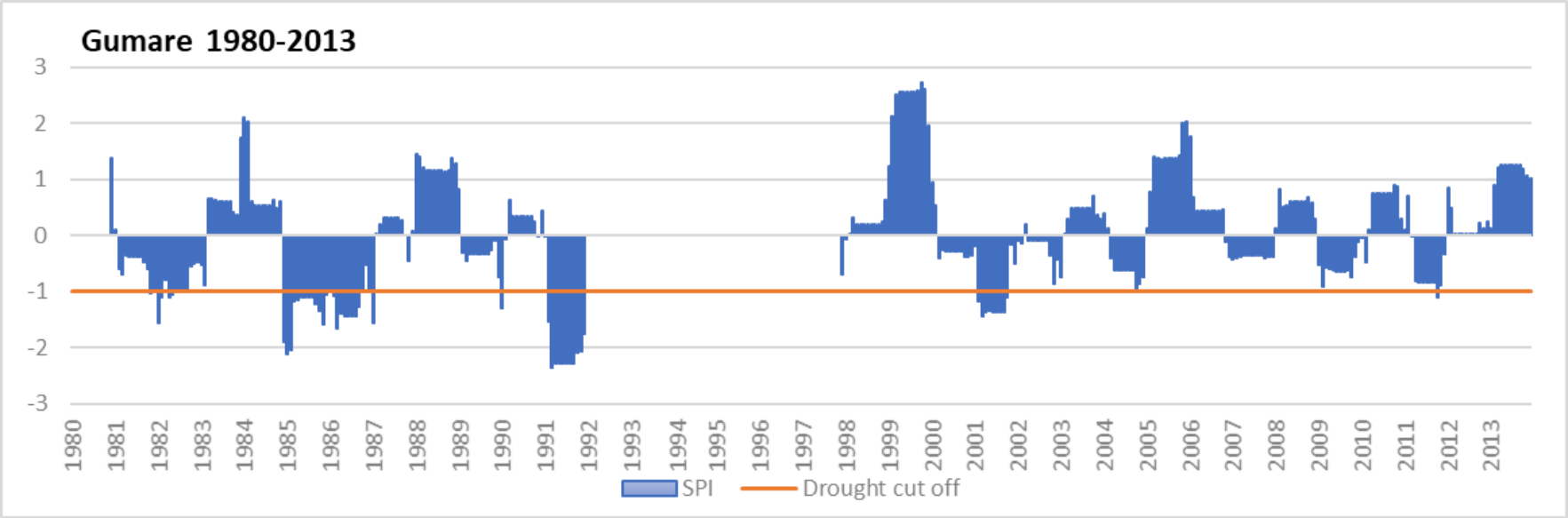

Figure 8.2ae: The 12-month SPI for Gumare

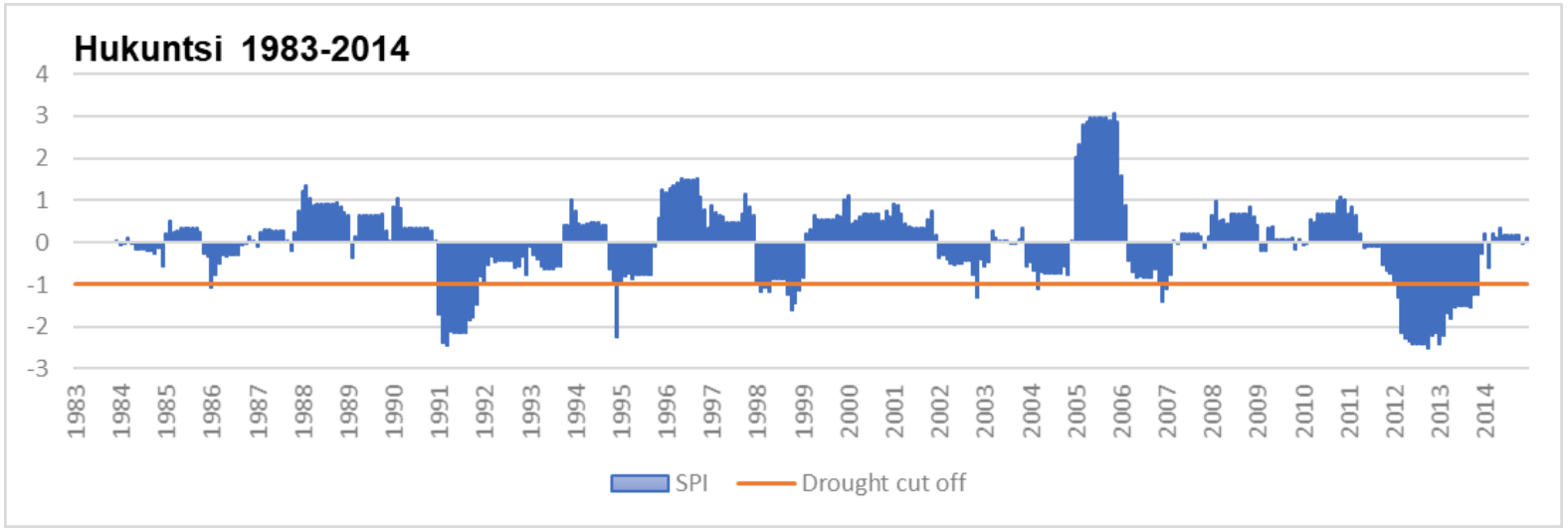

Figure 8.2af: The 12-month SPI for Hukuntsi

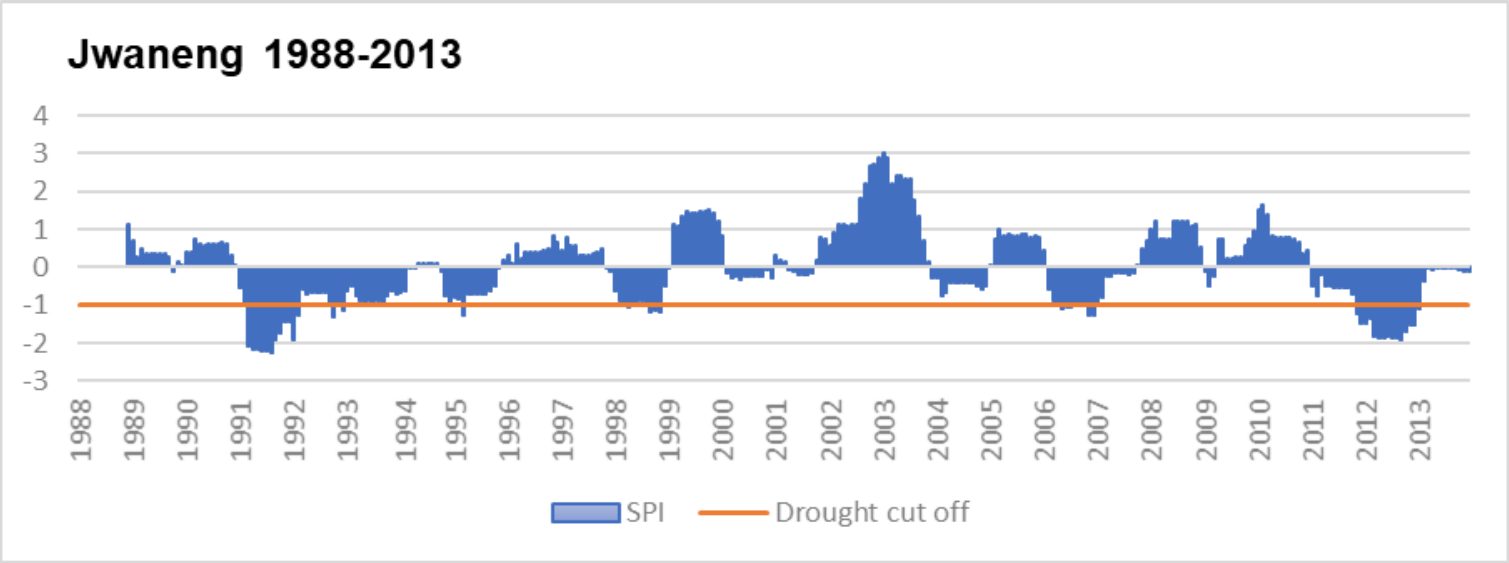

Figure 8.2ag: The 12-month SPI for Jwaneng

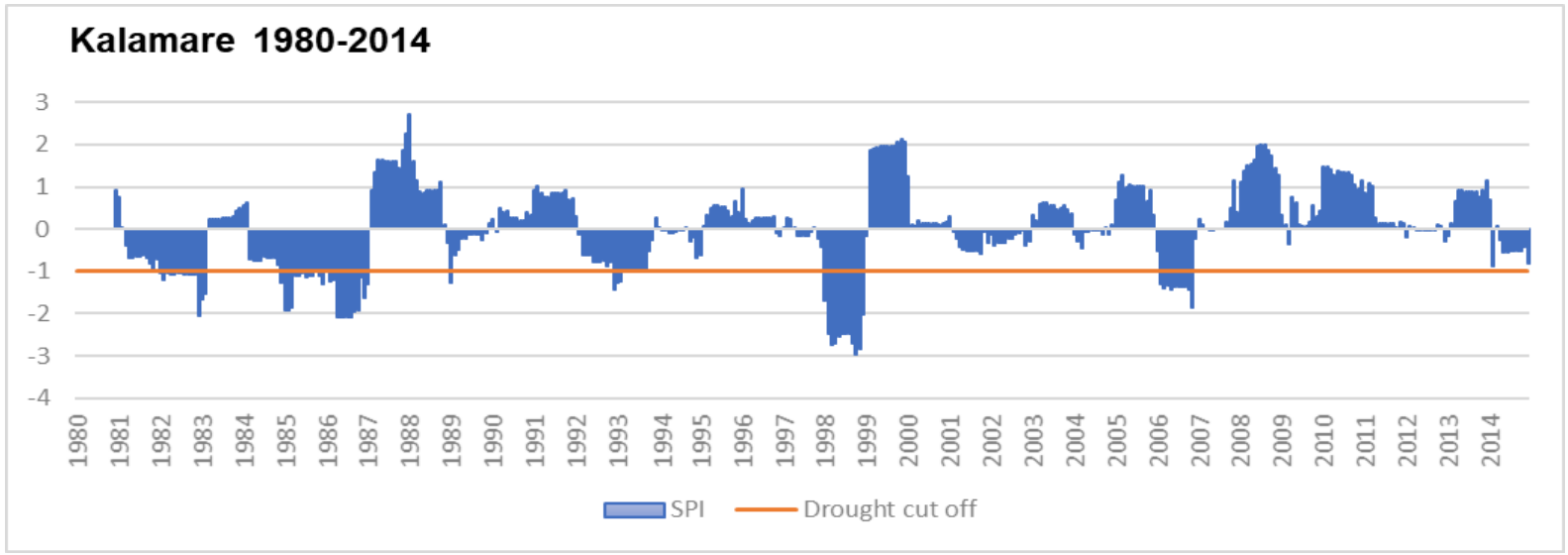

Figure 8.2ah: The 12-month SPI for Kalamare

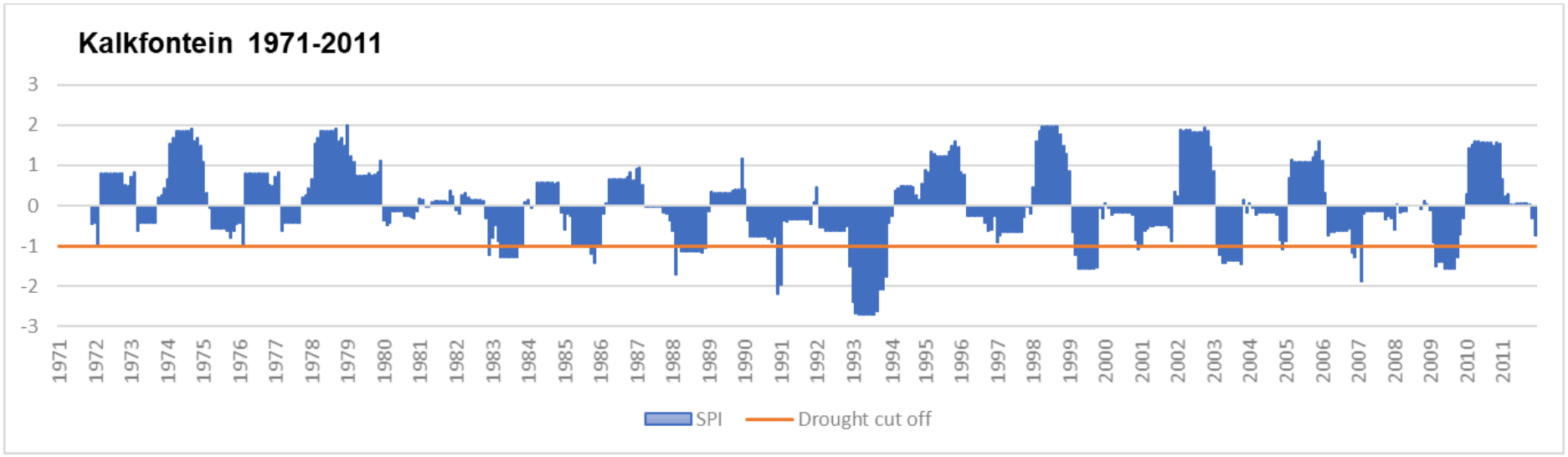

Figure 8.2ai: The 12-month SPI for Kalkfontein

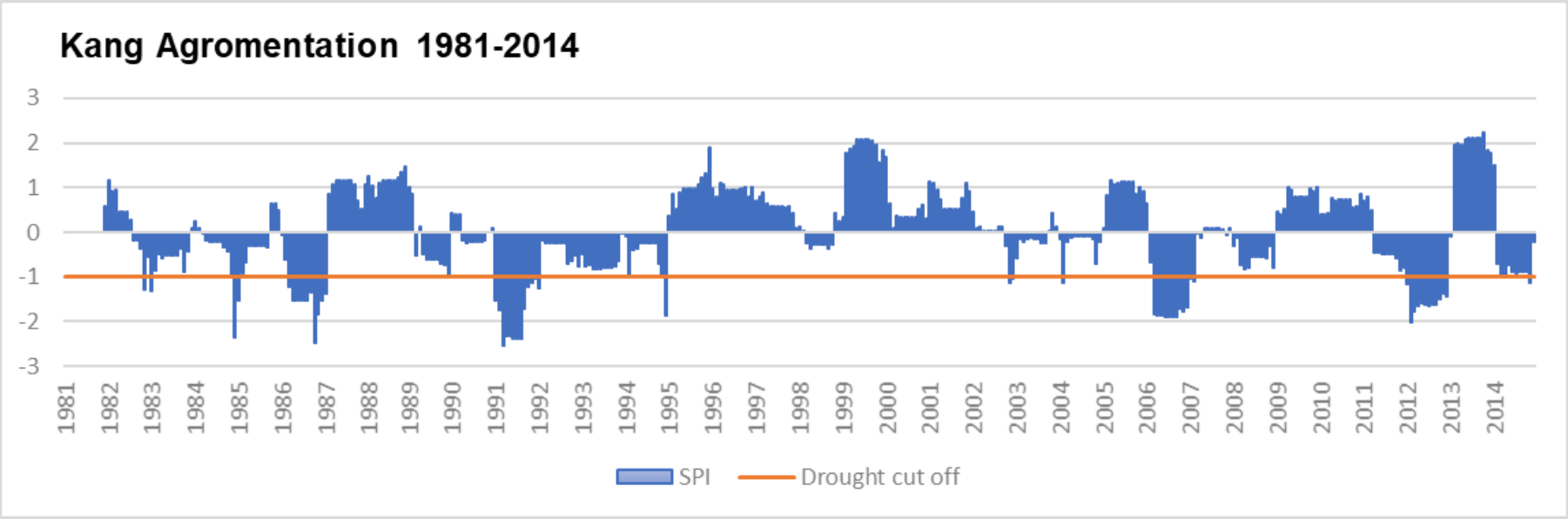

Figure 8.2aj: The 12-month SPI for Kang Agromentation

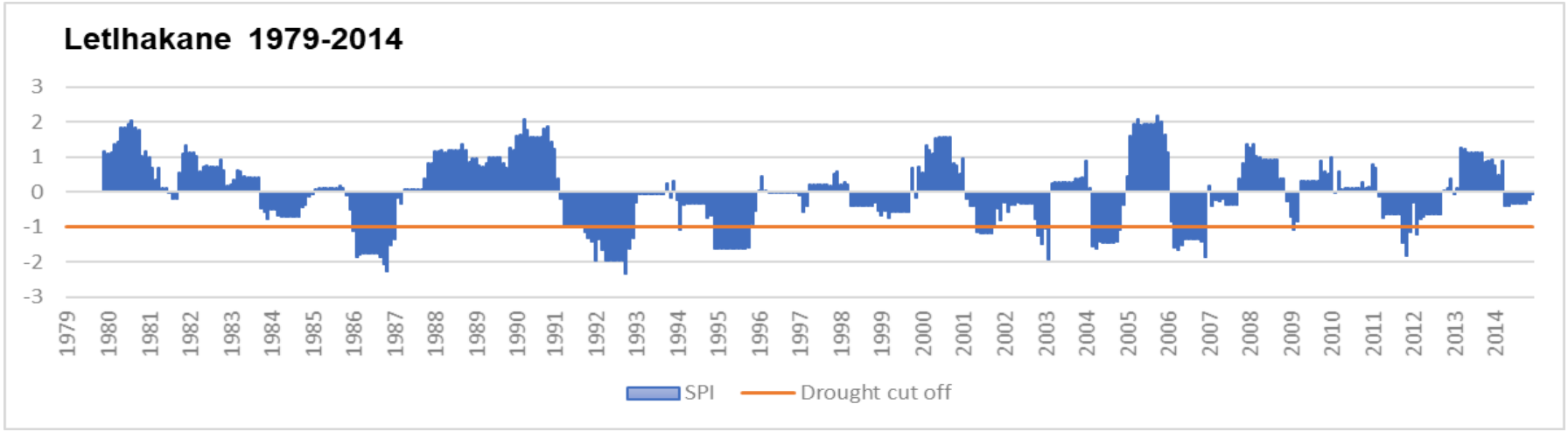

Figure 8.2ak: The 12-month SPI for Letlhakane

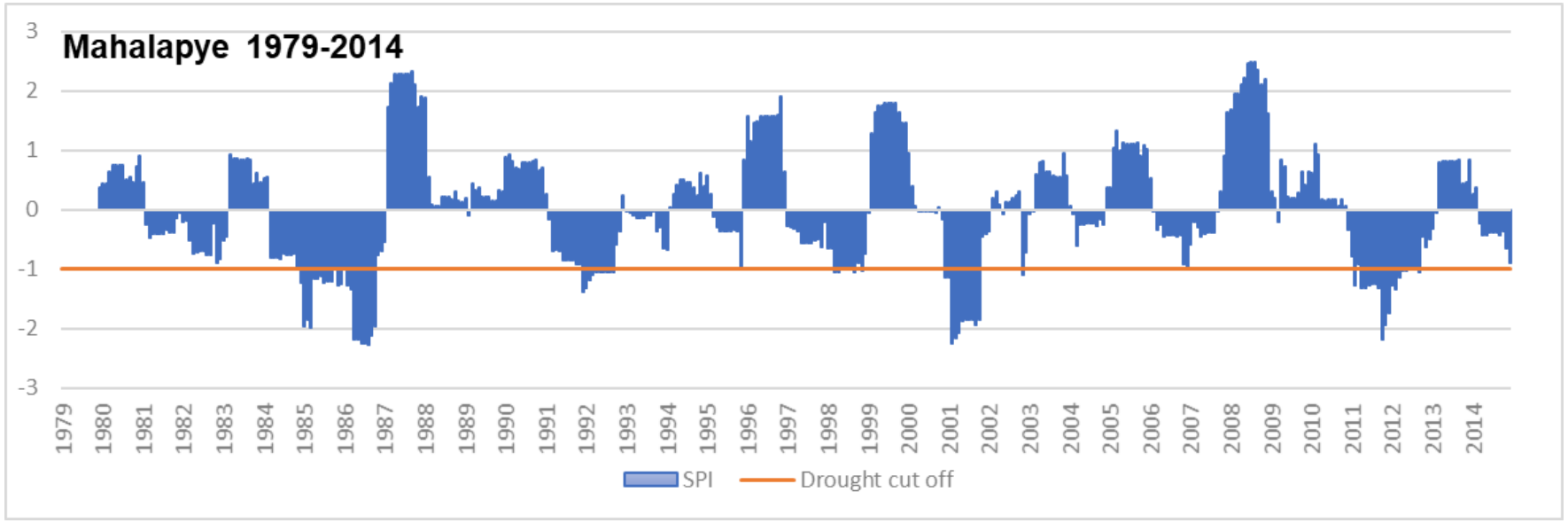

Figure 8.2al: The 12-month SPI for Mahalapye

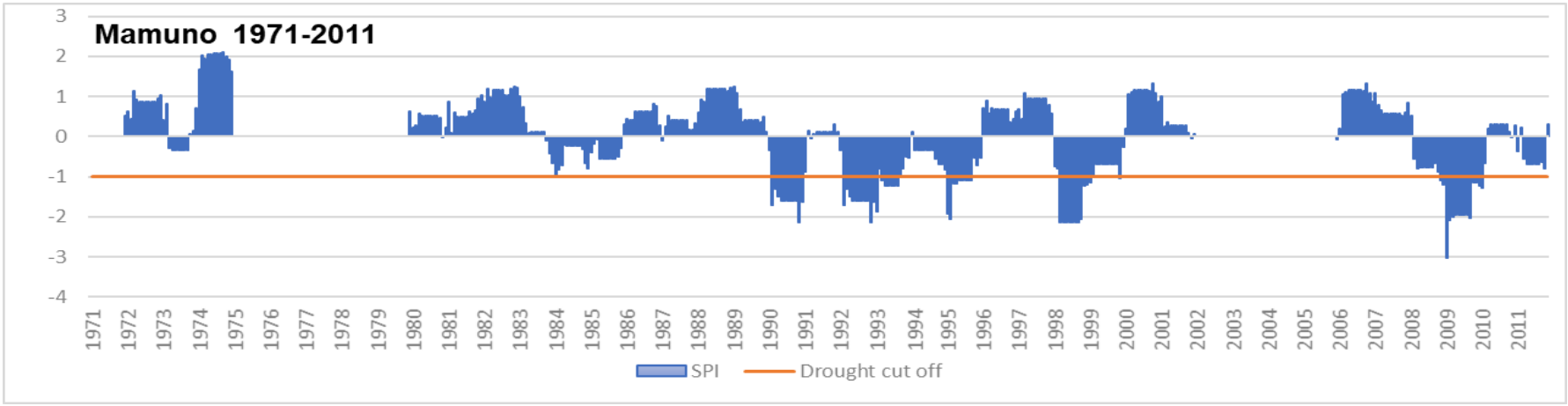

Figure 8.2al: The 12-month SPI for Mamumo

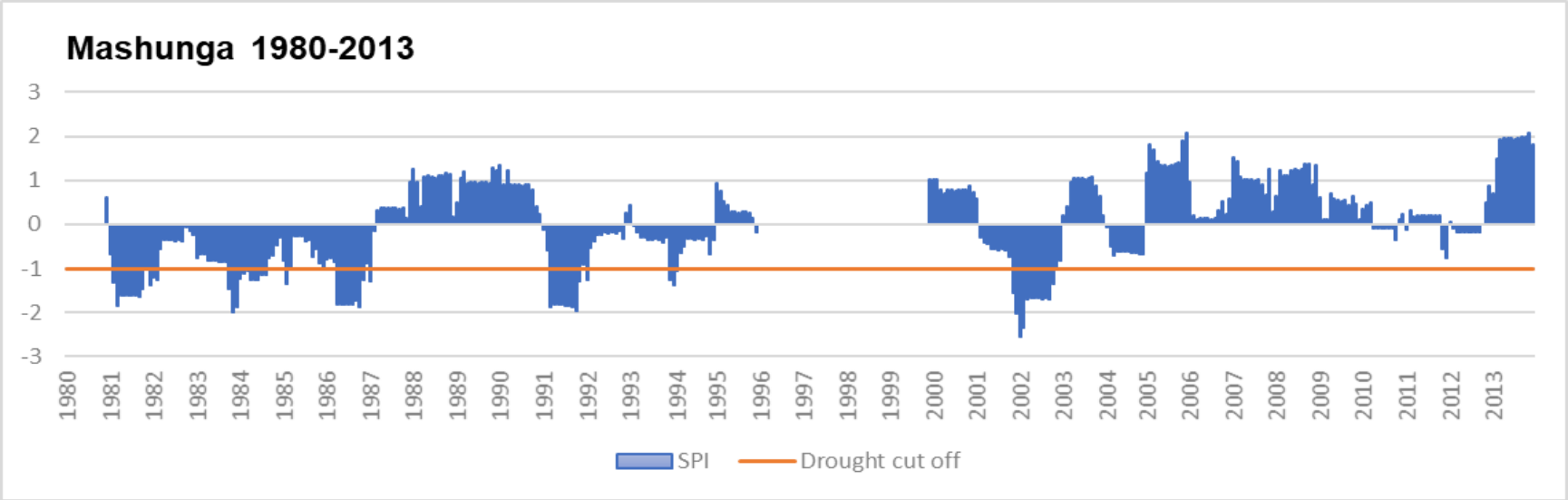

Figure 8.2am: The 12-month SPI for Mashunga

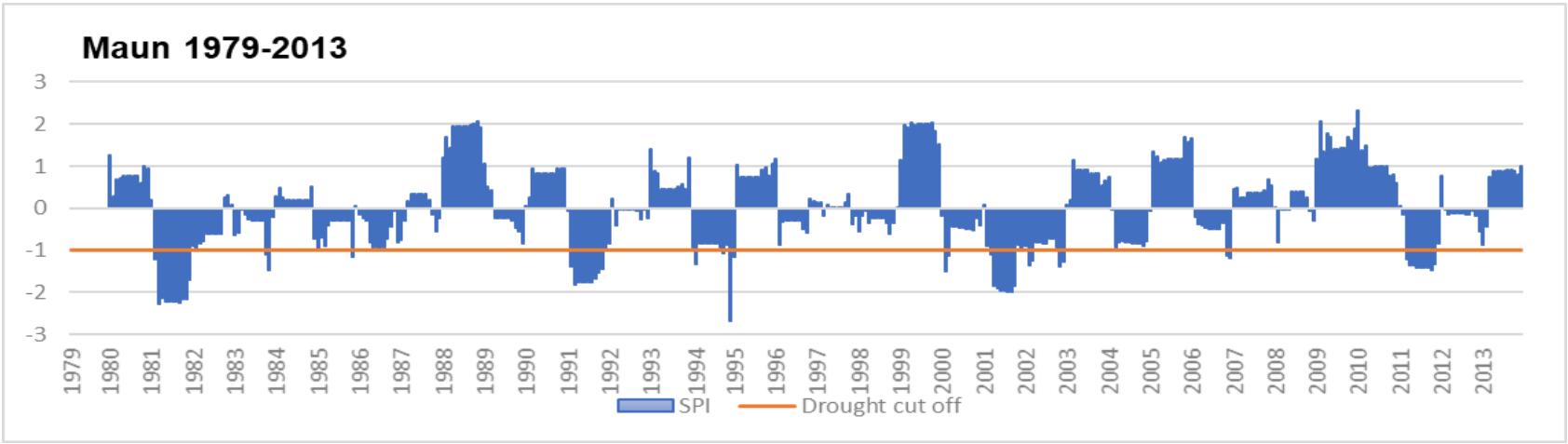

Figure 8.2an: The 12-month SPI for Maun

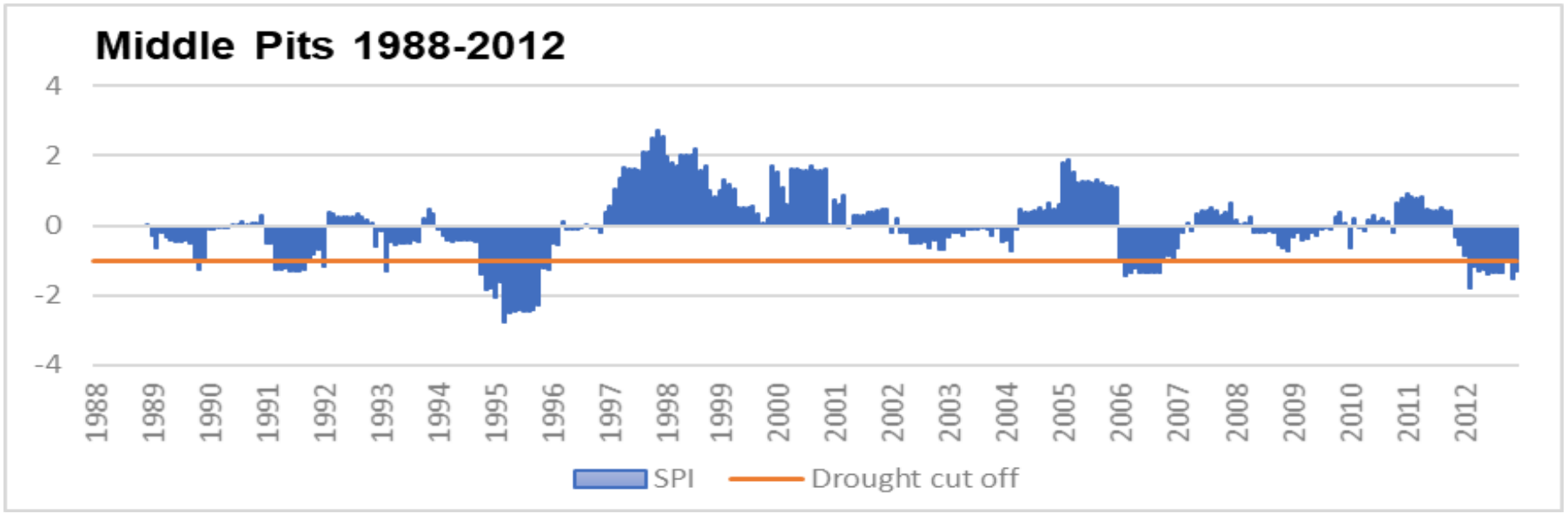

Figure 8.2ao: The 12-month SPI for Middlepits

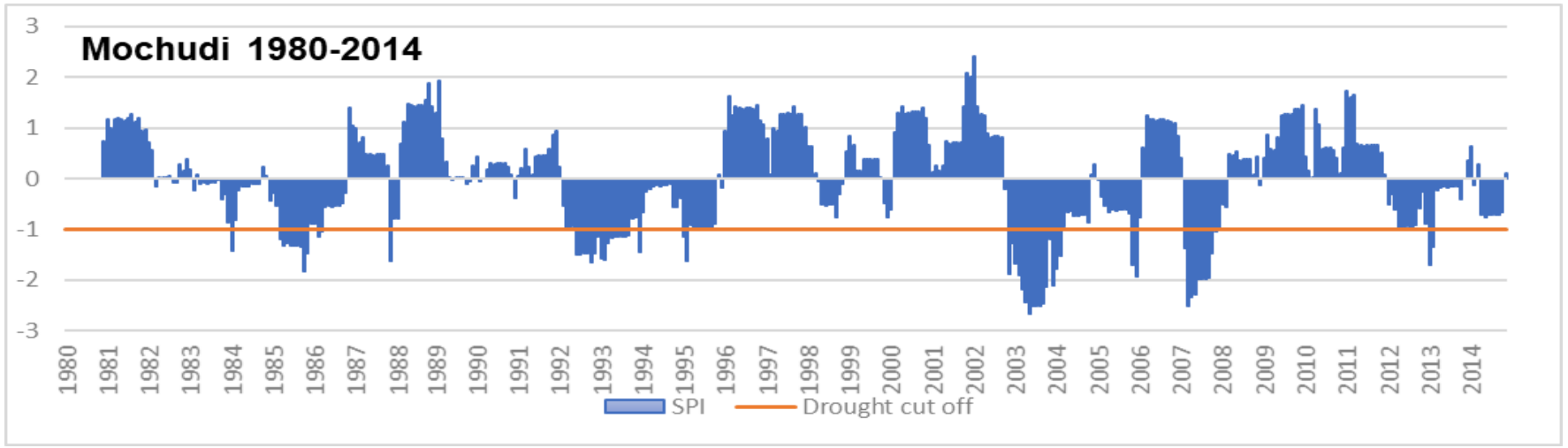

Figure 8.2ap: The 12-month SPI for Mochudi

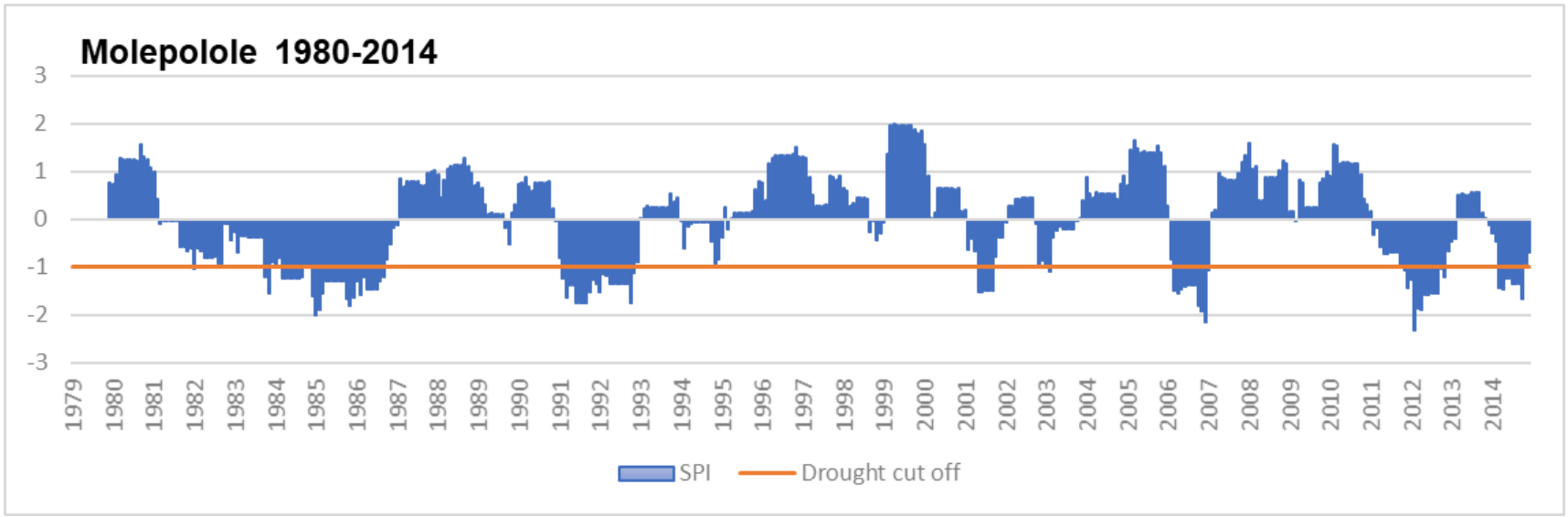

Figure 8.2aq: The 12-month SPI for Molepolole

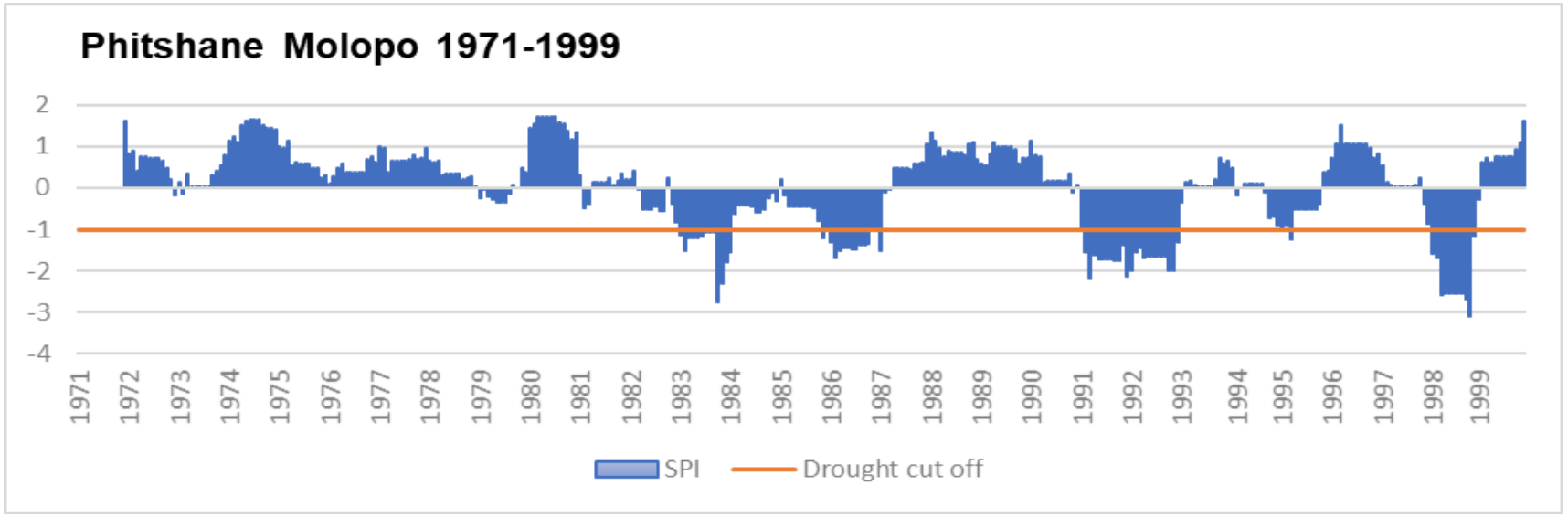

Figure 8.2ar: The 12-month SPI for Phitshane Molopo

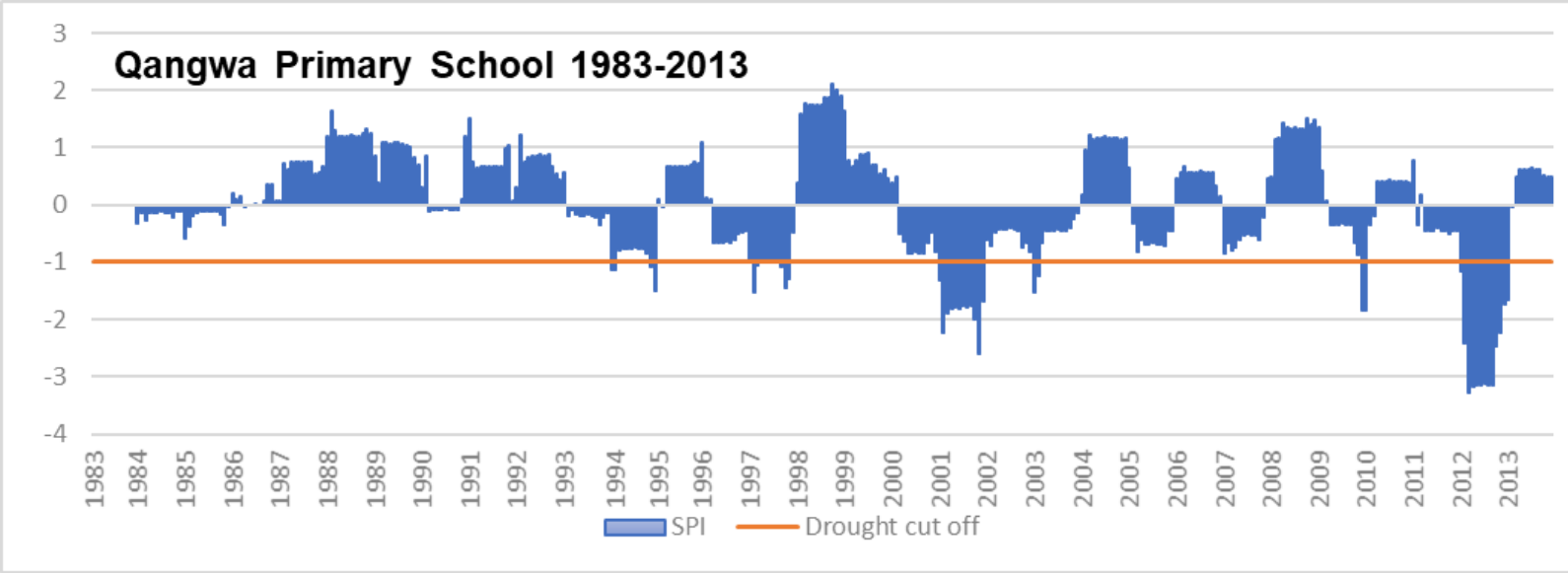

Figure 8.2as: The 12-month SPI for Qangwa Primary School

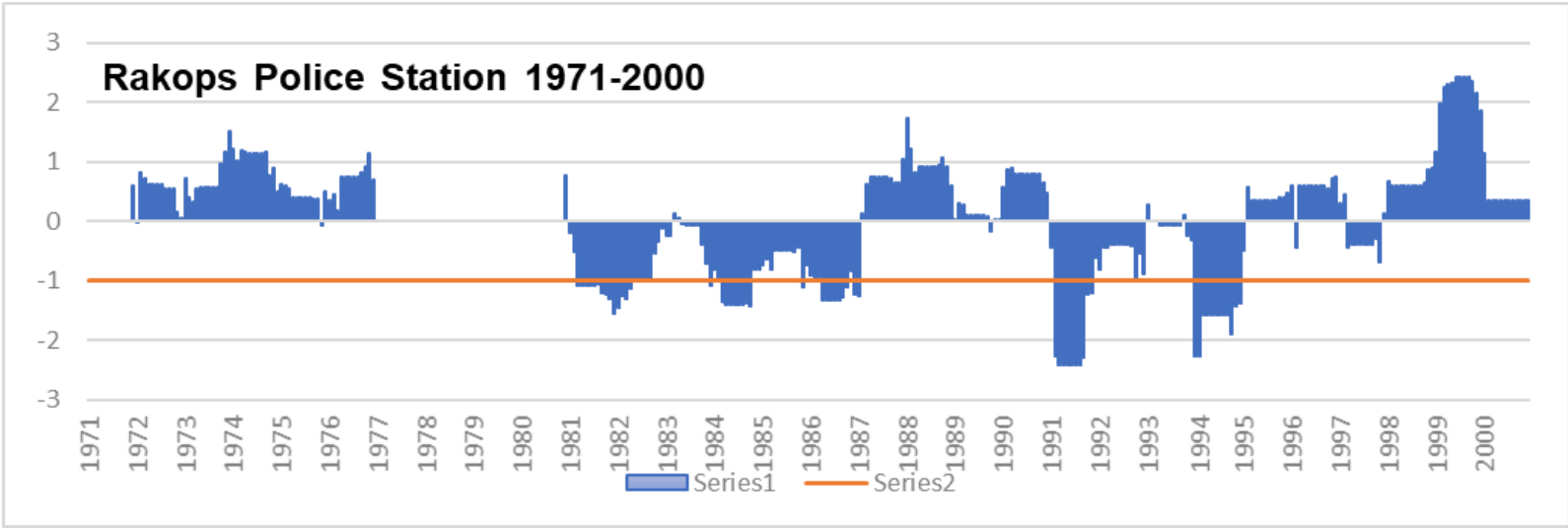

Figure 8.2at: The 12-month SPI for Rakops Police Station

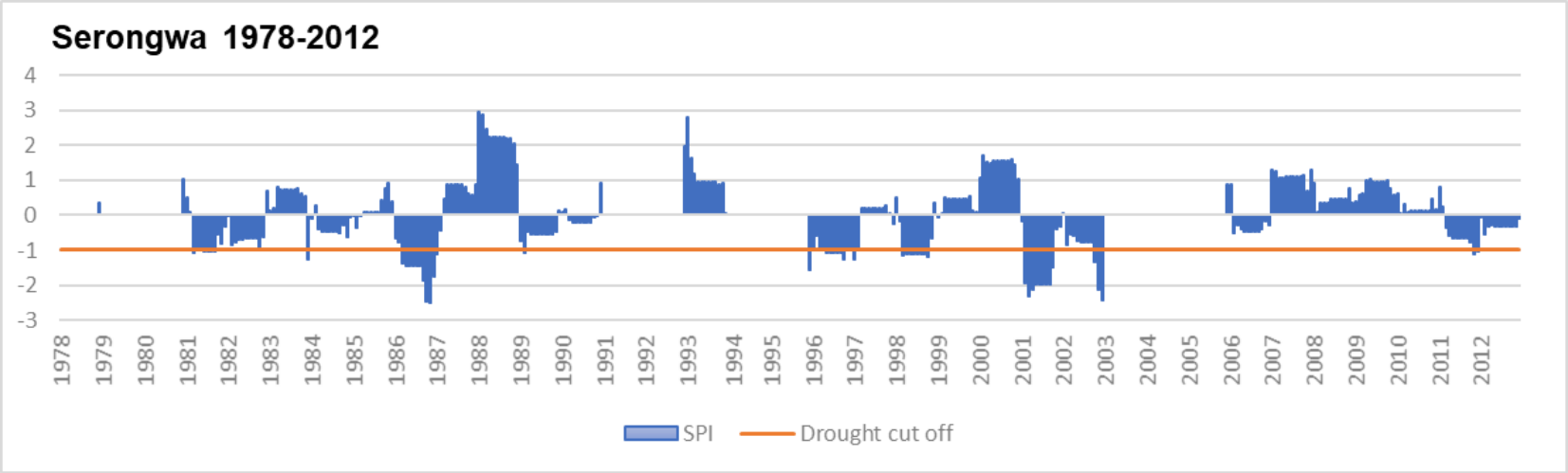

Figure 8.2au: The 12-month SPI for Serongwa

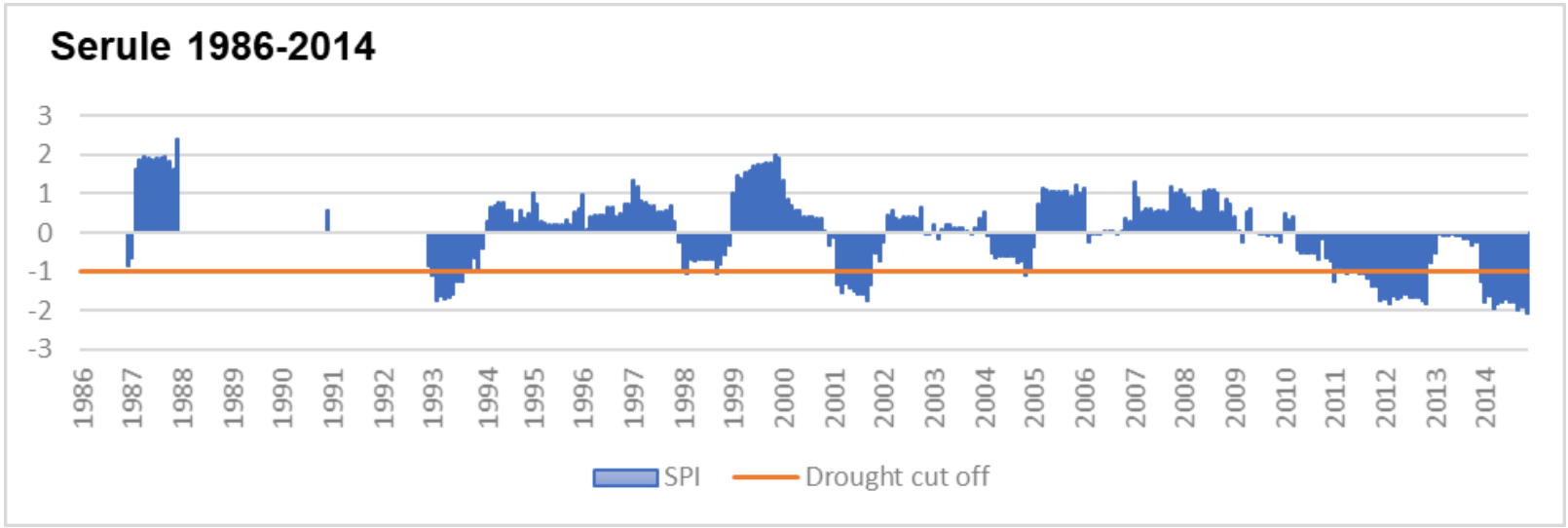

Figure 8.2aw: The 12-month SPI for Serule

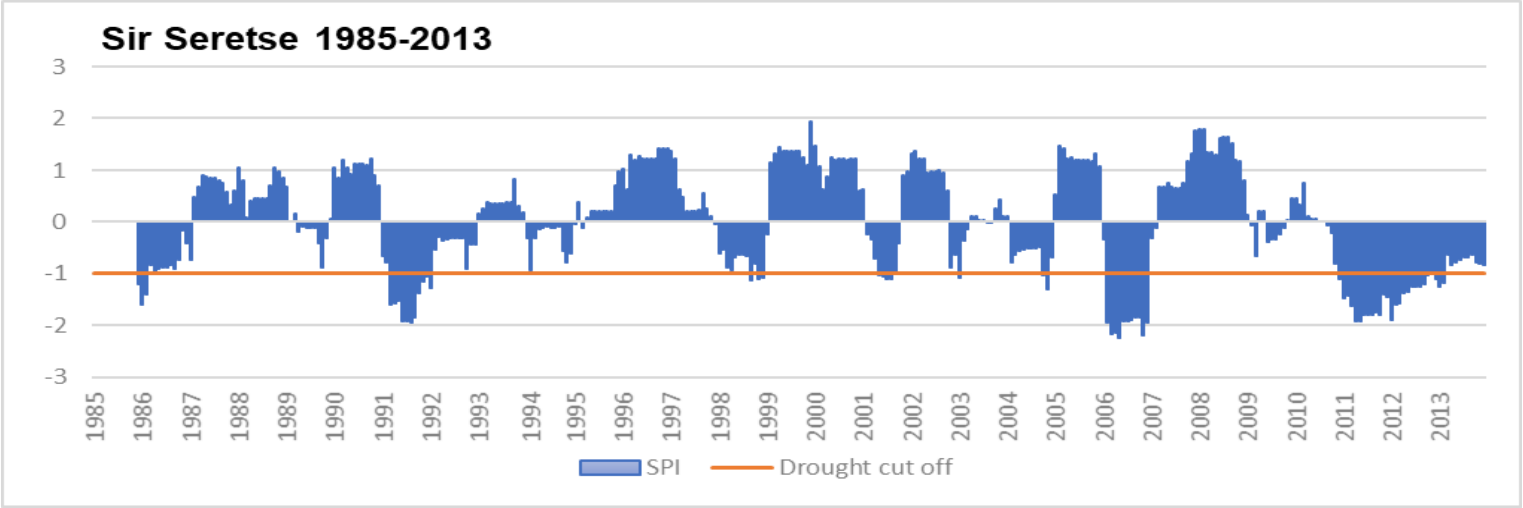

Figure 8.2ax: The 12-month SPI for Sir Seretse

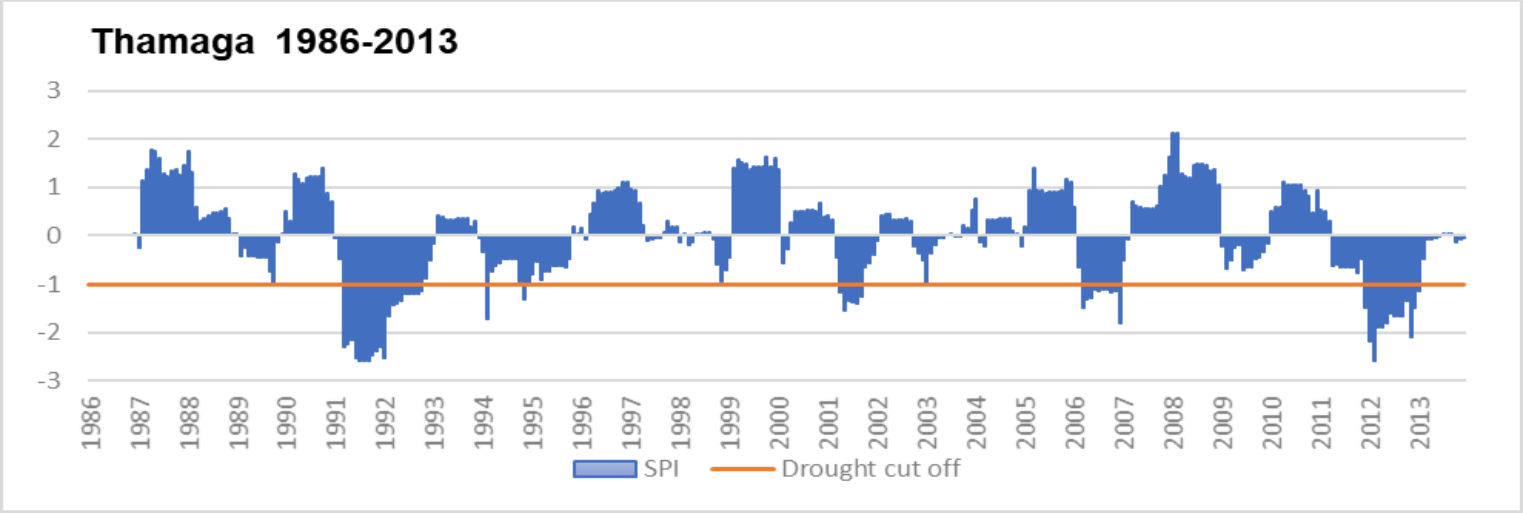

Figure 8.2ay: The 12-month SPI for Thamaga

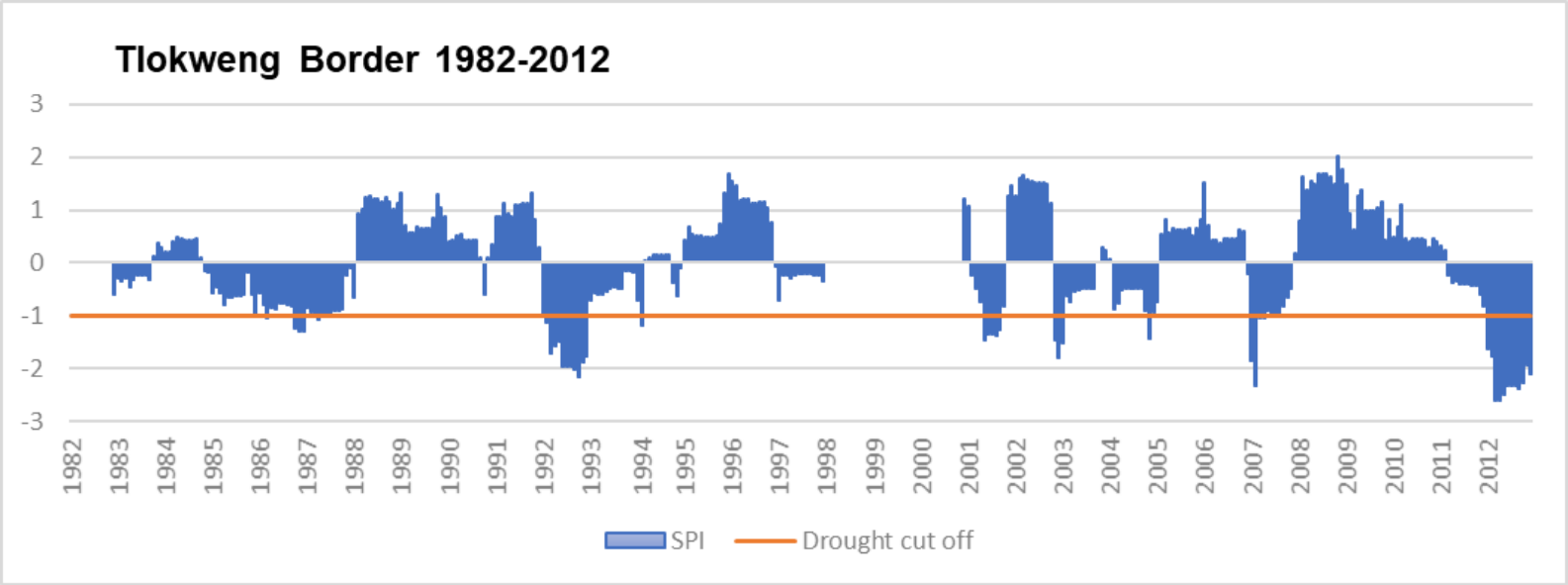

Figure 8.2az: The 12-month SPI for Tlokweng Border

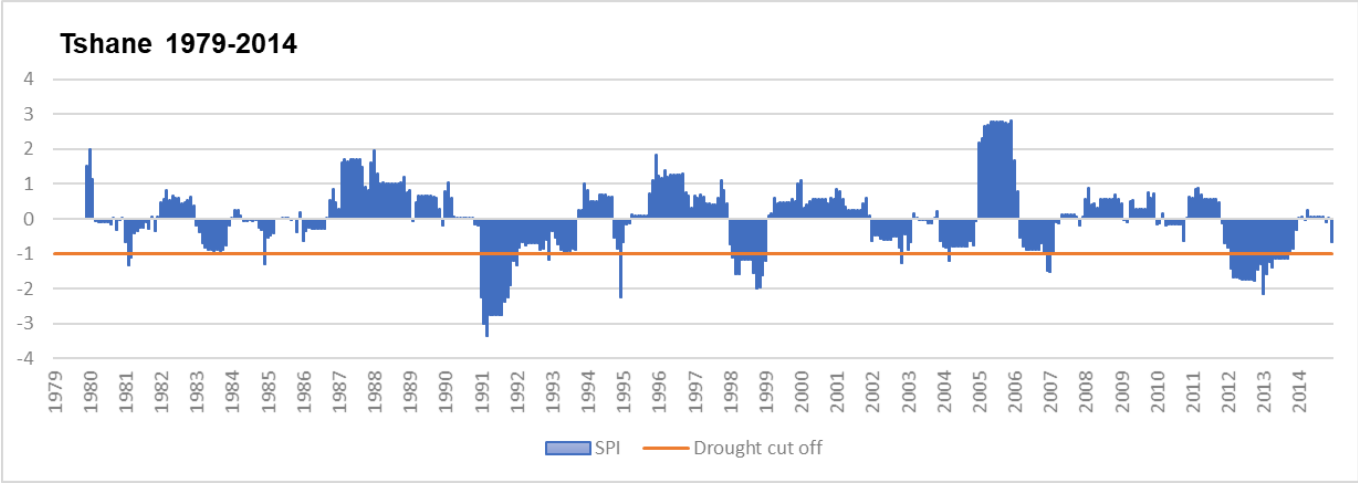

Figure 8.2ba: The 12-month SPI for Tshane

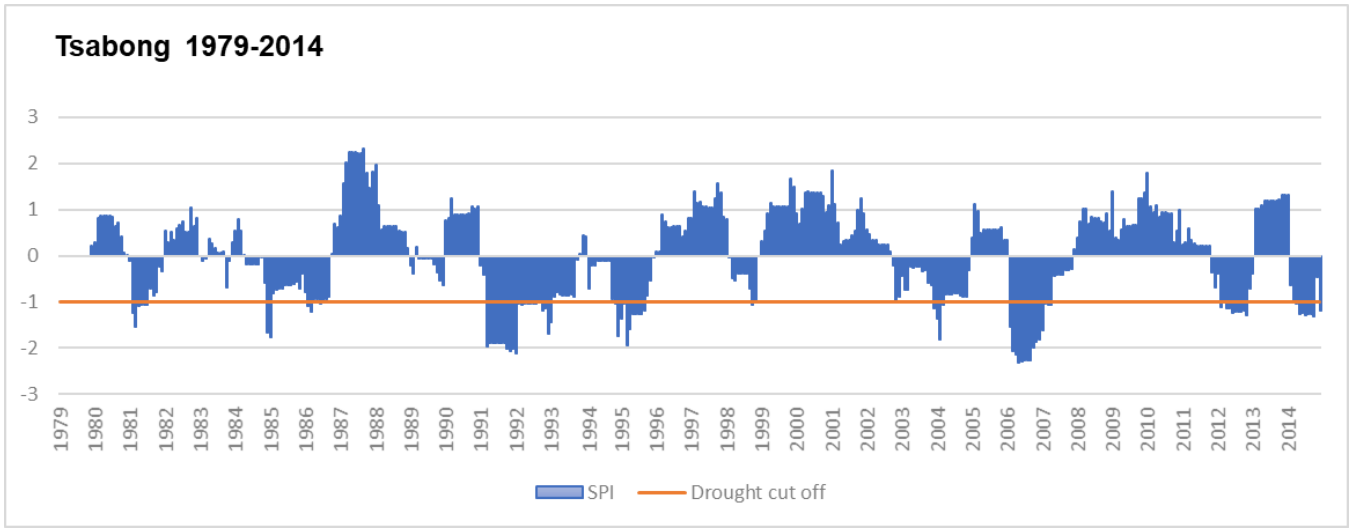

Figure 8.2bb: The 12-month SPI for Tsabong

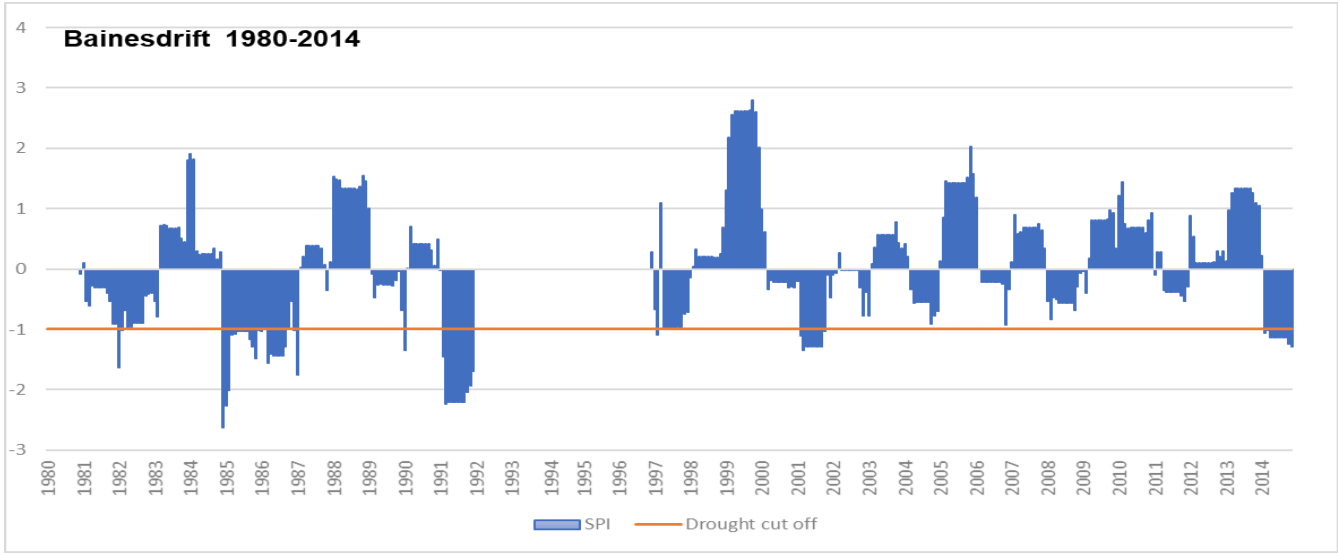

Figure 8.2bc: The 12-month SPI for Bainesdrift

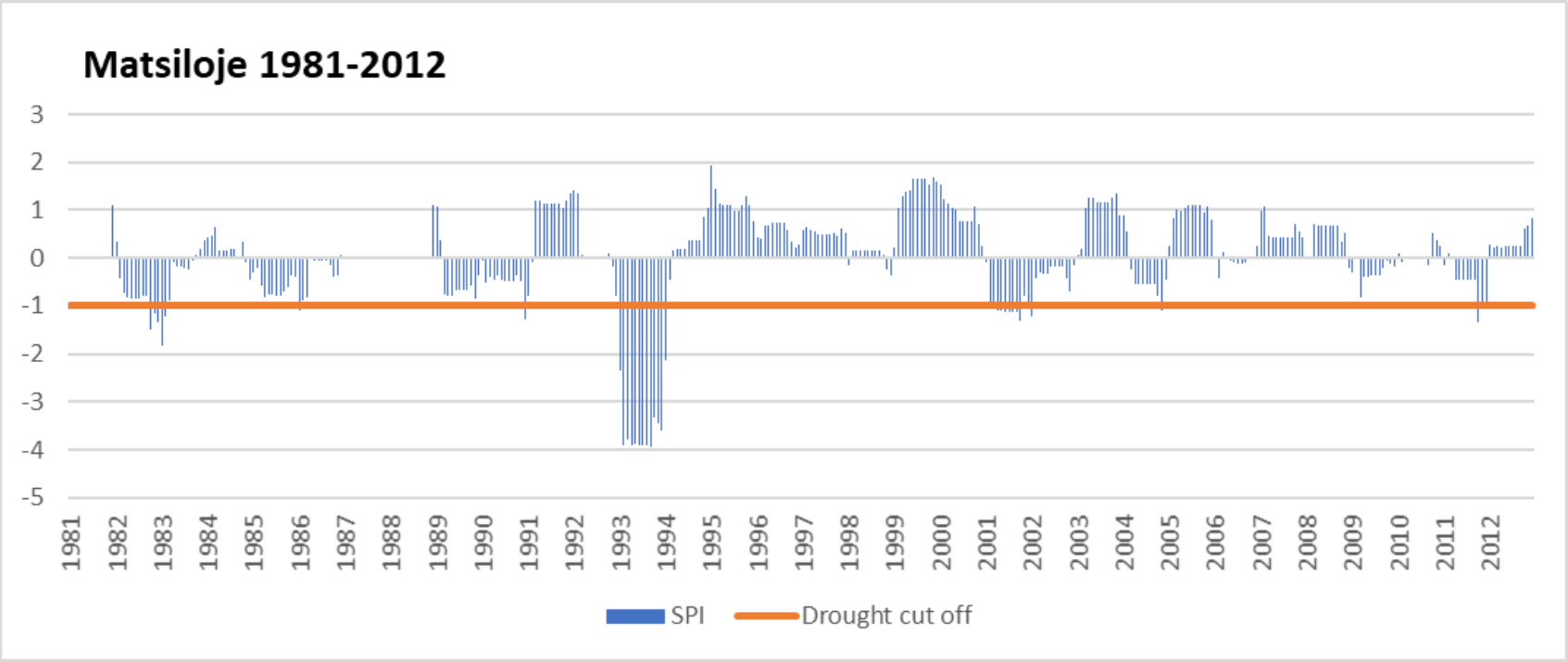

Figure 8.2bd: The 12-month SPI for Matsiloje

8.3. Inverse Distance Weighting

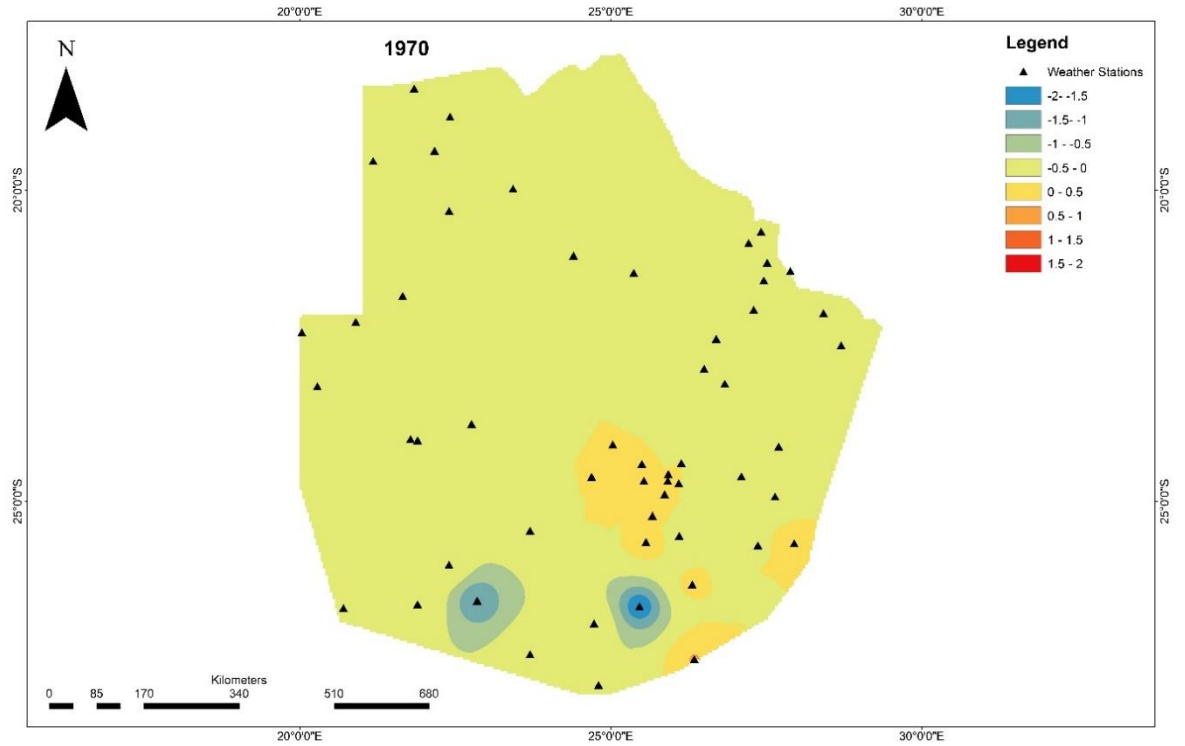

Figure 8.3a: IDW SPI 1970

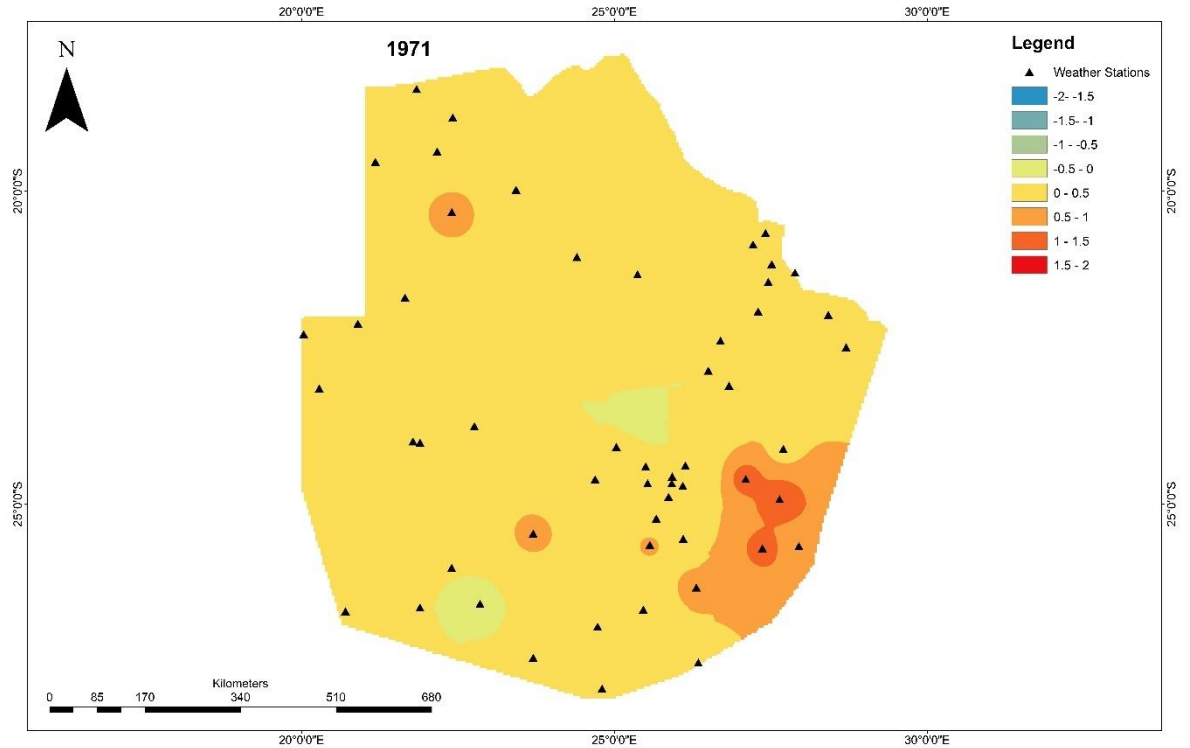

Figure 8.3b: IDW SPI 1971

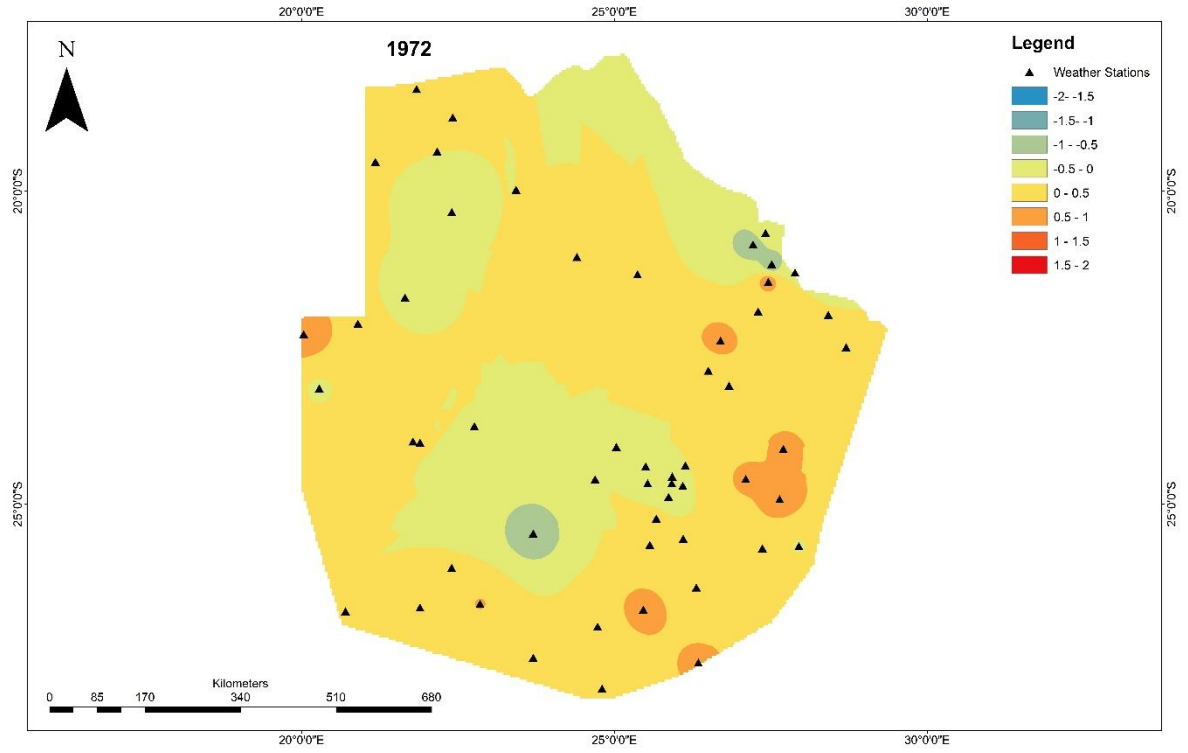

Figure 8.3c: IDW SPI 1972

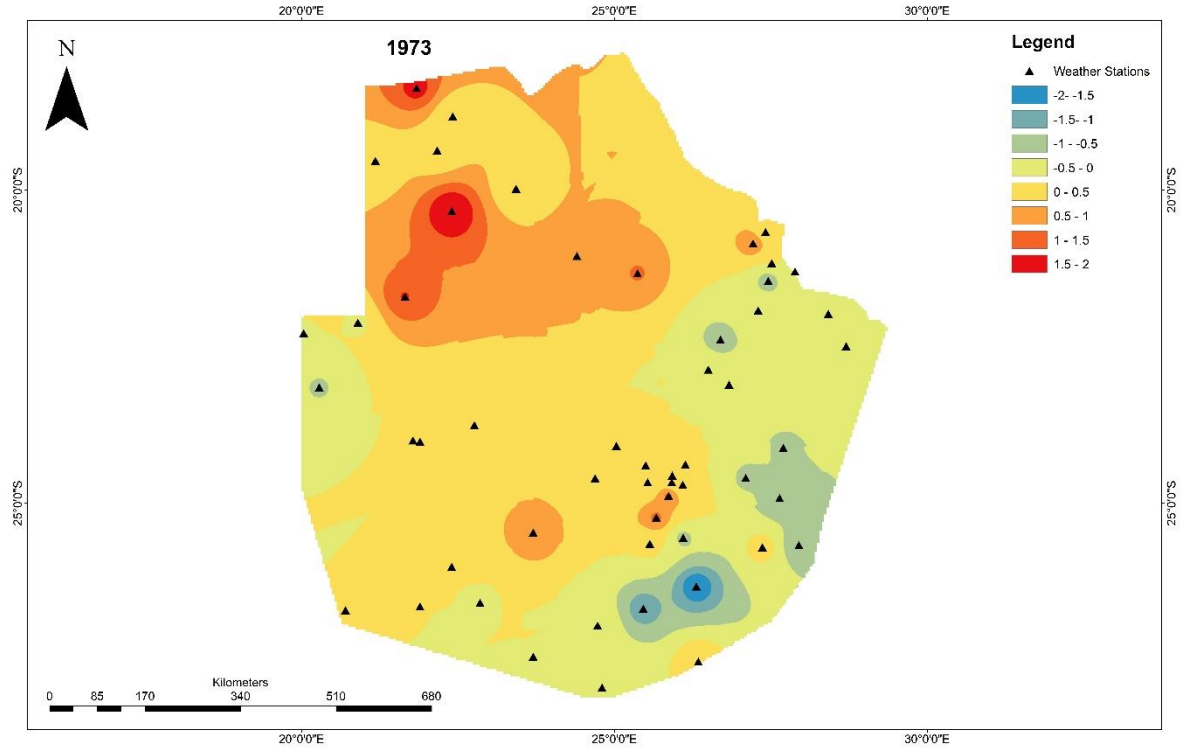

Figure 8.3d: IDW SPI 1973

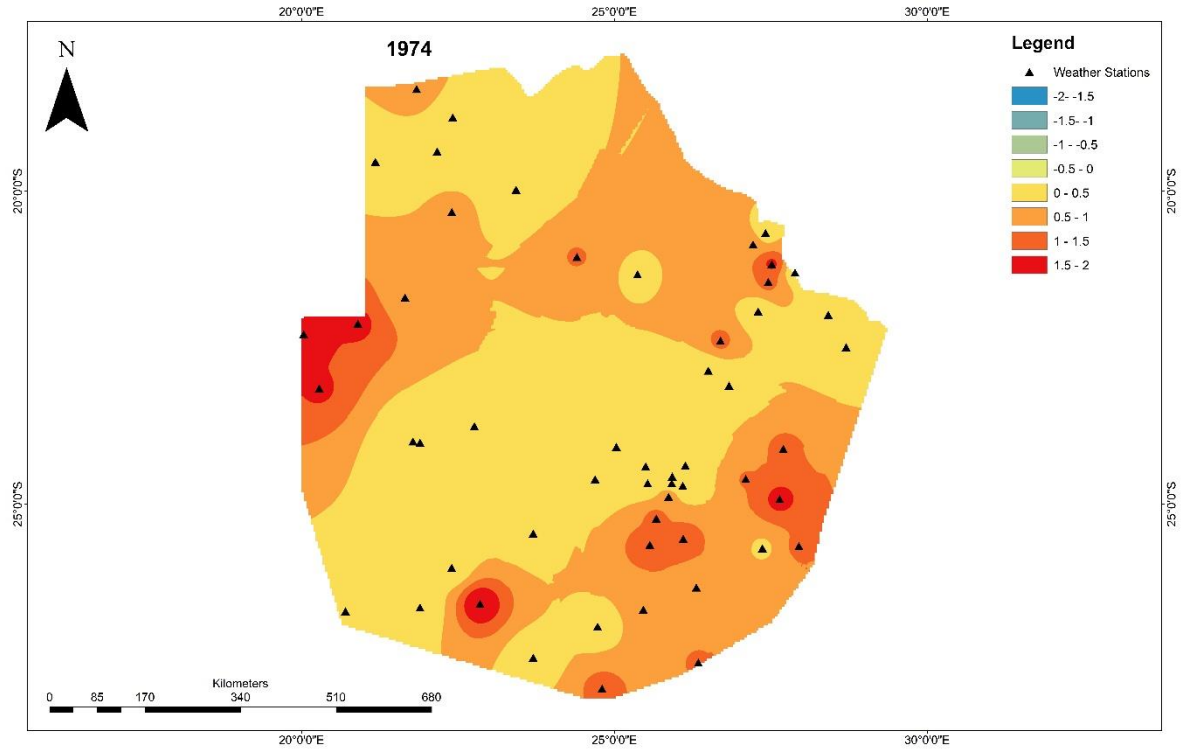

Figure 8.3e: IDW SPI 1974

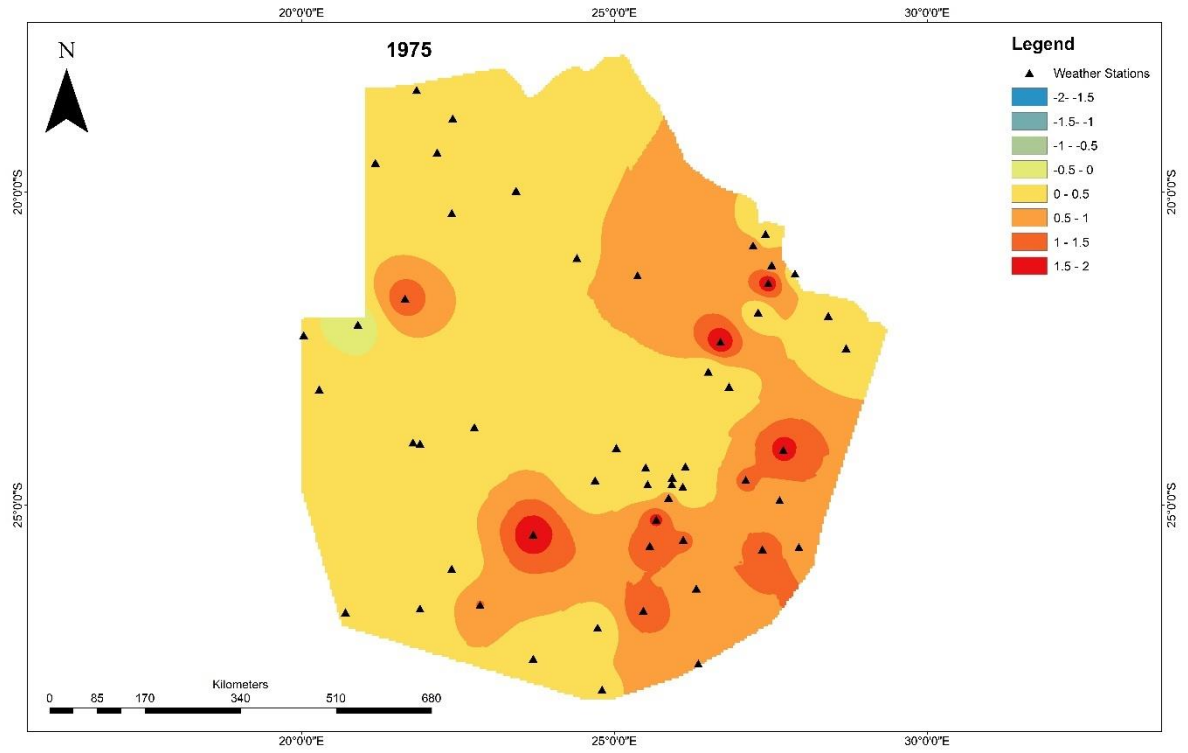

Figure 8.3f: IDW SPI 1975

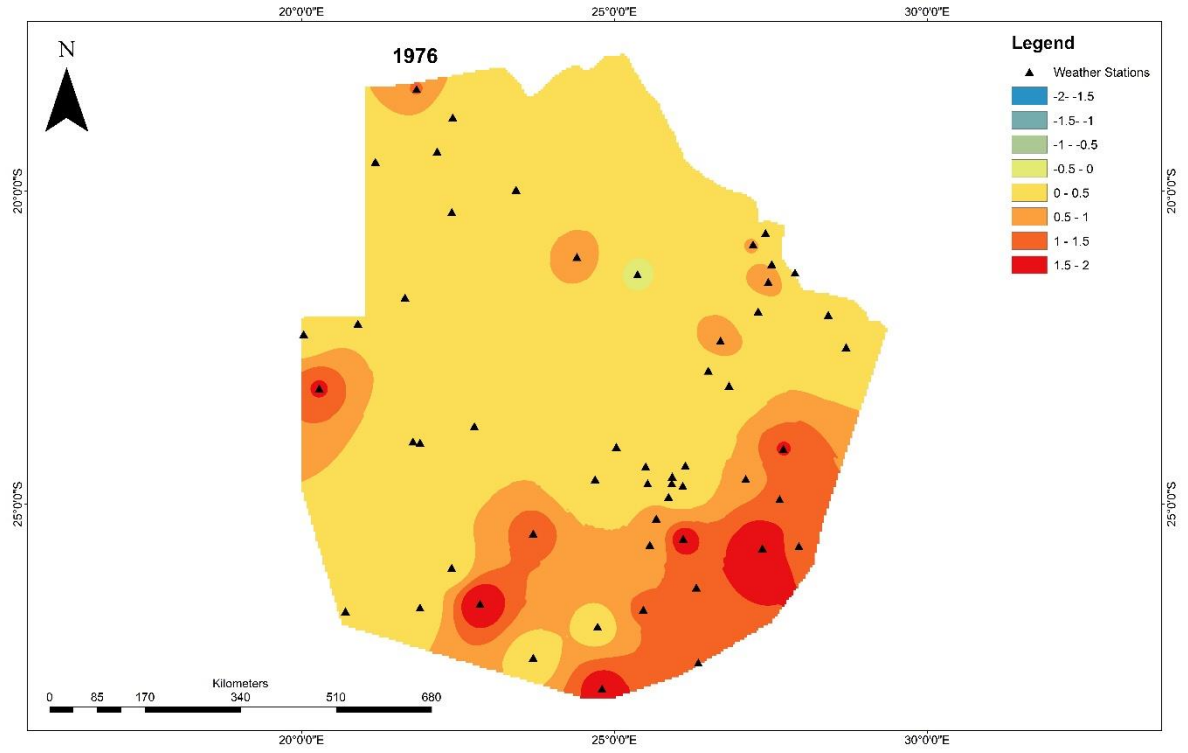

Figure 8.3g: IDW SPI 1976

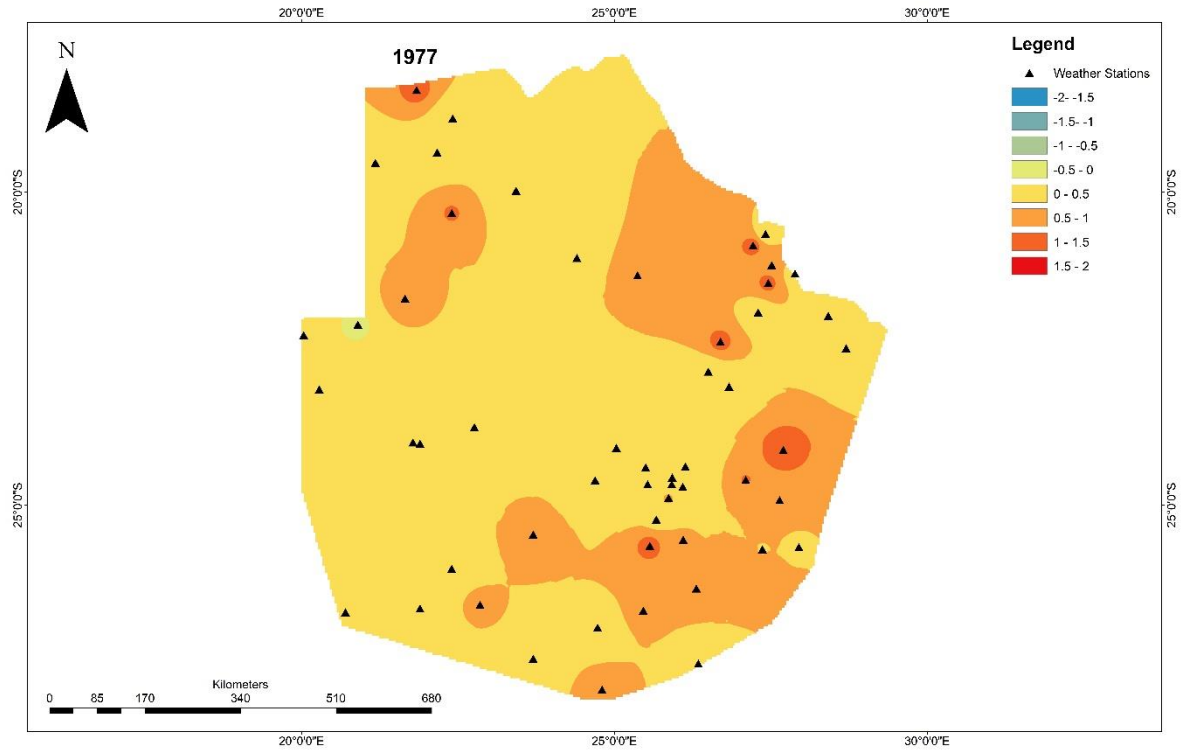

Figure 8.3h: IDW SPI 1977

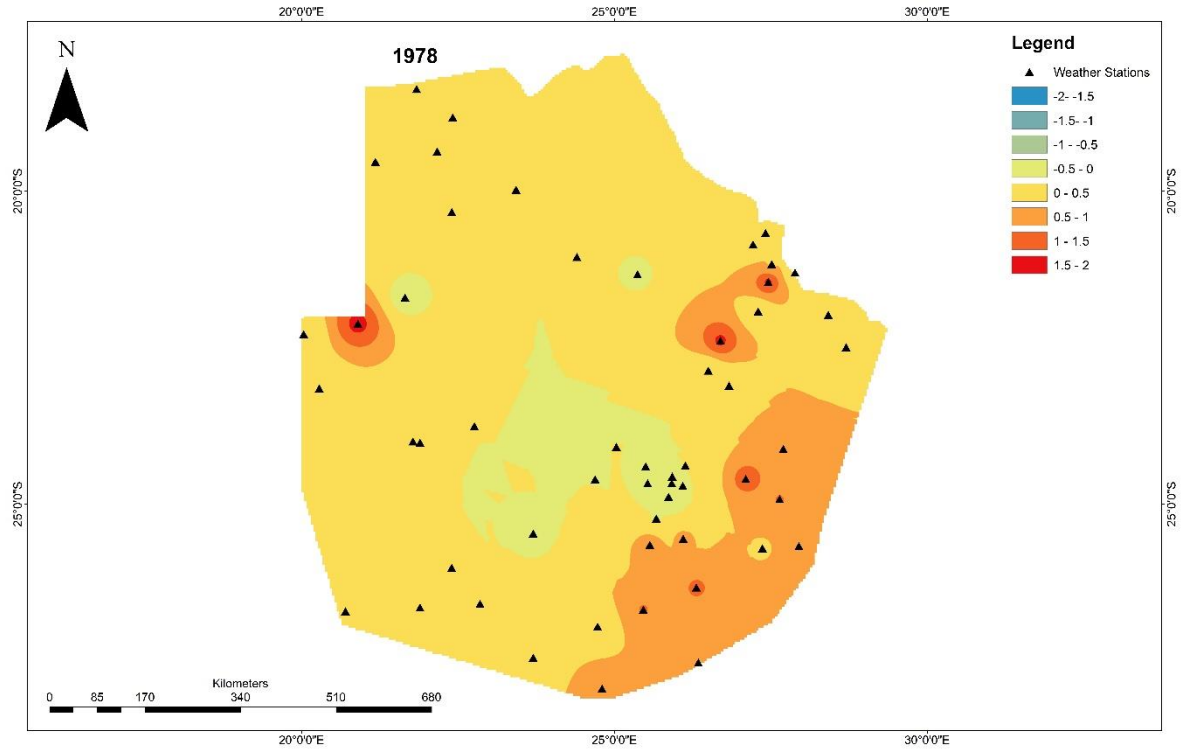

Figure 8.3i: IDW SPI 1978

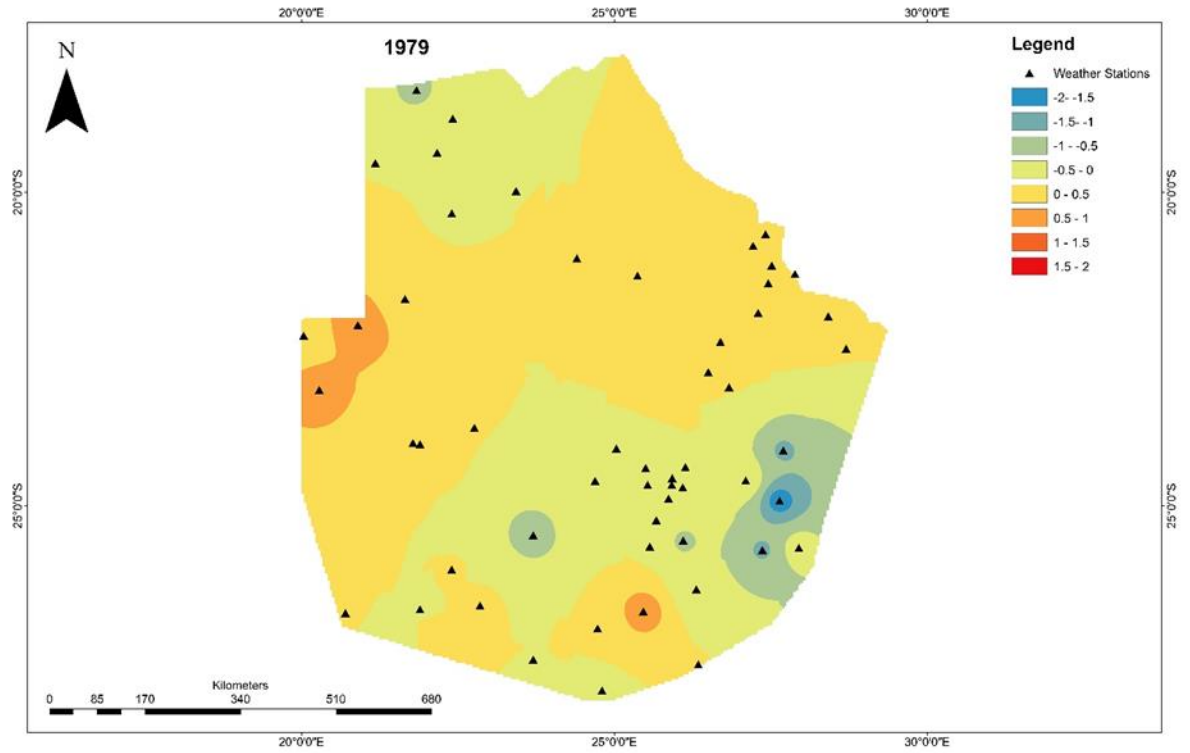

Figure 8.3j: IDW SPI 1979

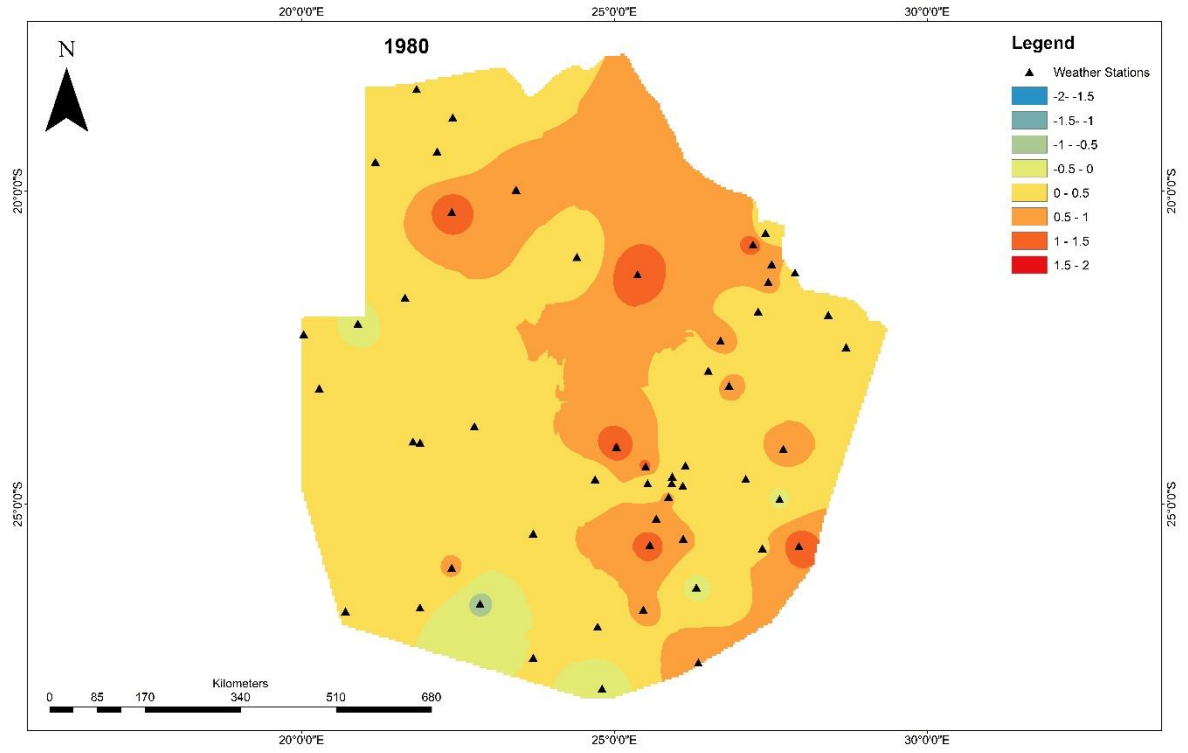

Figure 8.3k: IDW SPI 1980

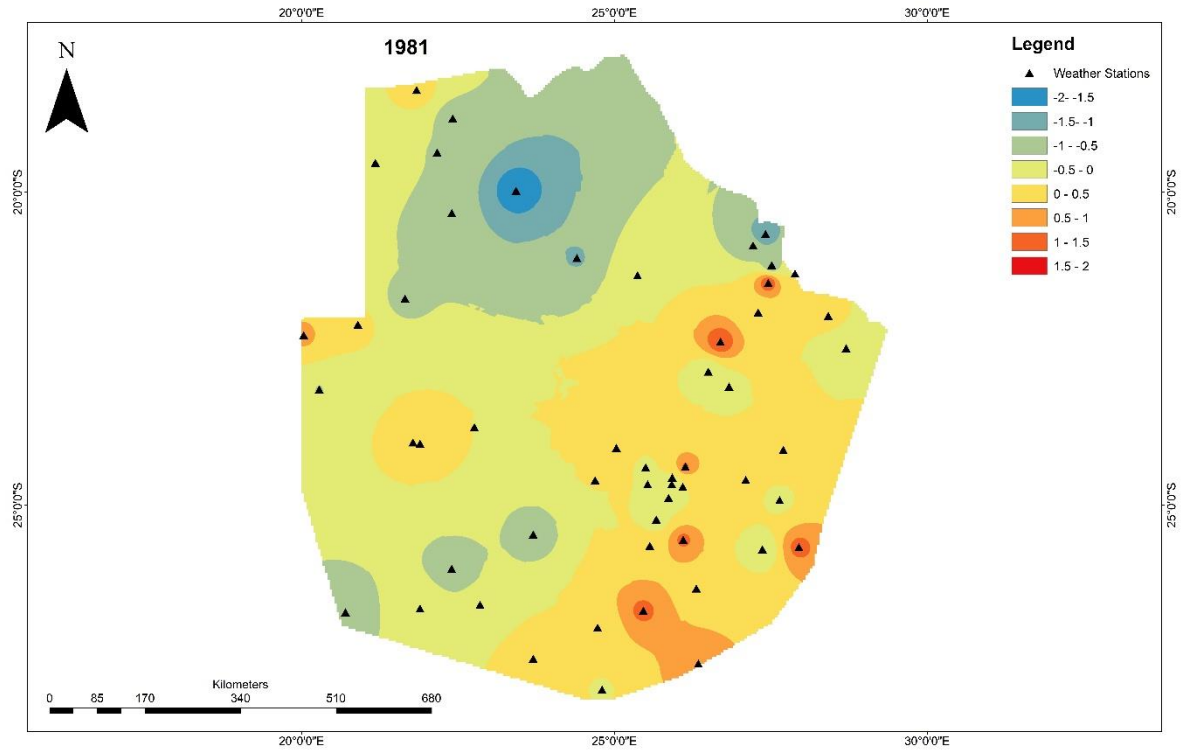

Figure 8.3l: IDW SPI 1981

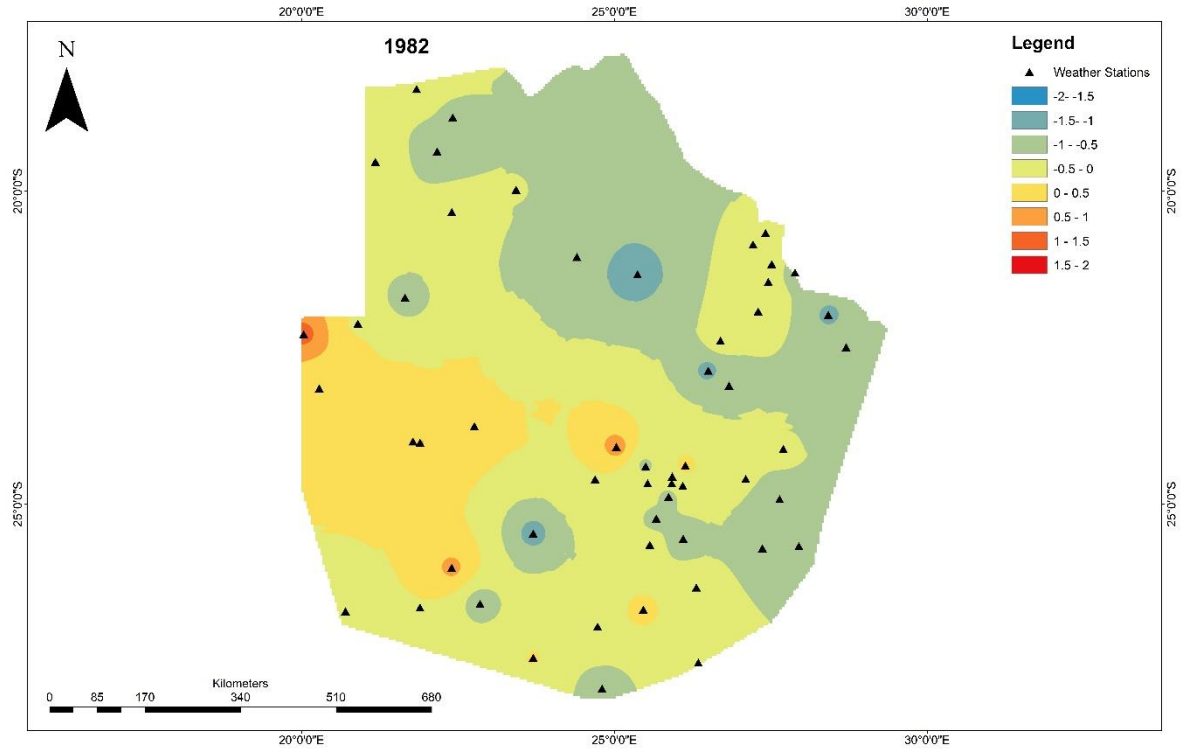

Figure 8.3m: IDW SPI 1982

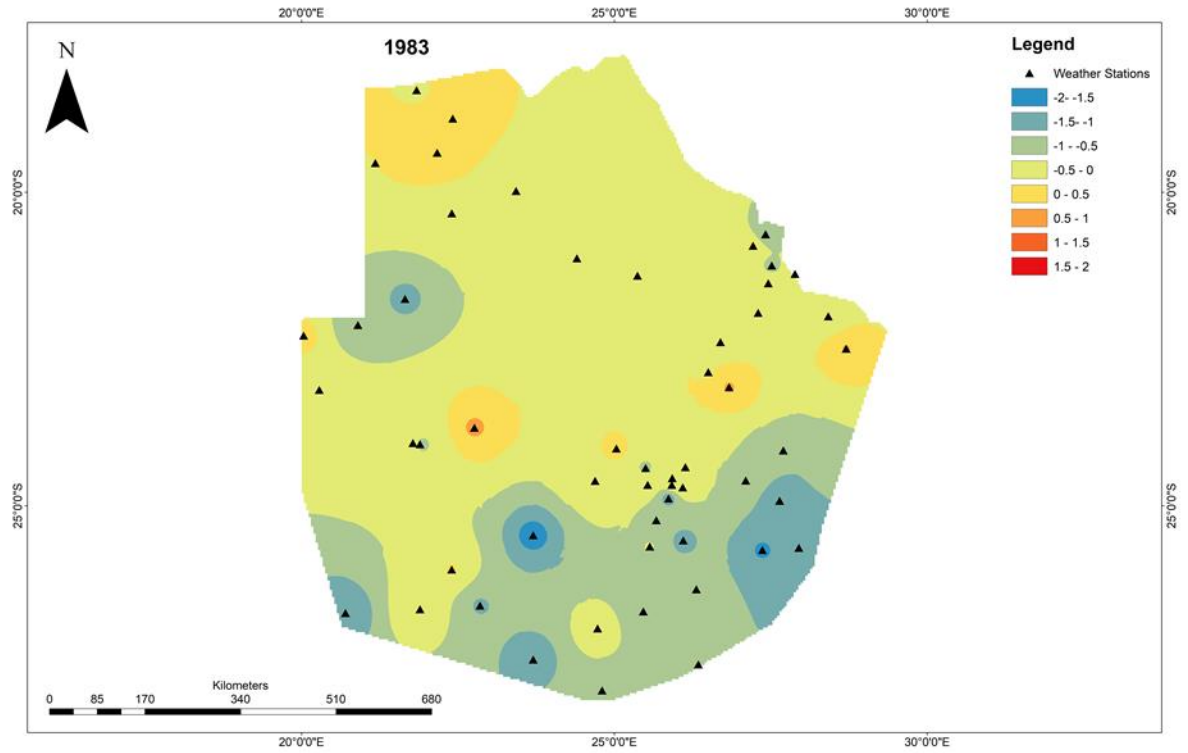

Figure 8.3n: IDW SPI 1983

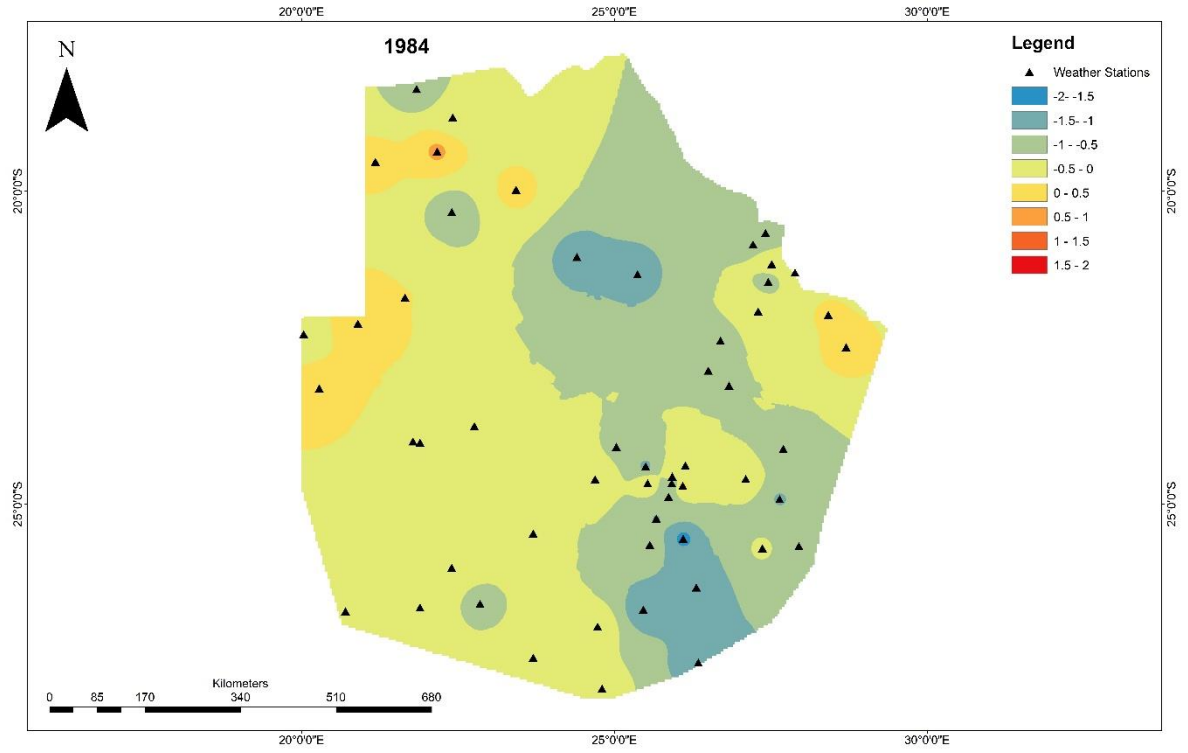

Figure 8.3o: IDW SPI 1984

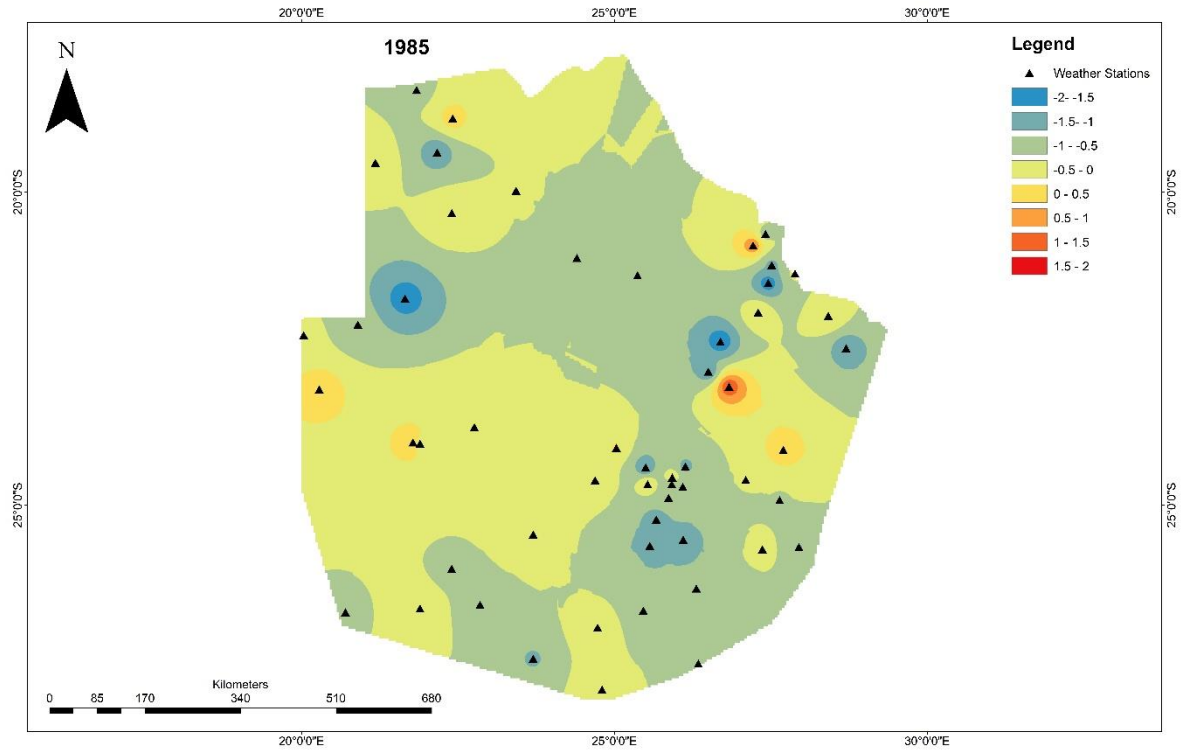

Figure 8.3p: IDW SPI 1985

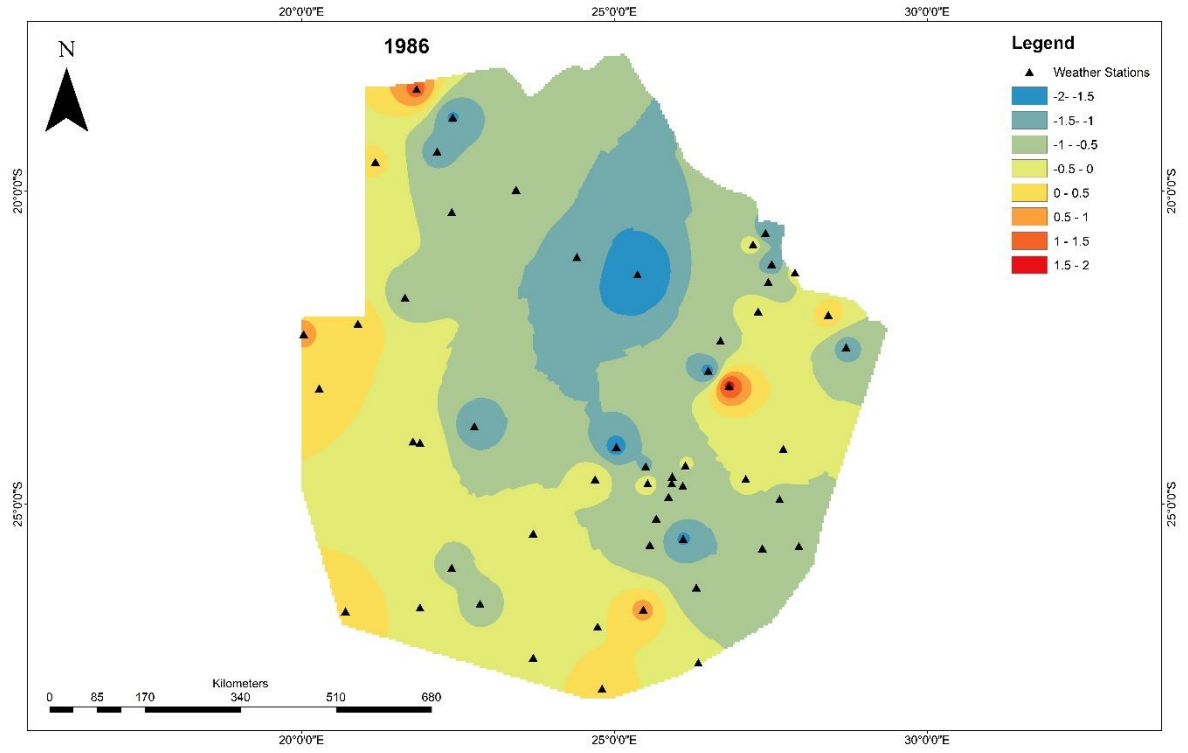

Figure 8.3q: IDW SPI 1986

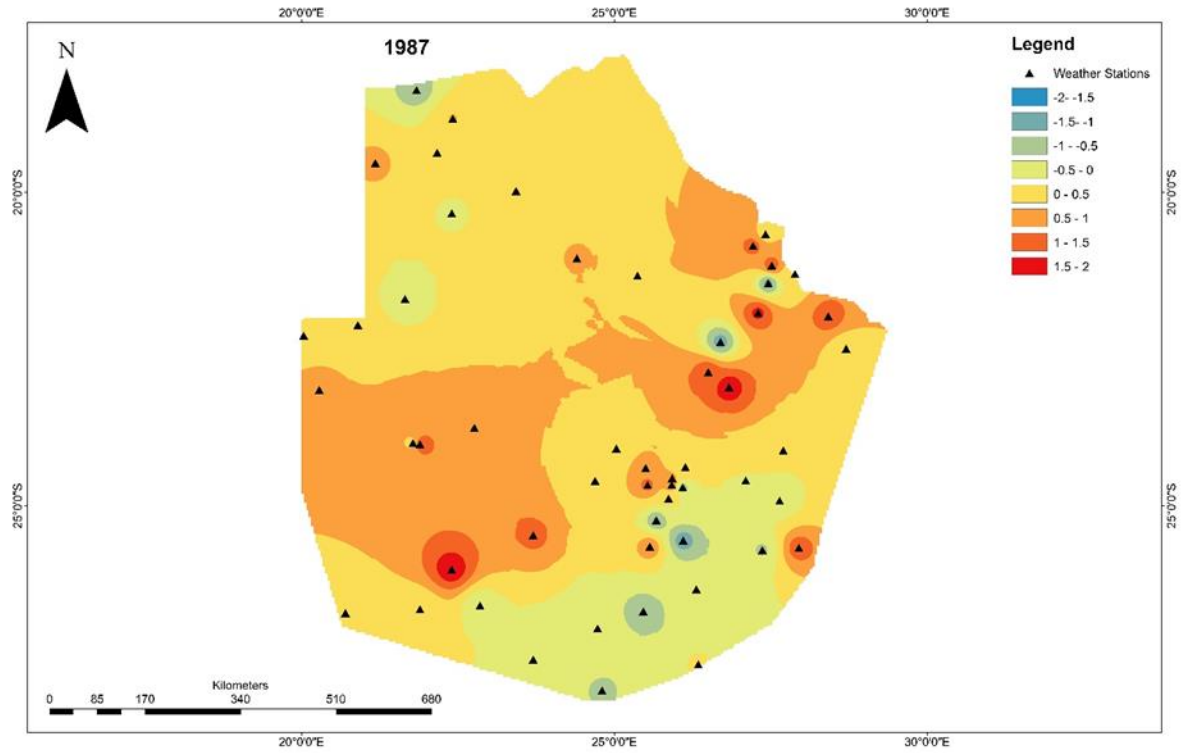

Figure 8.3r: IDW SPI 1987

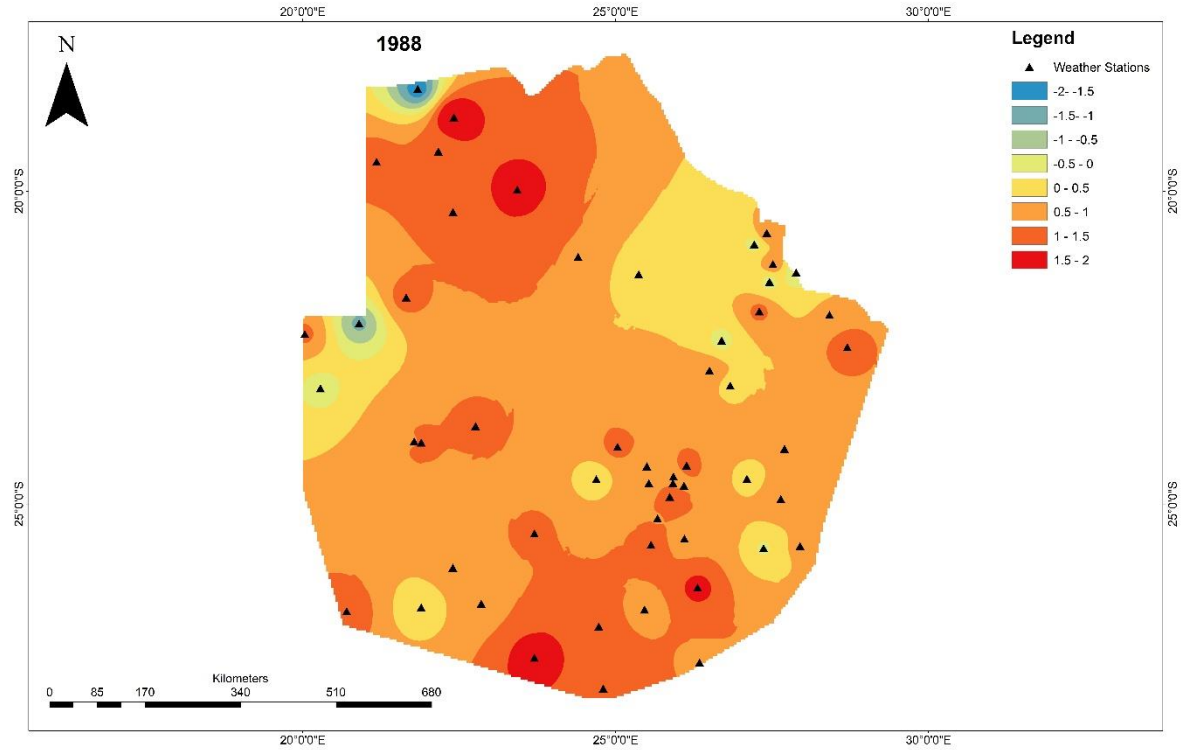

Figure 8.3s: IDW SPI 1988

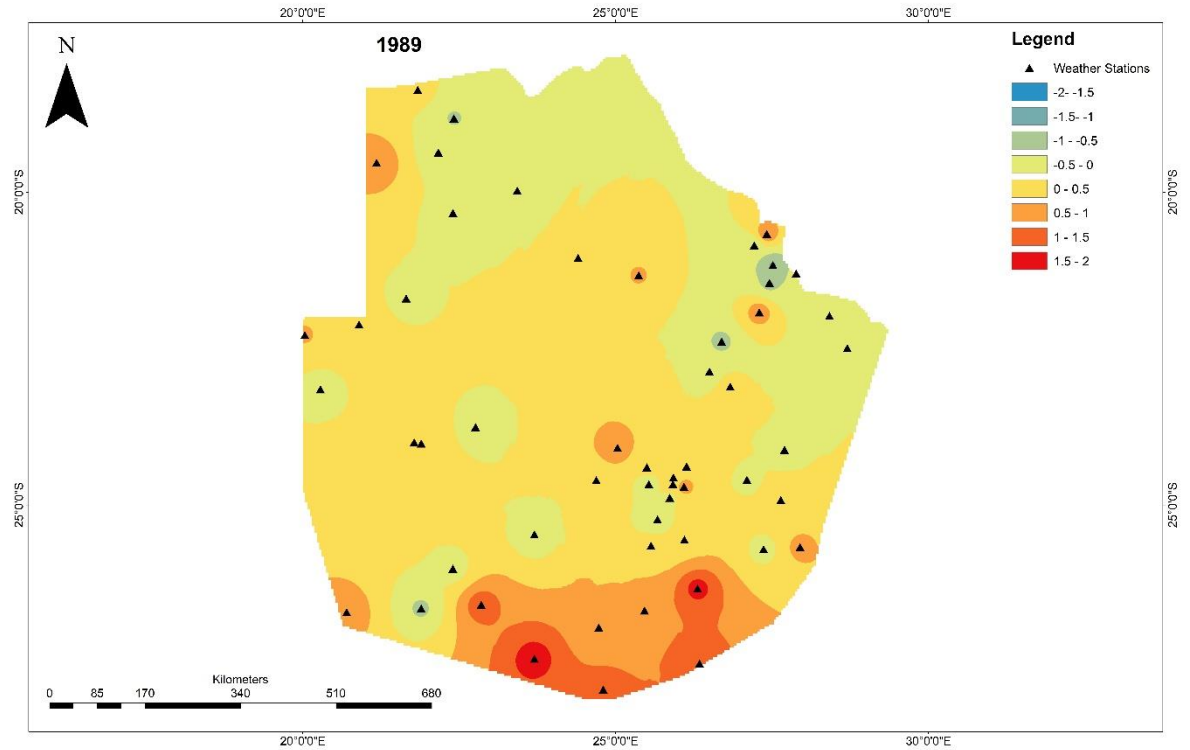

Figure 8.3t: IDW SPI 1989

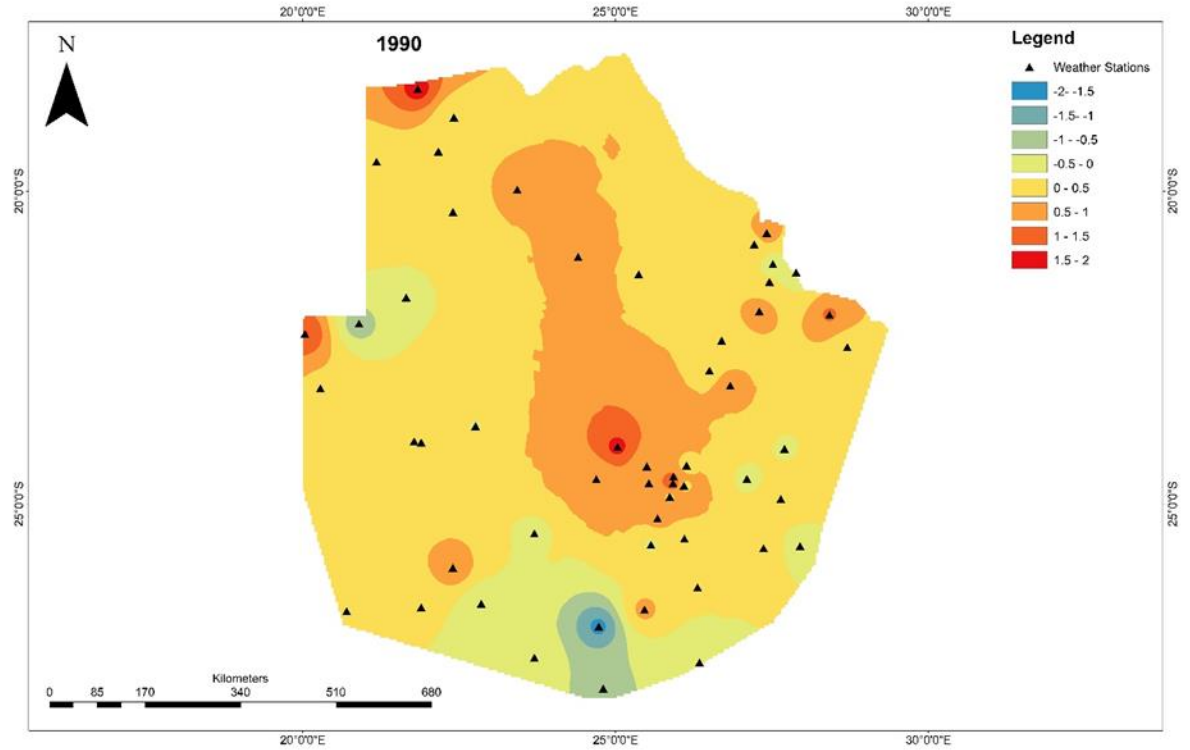

Figure 8.3u: IDW SPI 1990

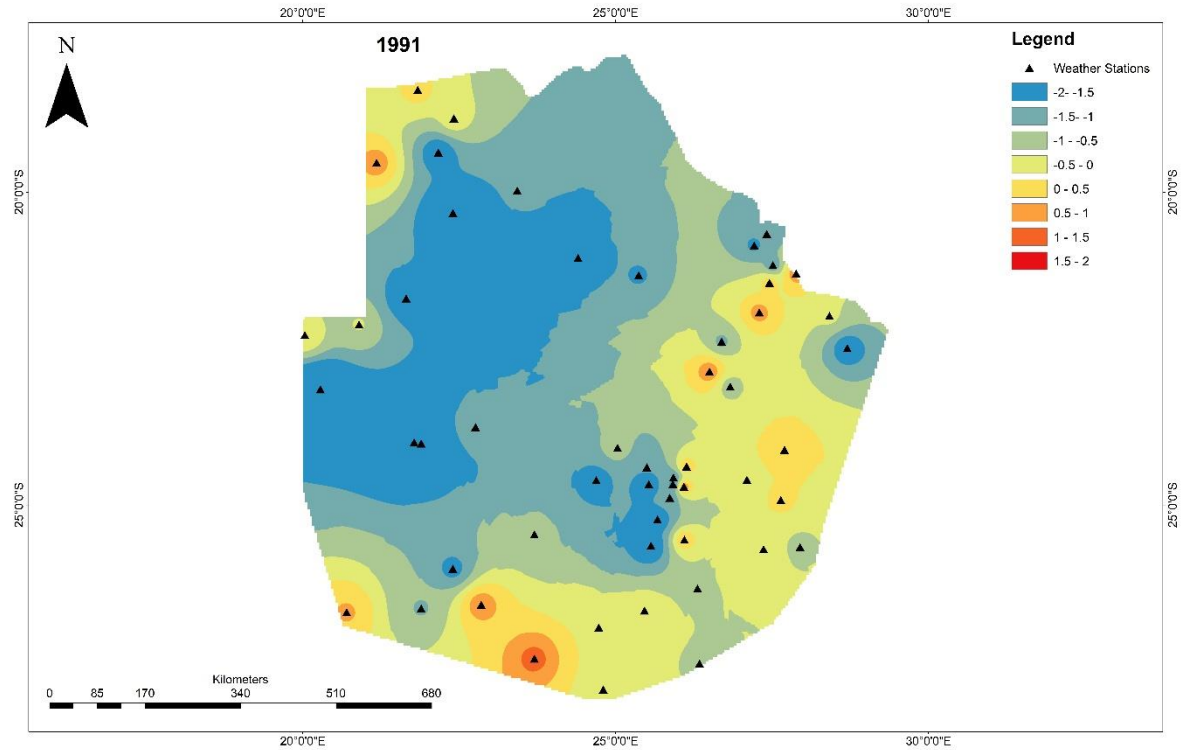

Figure 8.3v: IDW SPI 1991

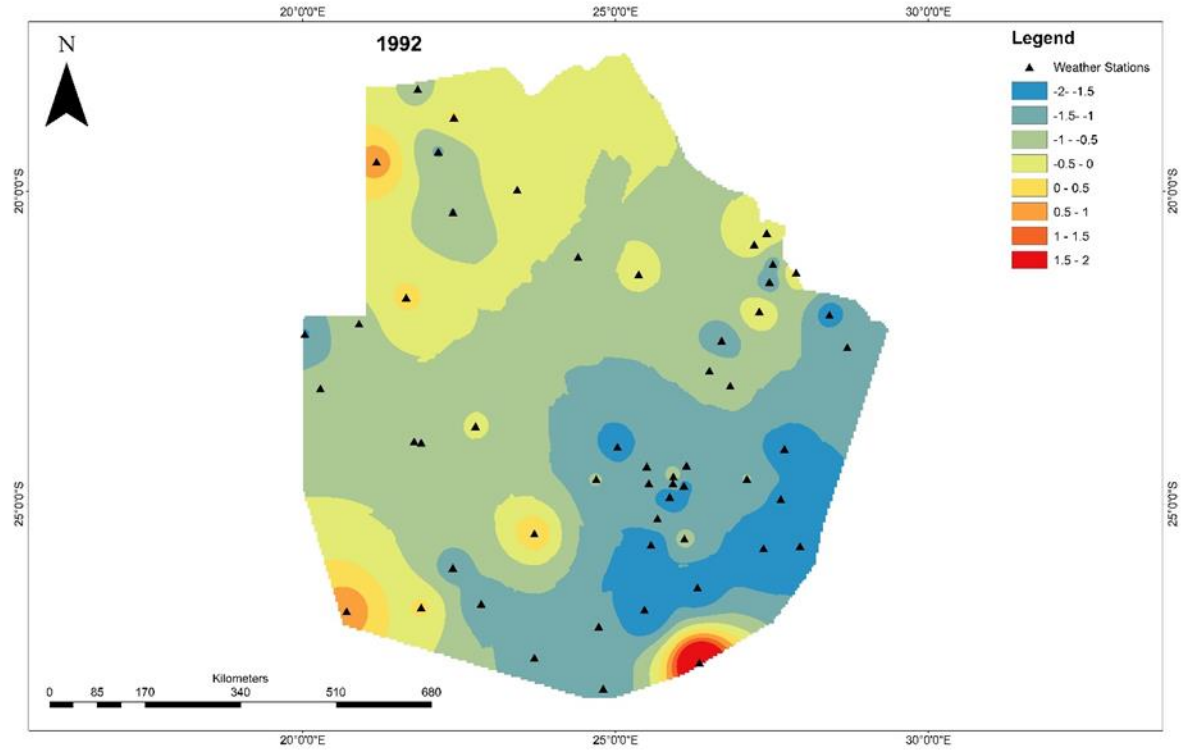

Figure 8.3w: IDW SPI 1992

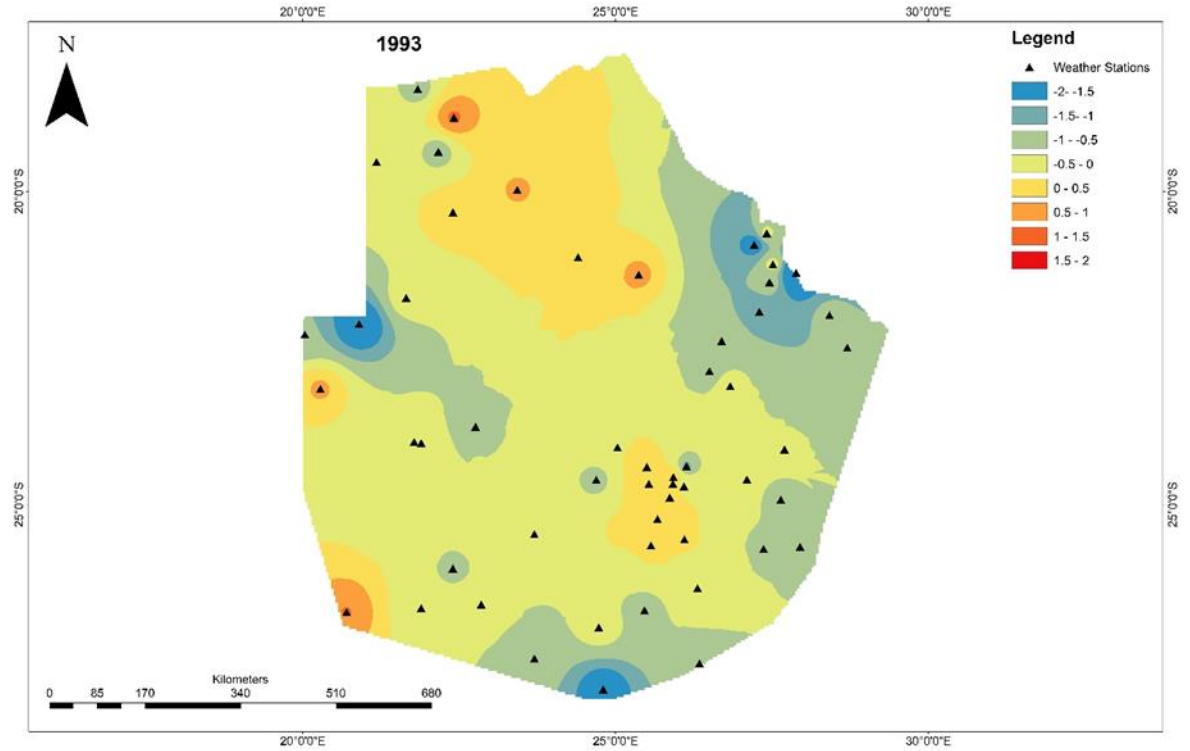

Figure 8.3x: IDW SPI 1993

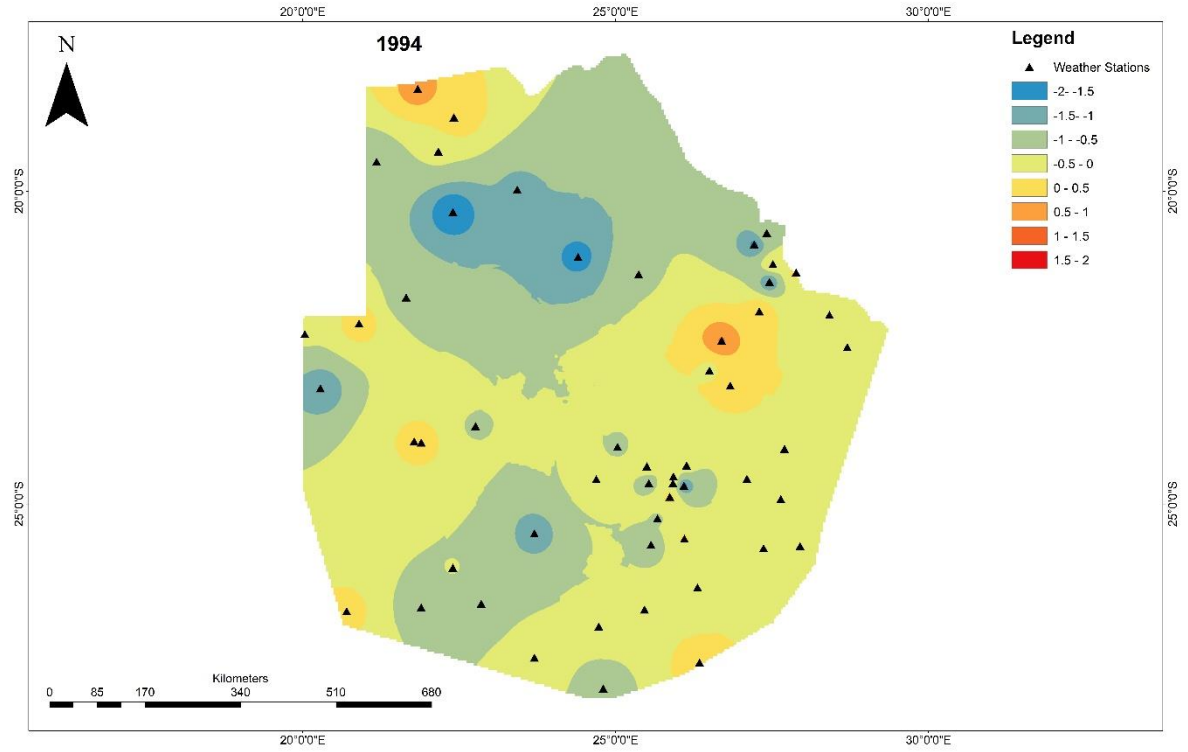

Figure 8.3y: IDW SPI 1994

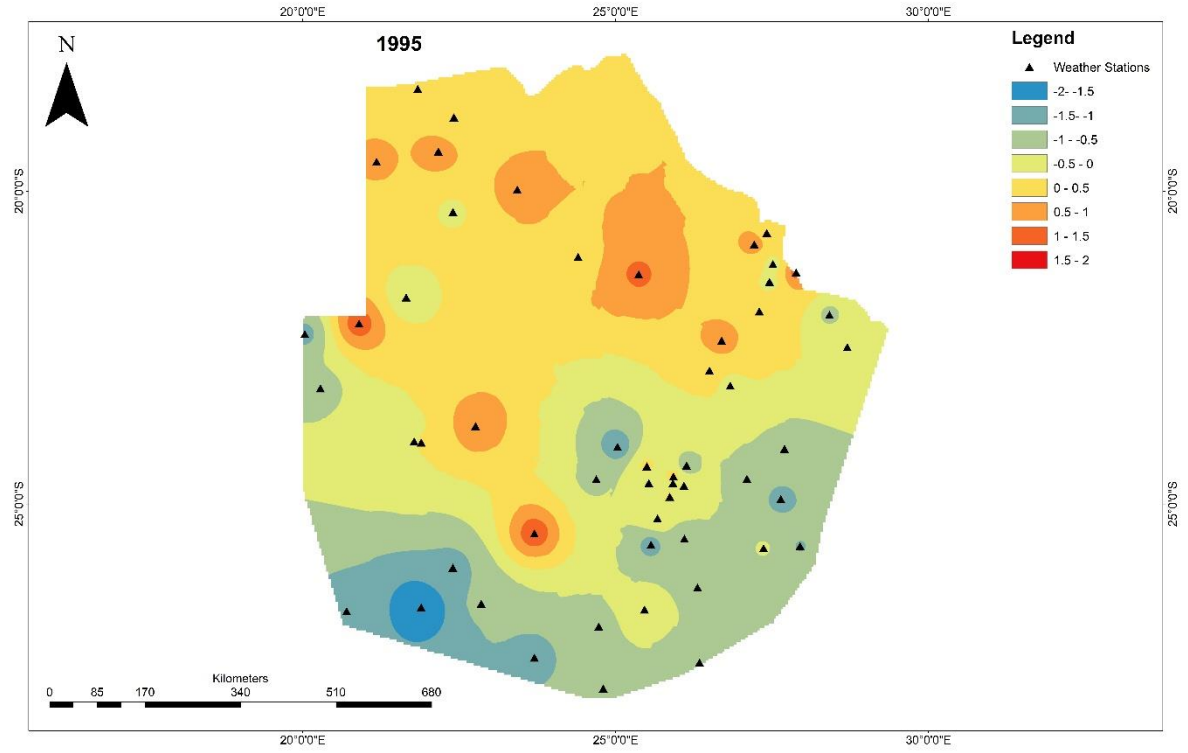

Figure 8.3z: IDW SPI 1995

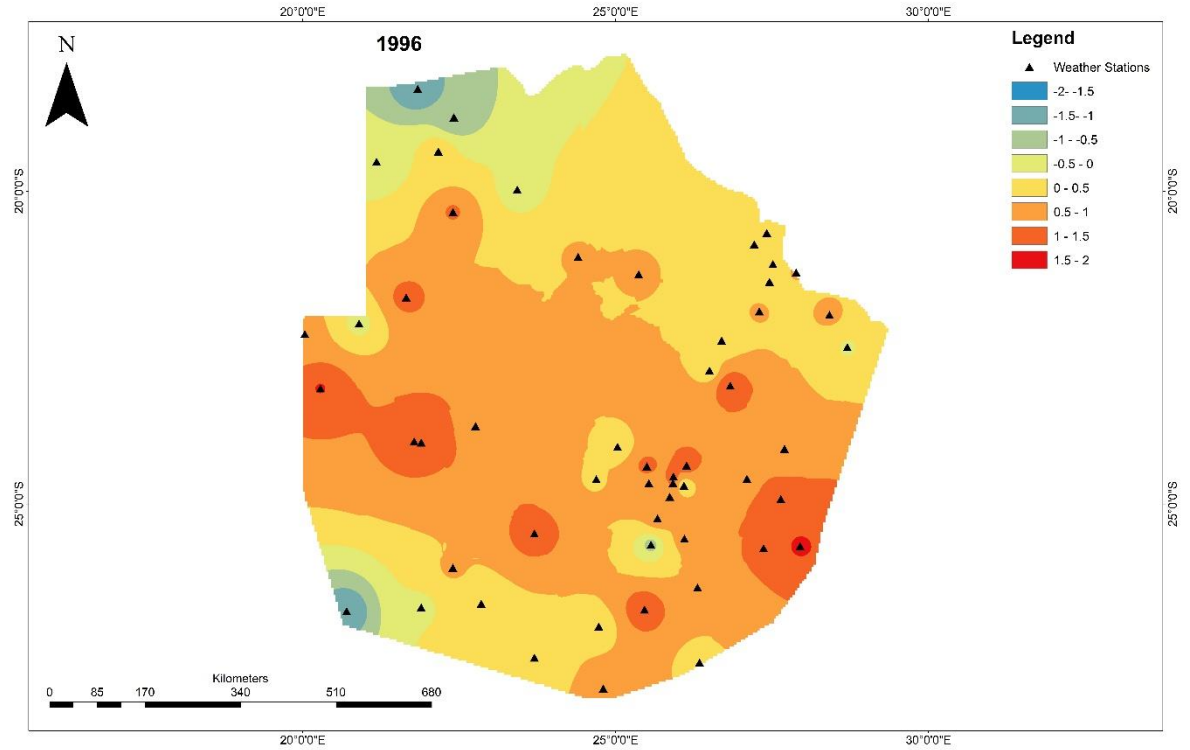

Figure 8.3aa: IDW SPI 1996

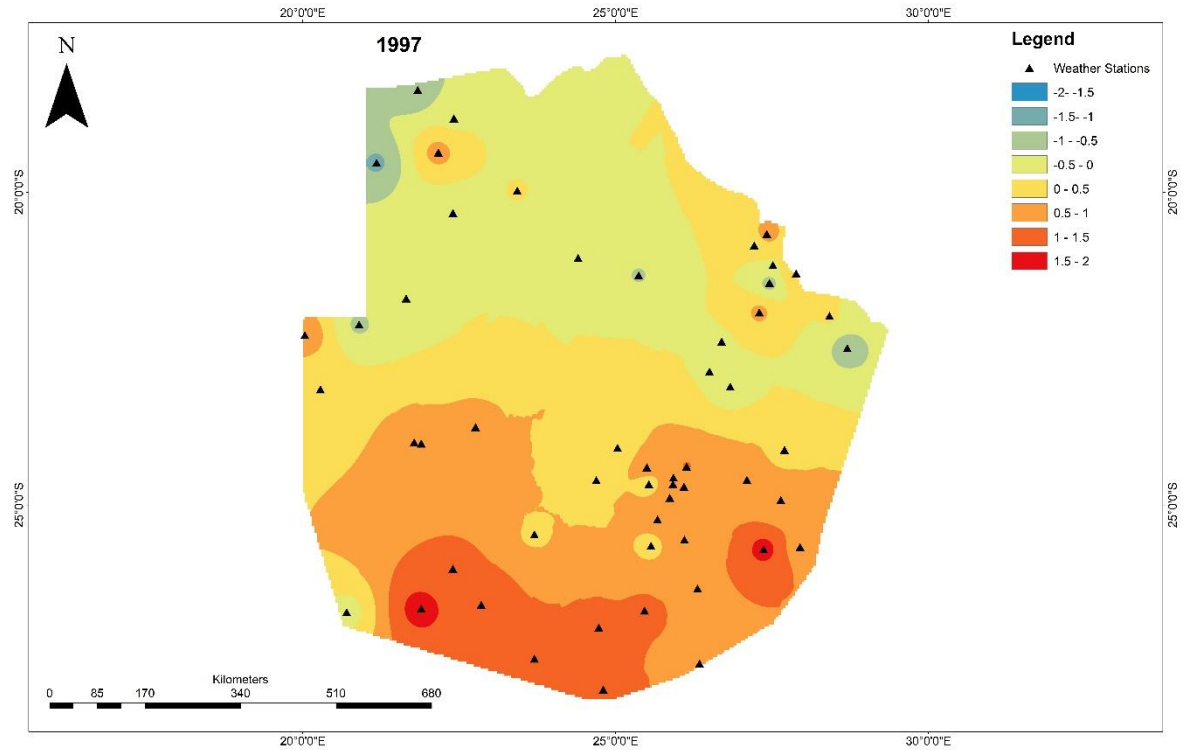

Figure 8.3ab: IDW SPI 1997

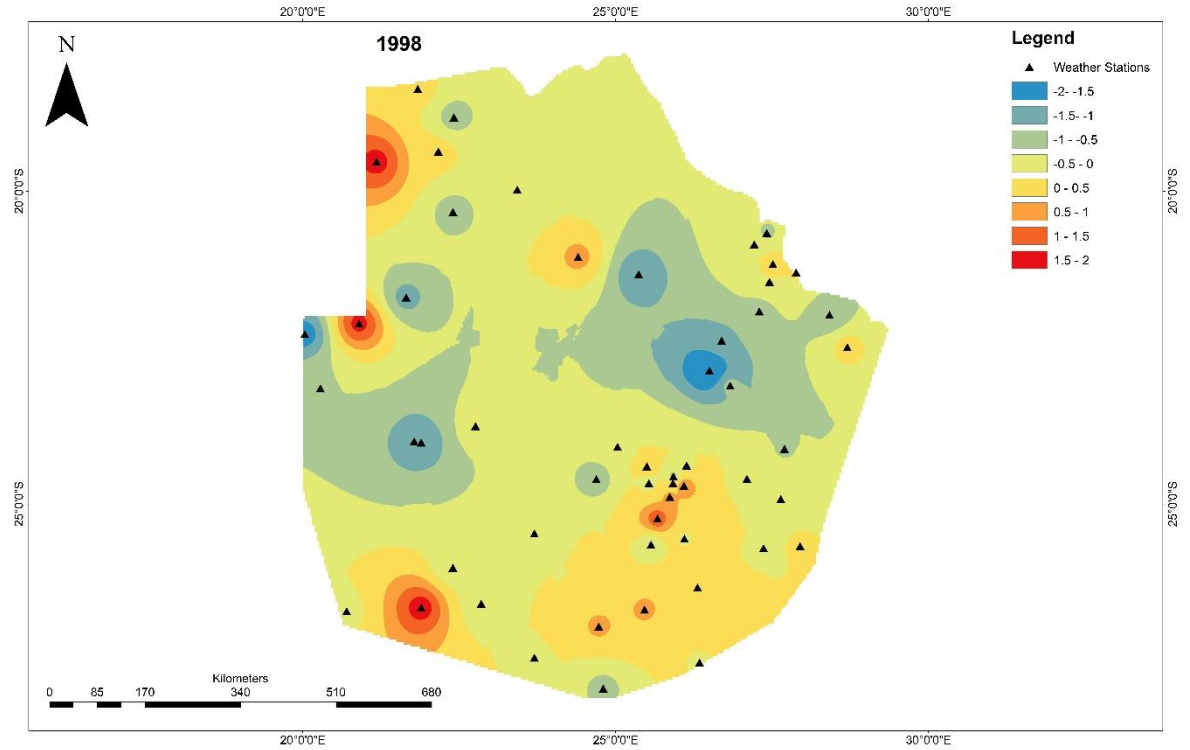

Figure 8.3ac: IDW SPI 1998

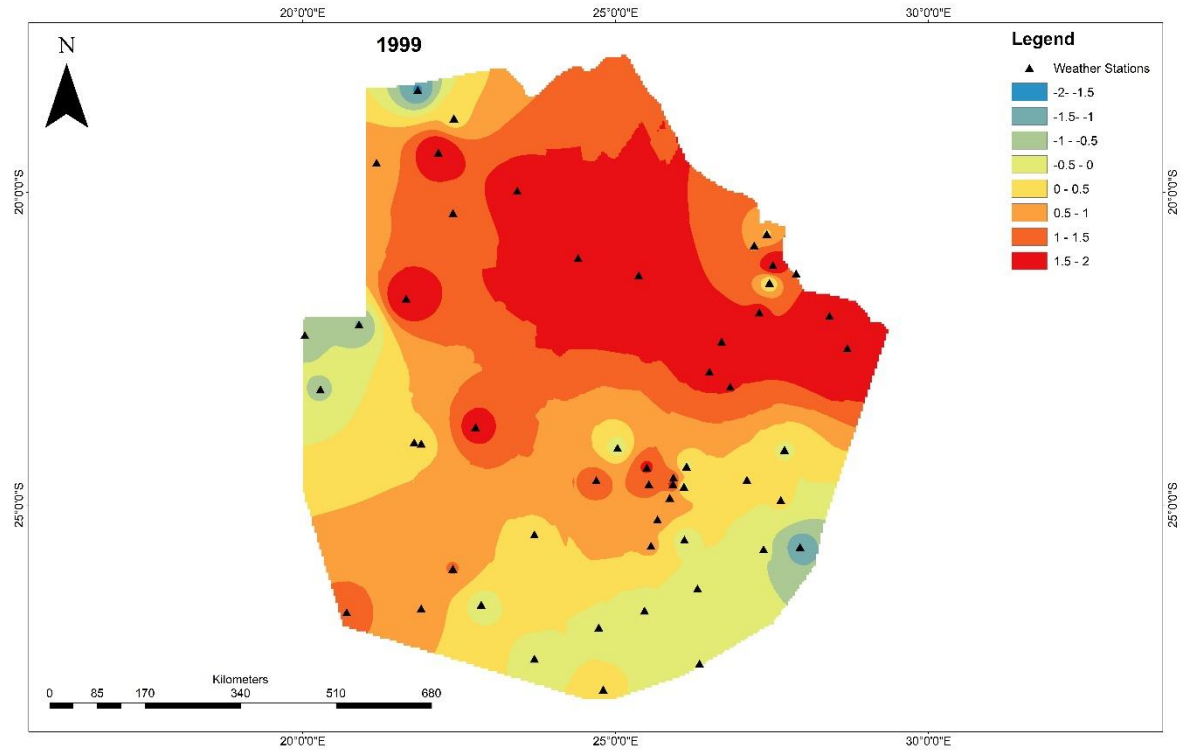

Figure 8.3ad: IDW SPI 1999

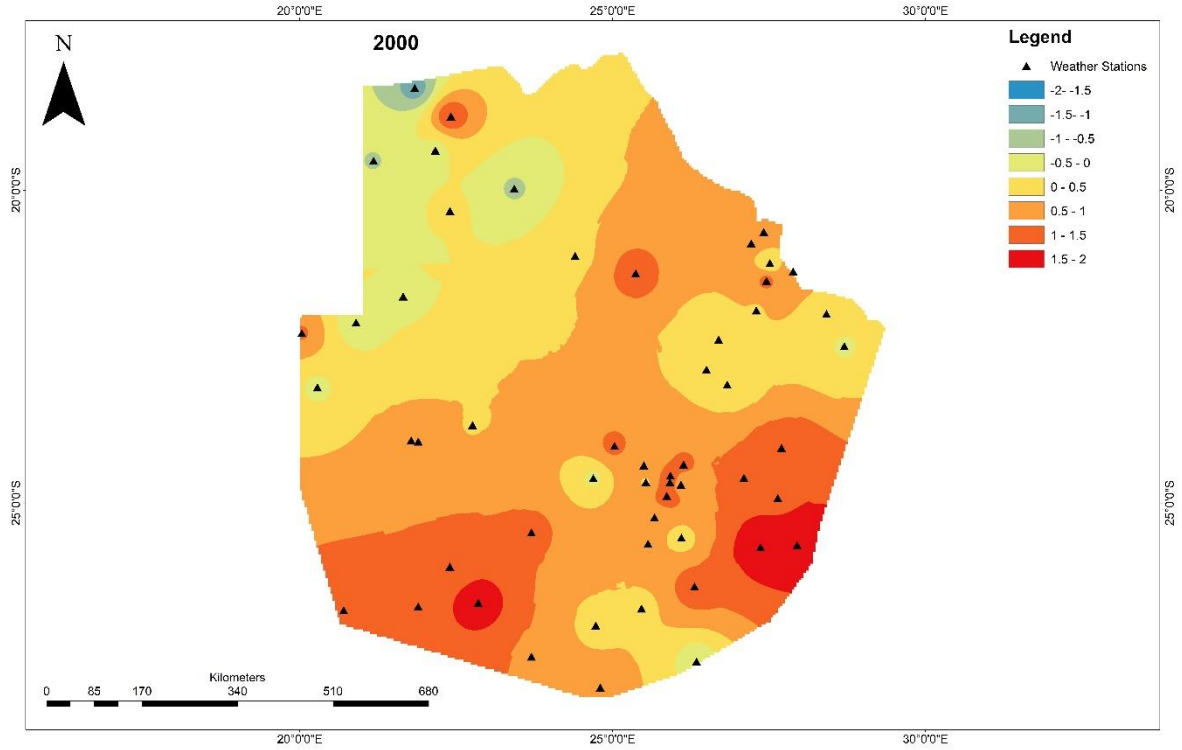

Figure 8.3ae: IDW SPI 2000

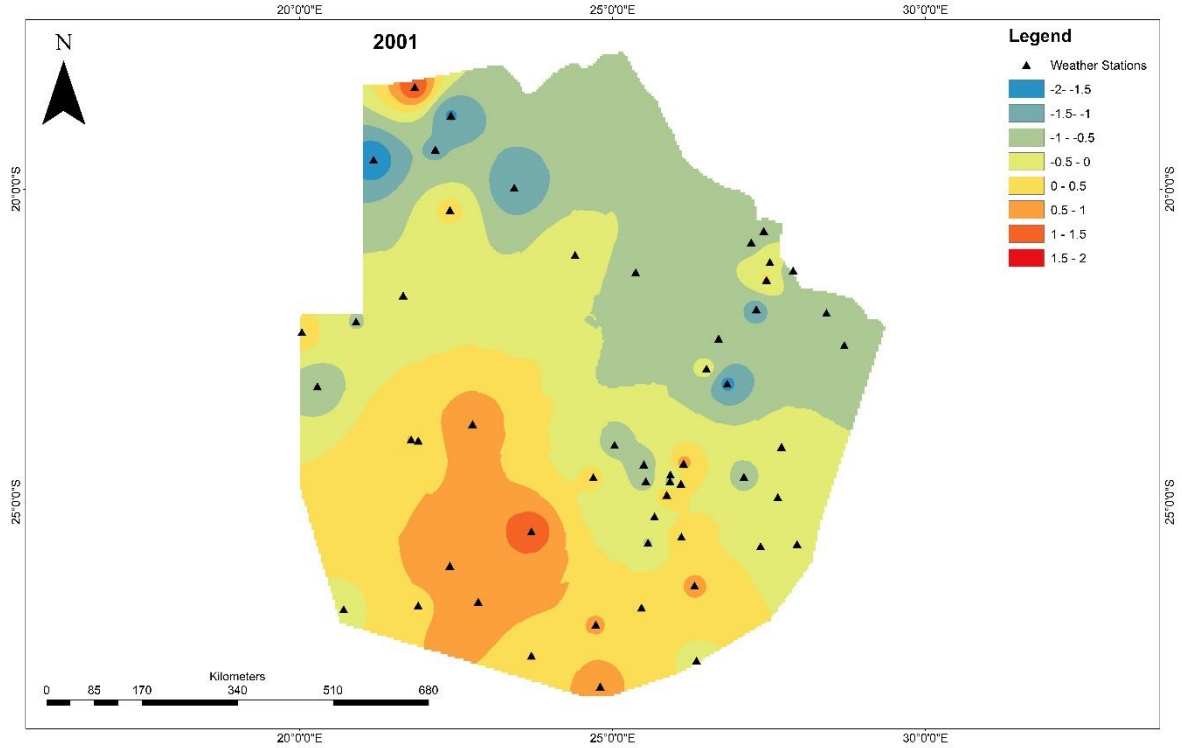

Figure 8.3af: IDW SPI 2001

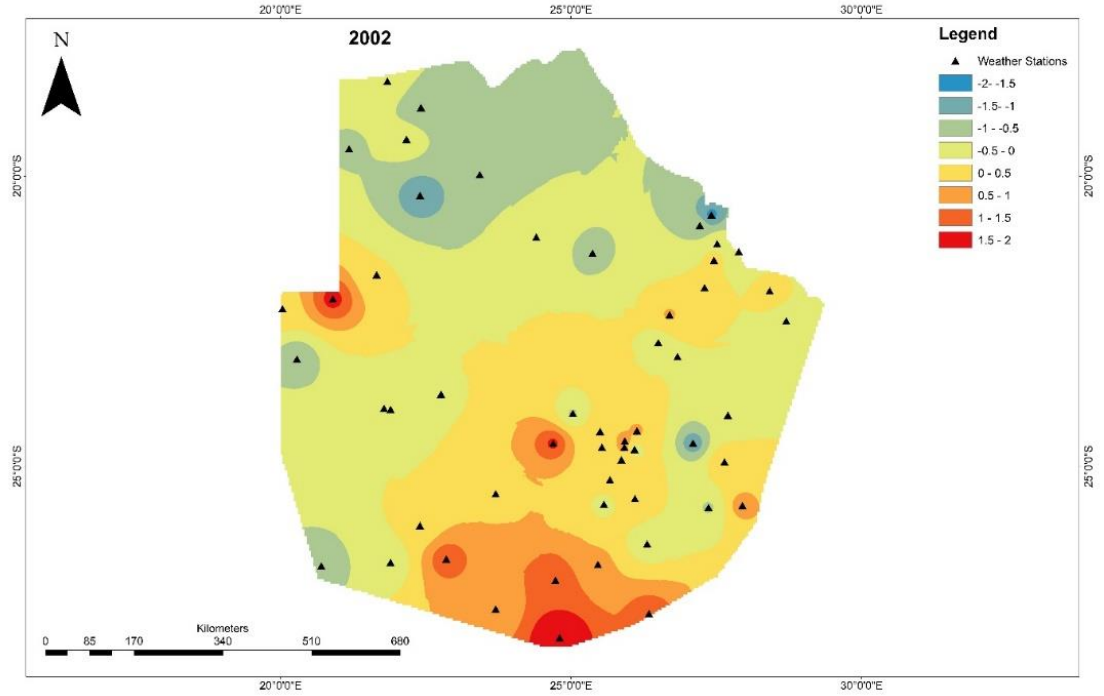

Figure 8.3ag: IDW SPI 2002

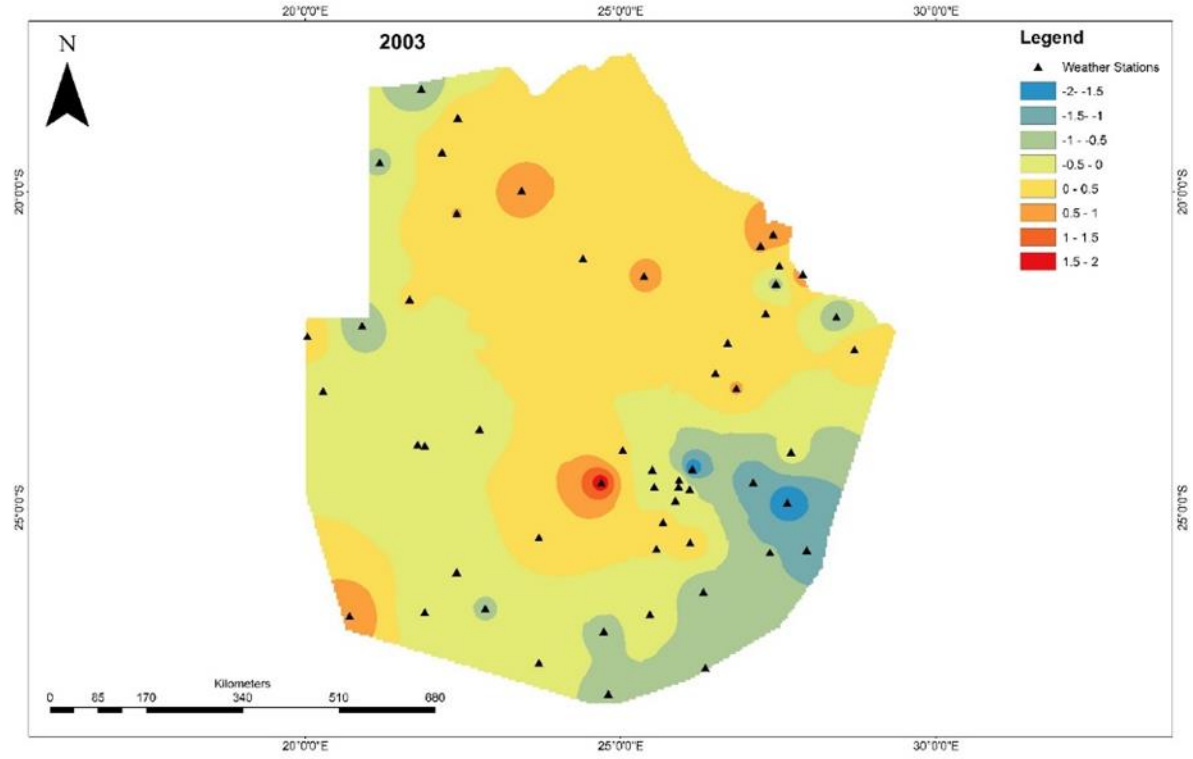

Figure 8.3ah: IDW SPI 2003

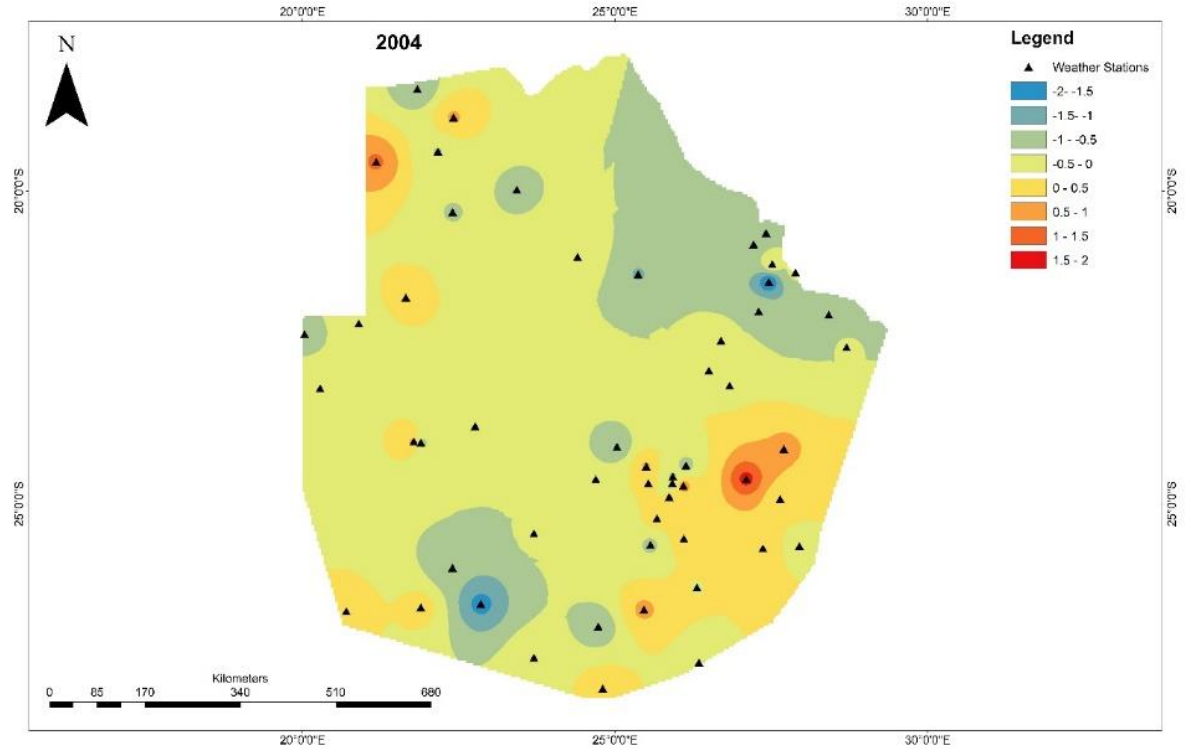

Figure 8.3ai: IDW SPI 2004

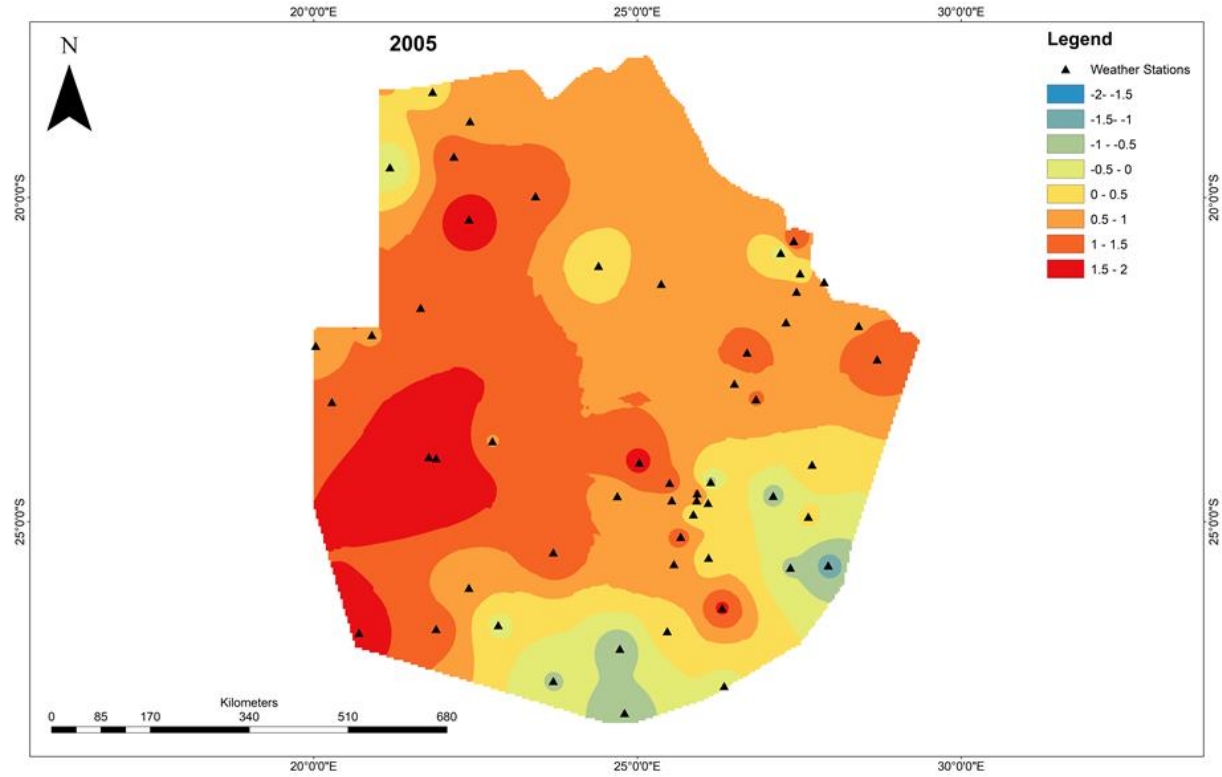

Figure 8.3aj: IDW SPI 2005

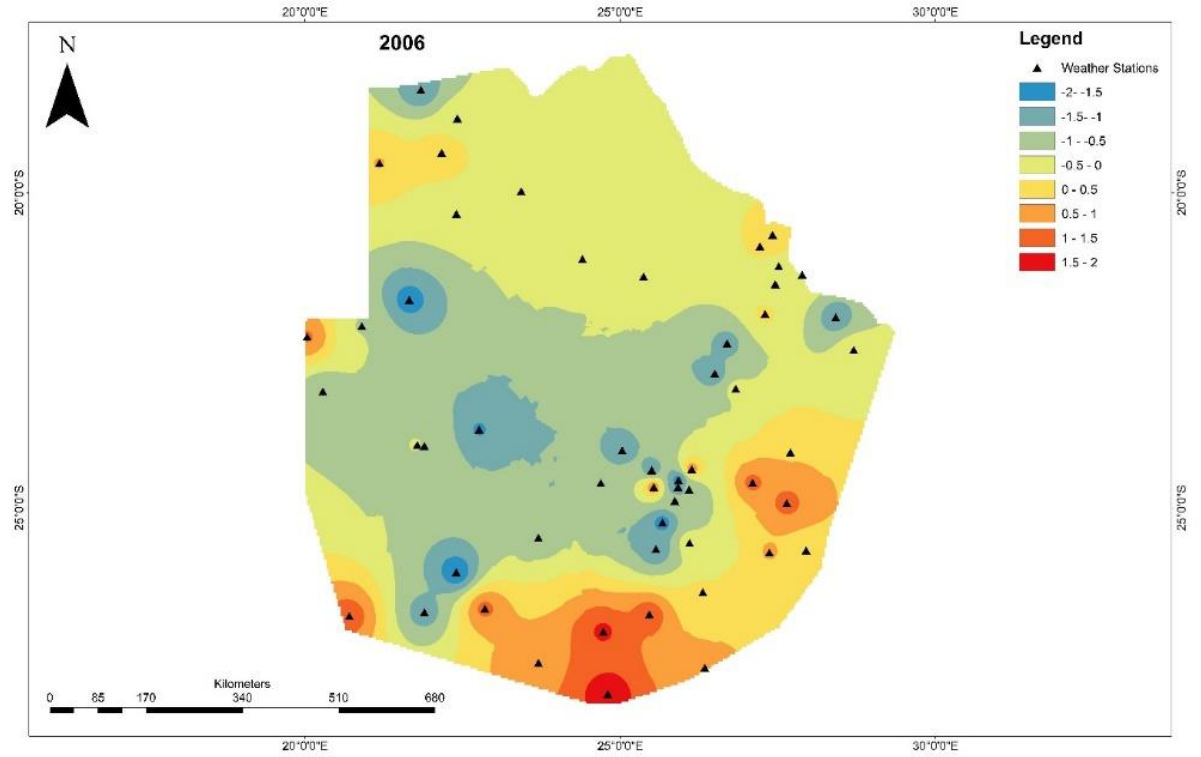

Figure 8.3ak IDW: SPI 2006

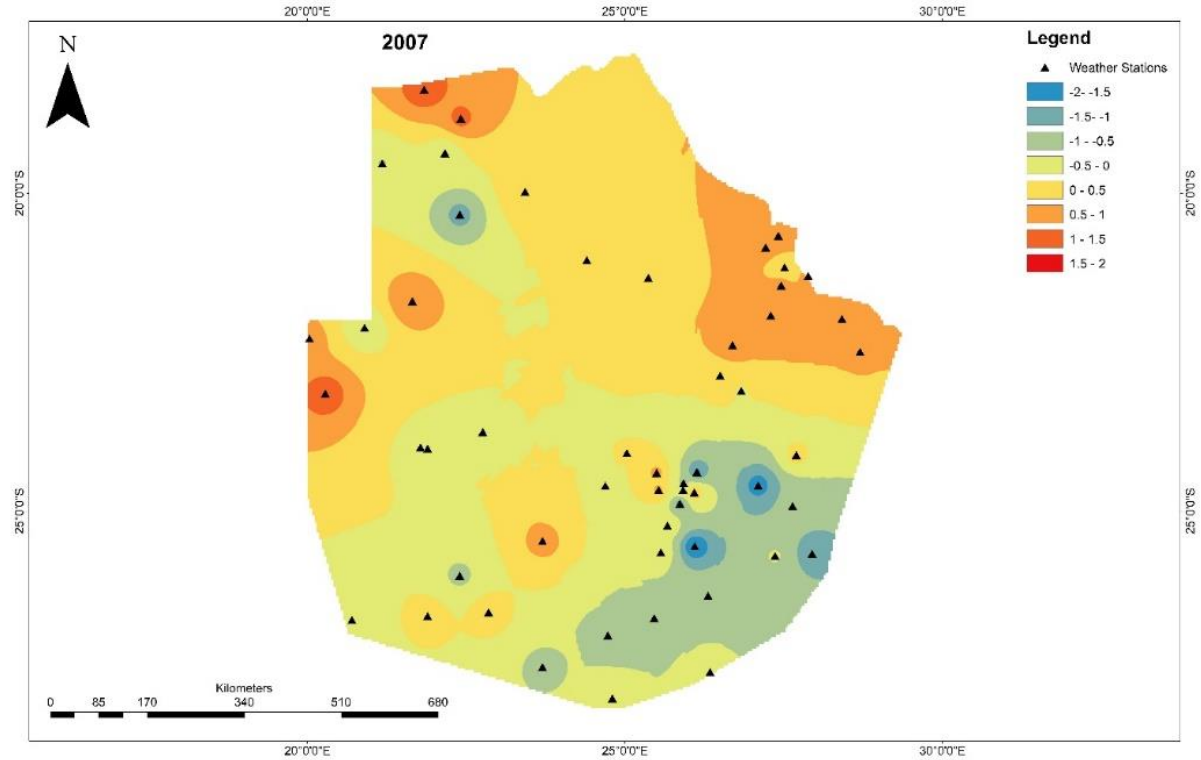

Figure 8.3al: IDW SPI 2007

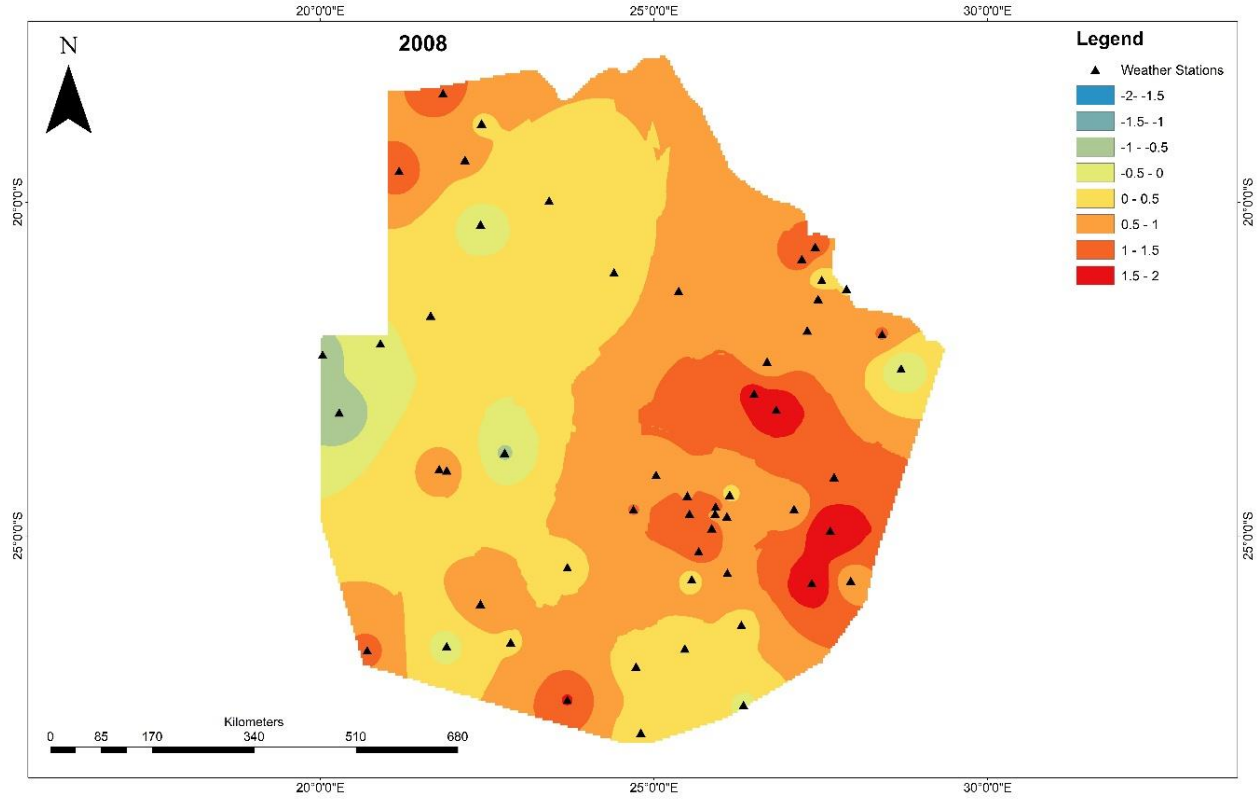

Figure 8.3am: IDW SPI 2008

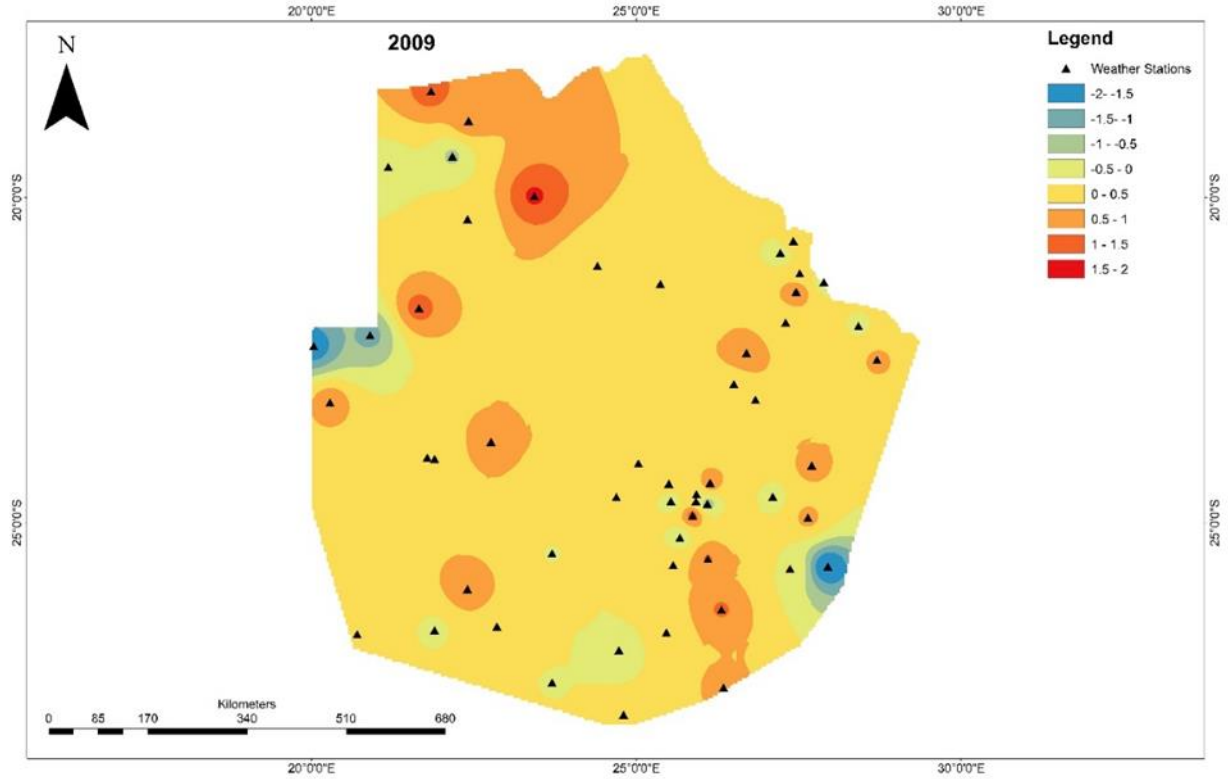

Figure 8.3an: IDW SPI 2009

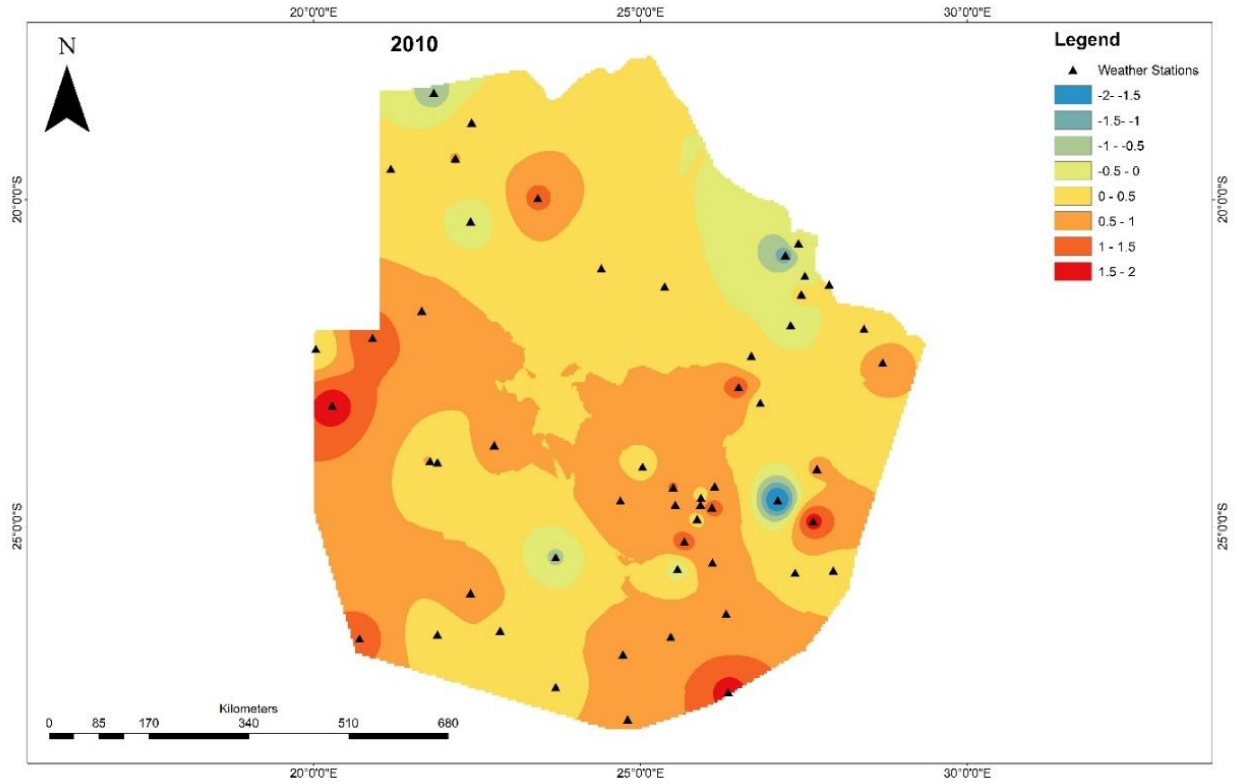

Figure 8.3ao: IDW SPI 2010

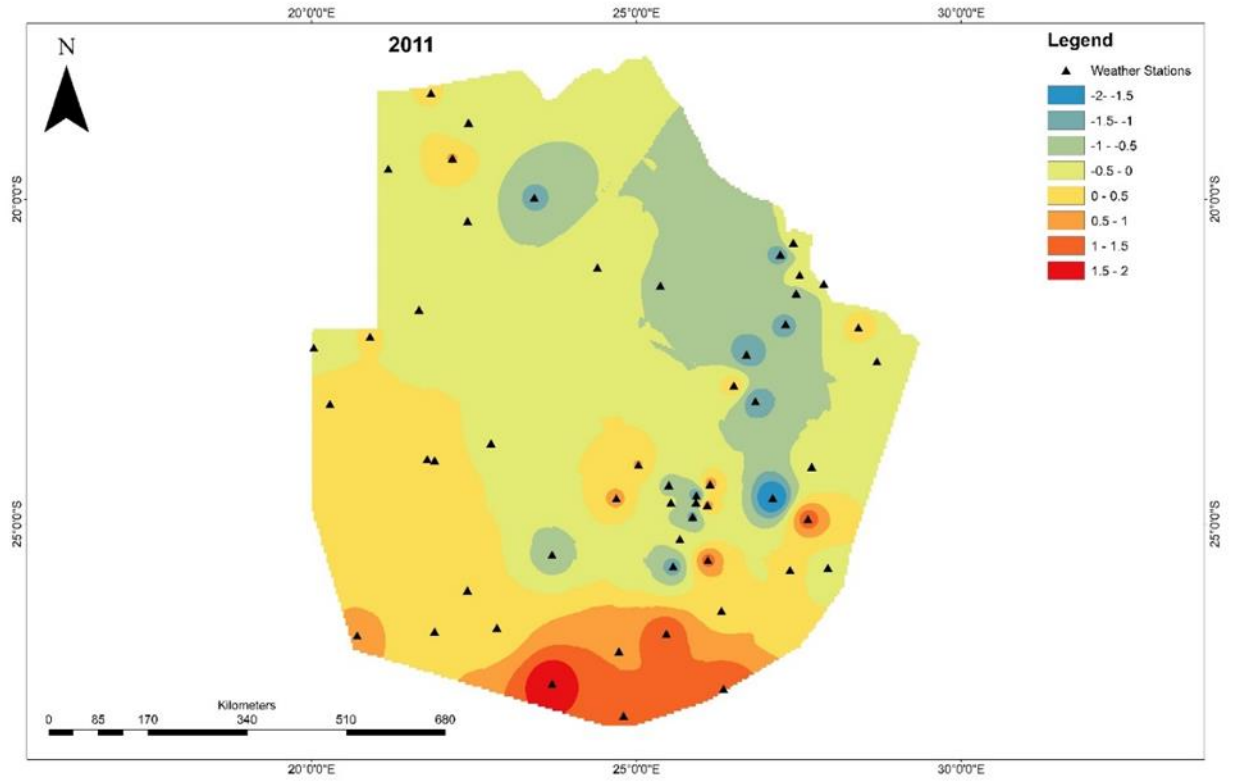

Figure 8.3ap: IDW SPI 2011

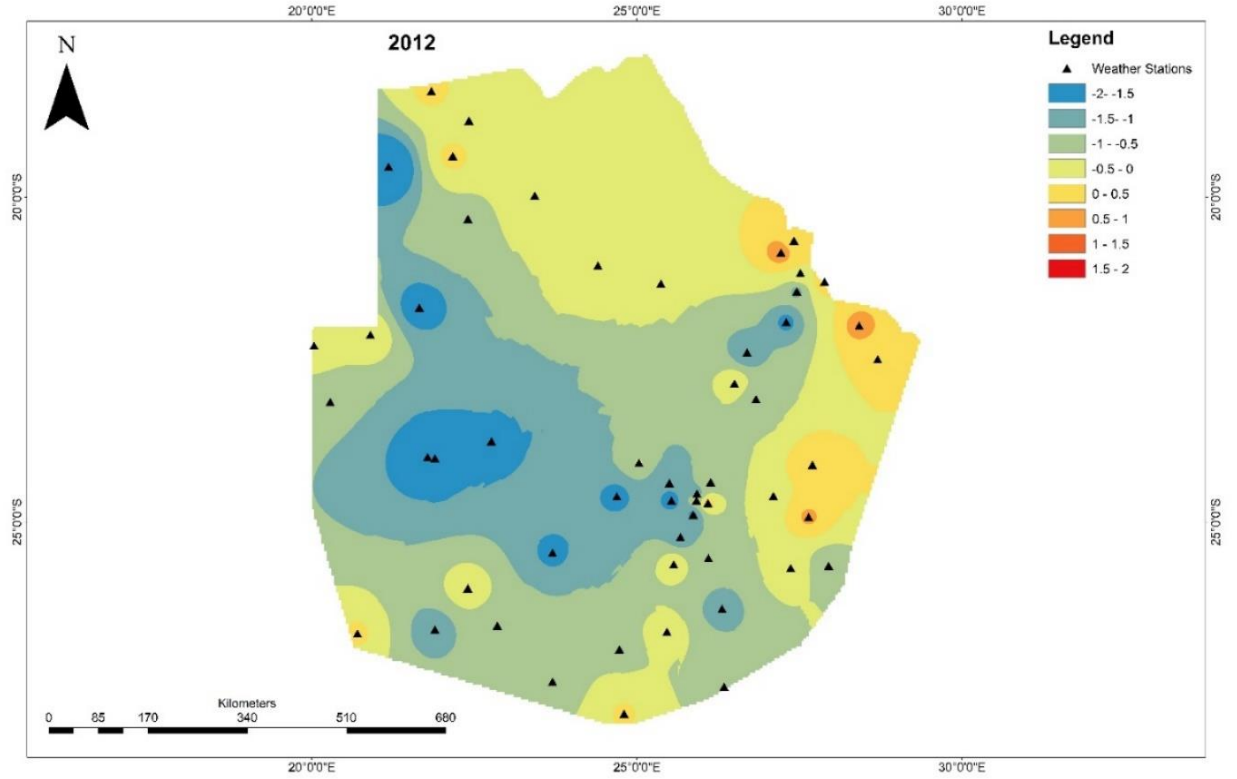

Figure 8.3aq: IDW SPI 2012

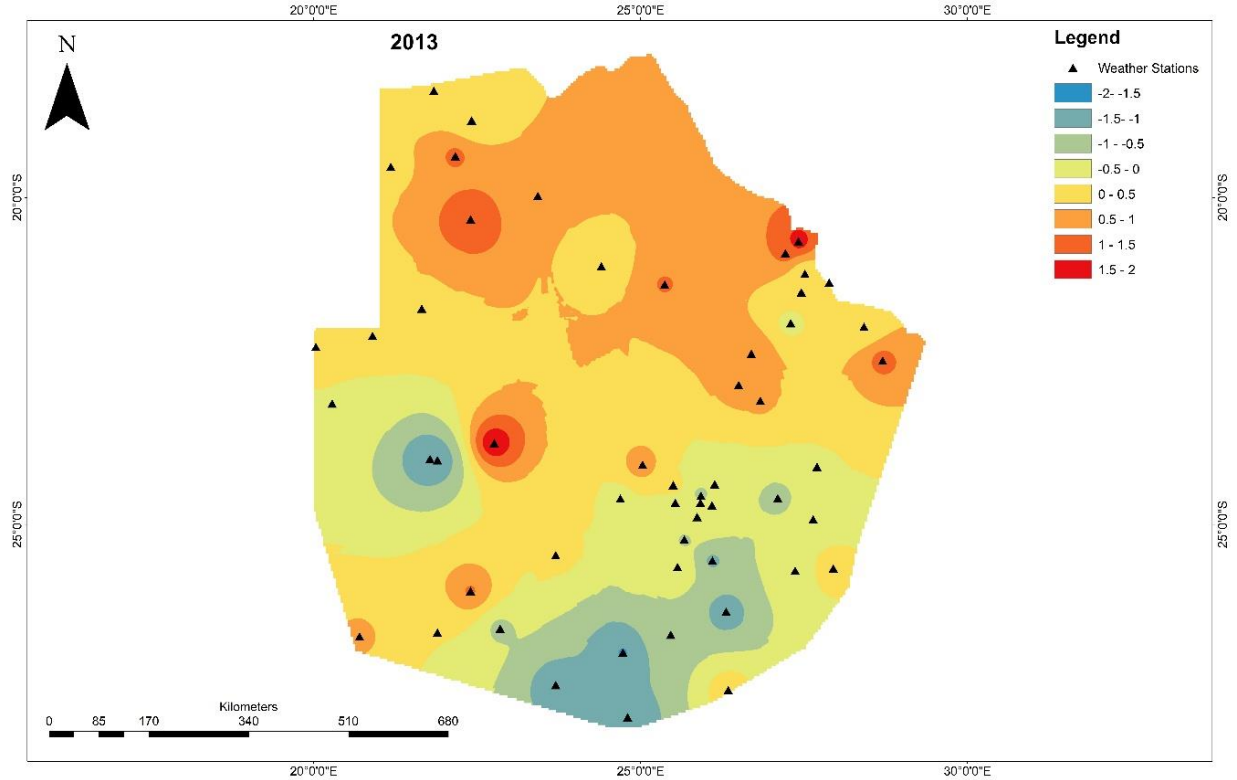

Figure 8.3ar: IDW SPI 2013

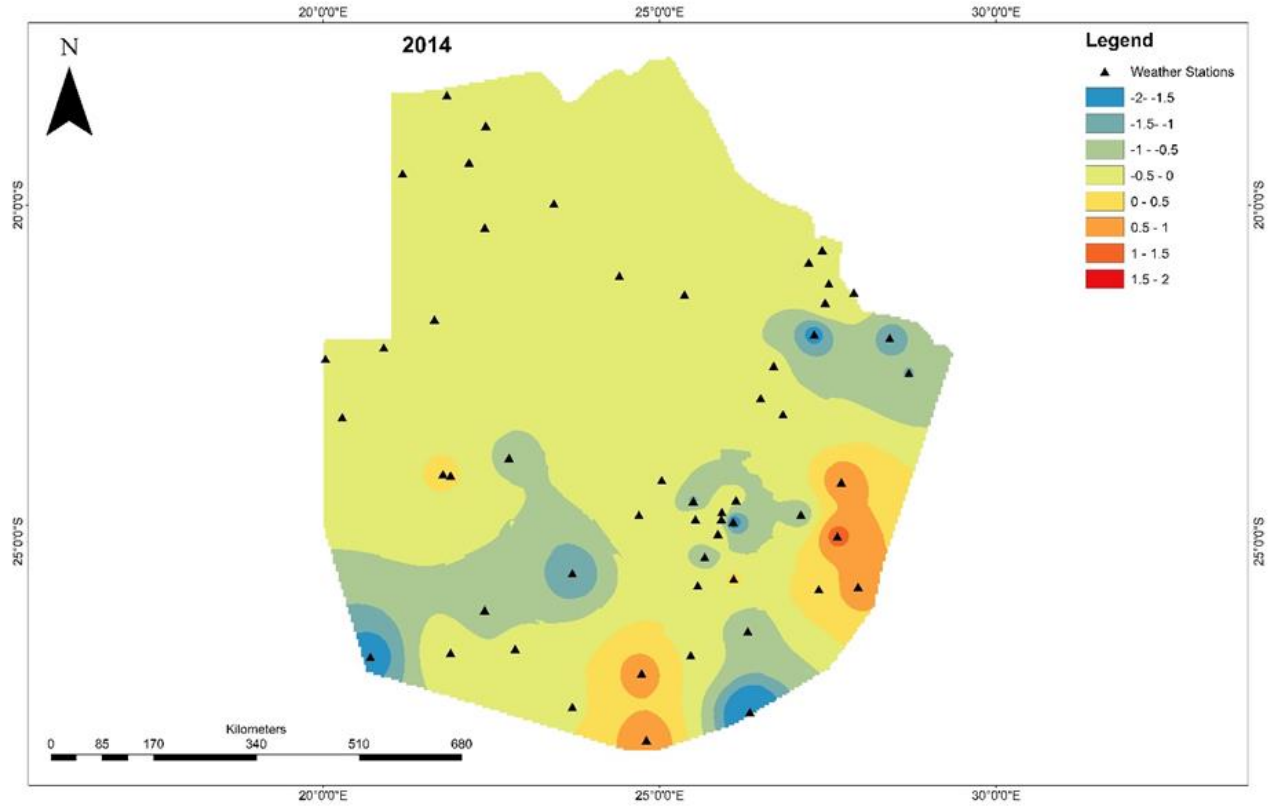

Figure 8.3as IDW: SPI 2014

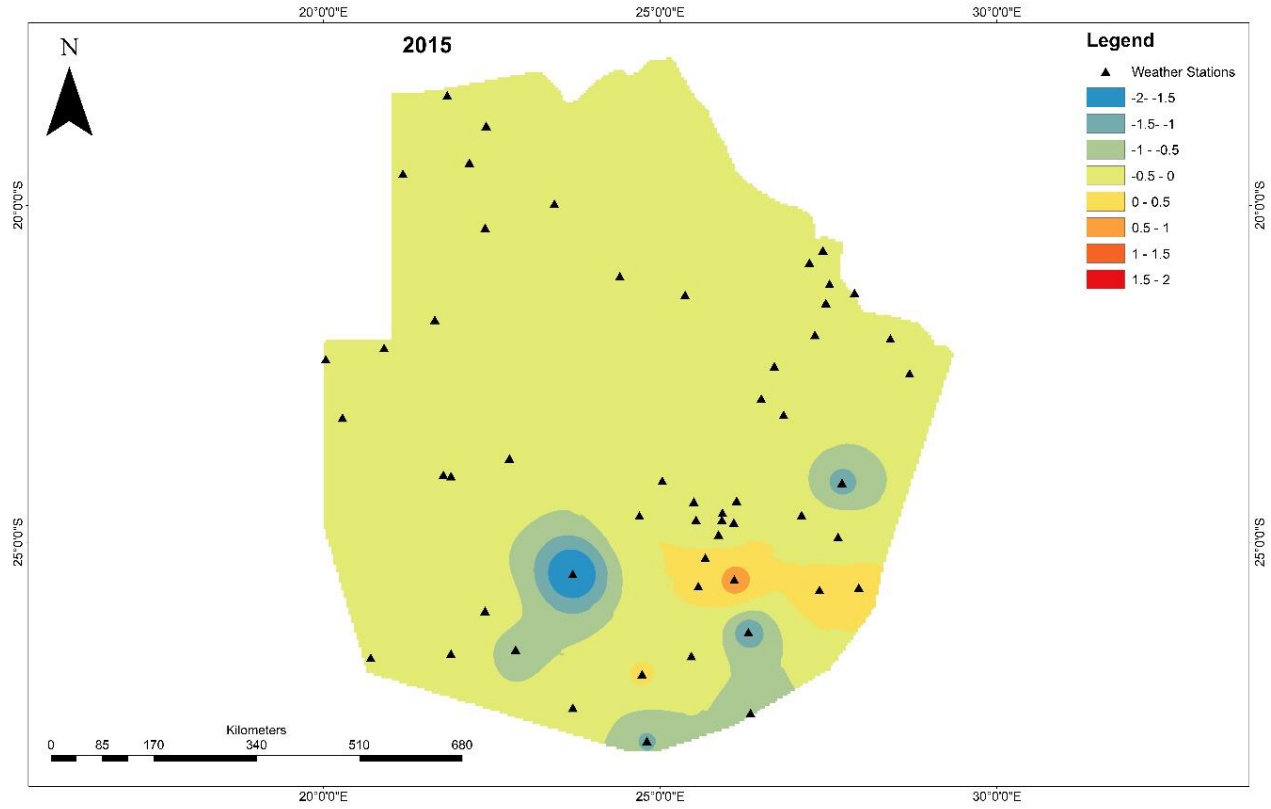

Figure 8.3at: IDW SPI 2015

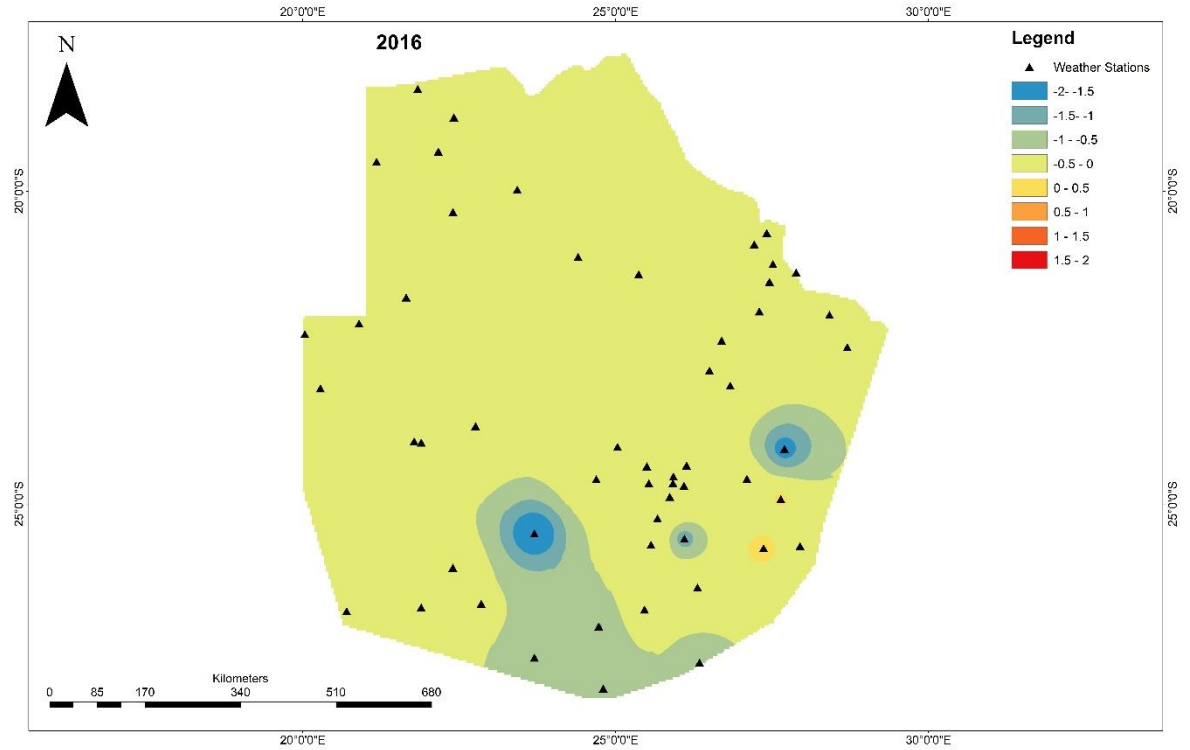

Figure 8.3au: IDW SPI 2016

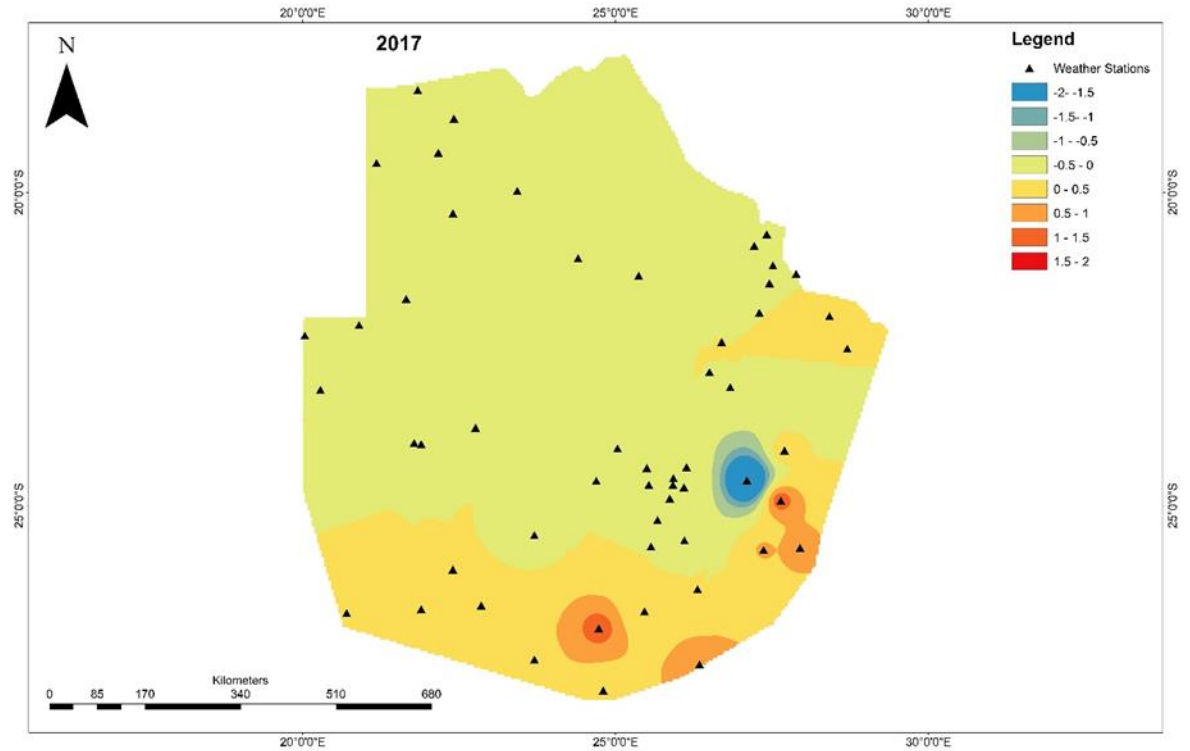

Figure 8.3av: IDW SPI 2017

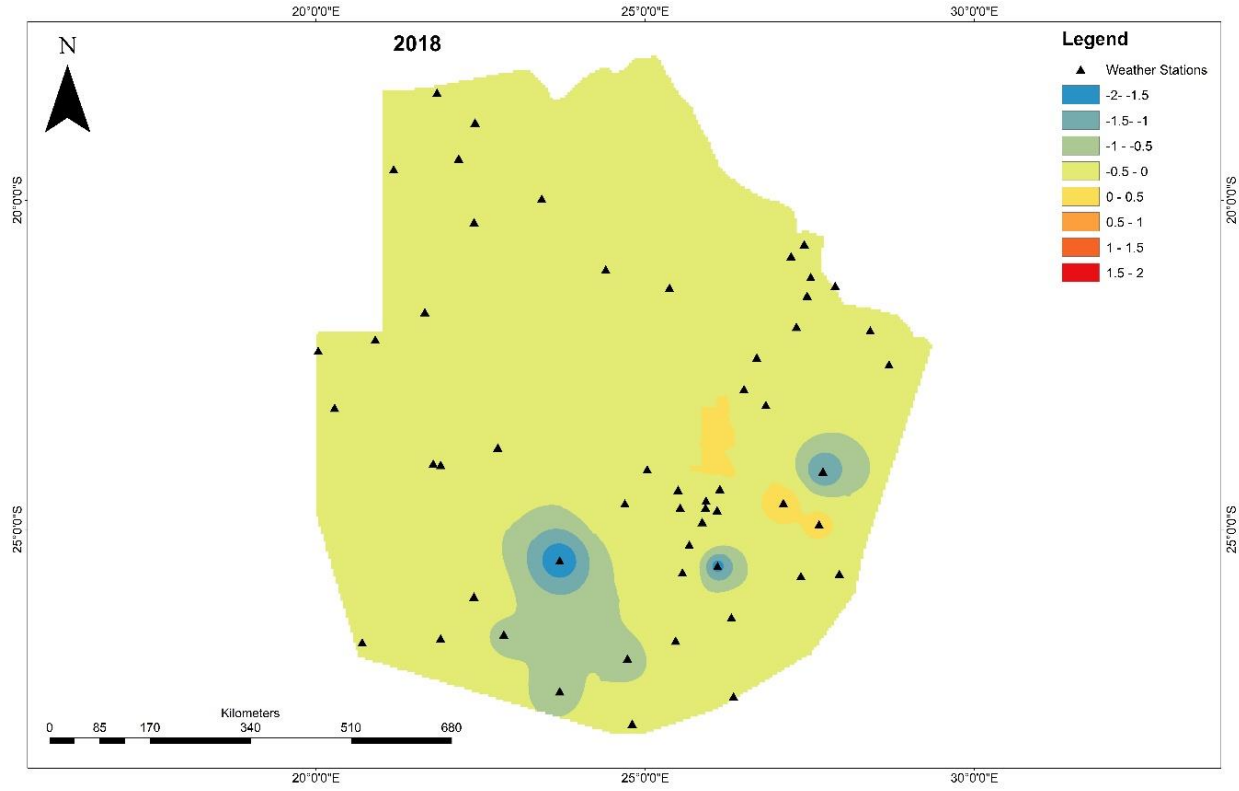

Figure 8.3aw: IDW SPI 2018

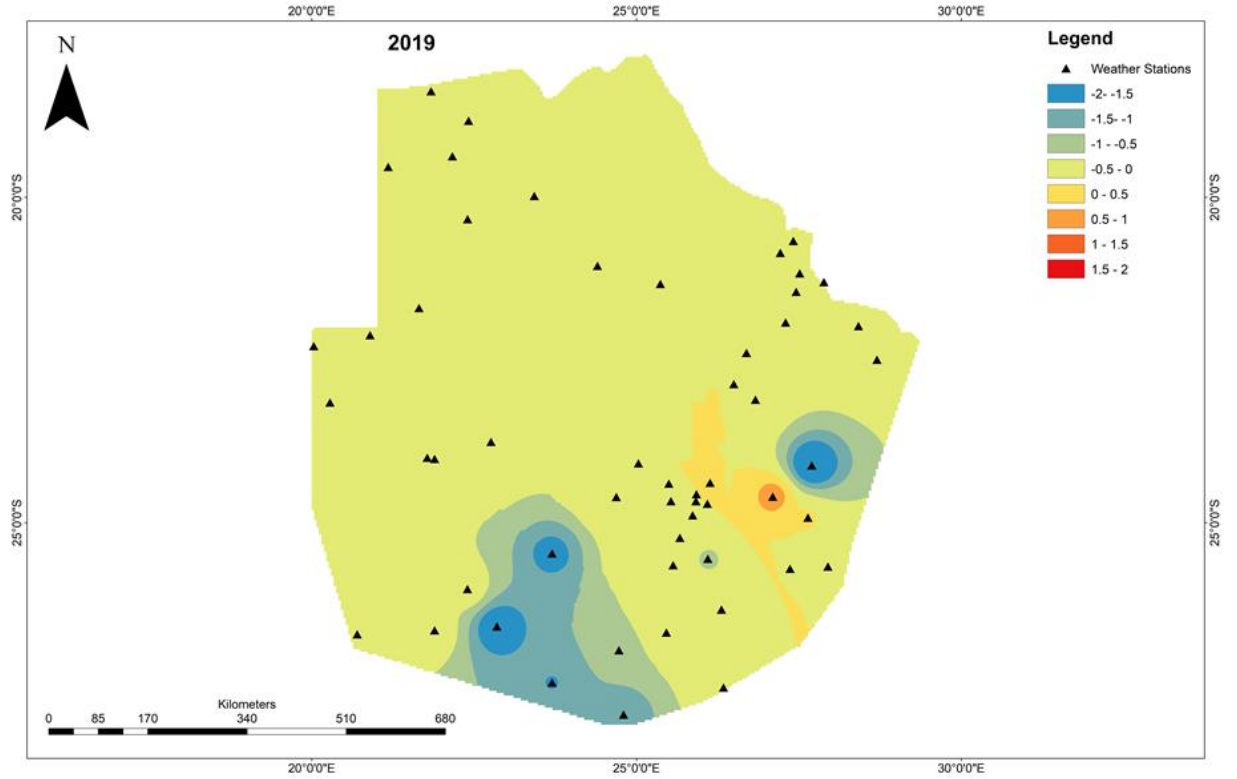

Figure 8.3ax: IDW SPI 2019

8.4. Ordinary Kriging

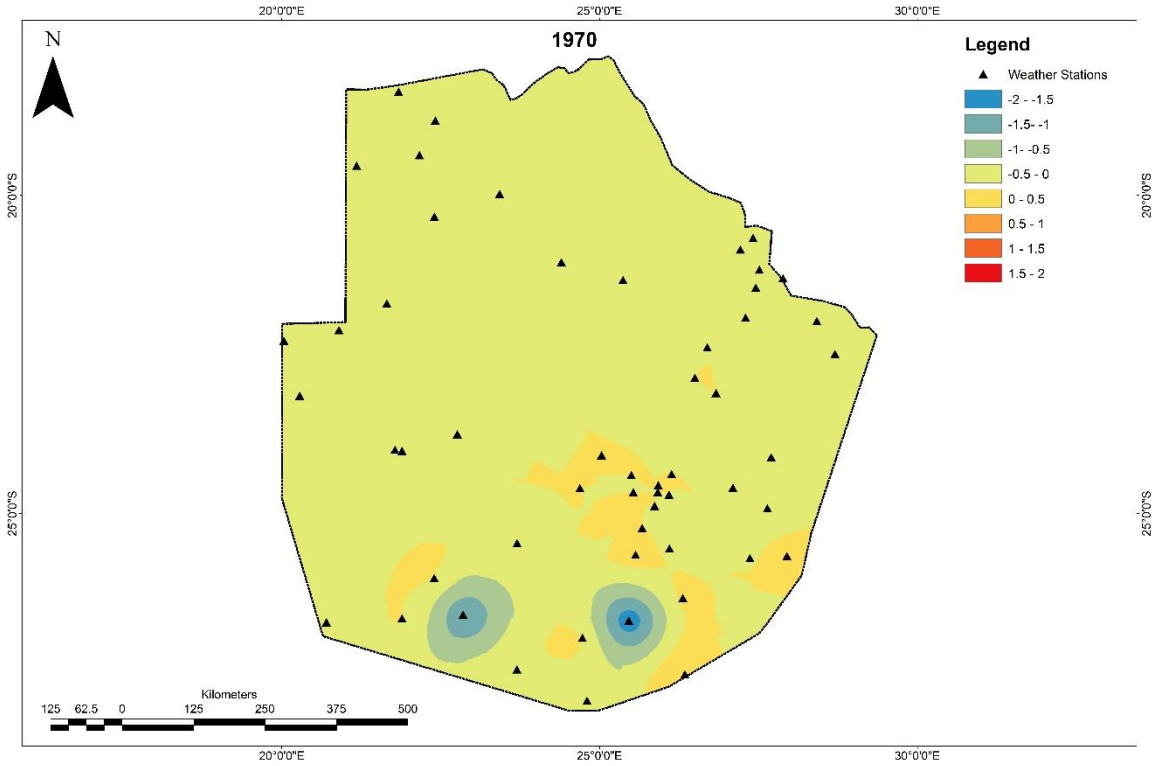

Figure 8.3a: OK SPI 1970

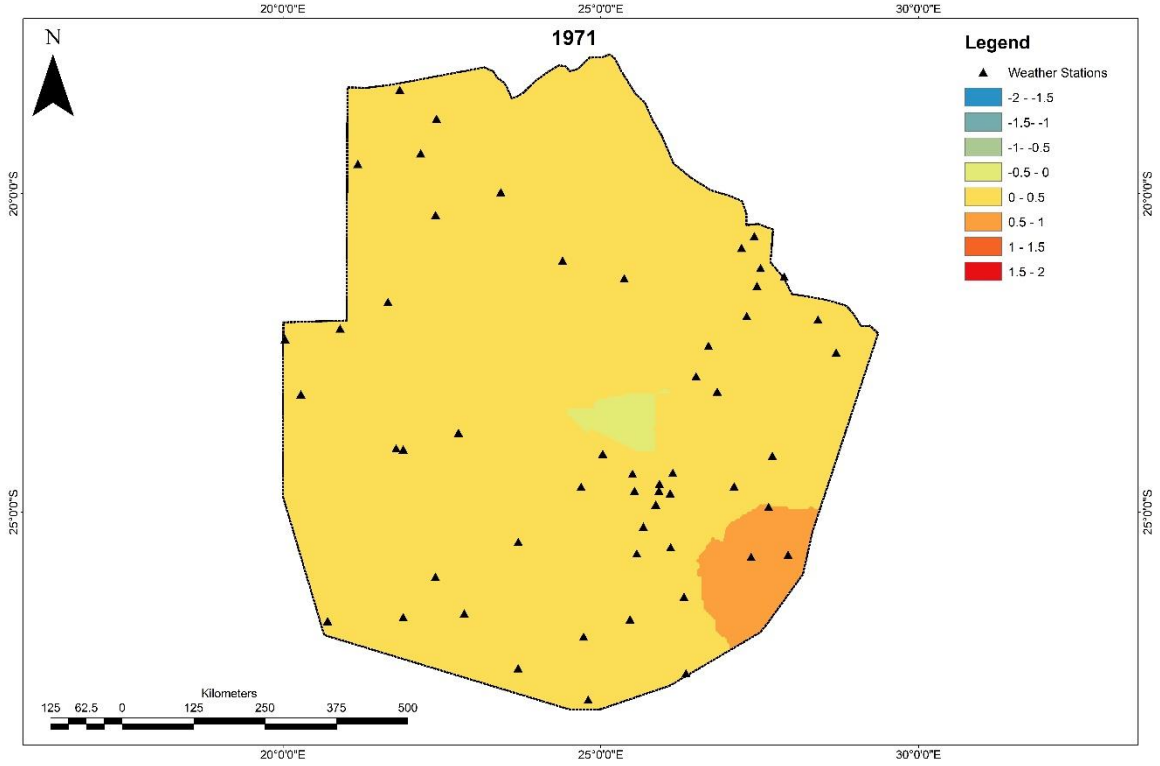

Figure 8.3b: OK SPI 1971

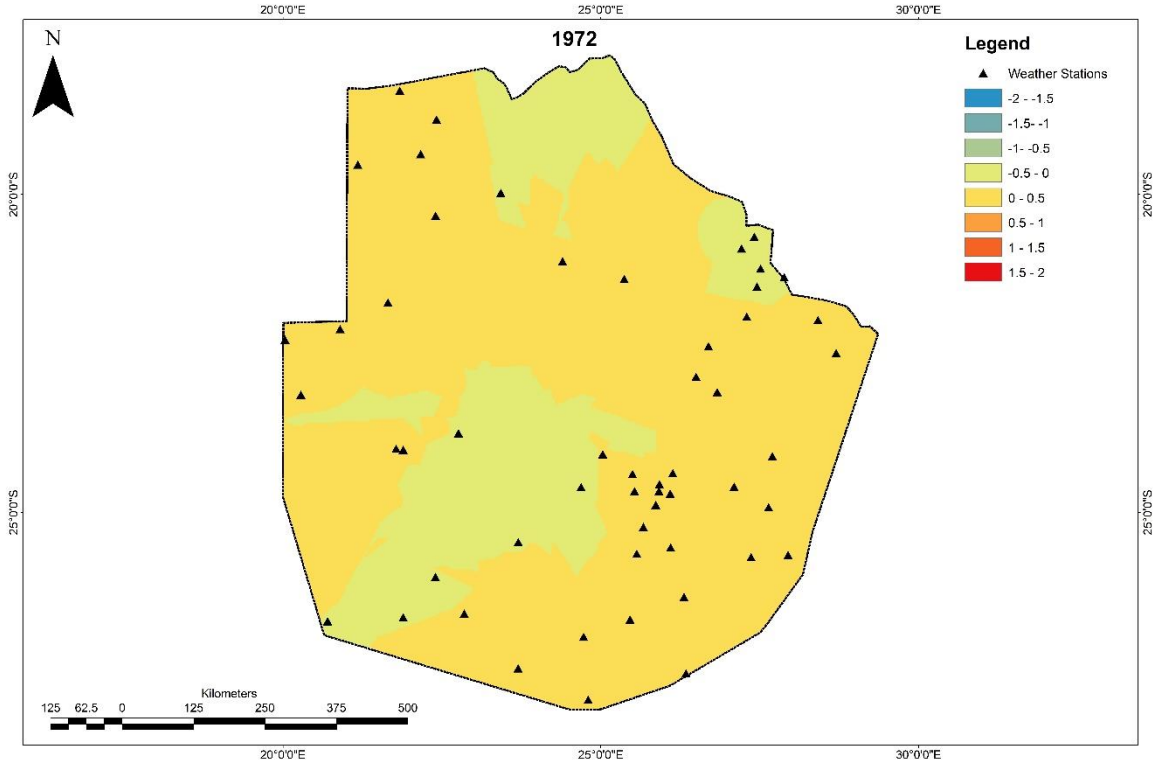

Figure 8.3c: OK SPI 1972

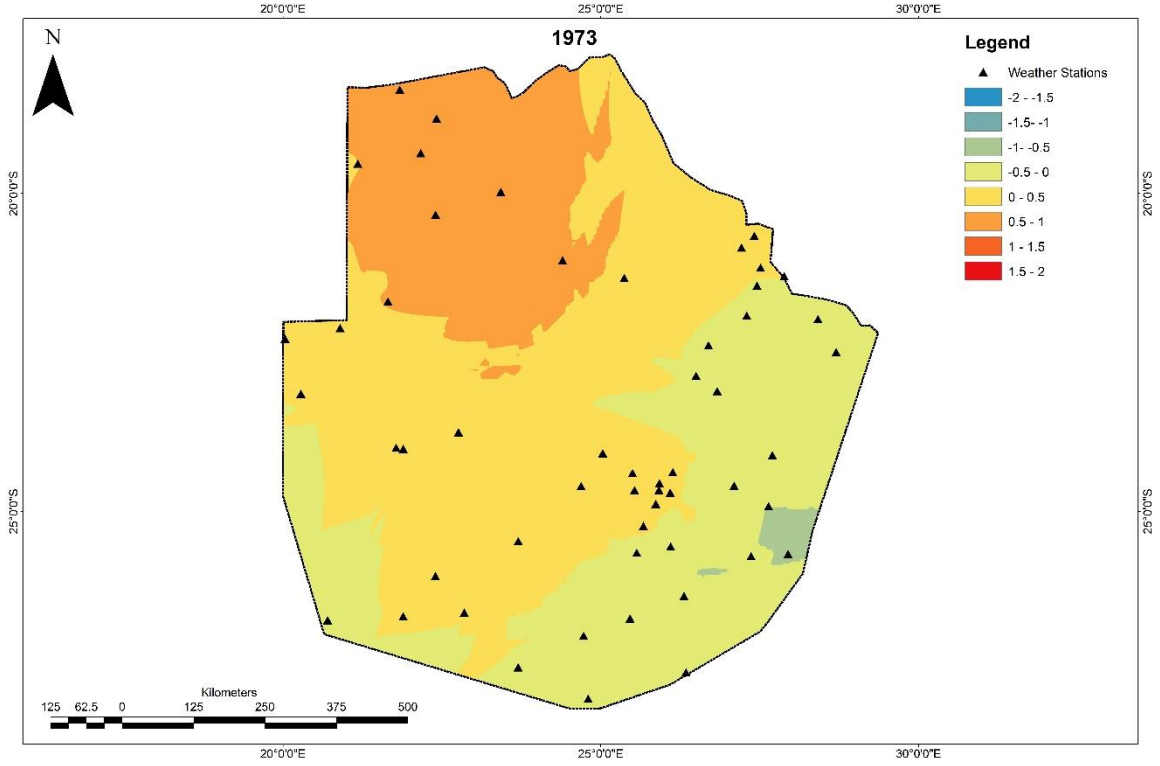

Figure 8.3d: OK SPI 1973

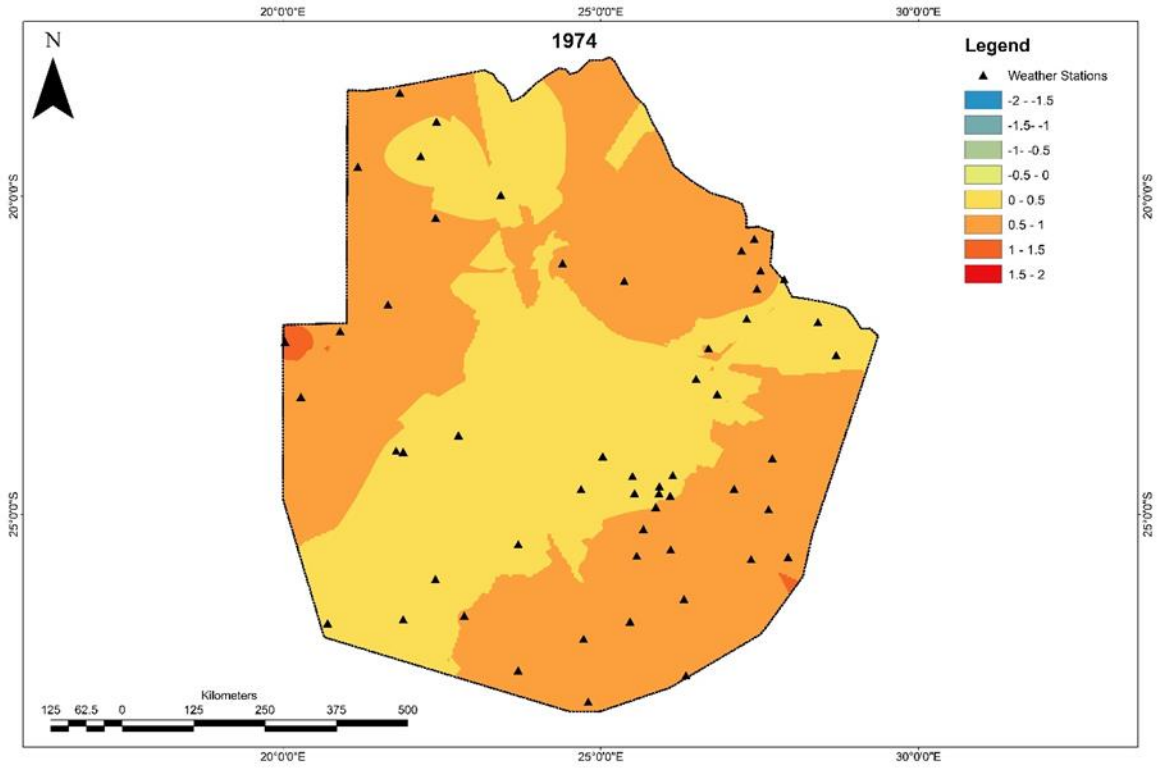

Figure 8.3e: OK SPI 1974

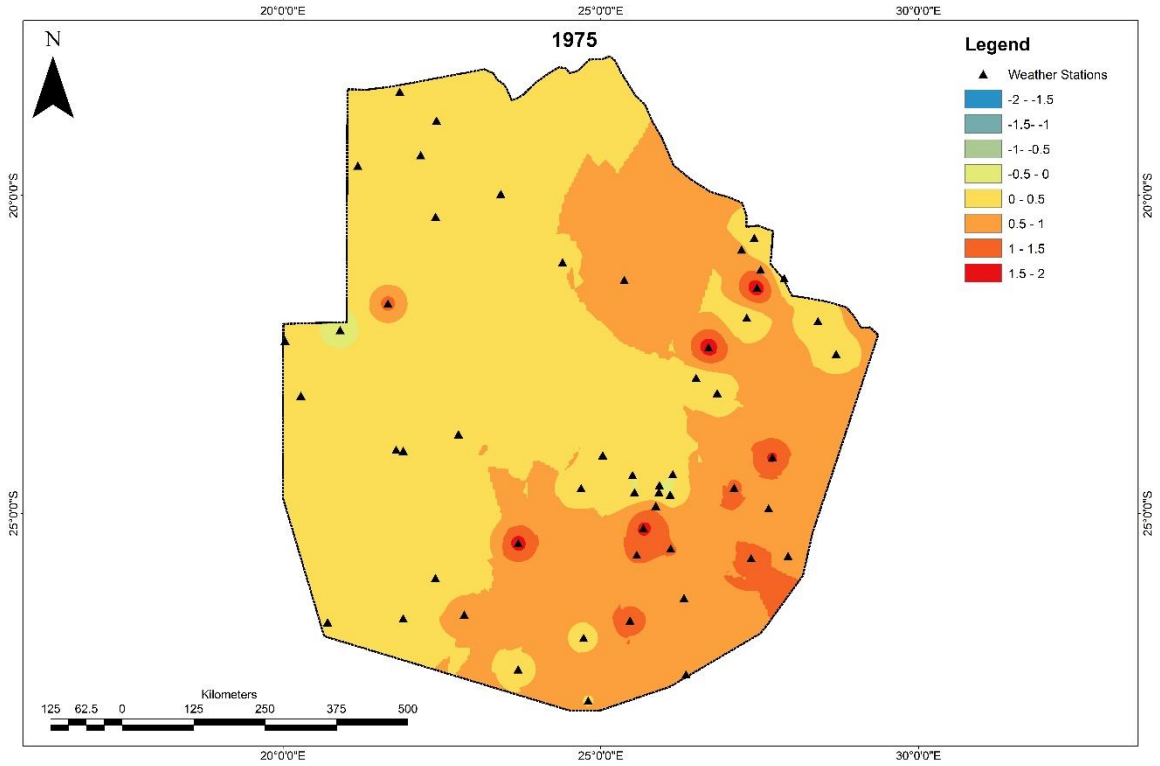

Figure 8.3f: OK SPI 1975

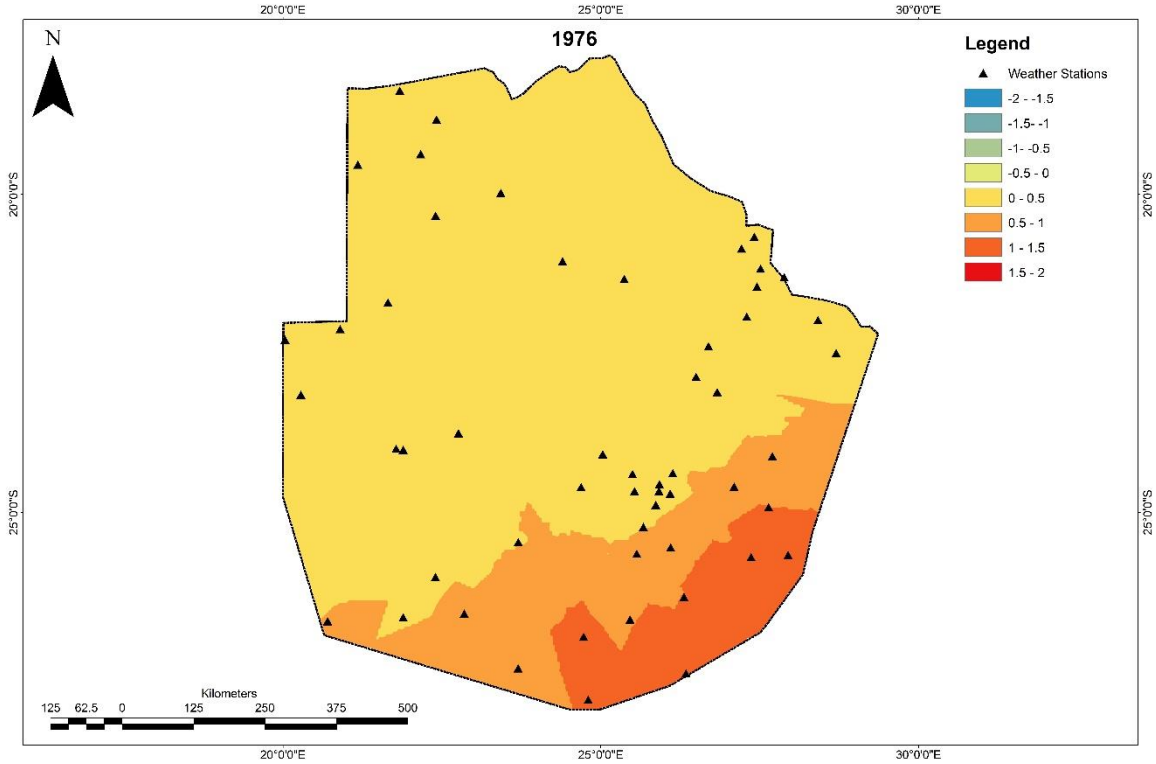

Figure 8.3g: OK SPI 1976

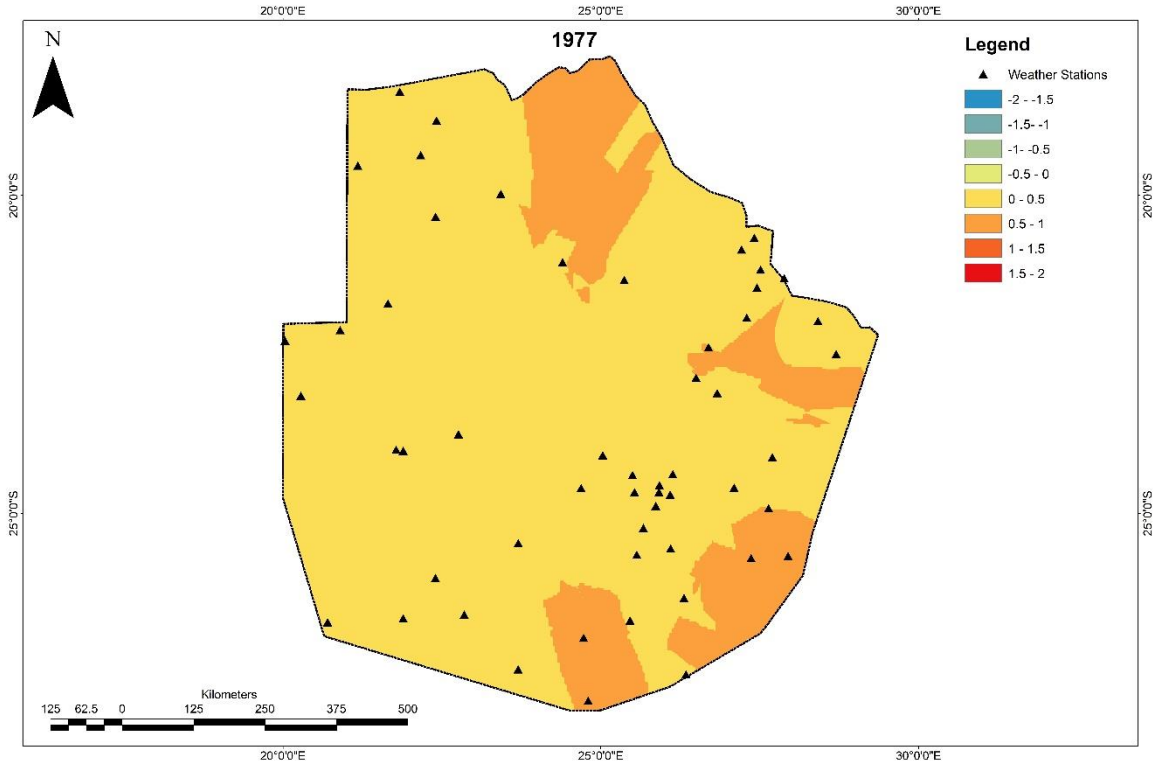

Figure 8.3h: OK SPI 1977

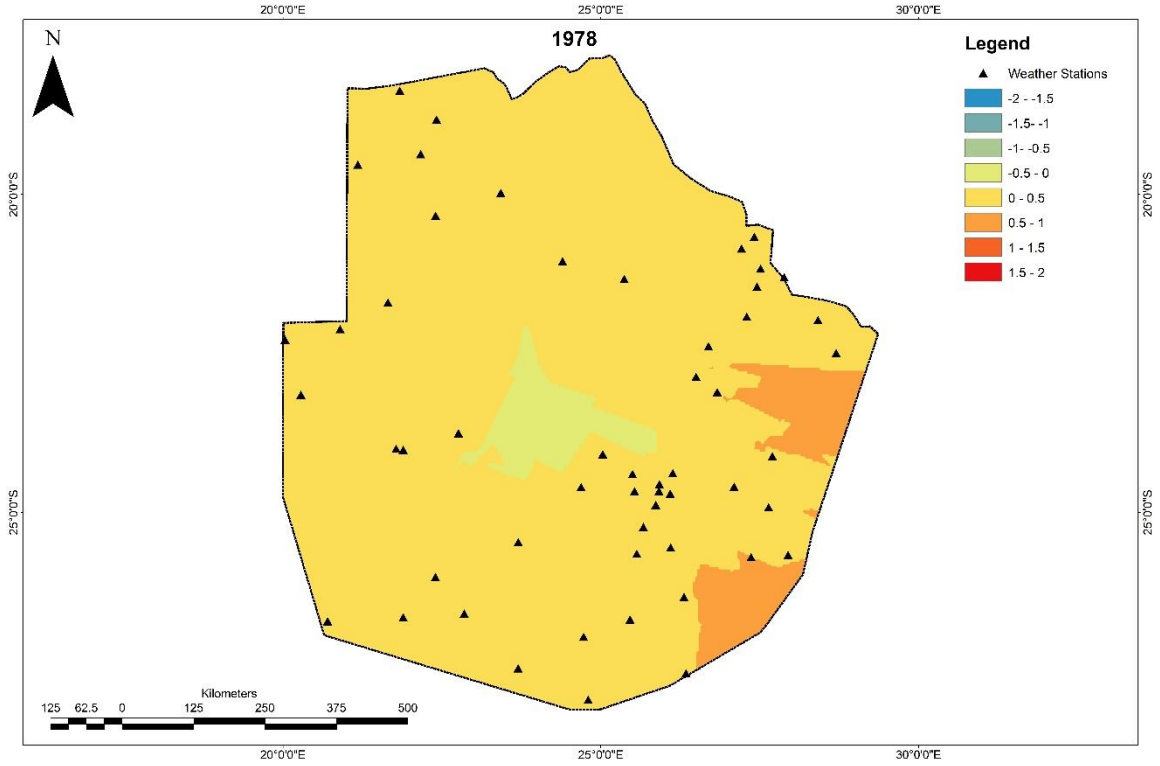

Figure 8.3i: OK SPI 1978

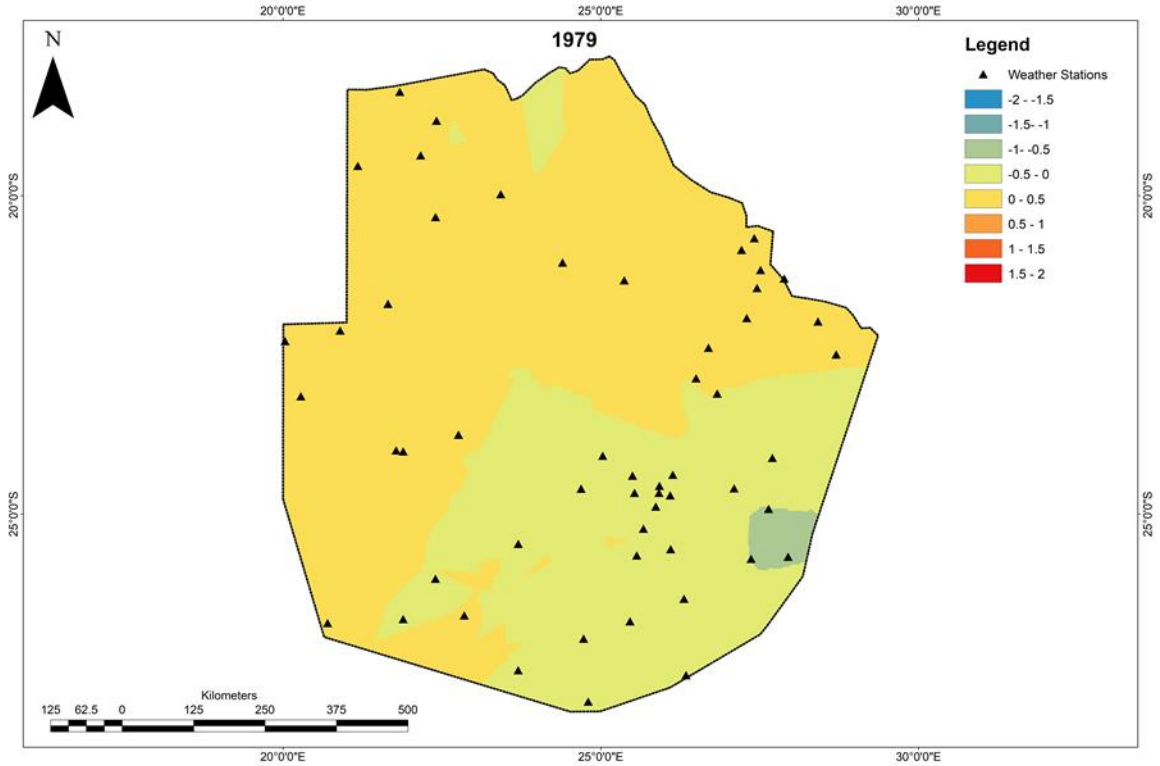

Figure 8.3j: OK SPI 1979

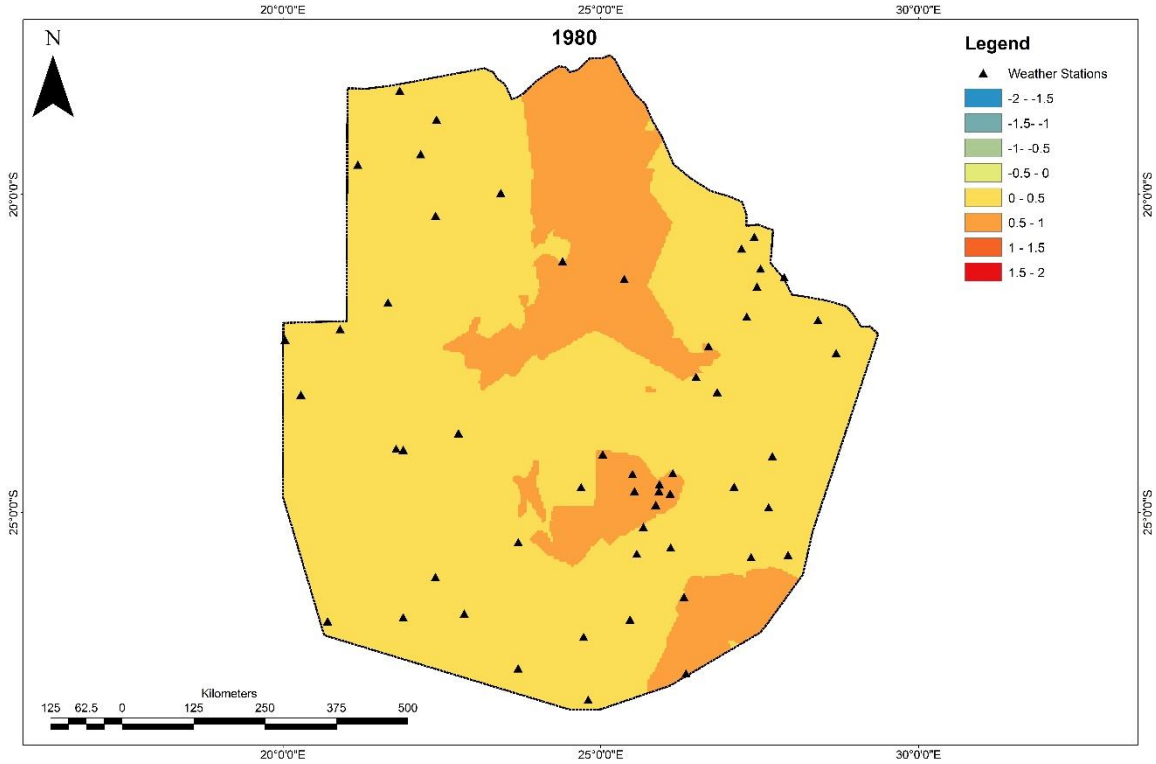

Figure 8.3k: OK SPI 1980

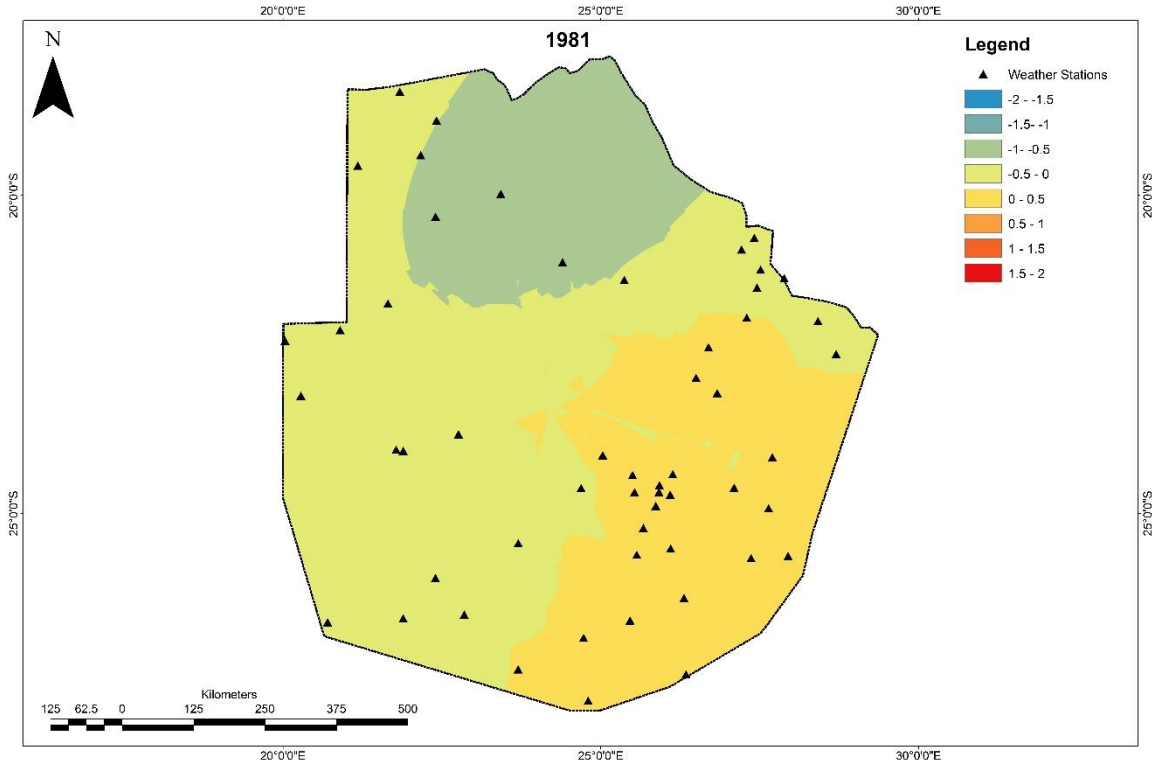

Figure 8.3l: OK SPI 1981

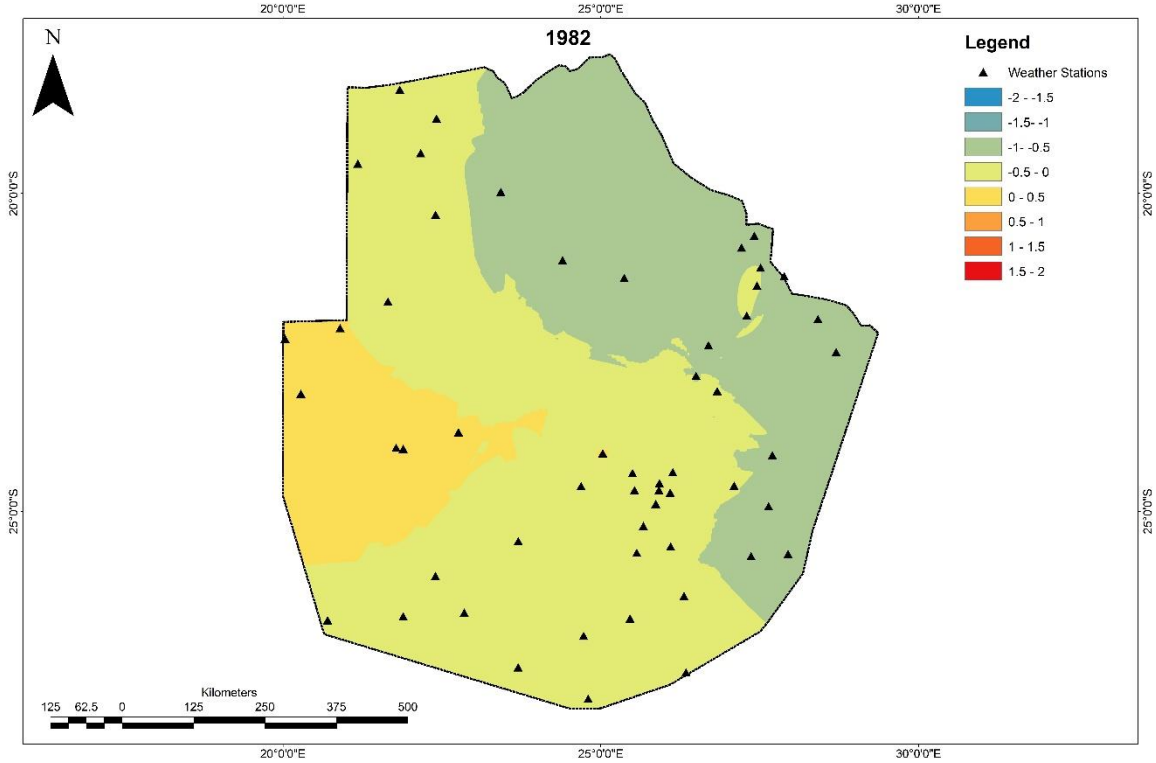

Figure 8.3m: OK SPI 1982

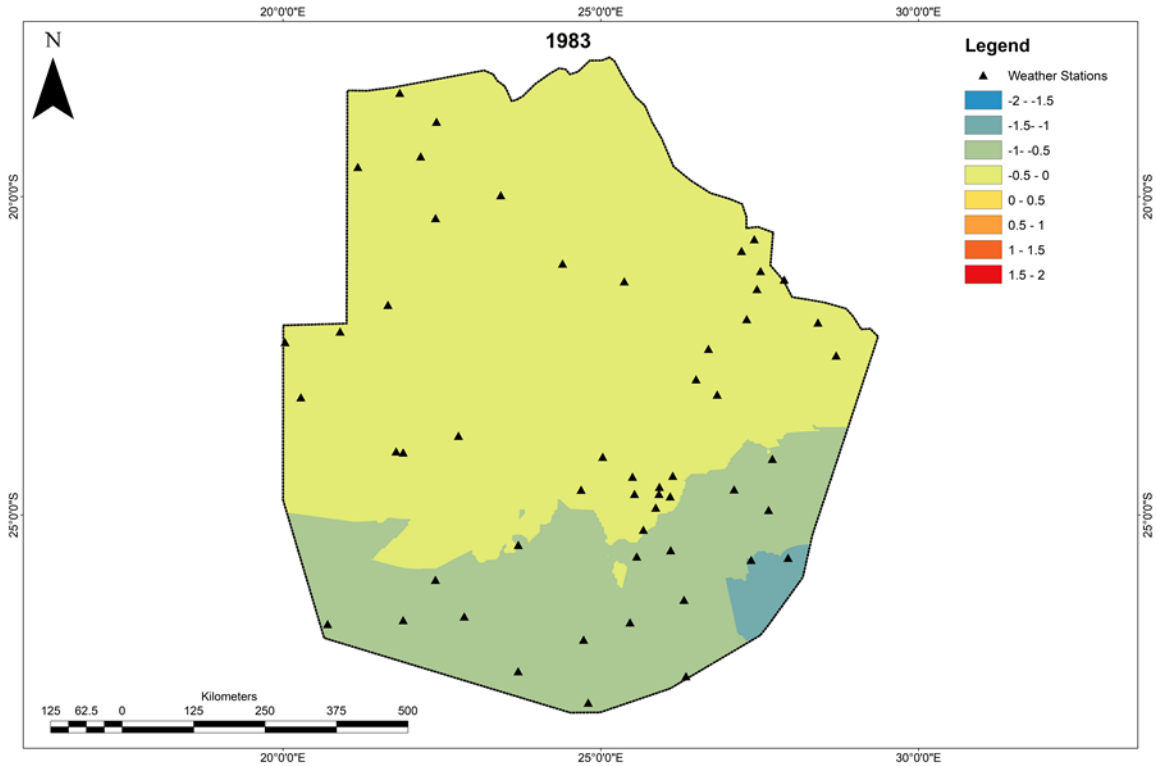

Figure 8.3n: OK SPI 1983

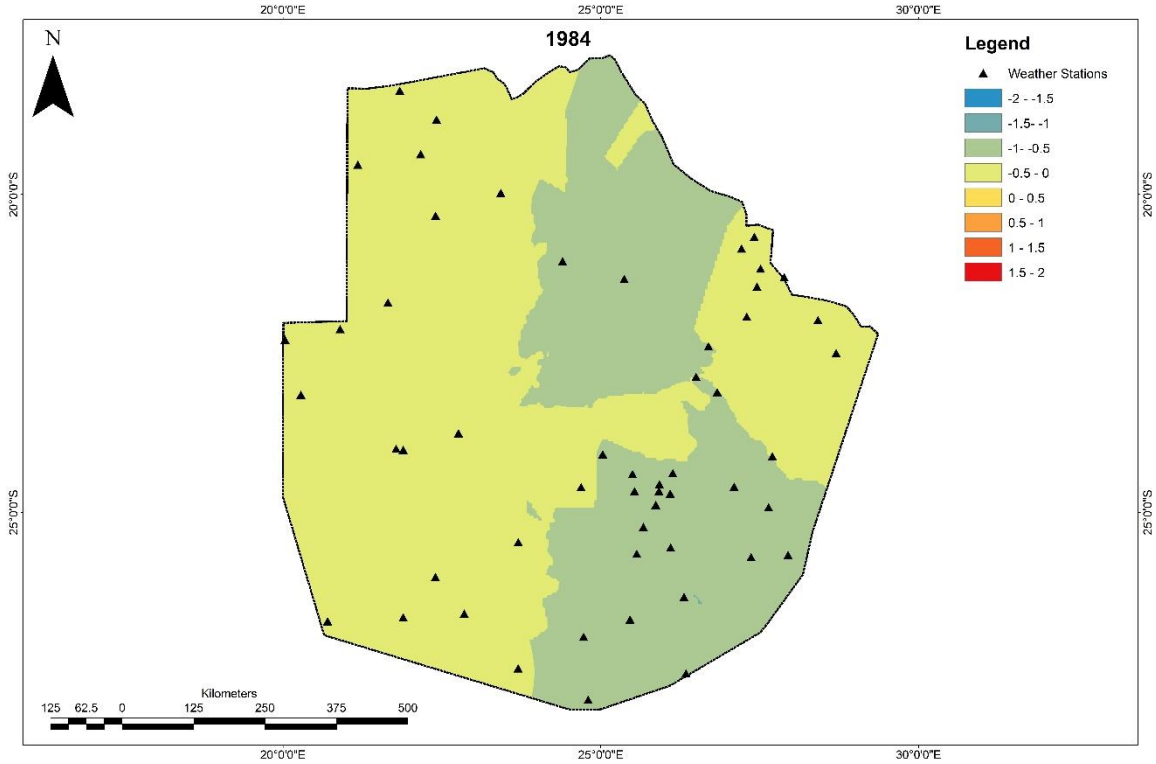

Figure 8.3o: OK SPI 1984

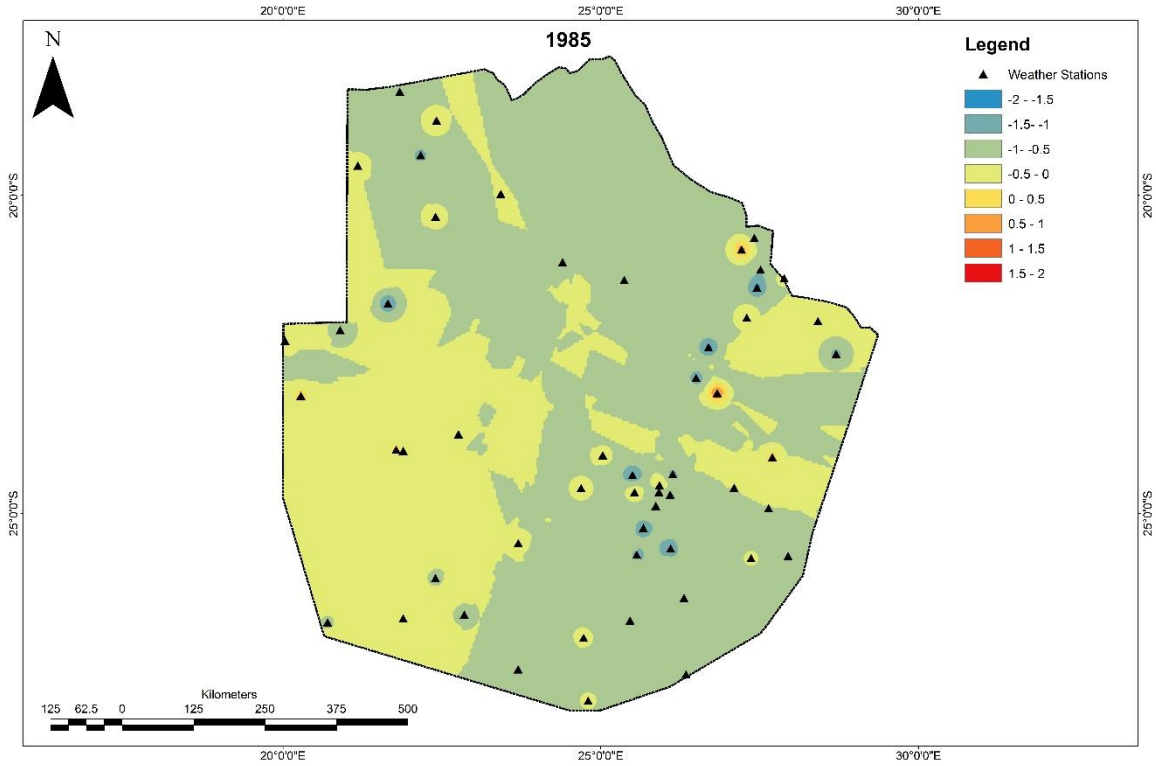

Figure 8.3p: OK SPI 1985

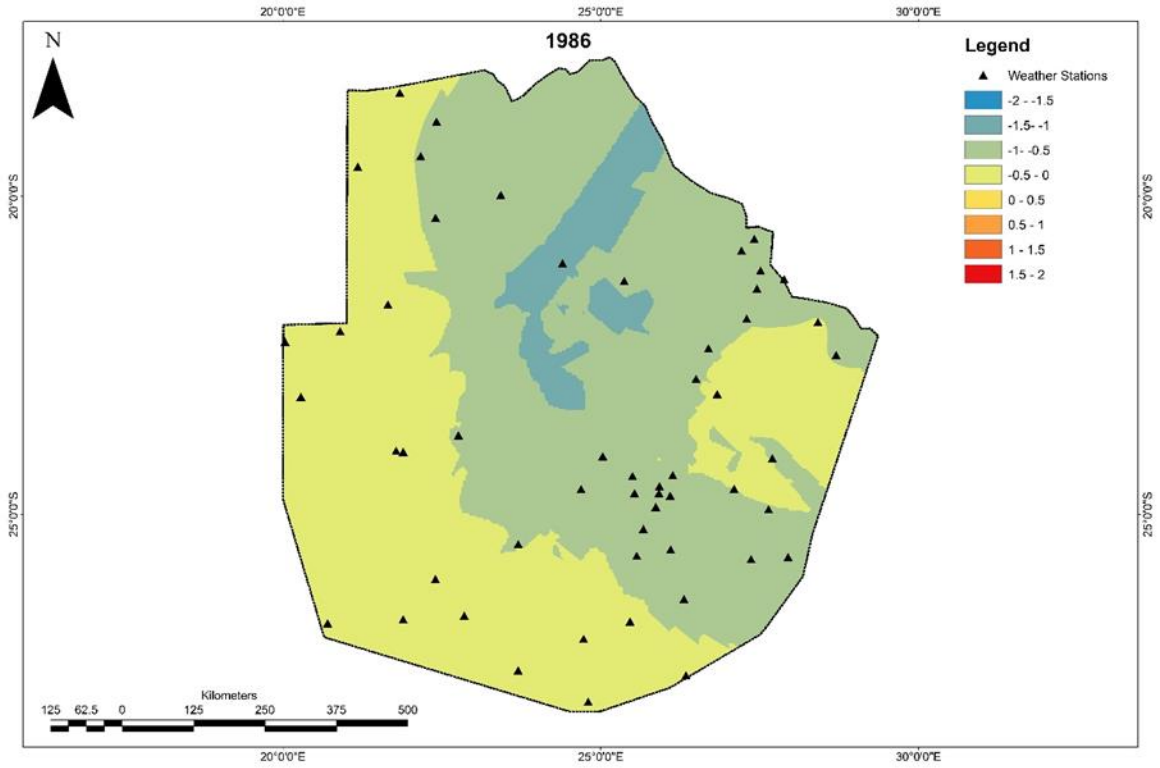

Figure 8.3q: OK SPI 1986

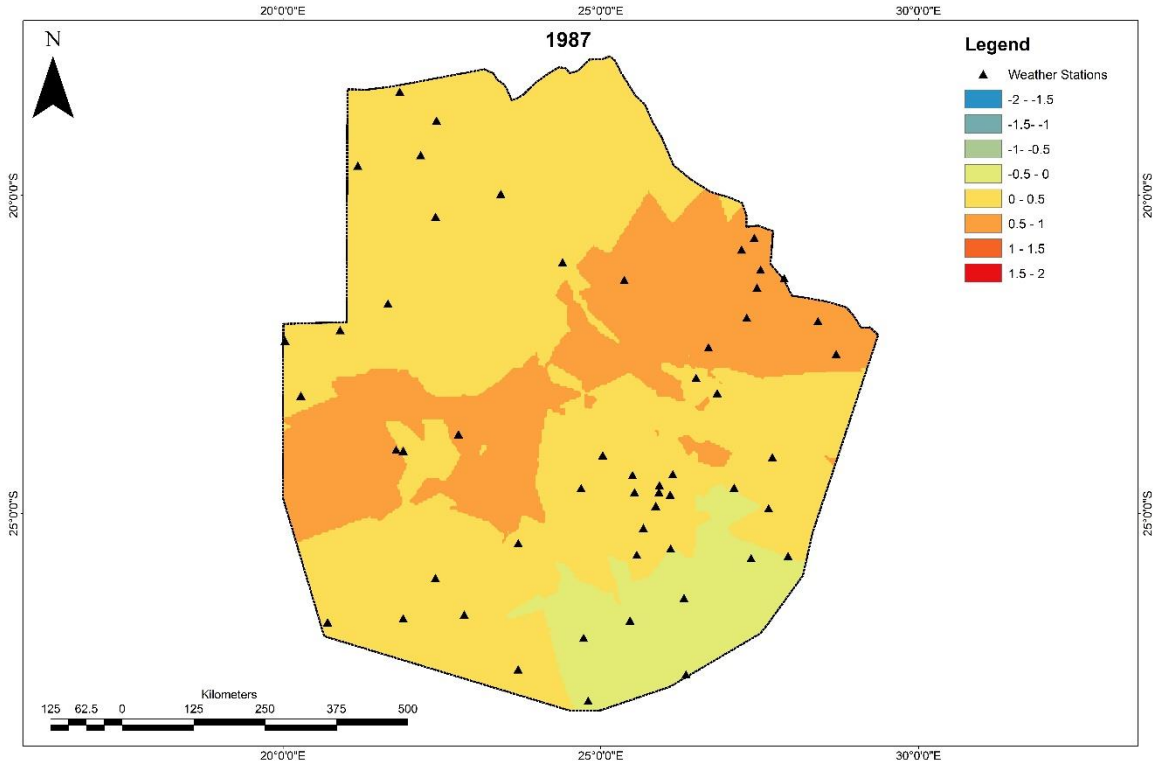

Figure 8.3r: OK SPI 1987

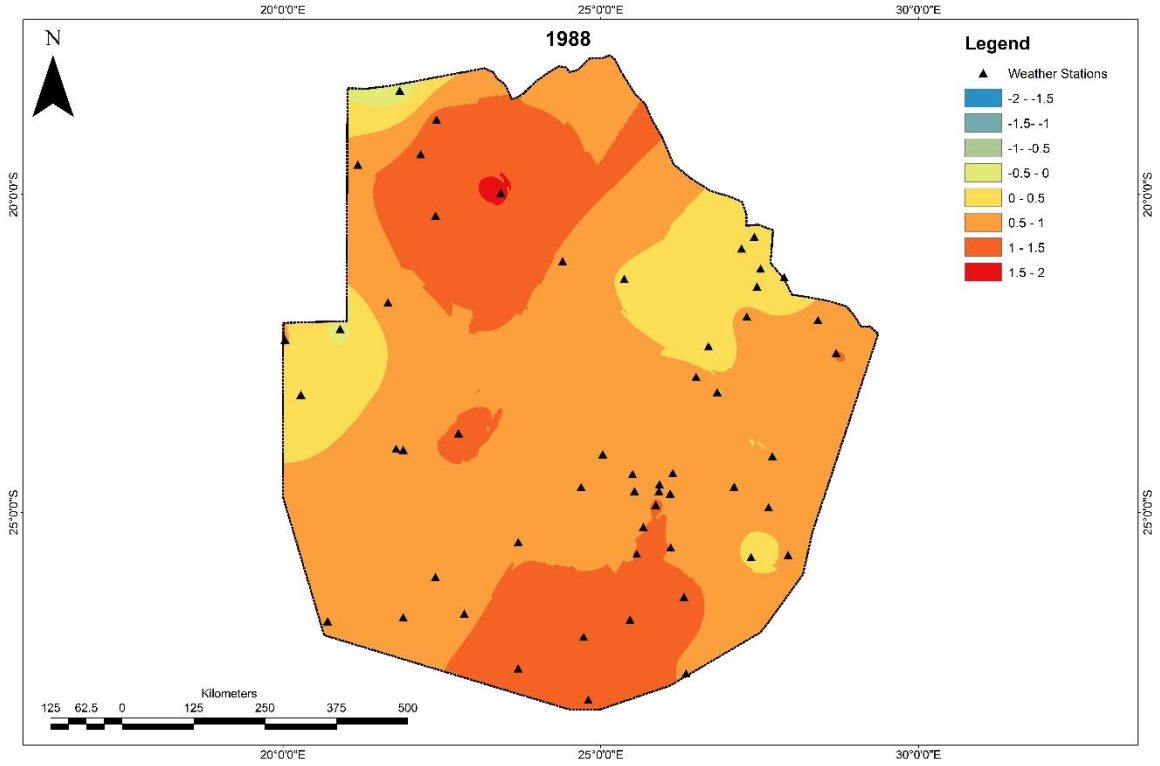

Figure 8.3s: OK SPI 1988

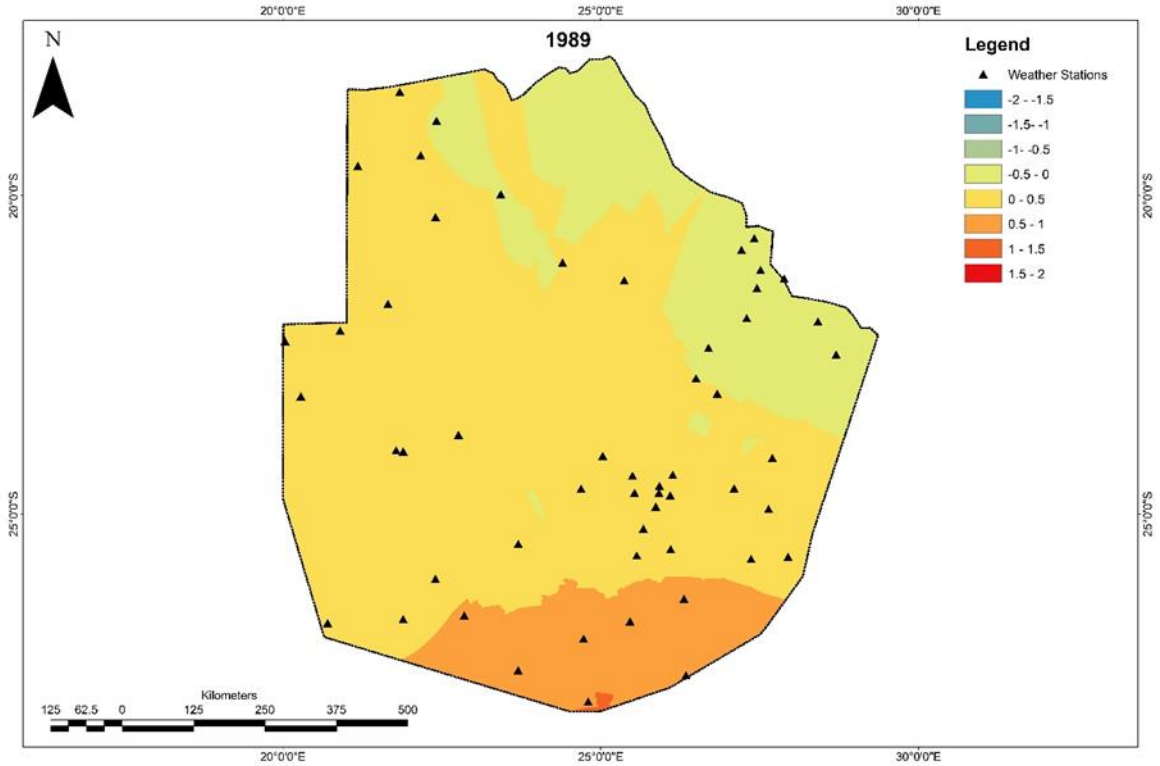

Figure 8.3t: OK SPI 1989

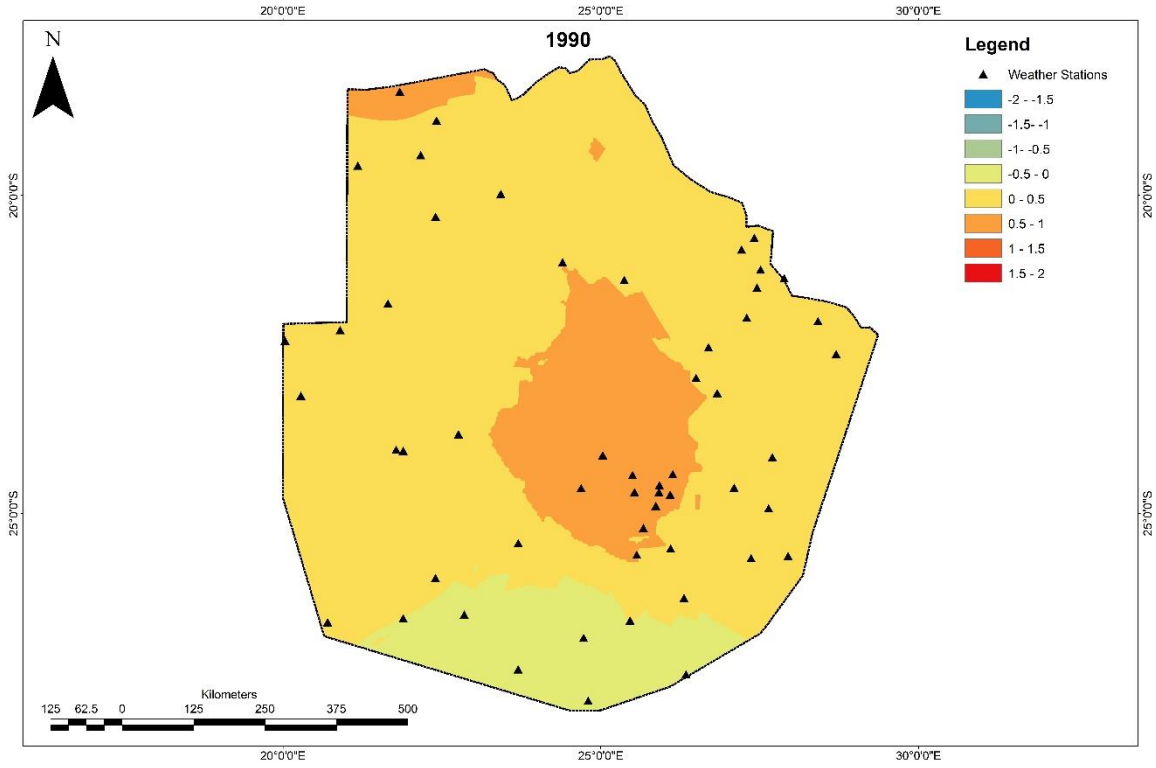

Figure 8.3u: OK SPI 1990

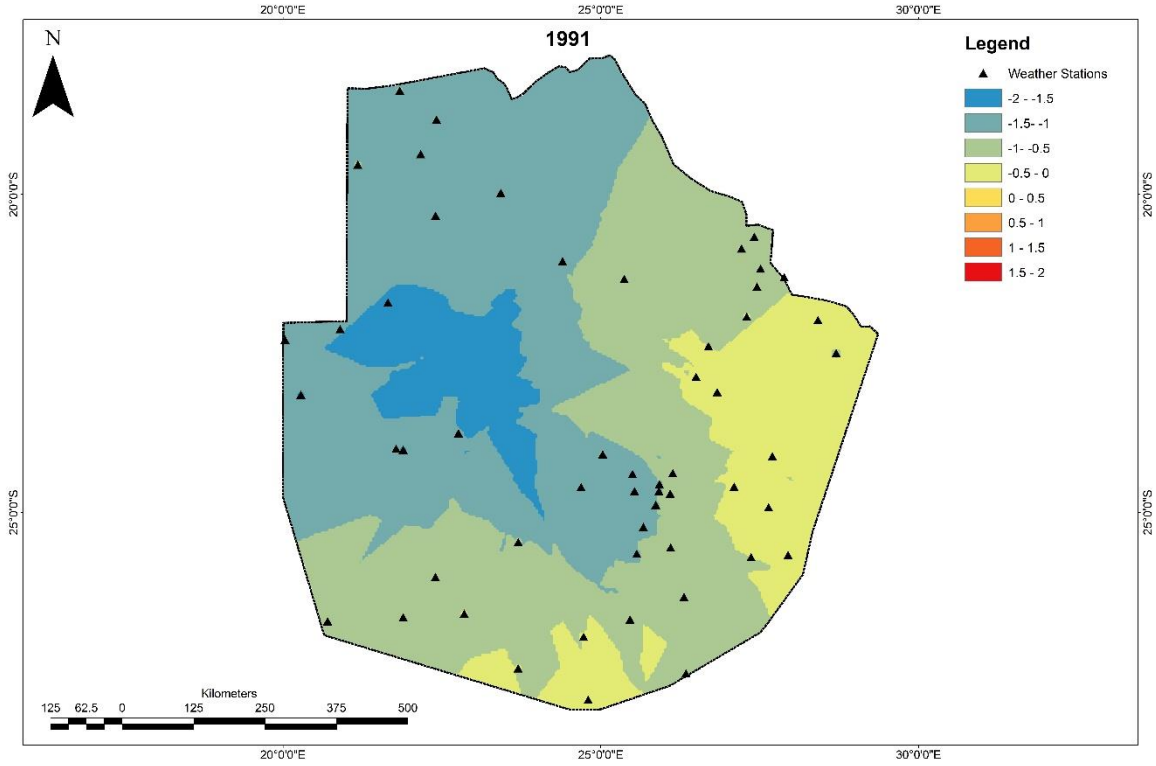

Figure 8.3v: OK SPI 1991

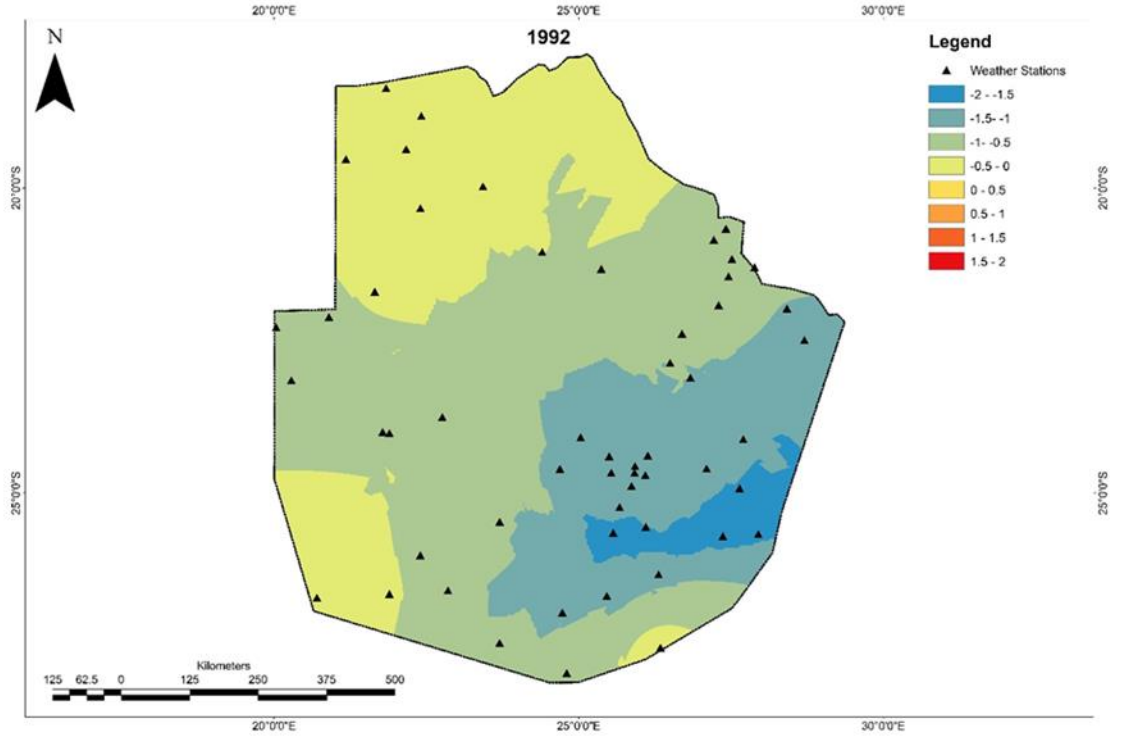

Figure 8.3w: OK SPI 1992

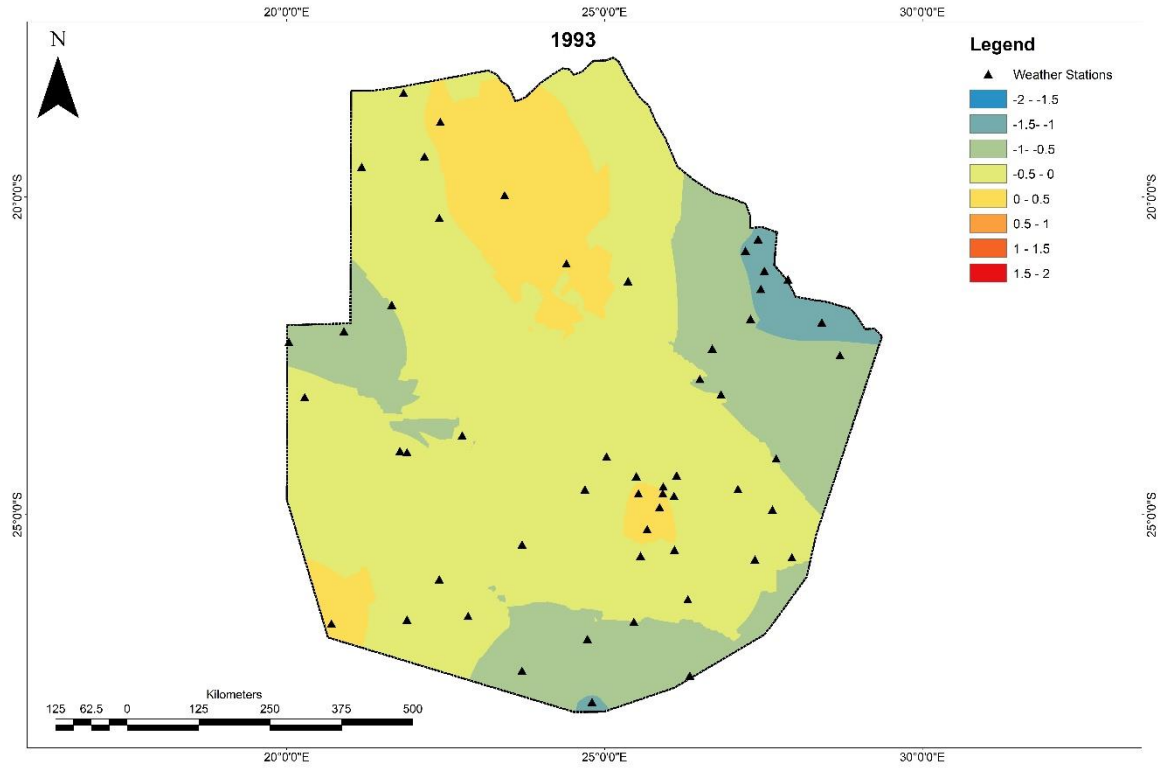

Figure 8.3x: OK SPI 1993

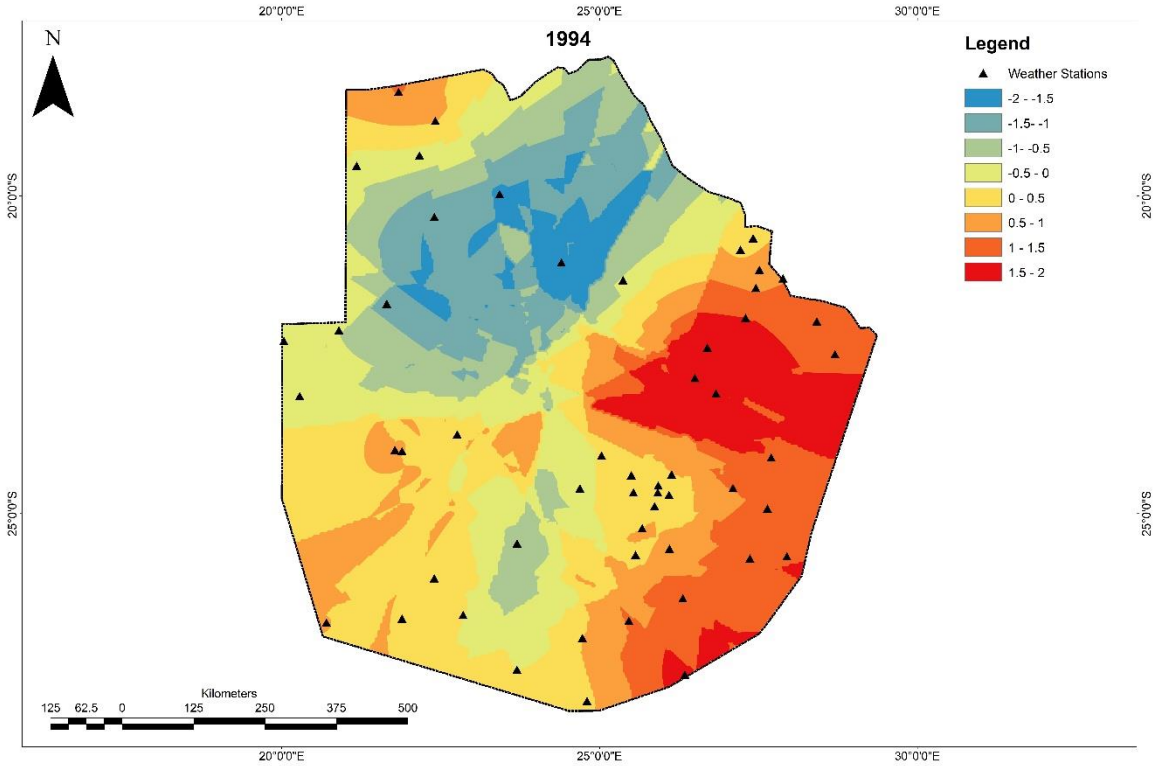

Figure 8.3y: OK SPI 1994

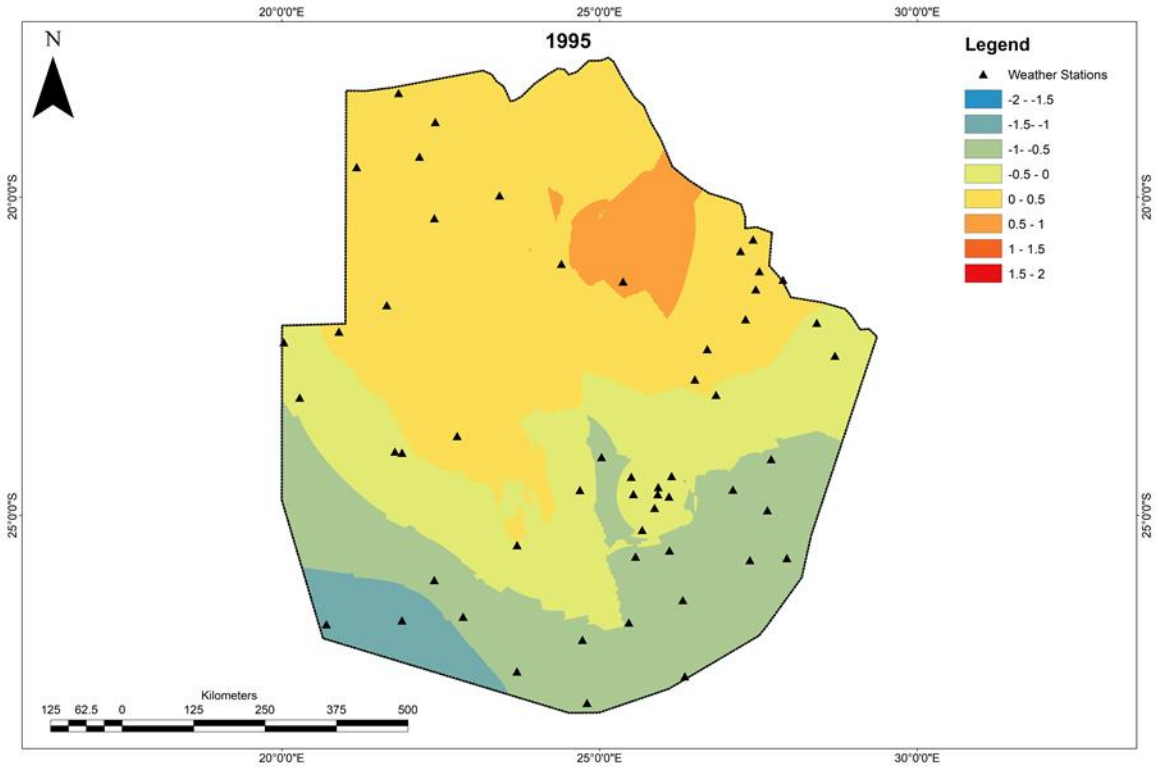

Figure 8.3z: OK SPI 1995

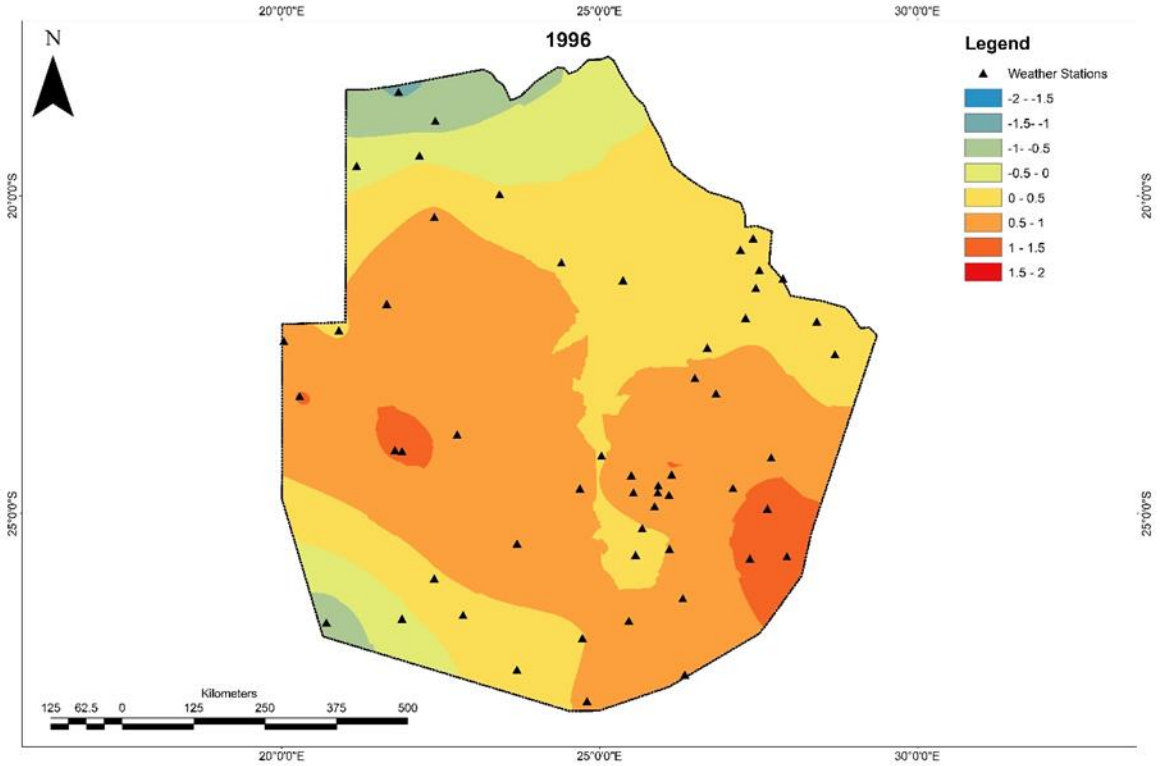

Figure 8.3aa: OK SPI 1996

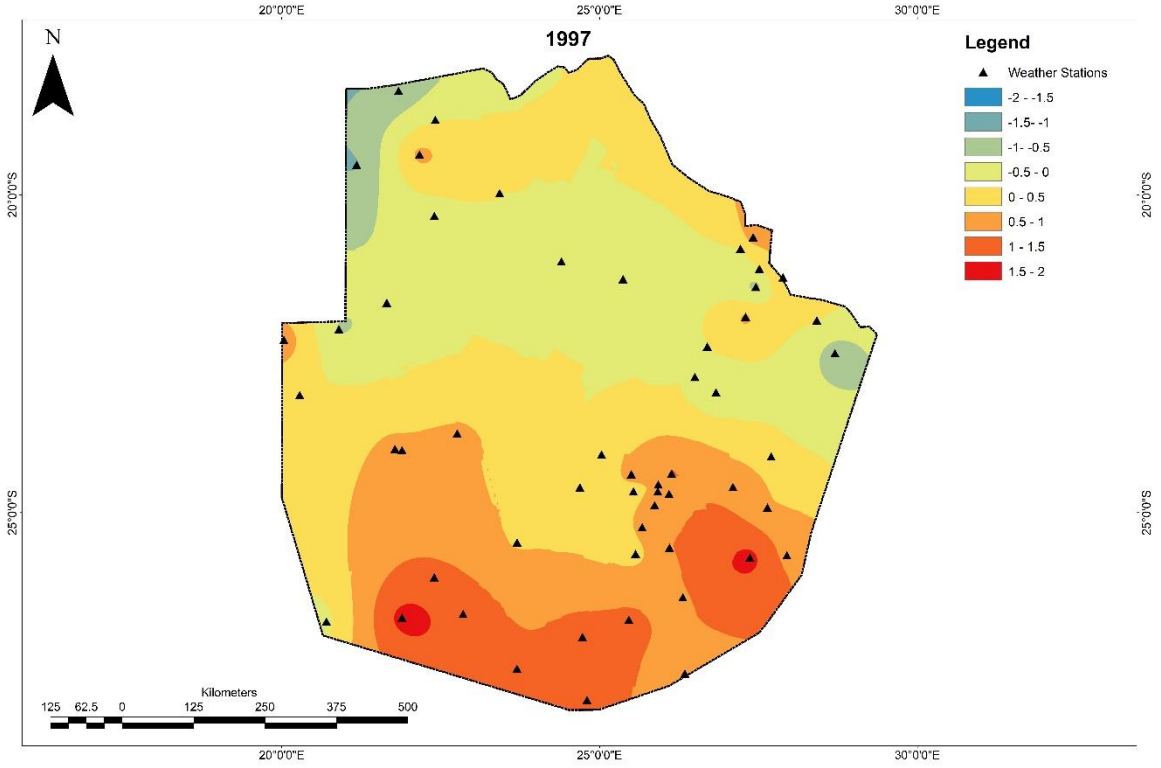

Figure 8.3ab: OK SPI 1997

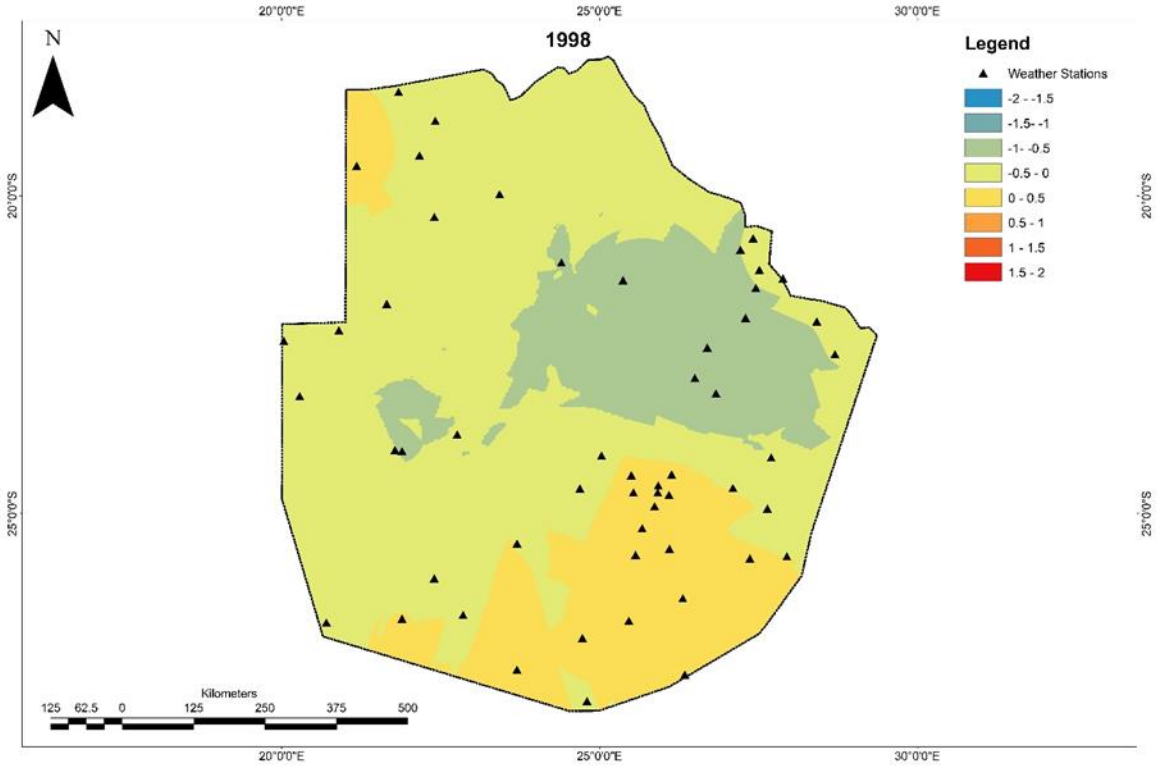

Figure 8.3ac: OK SPI 1998

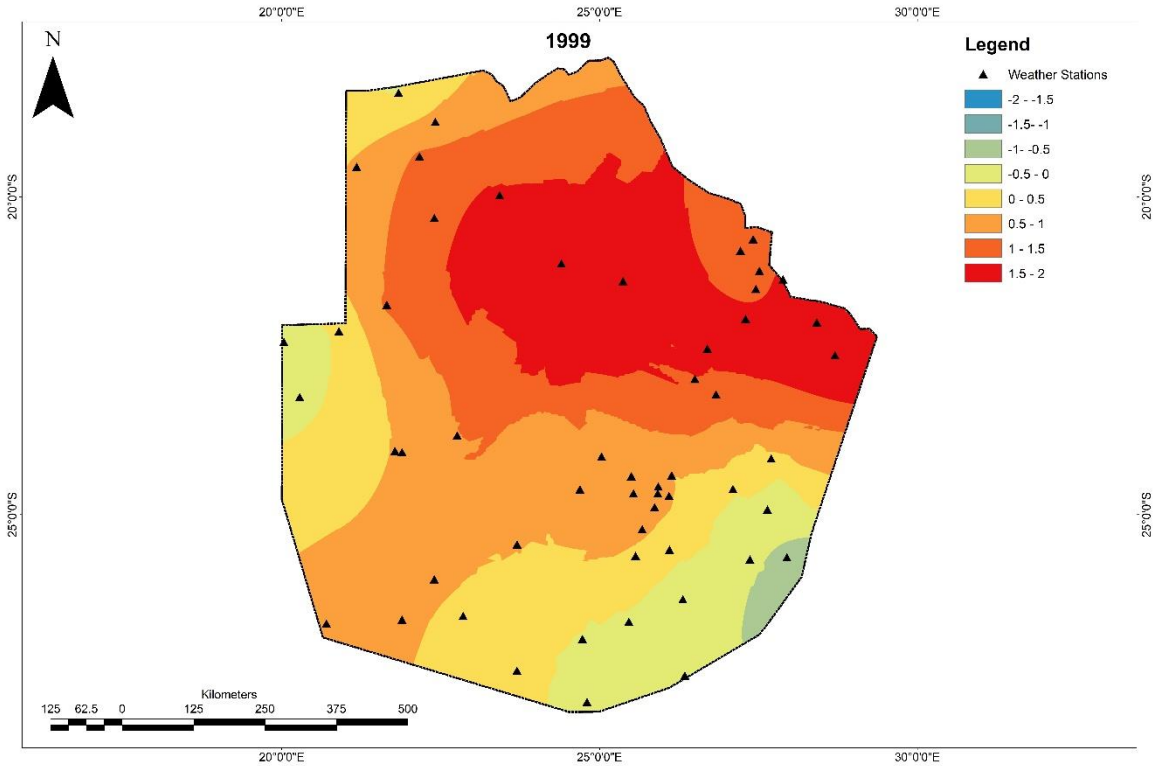

Figure 8.3ad: OK SPI 1999

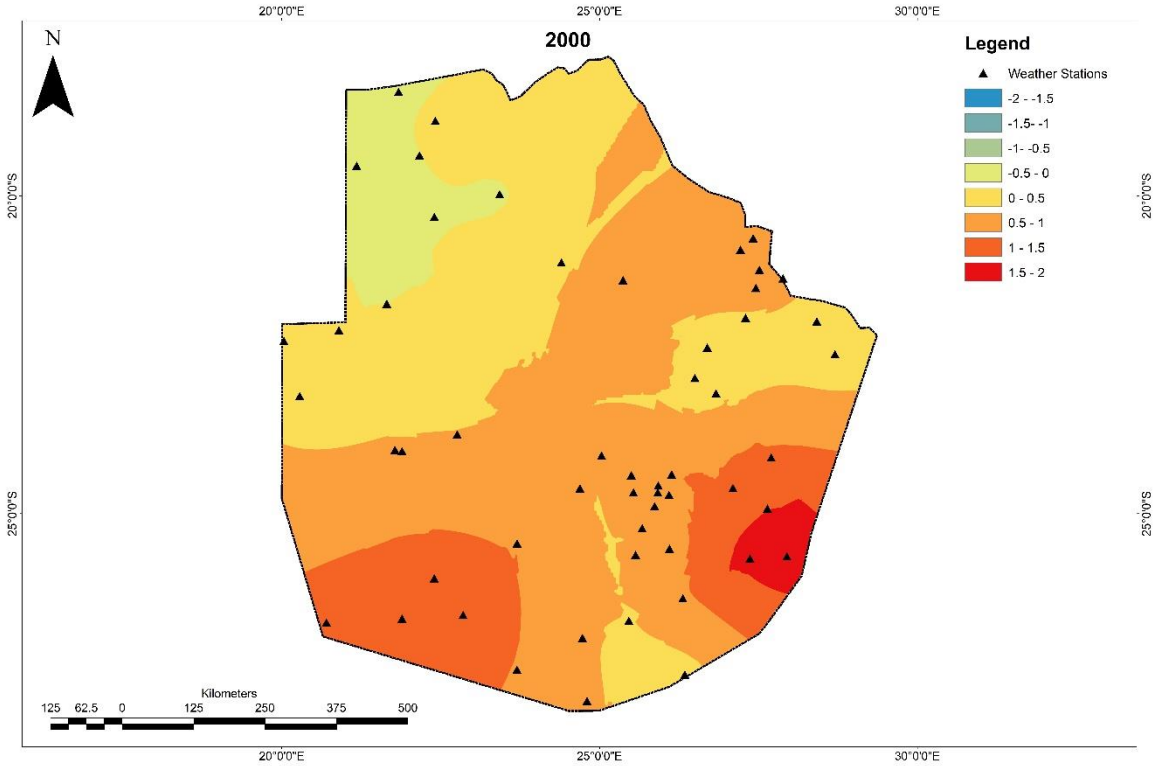

Figure 8.3ae: OK SPI 2000

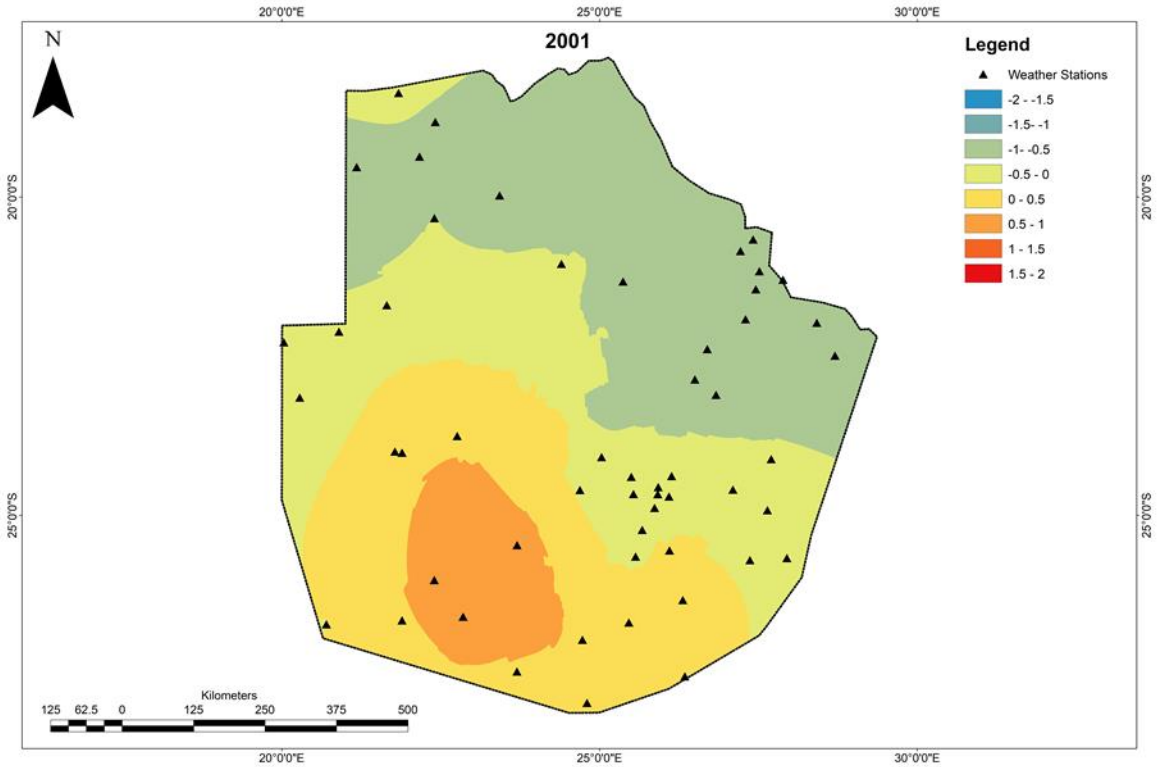

Figure 8.3af: OK SPI 2001

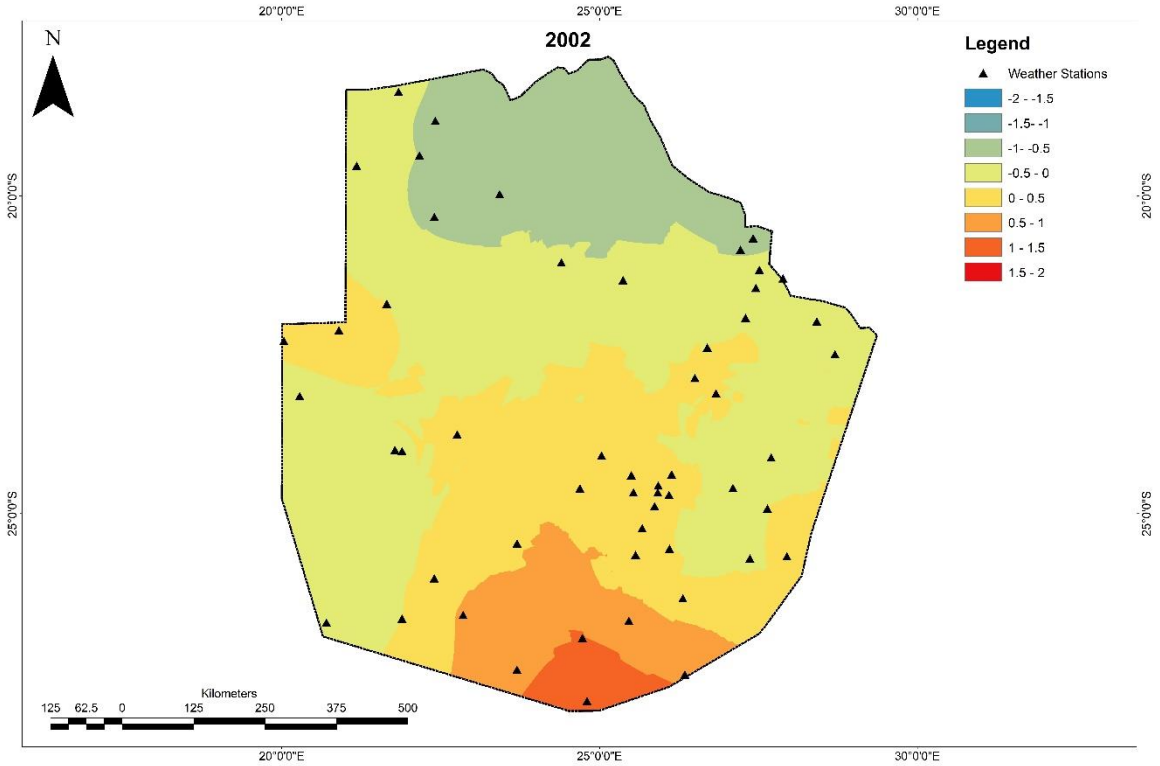

Figure 8.3ag: OK SPI 2002

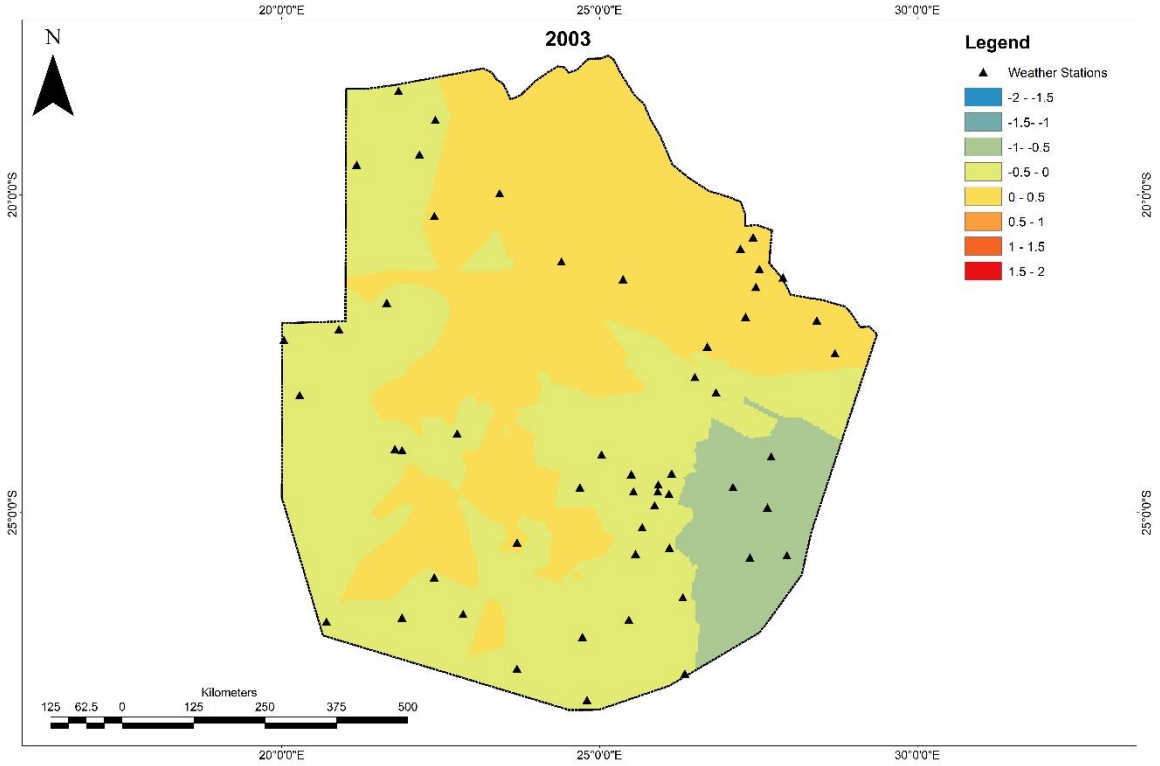

Figure 8.3ah: OK SPI 2003

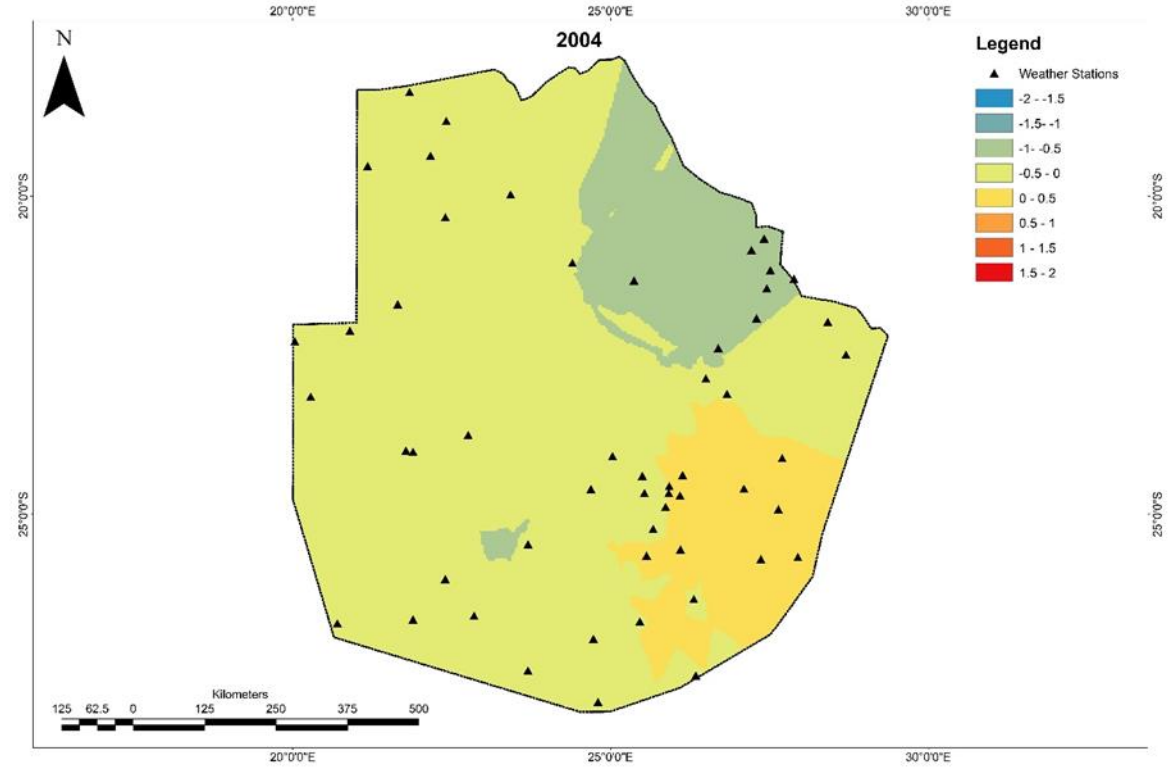

Figure 8.3ai: OK SPI 2004

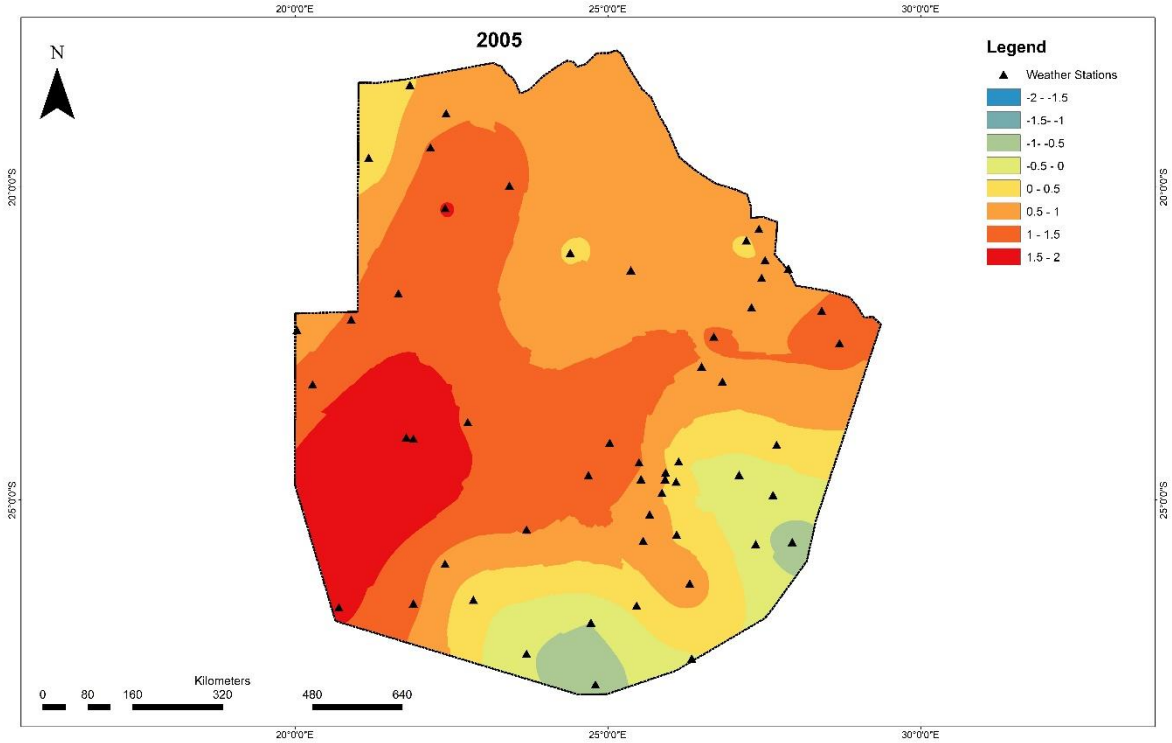

Figure 8.3aj: OK SPI 2005

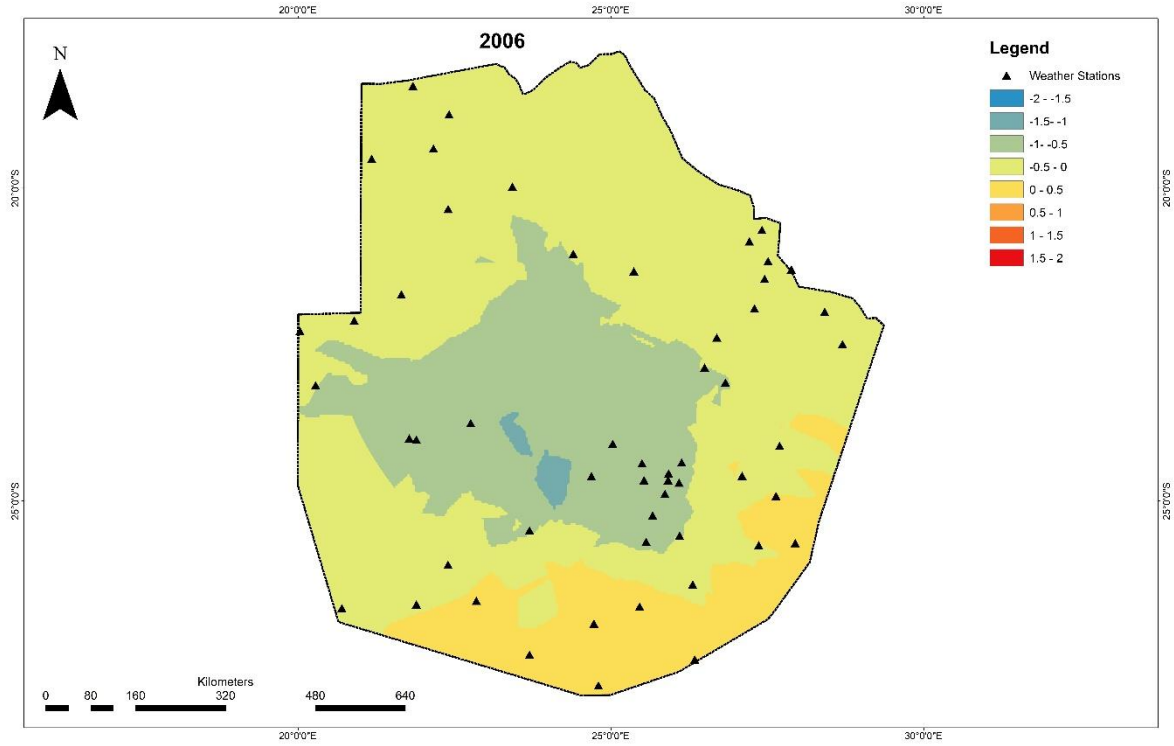

Figure 8.3ak: OK SPI 2006

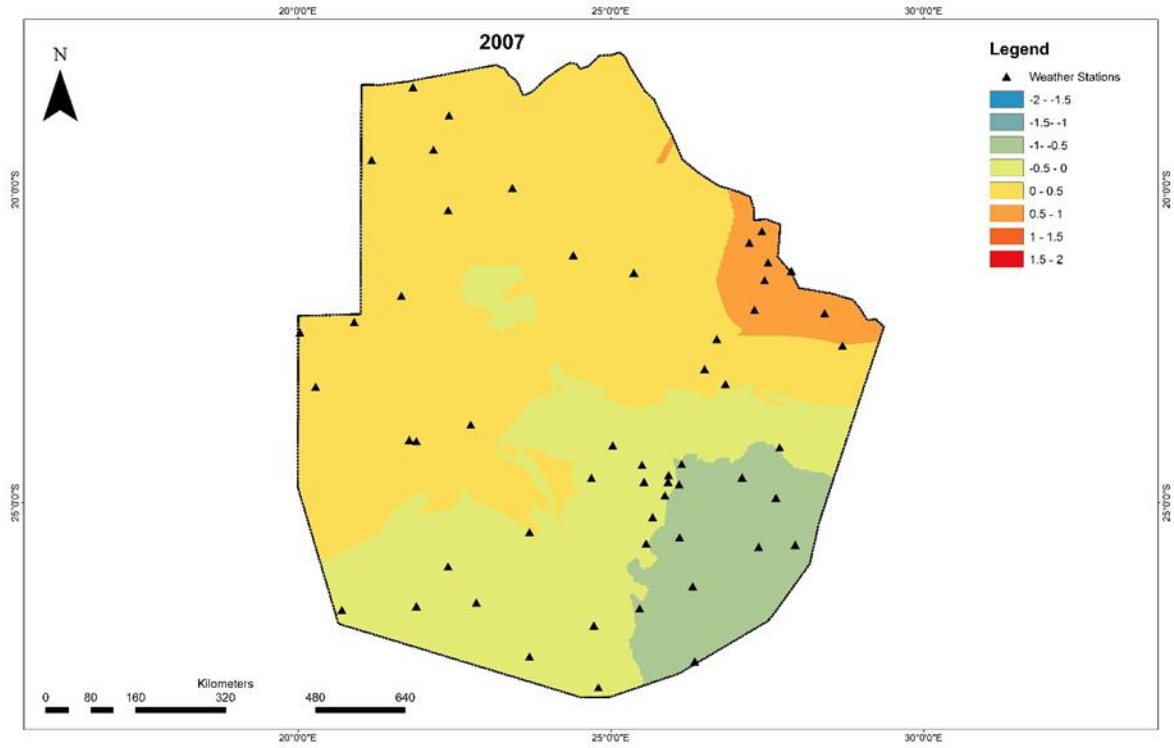

Figure 8.3al: OK SPI 2007

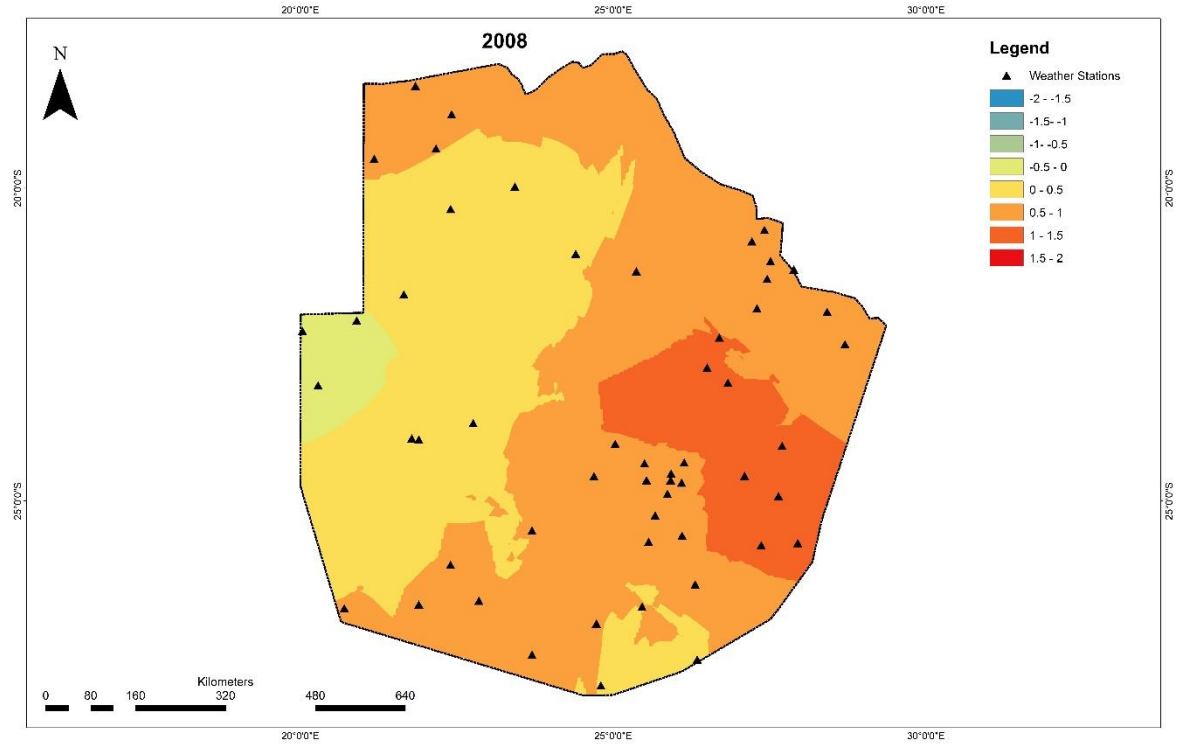

Figure 8.3am: OK SPI 2008

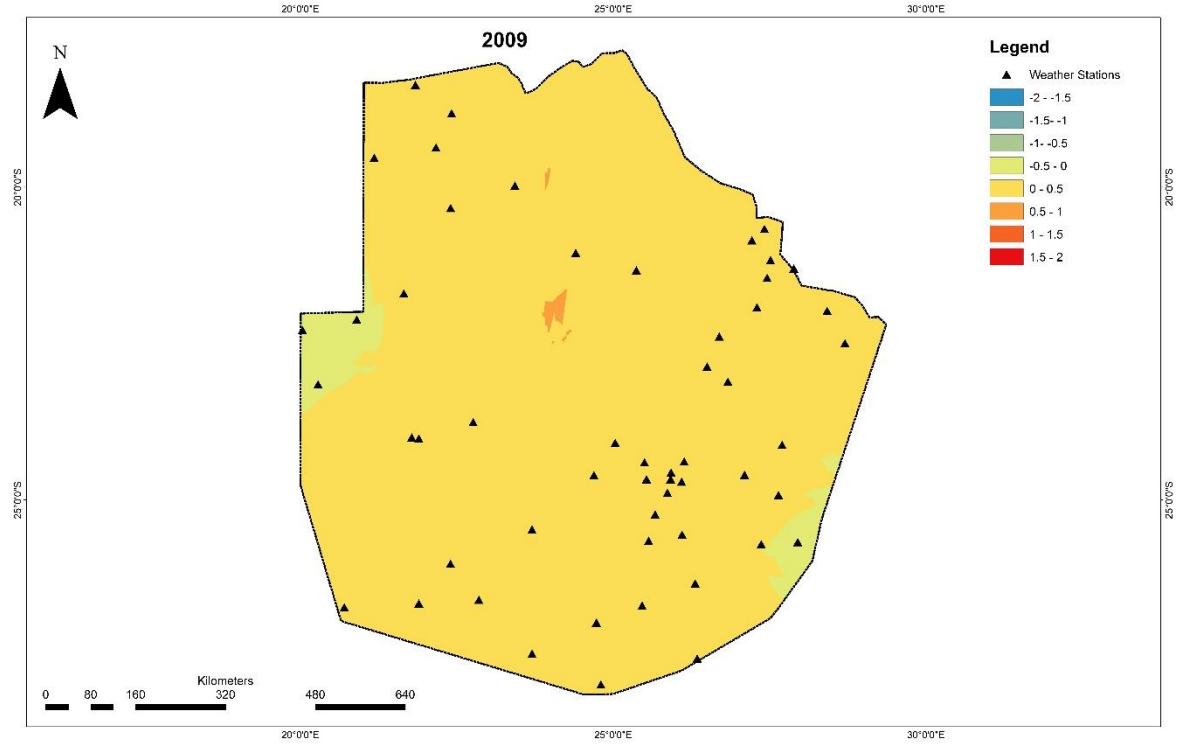

Figure 8.3an: OK SPI 2009

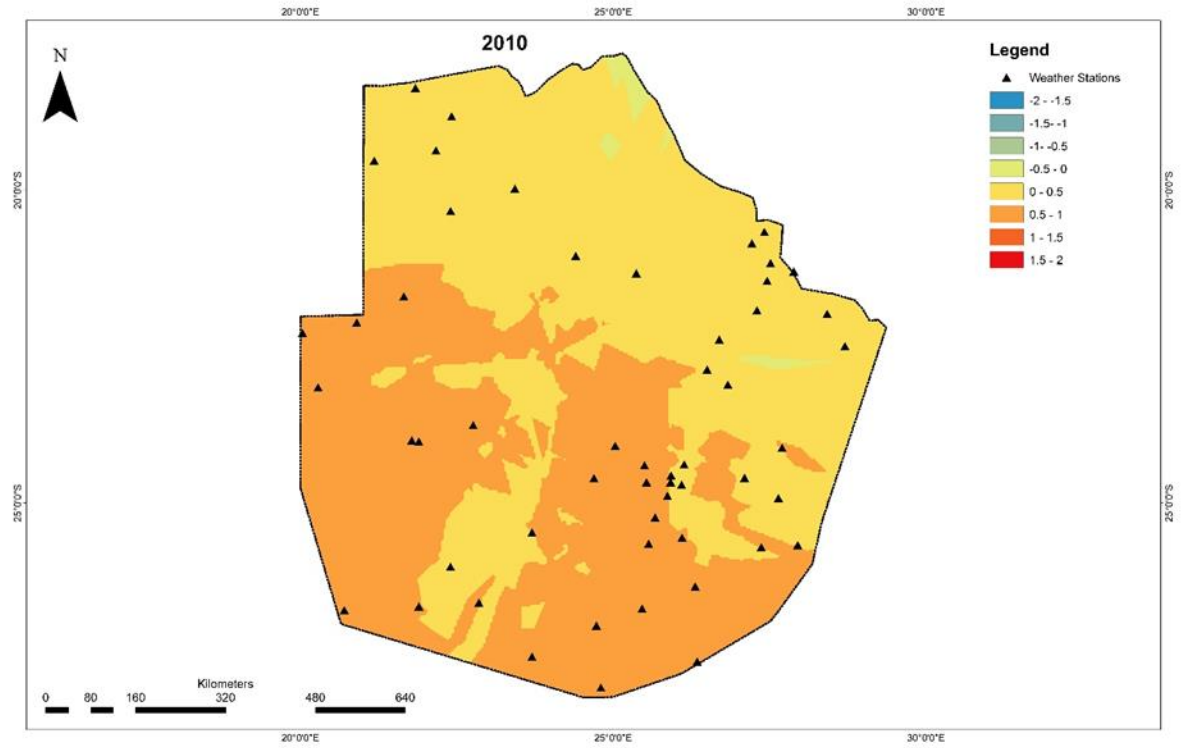

Figure 8.3ao: OK SPI 2010

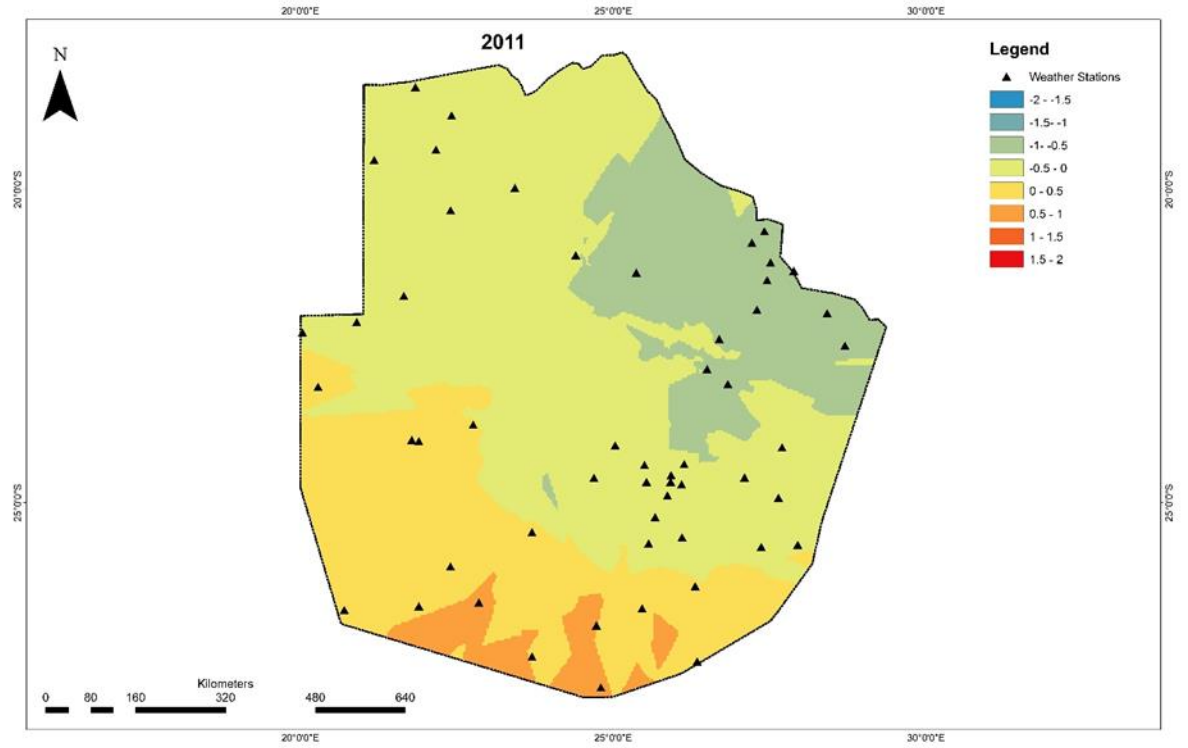

Figure 8.3ap: OK SPI 2011

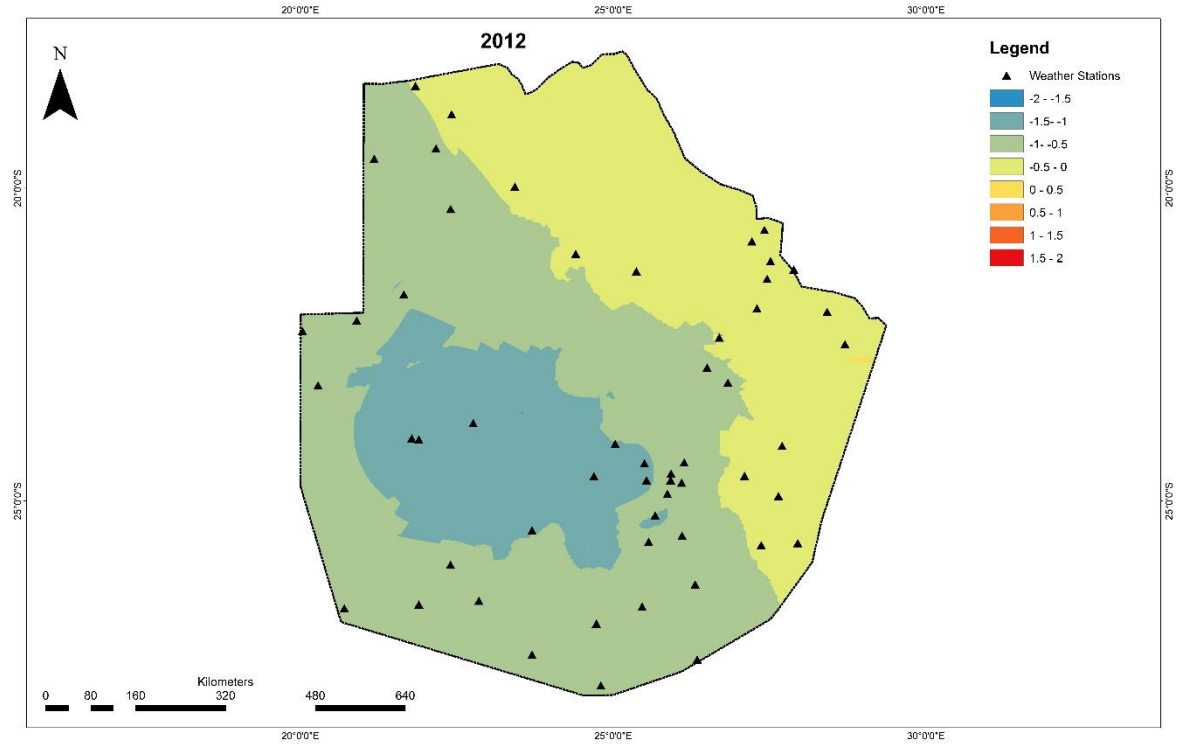

Figure 8.3aq: OK SPI 2012

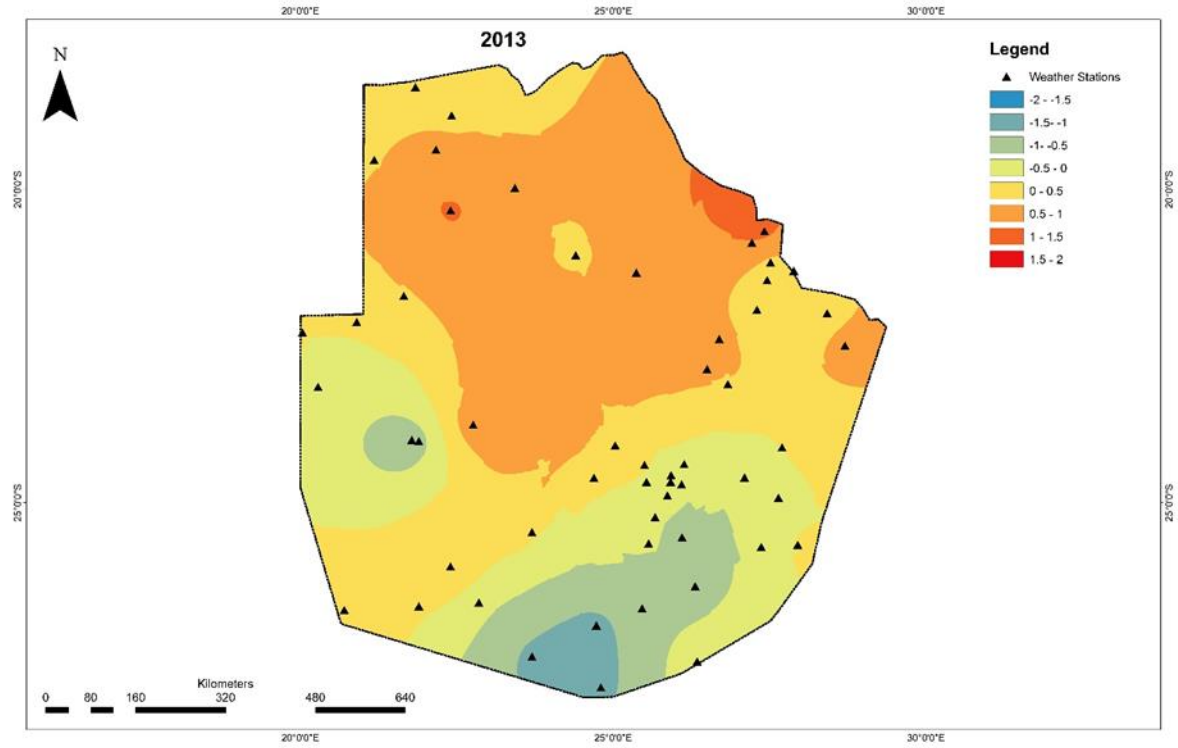

Figure 8.3ar: OK SPI 2013

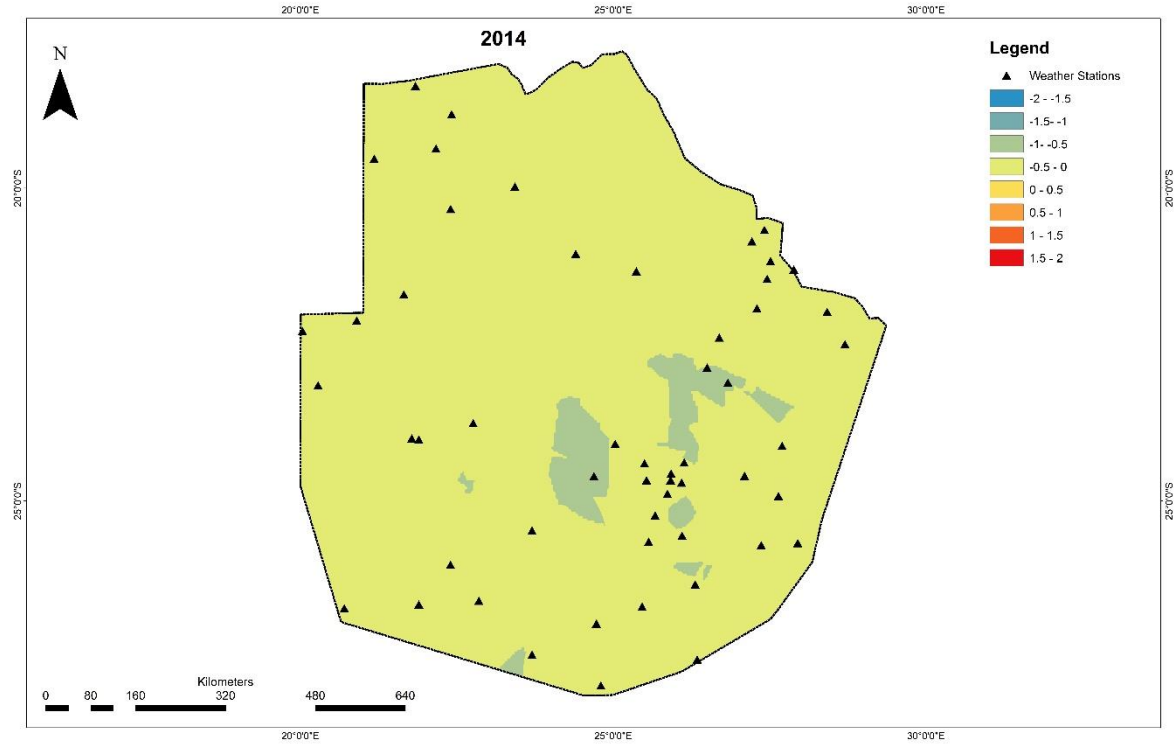

Figure 8.3as: OK SPI 2014

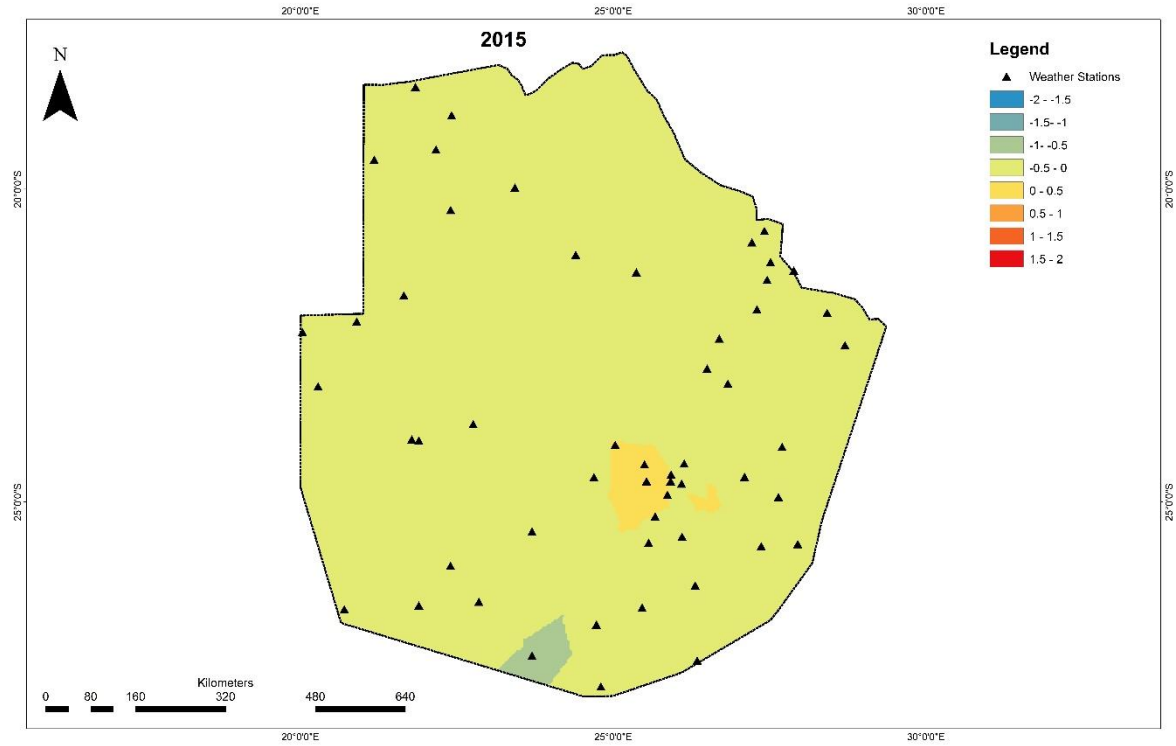

Figure 8.3at: OK SPI 2015

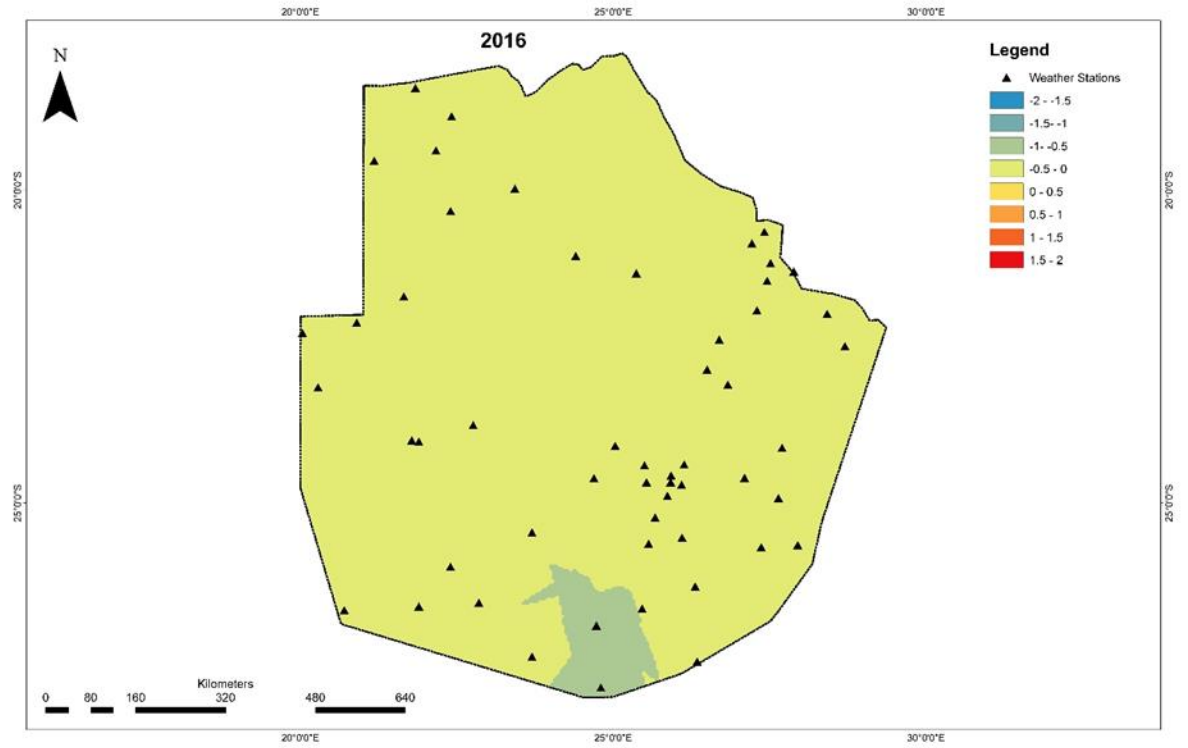

Figure 8.3au: OK SPI 2016

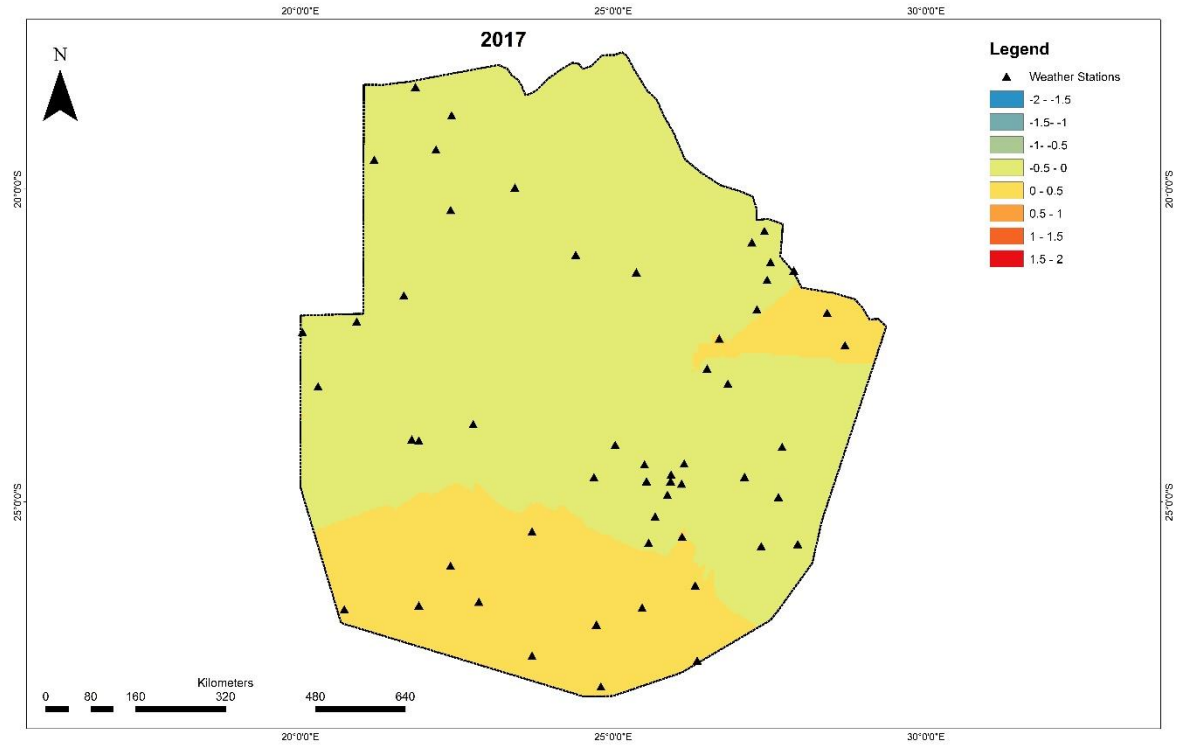

Figure 8.3av: OK SPI 2017

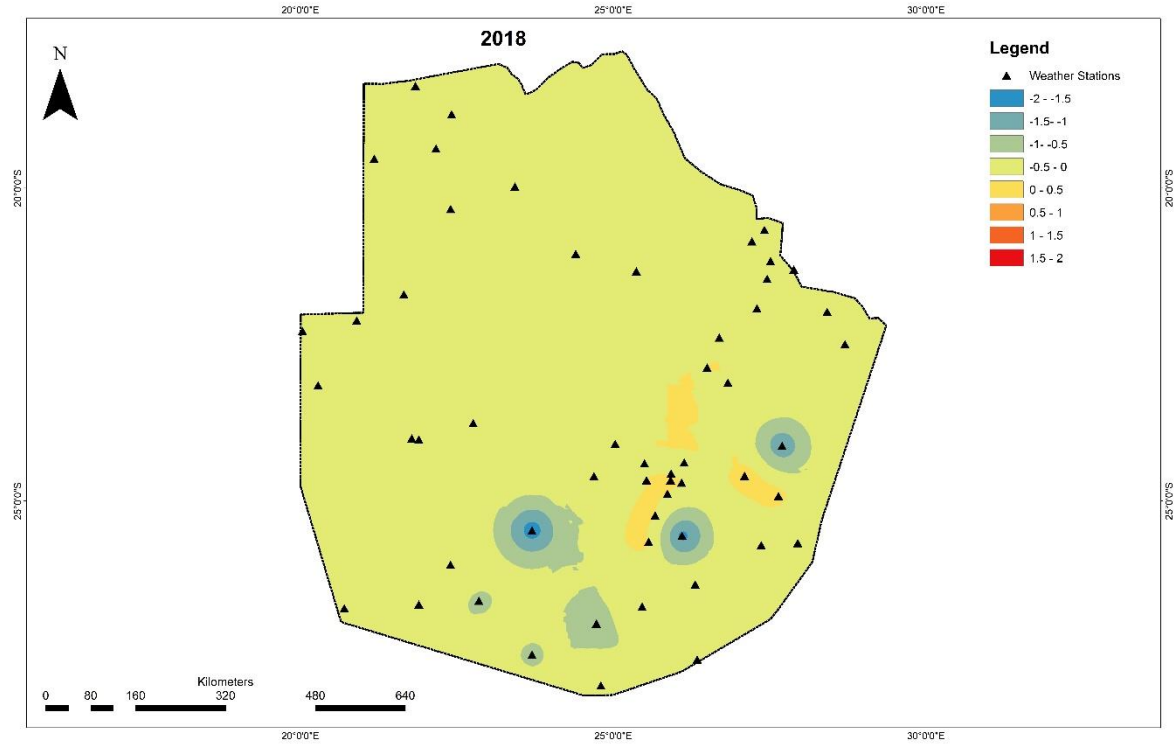

Figure 8.3aw: OK SPI 2012

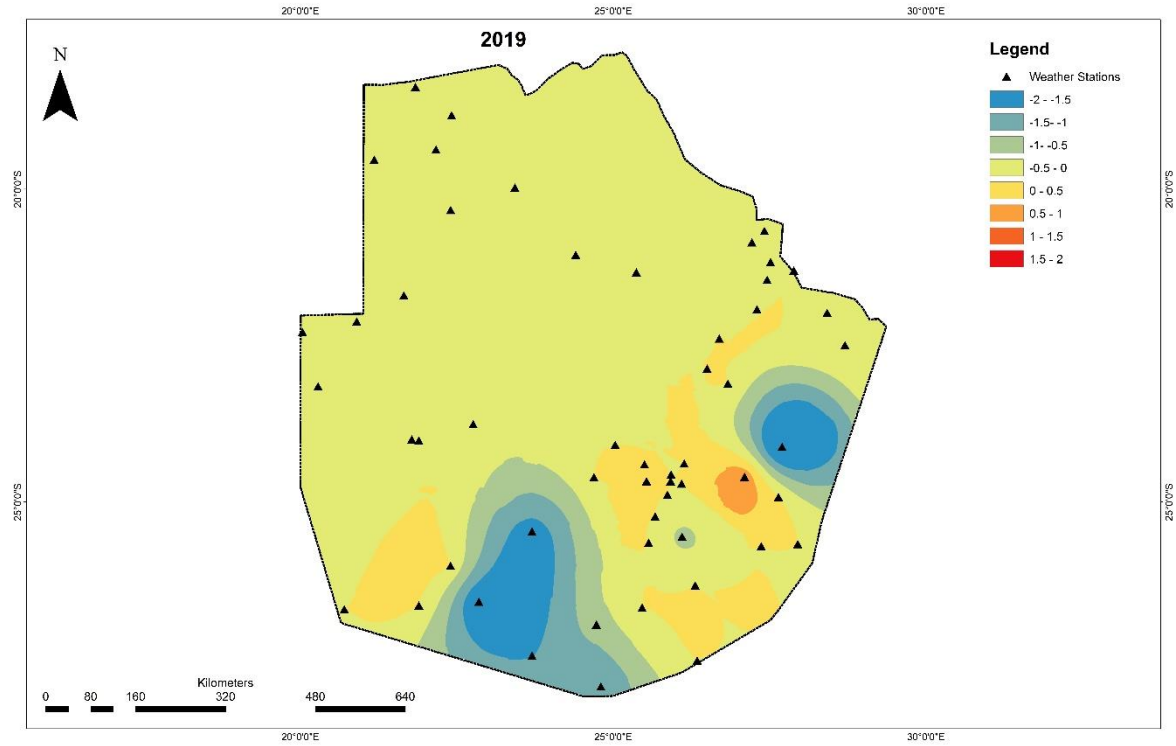

Figure 8.3ax: OK SPI 2010